BRNO UNIVERSITY OF TECHNOLOGY

VYSOKÉ UČENÍ TECHNICKÉ V BRNĚ

FACULTY OF ELECTRICAL ENGINEERING AND COMMUNICATION

FAKULTA ELEKTROTECHNIKY
A KOMUNIKAČNÍCH TECHNOLOGIÍ

DEPARTMENT OF BIOMEDICAL ENGINEERING

ÚSTAV BIOMEDICÍNSKÉHO INŽENÝRSTVÍ

STUDY OF ELECTROPHYSIOLOGICAL FUNCTION OF THE HEART IN EXPERIMENTAL CARDIOLOGY

STUDIUM ELEKTROFYZIOLOGICKÝCH PROJEVŮ SRDCE V EXPERIMENTÁLNÍ KARDIOLOGII

DOCTORAL THESIS
DIZERTAČNÍ PRÁCE

AUTHOR — **Ing. Marina Ronzhina**
AUTOR PRÁCE

SUPERVISOR — **doc. Ing. Jana Kolářová, Ph.D.**
ŠKOLITEL

BRNO 2016

BRNO UNIVERSITY OF TECHNOLOGY
FACULTY OF ELECTRICAL ENGINEERING AND COMMUNICATION

Doctoral Thesis

Doctoral study field **Biomedical Electronics and Biocybernetics**
Department of Biomedical Engineering

Student: Ing. Marina Ronzhina ***ID:*** 112287

Academic year: 2016/17

TITLE OF THESIS:

Study of Electrophysiological Function of the Heart in Experimental Cardiology

INSTRUCTION:

1) Provide the literature review in the field of recording, processing and analysis of electrical biological signals in experimental cardiology. Focus on the methods for ECG analysis in time and frequency domain and on the data classification tools recently used for automatic diagnosis of myocardial ischemia. 2) Create a database of ECG with and without myocardial ischemia patterns using experimental data available on the Department of Biomedical Engineering, Brno University of Technology. If need, design and carry out experiments with rabbit isolated heart in order to collect ECG under various conditions including induced myocardial ischemia. 3) Propose and implement approach for evaluation of ECG under various experimental conditions. Quantify the changes in ECG caused by myocardial ischemia and provide statistical evaluation of data. 4) Based on the results from step 3, design and implement approach for automatic detection of myocardial ischemia in experimental data. Validate the detection method using data collected under different conditions and evaluate the detection performance of proposed approach. 5) Discuss obtained results critically: describe advantages and limitations of proposed methods, compare the results with those of other authors and outline potential future development in this field.

Submission deadline: 27.10.2016

Head of thesis: doc. Ing. Jana Kolářová, Ph.D.

VYSOKÉ UČENÍ TECHNICKÉ V BRNĚ Fakulta elektrotechniky a komunikačních technologií
Ústav biomedicínského inženýrství
-2-

prof. Ing. Jiří Jan, CSc.
Subject Council chairman

WARNING:

ABSTRACT

Isolated heart is widely used in experimental cardiology to study myocardial ischemia and infarct, left ventricular hypertrophy, myocarditis, etc. Nevertheless, the standardized criteria for assessment of above disorders in animal models are missing that complicates interpretation of the results obtained in such studies. It is of special importance, if several pathologies are presented simultaneously, when possible co-effects cannot be simply identified and analysed. Besides the condition of the heart, there are many other factors playing important role in data acquisition and analysis. In this work, electrophysiological effects of increased left ventricular mass (intrinsic factor) and voltage-sensitive dye di-4-ANEPPS (external factor) are evaluated on rabbit isolated hearts under non-ischemic and ischemic condition. Although both phenomena are quite frequent in animal studies, their effects on ischemia manifestations and electrogram-based ischemia detection accuracy have not been quantitatively described yet. Results of quantification of ischemia-induced changes in heart function (under normal conditions, increased LV or dye administration) by analysis of various EG and VCG parameters are summarized. Such important aspects as recording electrodes placement, method of parameters calculation (using or without outcomes of manual EG delineation) and definition of the beginning of 'true' ischemic injury in preparation (methodological factors) are also addressed. Along with it, different tools for automatic detection of ischemia in data are presented. According to the results of statistical analysis of parameters and testing the detectors on different data, all above mentioned phenomena (both heart-related and methodological) should be taken into account to ensure successful study of the heart electrical activity.

KEYWORDS

Rabbit isolated heart; electrogram; vectorcardiogram; global myocardial ischemia; left ventricle size; di-4-ANEPPS; feature selection; automatic classification.

ABSTRAKT

Srdeční poruchy, jejichž příkladem je ischemie myokardu, infarkt, hypertrofie levé komory a myokarditida, jsou v experimentální kardiologii obvykle studovány na modelu izolovaného srdce. Kritéria pro detekci srdečních poruch však nejsou pro zvířecí modely standardizována, což komplikuje srovnání a interpretaci výsledků různých experimentálních studií. Obzvlášť složitá situace nastává při současném výskytu několika patologických jevů, jejichž vzájemná součinnost komplikuje rozpoznání jejich individuálních účinků. Korektní posouzení stavu srdce vyžaduje také zohlednění mnoha faktorů spojených s akvizicí dat. Tato práce je věnována kvantitativnímu hodnocení elektrofyziologických změn způsobených globální ischemií myokardu. Vliv ischemie byl hodnocen pro fyziologická srdce a srdce se zvětšenou levou komorou a dále pro srdce nabarvená napěťově-citlivým barvivem di-4-ANEPPS. Přestože jsou oba fenomény často zastoupeny v animálních studiích, nebyl dosud popsán jejich vliv na manifestaci ischemie v elektrogramech (EG), ani nebyl kvantifikován jejich vliv na přesnost detekčních algoritmů pro identifikaci ischemie. Práce shrnuje kvantitativní změny srdeční funkce vyvolané ischemií (v normálních podmínkách, při hypertrofii levé komory, a při administraci barviva) založené na hodnocení EG a VKG parametrů. Dále práce obsahuje rozbor důležitých aspektů akvizice záznamů, jako je umístění snímacích elektrod, způsob výpočtu deskriptorů z EG a VKG (s použitím výsledků manuálního rozměření záznamů, nebo bez něj) a identifikace okamžiku vývoje ischemie v preparátu. Nedílnou součást práce tvoří návrh, realizace a ověření metod pro automatickou detekci ischemie v experimentálních záznamech. Výsledky práce dokazují, že dosažení opakovatelných a věrohodných výsledků je podmíněno zohledněním všech výše uvedených faktorů souvisejících jak se stavem srdce, tak s metodikou záznamu a analýzy dat.

KLÍČOVÁ SLOVA

Izolované králičí srdce; elektrogram; vektorkardiogram; globální ischemie myokardu; velikost levé komory srdeční; di-4-ANEPPS; výběr příznaků; automatická klasifikace.

BIBLIOGRAPHIC CITATION

RONZHINA, M. *Study of electrophysiological function of the heart in experimental cardiology*. Brno: Brno University of Technology, Faculty of Electrical Engineering and Communication, 2016. 165 p. Academic advisor: doc. Ing. Jana Kolářová, Ph.D.

DECLARATION

I declare that I have written the doctoral thesis titled "Study of electrophysiological function of the heart in experimental cardiology" independently, under the guidance of the supervisor, and using the technical literature and other sources quoted within the thesis and detailed in the list of literature in the final section.

As the author of thesis, I furthermore declare that, as regards the creation of the work, I have not infringed any copyright. In particular, I confirm that I have not violated anyone's personal and/or ownership rights and I am fully aware of the consequences of breaking Regulation § 11 of the Copyright Act No. 121/2000 Coll., as amended, and intellectual property rights or changes in related Acts (the Intellectual Property Act), as amended, inclusive of possible consequences resulting from the provisions of the Criminal Act No. 40/2009 Coll., Section 2, Head VI, Part 4.

Brno, …….. ……..

Ing. Marina Ronzhina

ACKNOWLEDGEMENT

I would like to thank all the people who supported me during my doctoral studies. Especially, I would like to thank to my supervisor doc. Ing. Jana Kolářová, Ph.D. and my external supervisor prof. MUDr. Marie Nováková, Ph.D. for their interest, professional mentoring, ideas, and contributing suggestions. Furthermore, I wish to thank to my colleagues from the Department of Biomedical Engineering (Brno University of Technology) and also the Department of Physiology (Masaryk University) for valuable support in experimental part of the work and for constructive and suggestive discussions during my studies. I also thank to prof. Ing. Ivo Provazník, Ph.D., head of the Department of Biomedical Engineering, FEEC, BUT for providing excellent conditions for the study and research. Special thanks belong to my family, parents and friends for their great patience, inspiration and generous support.

I also acknowledge institutional support given by research projects, namely FNUSA-ICRC (CZ.1.05/1.1.00/02.0123) in the years 2012-2015 and the grant projects of the Czech Science Foundation GA102/07/1473 in the years 2010-2011, and GAP102/12/2034 in the years 2012-2016.

Brno, …….. ……..
Ing. Marina Ronzhina

TABLE OF CONTENTS

Introduction **9**

1 Brief summary of electrophysiological studies of myocardial ischemia **10**

1.1 Electrocardiography **10**

1.2 ECG based diagnostics of myocardial ischemia **11**

1.3 Study of myocardial ischemia using rabbit model **15**

2 Aims of the doctoral thesis **18**

3 Experiments with rabbit isolated hearts: overview of experimental setup and data acquisition and analysis **19**

3.1 Experimental protocols **19**

3.2 Electrogram recording **20**

3.3 Data processing and analysis **21**

3.3.1 Processing of electrograms recorded during fixed heart orientation 21

3.3.2 Processing of electrograms recorded during heart rotation 26

3.3.3 Calculation of electrogram parameters 28

4 Electrical activity of the heart under normal and pathological conditions **35**

4.1 General characteristics of electrogram under normal and ischemic conditions **35**

4.1.1 Background 35

4.1.2 Methods 36

4.1.3 Results 38

4.1.4 Discussion 55

4.2 Effects of left ventricle mass on electrogram under non-ischemic and ischemic conditions **59**

4.2.1 Background 59

4.2.2 Methods 60

4.2.3 Results 61

4.2.4 Discussion 68

4.3 Effects of voltage-sensitive dye di-4-ANEPPS on electrogram under normal and ischemic conditions **71**

4.3.1 Background 71

4.3.2 Methods 72

4.3.3 Results 74

4.3.4 Discussion 85

5 Automatic detection of ischemia in electrograms **89**

5.1 Background **89**

5.2 Methods **92**

5.2.1 Feature selection 93

5.2.2 Data classification 95

5.2.3 Evaluation of classification performance 99

5.3 Results **100**
5.3.1 Selected feature sets 100
5.3.2 Binary classification: single-feature decision rules and multi-feature techniques 102
5.3.3 Multiclass classification results: single-feature decision tree and multi-feature techniques 112
5.4 Discussion **117**

Overall conclusions **122**

References **126**

List of abbreviations **136**

List of figures **137**

List of tables **139**

Appendix A – Parameters calculated from electrograms and vectorcardiograms **140**

Appendix B – Electrogram and VCG during ischemia **142**

Appendix C – Values of parameters in stabilization and ischemia **144**

Apppendix D – Results of paired test for control group parameters **147**

Appendix E – Discriminating ability indexes in control group during ischemia **148**

Appendix F – Discriminating ability indexes in different groups of parameters in control heart group **151**

Appendix G - Discriminating ability of lead III parameters **154**

Appendix H – Results of paired test for the hearts with high LV mass fraction **155**

Appendix I – Discriminating ability indexes in hearts with high LV mass fraction during ischemia **156**

Appendix J – Results of paired test for parameters from the hearts stained with VSD di-4-ANEPPS **159**

Appendix K – Discriminating ability indexes in hearts stained with VSD di-4-ANEPPS **160**

Appendix L – Selected classification features **163**

INTRODUCTION

Although ischemic and reperfusion injury has been intensely studied, it is worth of further interest, since the coronary artery disease still represents one of the major causes of morbidity and mortality in many countries around the world. Particularly, in Europe region, coronary heart disease (which is a result of coronary artery disease) caused 19 % of deaths in men and 20 % of deaths in woman last year [1]. Myocardial ischemia and concomitant arrhythmias result in incorrect electrical and mechanical activity of the heart and often lead to the sudden death.

Mechanisms of various heart disorders are well known due to available diagnostic tools such as electrocardiography, echocardiography, heart catheterization, etc. First two techniques are fundamental methods widely used for clinical diagnostics of heart diseases in both acute and chronic forms by assessment of the pathological changes in electrical conduction system, morphological structure and function of the heart. There are standardized guidelines for diagnostics and management of heart diseases reported by American Heart Association (AHA), American College of Cardiology Foundation (ACCF) and Heart Rhythm Society (HRS) [2]. Recommendations from the guidelines are regularly updated according to the results of new studies. Nevertheless, there are still areas requiring an improvement of available methods and/or development of new ones with sufficient sensitivity and specificity.

Open questions in the development of the disease, its diagnostics and corresponding treatment may be successfully solved using various animal models, from subcellular level to that of the whole organism. The isolated heart perfused according to Langendorff is possible predominant model used to study myocardial ischemia and infarction [3],[4]. In experimental cardiology, above and many other aspects are usually examined by means of electrophysiological, biochemical and histological techniques. The first methods are mainly represented by analysis of heart electrical activity recorded as electrocardiogram (ECG, in animal *in vivo*), electrogram (EG, in isolated heart) or cardiac action potential (AP, any model including tissue and cells). Although the animals have been used in electrophysiological studies for a long time, the standardized criteria for assessment of cardiac disorders in animal models are missing, which often complicates interpretation of achieved results and their comparison with other reports. Particularly, lack of criteria for ischemia manifestation in rabbit heart (one of the most frequently used model [5]) may lead to discrepancy in obtained study results due to differences in the definition of ischemia beginning in preparation and/or in ECG or EG patterns used for ischemia assessment. This is of special importance, when there are several coexisting factors (such as LV enlargement, myocardial ischemia, drug effects, etc.) which may affect cardiac activity in different or similar way. The identification and elimination of such co-effects is rather difficult and requires performing more detailed analysis of recorded data or additional investigating of the phenomena on control group/s.

Besides above aspects, there are many others not associated with the heart or used diagnostics rules rather than with technical or methodological concept of the method, such as: placement, size and material of recording electrodes, the content and temperature of the solutions (*in vitro* studies), type of anaesthesia, administration of some drugs (heparin, electric-mechanical uncoupler, etc.), duration of stabilization period and the whole experiment, utilizing of some methods with potential undesirable effects (e.g. phototoxic effects of voltage-sensitive dye used for AP recording by optical way, etc.). All of them may affect the quality of obtained data and the reliability of study results. Thus, successful study of the heart electrical activity under normal as well as pathological condition is only possible in case of comprehensive approach, when heart-related factors and other methodological aspects are taken into account.

1 BRIEF SUMMARY OF ELECTROPHYSIOLOGICAL STUDIES OF MYOCARDIAL ISCHEMIA

1.1 ELECTROCARDIOGRAPHY

Heart is a pump that drives a blood through the vasculature. This mechanical function of the heart is the result of coordinated contractions of atria and ventricles which occur in response to the conduction electrical signal, so called action potential (AP). Various pathological conditions lead to dysregulation of the excitation-contraction coupling [6]. For example, ischemic heart is characterized by slow conduction and non-uniform excitability that make it more predisposed to ventricular fibrillation [7].

AP origins in the pacemaker cells of sinoatrial (SA) node and then is passing to the other sites of the heart through conduction system (Fig. 1a, left). APs from different heart locations have a specific morphology (Fig. 1, right), which also varies with species and heart rate and can be affected with drugs or hormones. In contrast to the cell of SA node (and other peacemaker cells) which have the smooth APs (Fig. 1a, right at the top), non-peacemaker ones (for instance, AP of ventricular myocytes; black in Fig. 1a, right at the middle) are characterized by AP with longer plateau phase (see below) that prevents re-excitation and generating the heart beat without preceding relaxation. [6].

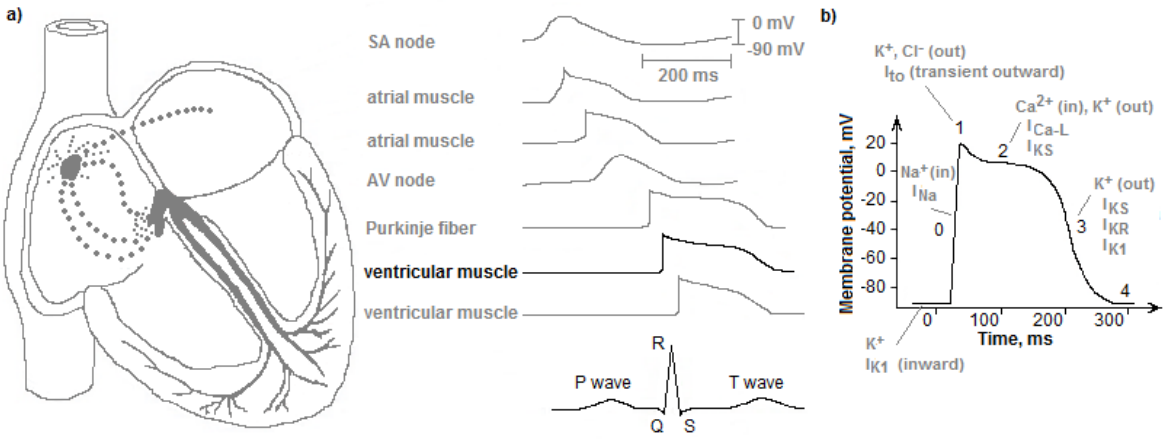

Figure 1. Electrical activity of the heart.
a) Conduction system of the heart (left), time courses of action potentials in its different parts and resulting ECG (right); b) cardiac ventricular action potential and corresponding ion currents.

Cardiac AP consists of 5 distinct phases (Fig. 1b): 0 – rapid depolarization, 1 – early repolarization, 2 - plateau, 3 - late repolarization, 4 - resting membrane potential [6]. Each phase of AP is characterized by changes of cell membrane permeability to the ions involved in the activation process. This knowledge is helpful for understanding the mechanisms of heart function. For example, during plateau phase of AP, membrane is keeping depolarized by keeping the Na^+ and Ca^{2+} channels inactivated that prevents re-excitation of the cell. Coordinated activation-relaxation alternation can be explained by AP duration (APD) that is generally almost as long as the Ca^{2+} transient and contraction. Calcium entering the cell membrane activates the myofilaments and induces the cardiac muscle contraction. So called L-type calcium channels (slow channels) play the most important role in activation process (mainly in the genesis of plateau phase of AP). Entering

Ca^{2+} into the cell triggers release of Ca^{2+} from sarcoplasmic reticulum that increases $[Ca^{2+}]_i$ additionally [8],[9].

Propagation of APs of different cell types through the heart results in origin of the electrical signal with specific shape – electrocardiogram (ECG) – that can be measured on the level of the whole organ (Fig. 1a, right bottom) [6]. Phases of APs are in the relationship with the parts of ECG. Particularly, for ventricular myocyte, the upstroke of AP corresponds with the onset of QRS complex and end of AP with the end of T wave [10]. ECG curve describes the depolarization and repolarization of the heart, where the P wave and QRS complex represent the depolarization of atria and ventricles, respectively, and T wave represents the repolarization of the ventricles.

Non-invasive measurement of electrical activity of the heart – electrocardiography – is the basic diagnostic method in cardiology. The standard clinical surface ECG includes recordings from 12 leads: three bipolar (lead I, II, III), six unipolar precordial leads (V1 through V6) and three modified unipolar limb leads (aVR, aVL and aVF) [11]. Other lead system – Frank system – consists of only three orthogonal leads (X, Y and Z) used for construction of so called vectorcardiogram (VCG). Although the standard 12-lead system is widespread used in clinic, the latter can better reflect the anatomic changes in the heart (e.g. providing better sensitivity and specificity than conventional ECG in the diagnosis of left ventricular enlargement), bring unique or additional 3D information about cardiac electrical activity important for detection of acute myocardial infarction, pulmonary valve stenosis, Brugada syndrome, etc. [12],[13].

1.2 ECG BASED DIAGNOSTICS OF MYOCARDIAL ISCHEMIA

Various cardiac diseases may be indicated on ECG as characteristic changes of its shape (including amplitude and/or time interval changes). ECG alterations during myocardial ischemia – the most common type of cardiovascular disease – originate from the changes in metabolic as well as electrophysiological systems. The lack of O_2 leads to the switching the oxidative phosphorylation to glycolysis for ATP production. Some ATP energy may be used to maintain the mitochondrion membrane potential, which may lead to fall in ATP and increasing ADP. Under these conditions, sarcolemmal ATP-sensitive K^+ channels have a greater probability to being open and produce an outward K^+ current (plateau phase, see Fig. 1b). This results in shortening APD, depolarization (decrease from -85 mV to -60 mV) of the resting membrane potential (see Fig. 2a) and, consequently, in reduction in excitability and conduction block. [14]

However, initially, AP is slightly prolonged, but changes rapidly to a shortening. This *transient AP prolongation* can be explained by various factors, such as increasing the local temperature, reduction in electrogenic pump current, a fall in I_{K1} due to intracellular acidosis, and an acute inhibition of I_{to}. K^+ currents, that cause *the prominent shortening of AP* after short-term lengthening, are specific currents that become activated only under ischemic conditions, especially on the plateau of AP. On the contrary, the K^+ currents, activated under physiological conditions, are inhibited by ischemic conditions (namely, hypoxia, metabolic blockade, exposure to oxygen stress, etc.). Gradual *decrease of excitability* is mainly caused by inactivation of the Na^+ channel due to depolarization. Reduction of excitability is especially pronounced in the subepicardial regions. *Conduction velocity* is determined by the amplitude and upstroke velocity of AP in the cells, resistance of the cell membrane, the longitudinal resistance of the cell, etc. In healthy myocardium, conduction is more rapid in the longitudinal than in transverse direction. Decreasing amplitude and upstroke velocity of AP in ischemia (mainly severe ischemia, Fig. 2a) negatively affect the conduction. [14]-[16]

Reperfusion restores the delivery of oxygen and substrates required for aerobic ATP generation and washes accumulated H^+ out, which results in the normalization of extracellular pH; external K^+ is also reduced by washout and resting potential quickly restores to normal values; the systolic and diastolic $[Ca^{2+}]_i$ level increases to the control values within approx. 15 min of reperfusion, which enables the normalization of heart mechanical function [7],[17],[18].

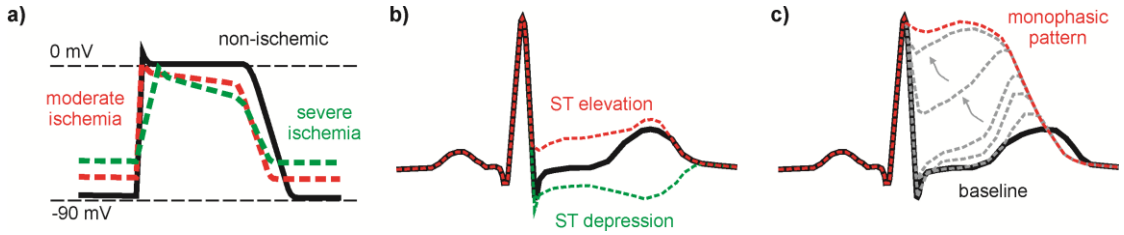

Figure 2. Electrophysiological manifestations of myocardial schemia.
AP changes in ischemia (a); ST deviations (b); the grades of ischemia in ECG (c).

Corresponding ECG changes may be indicated by leads facing the ischemic region. Initial shortening of APD in ischemic zone without concurrent changes in conduction velocity (usually in subepicardial region) leads to *tall, symmetrical* and *peaked T wave*. Decreased APD also results in *shortening of QT* interval. ST segment corresponds with the period when the ventricles are depolarized, i.e. the ventricular APs are all in the plateau phase (see Fig. 1). If all regions of ventricles have the same transmembrane potential, such as in healthy heart, this period is isoelectric in ECG. However, above changes over the myocardium (mainly shortening and decreased amplitude of AP and depolarization – i.e. less negative resting membrane potential, see Fig. 2a) are not homogenous (especially at the border zone) and a voltage gradient between normal and ischemic zones appears, which results in flow of the current (so called injury current) between these regions. On the surface ECG, these currents are represented by *deviation of ST segment* above (ST segment elevation) or below (ST segment depression) the baseline. ST elevation or depression appears in ECG (Fig. 2b), if the injury currents are directed toward or away from the recording electrode. After about 5 minutes of ischemia, the ST segment becomes further elevated because of the shorter AP in ischemic region of the heart and later, the ST becomes markedly elevated due to delayed activation in ischemic region. This can be accompanied by pronounced inverted T wave. When cells in the middle of infarct zone become unexcitable, the *'monophasic patterns'* are presented in ECG (Fig. 2c). The changes in depolarization leads to slowed conduction of electrical impulses through the ventricles, which is manifested in ECG as *widening of QRS* or/and *reduction of R peak steepness*.

In a clinical setting, myocardial ischemia is identified from the ECG according to the AHA/ACCF/HRS recommendations primarily based on ST segment changes that occur during the early acute phase of acute coronary syndromes [2]. According to the guidelines, diagnosis of acute ischemia/infarction is indicated, if ST deviation reaches the predetermined threshold value in 2 or more anatomically contiguous body surface ECG leads. Threshold values for ST segment – 0.1 mV or 0.2 mV for ST elevation and -0.05 mV or -0.1 mV for ST depression – depend on gender, age and used ECG leads. Furthermore, hypertrophy, effects of some drugs, electrolyte abnormalities and other factors may also cause ST segment deviation which may result in false positive diagnosis of ischemia and complicate differentiation between these abnormalities and acute ischemia. Other source of wrong ECG interpretation is the absence of ST changes in patients with ischemic chest pain, which may be explained by different mechanisms, such as perpendicular

orientation of ST vector to the recording plane, cancellation of electrical forces caused by ischemia at opposites sites, absence of coronary occlusion and corresponding ST changes at the time of ECG recording [19].

The changes in electrical activation within ischemic or infarcted region are also reflected in the changes of QRS complex. Particularly, the magnitude and extent of QRS alterations depend on the size and location of the ischemic region (and, consequently, on the vessel occluded) and the mutual placement of this region and recording lead [2].

The most frequently used tool for diagnosis of cardiac artery disease is *stress test* including physical exercise which leads to increased oxygen demand in myocardium and, therefore, may unmask the disease during test. Simultaneously with the exercise, ECG is recorded and ST segment is evaluated. According to the previously reported results of meta-analysis, the sensitivity (Se) and specificity (Sp) of stress-induced ST deviations in ischemia detection reach 50-68 % and 77-90 %, respectively [20].

The accuracy (Acc) of ischemia detection using ST-deviation criteria can be verified by coronary angiography, at autopsy or by modern non-invasive technologies, such as nuclear scintigraphy, echocardiography or magnetic resonance imaging. These methods are used as a *gold standard* and the results of ECG detection are compared with finding obtained using such tests. However, the diagnostic Acc of the detection of myocardial ischemia by nuclear and echocardiographic imaging test is only 75-90 %. Thus, the diagnosis of ischemia in ECG may possible be correct, even if the presence of ischemic injury was not detected by the imaging techniques, which complicates interpretation of the results. [21]

Various aspects of ischemia assessment by ECG have been recently studied with the purpose of improving the detection Acc. Man et al. evaluated the effect of definition of the point used for ST level measurement on the stability of ST-segment elevated myocardial infarction diagnosis in patients with acute coronary syndrome and observed, that, among all tested positions from J-20 ms to J+80 ms, the diagnosis is quite stable only between 10 and 40 ms after the J point [22].

According to Fayn, the subset of three leads (I, II and V2) can bring as much information as the standard 12-lead system, which results in the same Acc = 96.9 % provided by both methods [23]. Such advanced results were, however, obtained using linear discriminant analysis; if standard criteria for 12-lead ST deviations (age-dependent, [2]) were applied, Se, Sp and Acc reached only 64.4 %, 84.3 % and 75.0 %, respectively. Approaches based on more advanced statistical and machine learning techniques will be addressed in more detail in last chapter of the thesis. Haeberlin et al. evaluated the individual performance of ECG leads in detection of transient ischemia induced during controlled occlusion of three main coronary arteries and found that V3, V6 and aVF are the most reliable for detection of ischemia in any region [24].

Quite low diagnostic ability of ST criteria led to the development of new methods based on analysis of other parts of ECG (mainly QRS complex) or discriminators derived from ST-T interval. In the first group of studies, potential use of QRS prolongation as a marker of myocardial ischemia was investigated. Michaelides et al. found, that QRS prolongation observed in patients during typical anginal pain was more sensitive to myocardial ischemia (Se = 70 %, Sp = 89 %) than standard ST-segment changes (Se = 56 %, Sp = 89 %) [25]. According to Takaki et al., visual detection of QRS prolongation in standard ECG is only possible in patients with more severe or global ischemia; on the contrary, in a high-resolution ECG recorded during exercise test, significant prolongation of QRS complex can be detected even in patients with mild (e.g. single vessel) coronary artery disease [26].

Many various studies were inspired by the concept of so called high-frequency (HF) QRS complex, which was introduced by Goldberger et al. for the first time [27]. The method consists of the analysis of low-voltage potentials presented in QRS region in frequency range 80-300 Hz. Ischemia leads to the slowed conduction velocity in particular regions of myocardium, which results in the reduction of fragmented depolarization wave in the tissue and, consequently, shifting the spectral content of QRS to frequencies lower than mentioned range. Decrease of the amplitude of HF-QRS components then can be evaluated by corresponding HF parameters (the root-mean-square value – RMS [27], reduced amplitude zone [28] and HF morphology index [29]). In more recent study with stress-induced ischemia confirmed by myocardial perfusion imaging, it was found, that the diagnostic performance of HF-QRS analysis (Se = 69 %, Sp = 86 %) was enhanced as compared to conventional ST segment method (Se = 39 %, Sp = 82 %) [30].

Other group of QRS-related methods is based on the analysis of QRS slopes (upward and downward). Pueyo et al. found that the QRS slopes are considerably less steep during artery occlusion performed within percutaneous transluminal coronary angioplasty (PTCA) procedure and proposed use of QRS slopes for ischemia detection. According to the results of the study [31]: a) slopes changes during the procedure are mostly due to a widening of QRS or a decrease of its amplitude (and due to a reduction of HF content); b) the slopes outperform RMS of HF components (band 150-250 Hz) in terms of ischemic changes sensor (reflects the capacity of a parameter to detect the ischemic changes beyond background noise level [32]). However, Se, Sp and Acc of the detection were not addressed by authors. In other work, linear discriminant analysis of QRS slopes calculated from V2 and aVR provided the same results of ischemia detection as ST elevation criteria with poor Se = 24 % and high Sp = 93 % [33]. Thus, separate use of QRS slope information to detect ischemia is disputable; it can, nevertheless, be used as an adjunct to the conventional ST segment analysis.

Standard guidelines for assessment of myocardial condition are defined for only standard ECG and not available for VCG [34, 2]. Nevertheless, many new VCG descriptors have been proposed in recent studies for ischemia and myocardial infarction detection. In most cases, the new parameters allowed improving detection performance. Particularly, Treskes et al. proposed use of ST (at J point) and ventricular gradient (VG) difference vectors (relative to the reference) for detection of acute myocardial ischemia during PTCA (where ‘ischemic’ ECGs were selected after 3 minutes of balloon occlusion) and obtained similar or even higher Se and Sp of this method (ST difference vector: Se = 78.6 %, Sp = 96.5 %, VG difference vector: Se = 71.4 %, Sp = 89.3 %) as compared to standard ST criteria (Se = 70.2 %, Sp = 89.1 %) [35]. Correa et al. compared detection performance of seven QRS-loop parameters (volume, maximum vector magnitude, planar area, maximum distance between centroid and loop, angle between XY and optimum plane, perimeter, and area-perimeter ratio) with that of conventional ST-vector magnitude and found, that [36]: a) QRS-loop volume is the best among all parameters with Se = 64.5 % and Sp = 74.6 %; b) Se and Sp of ST-vector magnitude is 73.2 % and 73.9 %, respectively, c) combination of all QRS-loop and ST-vector parameters improves the performance resulting in Se = 88.5 % and Sp = 92.1 % (all results obtained by linear discriminant analysis). The same feature set (except for volume) combined with standard ST-change vector magnitude, QRS-vector difference and spatial ventricular gradient allowed reaching Se = 95.5 % and Sp = 95.2 % in data recorded during PTCA and minute-by-minute discriminant analysis [37].

In view of the above, still further enhancement of myocardial ischemia detection using ECG is possible by improvement of conventional approach or by development of new methods employing new descriptors and more advanced techniques for data analysis.

1.3 STUDY OF MYOCARDIAL ISCHEMIA USING RABBIT MODEL

Many various aspects of the development of heart disease, its diagnostics and treatment may be successfully investigated using animals. Among various species, rabbit is one of the most popular models used in studies of cardiovascular system [5]. The main advantages of small animal models such as mouse, rat, hamster, and guinea pig are: a) low cost, b) short time for disease progression and c) short gestation time. The main benefits of large animal models (such as dog and pig) are: a) the similarity of physical dimensions of the hart to that of human, which may be crucial for study of arrhythmogenic mechanisms; b) easy surgical and catheter-based interventions and cardiac mapping studies due to large size; c) sufficient assessment of human-scale interventions such as cardiac ablation, implantable cardiac defibrillator, etc. However, such studies are approx. 5 - 15 times more expensive than those on small animals. The studies on rabbits are much easier than studies on dogs or pigs. The rabbit heart has an intermediate size which is large enough to perform various surgical interventions (such as a coronary artery ligations, catheterization, etc.). Moreover, the cardiac physiology of rabbit is similar to that of human, namely: a) similar basic cardiac electrophysiological parameters [38]; b) the same repolarizing ionic currents in the ventricles influencing AP duration (delayed rectifier K^+ currents I_{Kr} and I_{Ks}) [39]; c) similar transport of Ca^{2+} [6]. The two last observations are especially relevant for the study of arrhythmias [40].

Isolated rabbit heart is used in a wide range of studies including biochemical, pathophysiologic, metabolic and pharmacological studies. One of the main areas is the study of ischemia-reperfusion injury and mechanisms of ischemic or pharmacological preconditioning [41]. Three *types of ischemia* can be induced in isolated heart: 1) by complete stopping of coronary flow (global ischemia), 2) by partially restricting coronary flow (low-flow ischemia), 3) by occluding a coronary artery (mostly the left anterior descending artery, LAD) (regional ischemia). The first and the third approaches are most widely used and each of them has both advantages and limits. In human, in most cases ischemia affects a specific region of the myocardium because of stenosis in a coronary artery. This situation can be simulated by animal model of regional ischemia, where the coronary flow is reduced by various ways, such as use of hydraulic occluder positioned around the coronary artery, intracoronary placement of a hollow plug attached to a catheter or other mechanical devices [3]. Significant benefits of above method is that they can be performed in open- and even closed-chest preparations *in situ* and may mimic ischemia of different degree: severe in case of complete occlusion and mild or moderate in case of reduction of coronary flow to some percentage of value at rest. In low-flow setup, however, the methods produce concentric stenoses which are not characteristic for human, where about 70 % of stenoses are eccentric. Eccentric stenoses can be induced by partial inflation of an intraluminal ballon, which is, however, difficult to perform due to movements of the ballon inside the artery resulting in variable of residual lumen geometry and consequently in non-stable severity of the obstruction [42]. The simplest (and the most frequently used) way to induce severe regional ischemia is complete cessation of a coronary flow by ligating of a coronary artery.

However, the anatomy of the heart coronary system should be taken into account in case of regional ischemia model. Regional ischemia cannot be easily induced in species with extent collateralisation (such as in guinea-pig or hamster and to a lesser extent in a dog), where the ligating one of the coronary arteries does not lead to infarct and even ischemia. In clinical studies, in patients with collateral circulation no changes were found in QRS during balloon angioplasty regardless the severity of ischemia [43]. In rabbit, mouse, pig, and rat, the collateral circulation is

limited, thus, these species can be sufficiently employed in regional ischemia studies. However, the significant intraspecies differences in anatomy of rabbit coronary system have been found previously [41],[44]: since the left coronary artery is always dominant, both bifurcation and trifurcation of the atria coronaria sinistra may be observed in the population. Thus, the reproducibility of experiments with regional ischemia in rabbit is quite low and strongly depends on the experience and knowledge of the investigator about the coronary arteries distribution.

Difficulties associated with the regional ischemia inducing can be avoided by using the global ischemia model. Global ischemia can be simply induced by stopping of the heart perfusion. In this case, the presence or absence of collateralisation is irrelevant; thus, highly reproducible results may be achieved. Generally, this model of ischemia mimics severe hypotension in patients or the situation, where the whole heart becomes ischemic during open-heart surgery with aortic-cross clamping [42]. Despite the fact that above phenomena are relatively rare, use of the heart model of global ischemia is of interest in heart surgery field and in ventricular fibrillation study. Since there are some important differences between the global ischemia model and human heart undergoing arrest for the surgery (particularly, method used for heart arresting – cold cardioplegia in human *vs* full stopping of perfusion in animal model, cold *vs* warm or cold ischemia in human and isolated heart, respectively, etc.), the use of isolated heart is only way to obtain valuable information about ischemia-reperfusion injury at the molecular and genomic level [45]. Rabbit isolated heart model is intensively used to study the evolution of arrhythmias and to test antiarrhythmic or proarrhythmic effects of available and new drug compounds [5],[46]. In cardiac arrhythmia studies, global ischemia is of interest especially due to its effects on the activation patterns of ventricular fibrillation [47]-[51]. One of the most critical factors affecting experimental results is the duration of ischemia. It should be determined taking into account the goal of the study: short-term ischemia leads to recoverable changes in myocardial function and does not negate the cardioprotective mechanisms, whereas 30-35 min of global ischemia results in infarction (about 40-50 % within the myocardium at risk) [41].

In all above investigation fields, the study of potential *preconditioning effect* of global ischemia is still topical. Ischemic preconditioning is defined as a delay and decrease of irreversible damage of cardiac tissue in response to ischemia after previous one or several short-term periods of reversible myocardial ischemia [52]. It can be easily examined in isolated heart model, where 3-10 minutes long global ischemia (or 3-5 ischemia-reperfusion repetitions) is frequently used as the preconditioning stimulus followed by the period of intermittent reperfusion and long-term (30 minutes or longer) test ischemia (global or regional) [53]-[57].

For *quantitative assessment of ischemia*, various electrophysiological variables and biochemical markers with prominent changes during ischemia can be used in experimental cardiology. Besides such advantages as the absence of neurohumoral regulation and possibility of fully controlled experimental conditions, isolated heart preparation provides good direct access to the epicardium, which makes it suitable for simultaneous monitoring of heart mechanical function and electrical activity under 'physiological' as well as pathological conditions. The most common electrophysiological records providing in experiments on isolated hearts are EG and monophasic AP (MAP). Cardiac electrical activity is usually measured using epicardial, endocardial or transmural electrodes attached to the tissue or inserted into the ventricular wall ([5],[53],[54],[58]) or by electrodes placed in the heart bath filled with the conductive physiological solution ([59]). More advanced – touch-less – techniques are based on recording of MAP using potentiometric voltage-sensitive dyes (VSDs) and corresponding optical devices [5],[49],[51],[58]-[63]. Different approaches can be applied simultaneously with aim to comprehensively investigate the

relationships between various physiological parameters, that is important in experiments focused on the study of effects of electrical stimuli or the drugs on heart electrical activity, the mechanisms of onset and evolution of serious cardiac arrhythmias (including the study of ventricle conduction velocity and pathways), etc. [3],[48],[64]-[67].

As in human, ECG/EG remains the most frequent tool used in experimental studies. However, to best of our knowledge, ECG criteria for detection of ischemia in animals are not available. Probably the only document summarizing some guidelines for ECG assessment of arrhythmias (such as ventricular premature beat VPB, atrioventricular (AV) block, etc.) associated with ischemia, infarction and reperfusion in animal studies is the Lambeth Conventions, which were recently updated [68]. According to the Conventions, qualitative assessment of severity of ischemia includes following indexes: visual inspection for cyanosis and dyskinetic regional wall motion; ST segment elevation and ST-T alternans; regional increasing of extracellular potassium and venous lactate concentration.

2 AIMS OF THE DOCTORAL THESIS

An electrophysiological study in the rabbit isolated heart is one of the basic tools in experimental cardiology, which particularly allows investigation of myocardial ischemia and other cardiac disorders. However, there are still many arguable aspects (methodological, technical, etc.) in this area, which are worthy of attention. Therefore, dissertation is mainly focused on the investigation of some factors which may affect various phases of animal study and on the summarizing of corresponding suggestions with aim to improve reliability of experimental data, analysis results and their interpretation. Particular main tasks addressed in this work can be formulated as follows:

1. to describe patterns of EG recorded in rabbit isolated heart under normal conditions (i.e. fully perfused heart without drug administration – control group);
2. to quantify the response of the heart to short-term repeated perfusion stopping (so called global ischemia) by means of various parameters derived from EGs and VCG and to determine the most appropriate placement of electrodes for monitoring ischemia-induced alterations in recorded electrograms;
3. to assess possible effects of increased LV mass on cardiac electrical activity under non-ischemic and ischemic conditions (including describing manifestations of increased LV in recorded data, developing the method for increased LV mass detection and quantifying ischemia-induced changes by means of EG and VCG parameters);
4. to validate the suitability of the voltage-sensitive dye di-4-ANEPPS administration in experiments with rabbit isolated heart (including assessment of possible electrophysiological effects of the dye on the heart under non-ischemic and ischemic conditions by analysis of recorded data);
5. to develop the tools for automatic detection of myocardial ischemia and to assess possible effects of above experimental conditions (changed LV mass or dye administration) on detection accuracy (including evaluating discrimination ability of EG and VCG parameters and selecting the most reliable of them for further classification, implementing single- and multi-feature approaches based on simple human-like decision rules as well as more advanced supervised techniques and testing them on real data from control group, hearts with increased LV mass and hearts stained with the dye, evaluating the effect of definition of ischemia beginning in preparation and the effect of parameters calculation method – using or without outcomes of manual EG delineation – on classification performance).

3 EXPERIMENTS WITH RABBIT ISOLATED HEARTS: OVERVIEW OF EXPERIMENTAL SETUP AND DATA ACQUISITION AND ANALYSIS

In this chapter, general information about experimental protocols and data recording and analysis are provided. Particular methodological aspects and results of data analysis are addressed in more detail in corresponding parts of the next chapters. Electrograms of rabbit isolated heart recorded in the framework of the thesis are the part of database of animal electrocardiographic signals available at the Department of Biomedical Engineering, BUT [69].

3.1 EXPERIMENTAL PROTOCOLS

The experiments on adult New Zealand rabbits were carried out in collaboration with research team from Physiology Department of Faculty of Medicine (Masaryk University, Brno) in accordance with the guidelines for animal treatment approved by local authorities and conformed to the EU law. The animals underwent general anesthesia with i.m. injection of xylazin and ketamin. Each animal was weighted before surgical intervention. To prevent ischemia during heart preparation, trachea was cannulated and the animal was artificially ventilated (ventilator for small laboratory animals, World Precision Instruments, USA). The heart was then rapidly excised, placed in the bath, filled with Krebs-Henseleit (K-H) solution (1.25 mM Ca^{2+}, 37° C), and retrogradely perfused with the solution according to Langendorff in the mode of constant perfusion pressure 85 mmHg and temperature 37° C. Perfusion pressure and temperature of perfusion solution as well as of the solution in the bath are checked during the whole experiment.

Three types of experimental protocol (Fig. 3) were chosen to study possible effects of different phenomena, such as global ischemia, increase of LV mass, and administration of voltage-sensitive dye di-4-ANEPPS (including co-incidence of ischemia and one of last two factors), on electrical activity of the rabbit isolated heart.

The first type of experiments (Fig. 3a) was aimed to describe the main patterns of EG under normal condition, to study of effects of short global ischemia and reperfusion on electrical activity of the heart, and to investigate the possibilities of using the orthogonal lead system in such experiment. The protocol included stabilization, ischemia, and reperfusion. During last 10 min of stabilization, the heart was rotated around its longitudinal axes (ro1). The change of the heart orientation was also performed in ischemia and reperfusion (ro2 and ro3, respectively) except the first 1-1.5 min of ischemia, where the artefact (periodic changes in EG magnitude) caused with the forced beating of the heart frequently occurred in EG. The forced movement of the heart relative to the electrodes is probably associated with the changes of some factors, such as temperature, amount of perfusate in the heart chamber, etc. The artefact distorts recorded EGs and in some cases even makes them unusable for further analysis. During preparation, the part of aorta connected to the cannula was kept as short as possible to avoid or at least to reduce this problem.

In *the second type* of experiments (Fig. 3b), the changes of electrical function caused with increased LV mass were studied under non-ischemic and ischemic conditions. Besides stabilization and three ischemia-reperfusion repetitions, the protocol included two periods with the heart rotation (similar to the previous protocol) and collection of perfusate samples (coronary effluent) in different periods of the experiment for further biochemical analysis (p1, p2, and p3 in Fig. 3b).

Last experiments (Fig. 3c) were focused on the study of possible effects of VSD di-4-ANEPPS on electrical function of the heart. Two different protocols – with and without VSD administration – were used to compare data obtained in both cases. The first one included 9

periods: stabilization, dye loading and washout, and three ischemia-reperfusion repetitions (Fig. 3c, top). More detailed information about this type of experiments can be found in next chapter and in [59]. In the second one, loading and washout were excluded from the experimental protocol and stabilization period was prolonged for 30-40 min (Fig. 3c, bottom). Thus, in both types of experiments, the parts before the first ischemia were of the same duration.

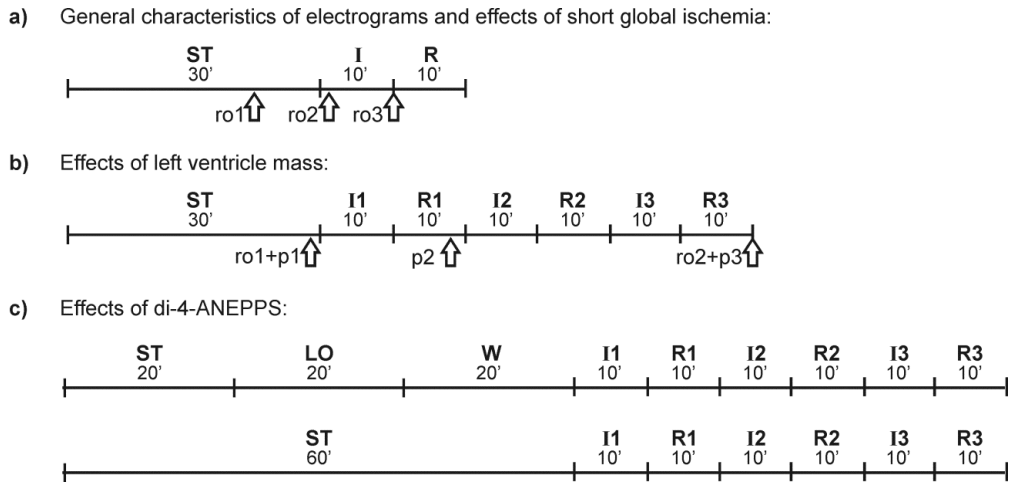

Figure 3. Experimental protocols.
Global ischemia in hearts rotated around its longitudinal axis during the whole experiment (arrows depict the beginning of the first rotation session in each experimental period) (a), repeated global ischemia in hearts rotated around its longitudinal axis in stabilization period and at the end of experiment including collection of perfusate samples (only one rotation session is performed in experimental periods) (b), repeated global ischemia in hearts loaded with voltage-sensitive dye di-4-ANEPPS (top) or without dye administration (bottom) (c). ST – stabilization, LO – loading with the dye, W – washout, I – ischemia, R – reperfusion, ro – rotation of the heart, p – perfusate collection.

3.2 ELECTROGRAM RECORDING

During whole experiments carried out according to the protocols from Fig. 3, EGs were recorded by three pairs of Ag-AgCl disc electrodes placed orthogonally on the inner surface of the bath filled with conductive K-H solution. In the third type of experimental protocol (Fig. 3c, top), MAP was also recorded from the local area of the LV surface with the optical technique based on the VSD di-4-ANEPPS. Thus, both EGs and MAP were recorded by touch-less methods, which do not lead to mechanical disturbance of myocardial tissue. The rest of the thesis will be focused on the analysis of EGs only. More information about MAP recording and analysis can be found in [59] or [69]. Recorded EGs were amplified by bioamplifiers DAM-50 (World Precision Instruments, Inc.), simultaneously digitized by 16-bit AD converters with sampling rate of 2 kHz with the LabView card PCI-6250 (National Instruments, USA), and stored on PC.

At the beginning of the experiments, the hearts were oriented relative to the electrodes in the same way, which is shown in left and middle parts of Fig. 4. The initial orientation of the heart is similar to its physiological orientation in the chest. In this case, horizontal leads (lead I and lead II) "look" at the middle part of LV and boundary region of LV, respectively (Fig. 4, middle). On view top of the heart, the placement of optical probe for MAP recording according to the first protocol is also shown for information.

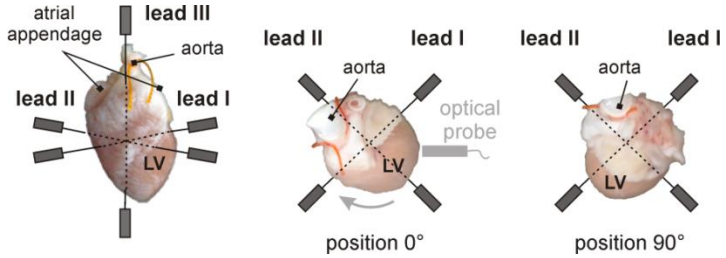

Figure 4. Orthogonal system of electrodes.
Front (left part of the figure) and top (middle and right part of the figure) views. Lead III is not shown on the top views. Direction of heart rotation is depicted with light grey arrow in the middle part of the figure. LV – left ventricle.

The changes in heart orientation relative to the electrodes included in some protocols was performed as the rotation of the heart around its longitudinal axis from initial position 0° to 90° in 10° steps, where position 0° corresponds to initial heart position in recording system (anterior wall facing forward, see Fig. 4, middle). The direction of the rotation is depicted with light grey arrow on top view of the heart in Fig. 4. The orientation of the heart at the end of rotation session is shown in right part of Fig. 4. Rotation of the heart in this way allows to record data from whole LV region (see next chapter for details). Each rotation session lasted approx. 1-1.5 min. Thus, EG recorded in each heart position was of approx. 5-8 s long (depending on actual heart rate). In case of protocol from Fig. 3b, the heart was rotated additionally from 0° to 30° at the end of each rotation session to verify whether some morphological changes appeared in EG during the rotation session (i.e. by comparing them with the EG from the beginning of rotation). If the rotation was repeated continuously during the whole experiment (protocol from Fig. 3a), EG from the beginning of each rotation session was compared with that from the beginning of the previous one to test the stability of EG morphology (see next paragraph).

3.3 DATA PROCESSING AND ANALYSIS

3.3.1 PROCESSING OF ELECTROGRAMS RECORDED DURING FIXED HEART ORIENTATION

The processing of EGs recorded in the hearts in initial position (signals from all types of experiments excluding the segments recorded during heart rotation) is schematically shown in Fig. 5. EGs recorded with different leads were processed separately except QRS complexes detection and P-QRS-T segments delineation.

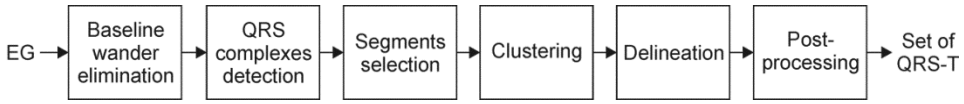

Figure 5. Flowchart of electrogram processing and analysis (fixed orientation of the heart).

Baseline wander elimination

The first step of EG processing is elimination of low-frequency baseline wander which complicates analysis of some signals. In clinical practise, the distortion of ST segment level and amplitudes of R and T wave may lead to false negative or positive detections of ischemia and infarction. Despite the absence of respiration which is the main reason of baseline wander in clinical ECG, the low frequency noise is often presented in isolated heart data recorded by lead III.

It is generally caused with the motion of the heart in chamber filled with K-H solution. Different methods of baseline wander elimination in EGs were tested, such as polynomial fitting and spline interpolation approaches, zero-phase (bidirectional) FIR filtering with different window types, and zero-phase Lynn's filter [70],[71]. The cut-off frequency was set to 0.5 Hz. This cut-off value is high enough to eliminate low-power wander without the distortion of important parts of EG such as ST segment and T wave. The best results were obtained using the latter approach combined with the padding of EG with flipped, reflected copy (mirror padding) of its beginning and ending parts (see Fig. 6). In this case, there was no phase distortion, time delay, and start-up and ending transients in the filtered signal.

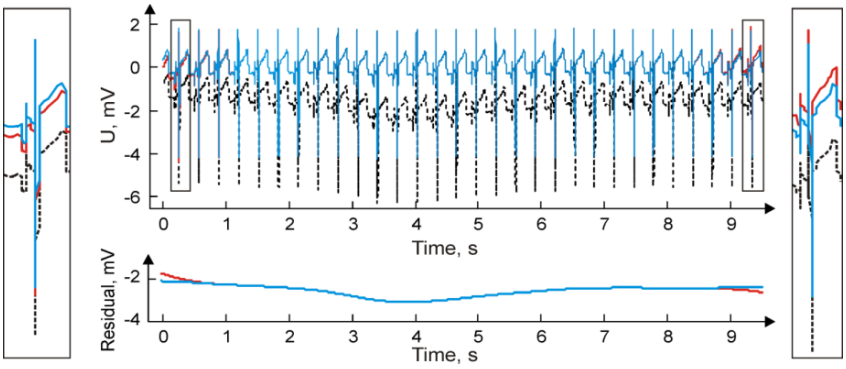

Figure 6. Baseline wander elimination in electrogram.
Zero-phase Lynn's filter with cut-off frequency of 0.5 Hz. Top: initial electrogram recorded with lead III (dashed black), filtered electrogram obtained without (red) and with (blue) padding the signal with mirror reflections of its beginning and ending part. Bottom: residuals after filtering with the first (red) and second (blue) approach. Left and right: the first and the last P-QRS-T segments, respectively.

QRS complexes detection

QRS complexes (so called fiducial points) were detected in filtered signals with the detector based on the wavelet transform adapted to EGs recorded in rabbits [72]. Before the detection, EGs were divided into particular parts according to the experimental periods because of the large differences in their morphology which may negatively affect the detection. Moreover, EGs recorded in ischemic periods are characterized with turning of the signal, i.e. with the changes of QRS complex or/and T wave polarity. Generally, these changes appear in the first half of the period and are accompanied by progressive increase and/or decrease of signal magnitude, which is especially prominent in lead II EG (see Fig. 7). This phenomenon causes the detection failure in more than 50% of records. QRS detection was also complicated in data from ischemic periods of some earliest experiments with VSD administration (2005-2006) due to discontinuities in lead III EG lasting about several minutes (recording interruptions caused by specific of lead system design).

In view of the above, single-lead detection approach usually based on lead I EG was chosen despite the availability of three simultaneously recorded EGs. In presence of misdetections caused with EG polarity change, signal from lead III was used instead. In case of insufficient quality of lead III EG, signal from lead I or lead II was used, but the detection was performed in non-overlapped 1 min long segments (chosen empirically; short enough for high detection accuracy) of the signal with further aggregating of particularly detection outputs.

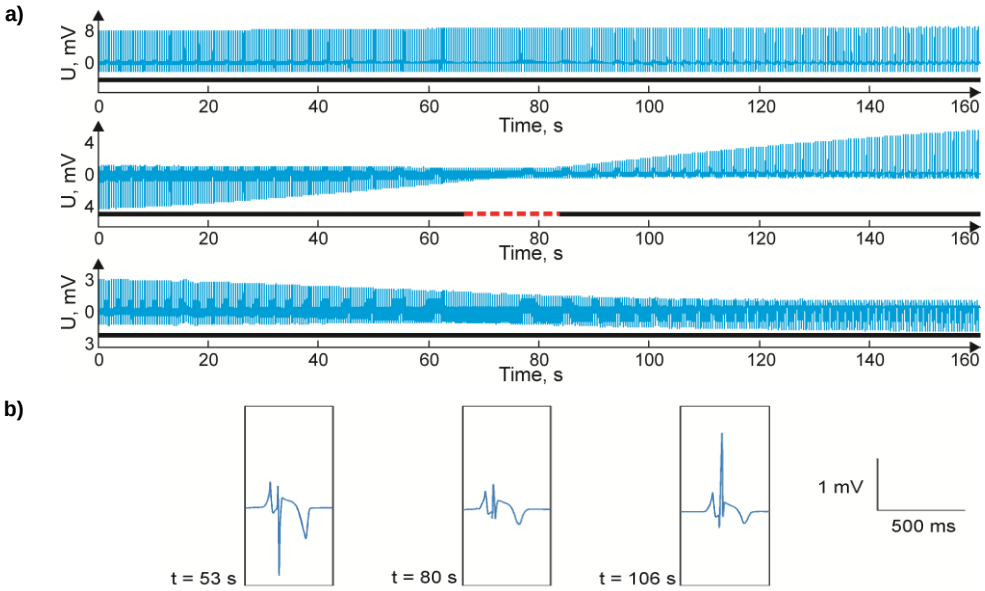

Figure 7. QRS complexes detection in electrograms from the first half of ischemic period. Electrograms from lead I, lead II, and lead III (top, middle, and bottom, respectively); successful detection and misdetections are depicted with black and dashed red line, respectively (a). Example of corresponding segments selected from lead II electrogram at different time moments (b).

Additional correction was then performed to unify the results of detection among whole data set: the index of detected QRS complex was shifted to maximal deviation (i.e. peak of Q or R wave dependent on morphology of the complex) of corresponding complex in EG recorded with lead I. The maximal deviation of QRS was found within the window of length 50-60 ms (50-60 samples before and after index of the detected QRS). All results were then verified and corrected manually. Mis- and over-detections were found mainly in data from ischemic period due to the presence of VPBs and AV blocks of second or even third degree.

Selection and clustering of P-QRS-T segments

The fiducial points of QRS were used to select the P-QRS-T segments as 150 samples before and 700 samples after the points with resulting length of the segments 851 samples (or approx. 426 ms). Manual delineation of the data from 2 h long experiment is very time-consuming. Automatic delineation is challenge task itself and is beyond the scope of the dissertation. Therefore, data clustering was performed to divide them into the groups with similar morphological characteristics, such as QRS beginning and QT interval length. Different clustering approaches such as non-hierarchical k-means method [73], self-organizing map [74]-[75] and hierarchical agglomerative unweighted average distance (UPGMA using Euclidean distance) [75] combined with gap statistics and silhouette value evaluation (both used for determination an optimal number of clusters, [75],[76]) were tested. Samples of P-QRS-T segments were used as an input to clustering algorithms. Surprisingly, the best results were obtained using the simplest method – UPGMA – with number of clusters empirically set at 40 for each experimental period data. The setting the number of clusters was also confirmed by high value of mean silhouette that reached 0.74-1 (represents appropriate choice of clusters' number [75]). Other clustering algorithms, such as k-means and self-organizing maps are not based on simple pairwise comparison of particular objects (or clusters), which results in combining segments with a rather different morphology into the same cluster. It was found that the optimization of cluster number by gap statistics is time consuming and

not effective, especially if data are not well separated such as in case of EG continuously changing during ischemia and the beginning of reperfusion.

As a result, the segments were combined into the groups mainly based on the similarity of QRS complexes morphology (the most prominent part of the whole P-QRS-T). It, nevertheless, was insufficient, if the changes of ST-T segment appeared even in the absence of those in QRS (see cluster c2 calculated for data recorded during reperfusion in Fig. 8). To obtain data proper for T wave end detection, additional clustering was applied to such the groups with number of clusters chosen individually for each case (usually 5-10). As shown in Fig. 6, P-QRS-T segments concluded in resulting clusters can be successfully delineated. The most prominent changes usually appear in EG at the first half of ischemia and at the beginning of reperfusion. It is evident from Fig. 8, that the segments from these parts of experiment (clusters c1 and c2) are divided into smaller clusters as compared with the rest of data (clusters c40).

Presented procedure allows reducing of time required for data delineation in several times (300-400 clusters instead of 8000-10000 segments for each experiment). Since each 10 minutes long ischemic period is represented by an average of 50 clusters (up to 80 in some case), time courses of parameters calculated from the segments are smooth enough to analyse ischemia-induced changes accurately.

Other benefit of clustering approach is easy detection of the segments with significant artefacts, pathological segments (such as VPBs), misdetections of QRS, etc. These phenomena are clearly visible on the courses of P-QRS-T belonging to the same cluster. In most cases, such the segments are involved into the separate clusters and can be easily excluded from the analysis by removing these clusters.

Delineation and post-processing of EG segments

Beginning of P (only in some experiments, see below) and Q wave, J point (the end of QRS complex), and the end of T wave were manually detected from QRS-T segments clusters, considering data from all three EG leads (dashed grey lines in Fig. 8). In particular, the Q beginning was detected in lead in which Q wave was presented as earliest (usually in EG from lead I or lead II). On the other hand, T wave end was detected in EG with the longest QT interval (usually in EG from lead III). The most difficult task is to establish the position of J point, especially at the end of ischemic periods, where elevated ST-T interval merges with R wave. In most cases, the EG from lead III is very helpful for J point detection because the changes in morphology of this signal (mainly in ST-T part) are not so prominent. Delineation was performed by author of thesis after consultation with the experts with multiyear experience on analysis of ECG/EG of small animals from University of Veterinary and Pharmaceutical Sciences Brno and Physiology Department of Masaryk University, Brno.

Modified version of software for manual delineation and annotation of ECG/EG was used to delineate the QRS-T segments [77]. Initial version of the software allows performing beat-per-beat analysis of data. This software was modified to enable the analysis of EG groups EG (results of data clustering) one by one.

The new software version allows manual indicating the particular points in EG segments (delineation), denoting the group of EG segments as unsuitable for analysis (for example, due to impulse artefact of high magnitude), providing manual annotation of EG (detection of various types of rhythm and beat), saving the results on PC and updating annotations made earlier. The main window of the software with an example of EG delineation is shown in Fig. 9. The segments labelled during delineation as ‘unclassifiable beats’ due to presence of some significant artefact

were excluded from the data set. The results of clusters' delineation (i.e. indexes of three or four detected points) were arranged according to the initial order of the segments within the groups representing particular experimental periods.

Before calculation of various parameters, the segment baseline was shifted exactly to the zero level with respect to detected beginning of QRS complex. Example of such a correction is shown in Fig. 10. The PQ deviation in some initial segments remained after baseline wander elimination could dramatically affect the values of important morphological characteristics of EG such as magnitude of R wave and T wave and level of ST segment. Particularly, total deviation of ST segment level in non-corrected EG could probably be considered as ST elevation due to ischemia.

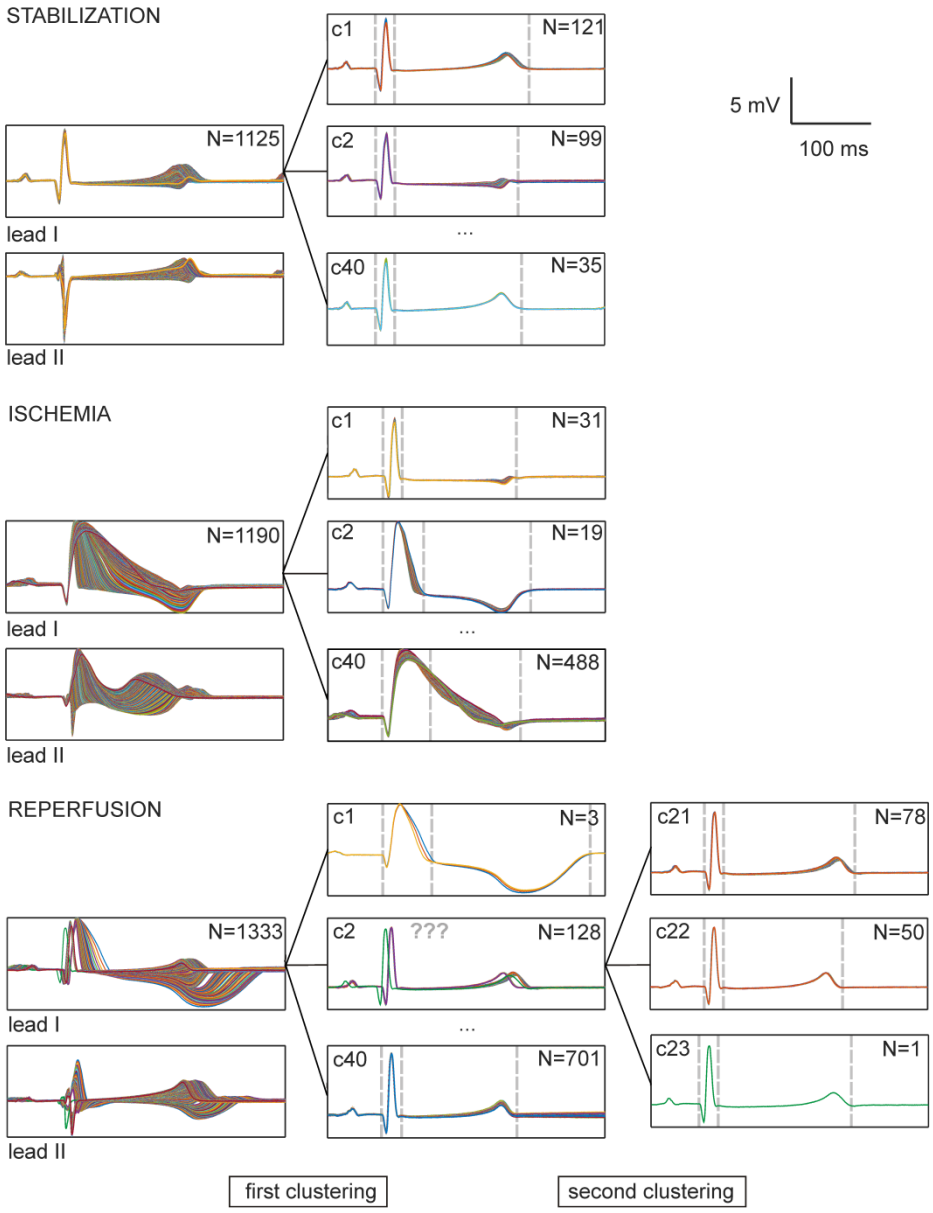

Figure 8. Example of two-level clustering of electrograms from one experiment.
N – number of P-QRS-T segments in initial group or cluster. Segments from lead III are not shown.

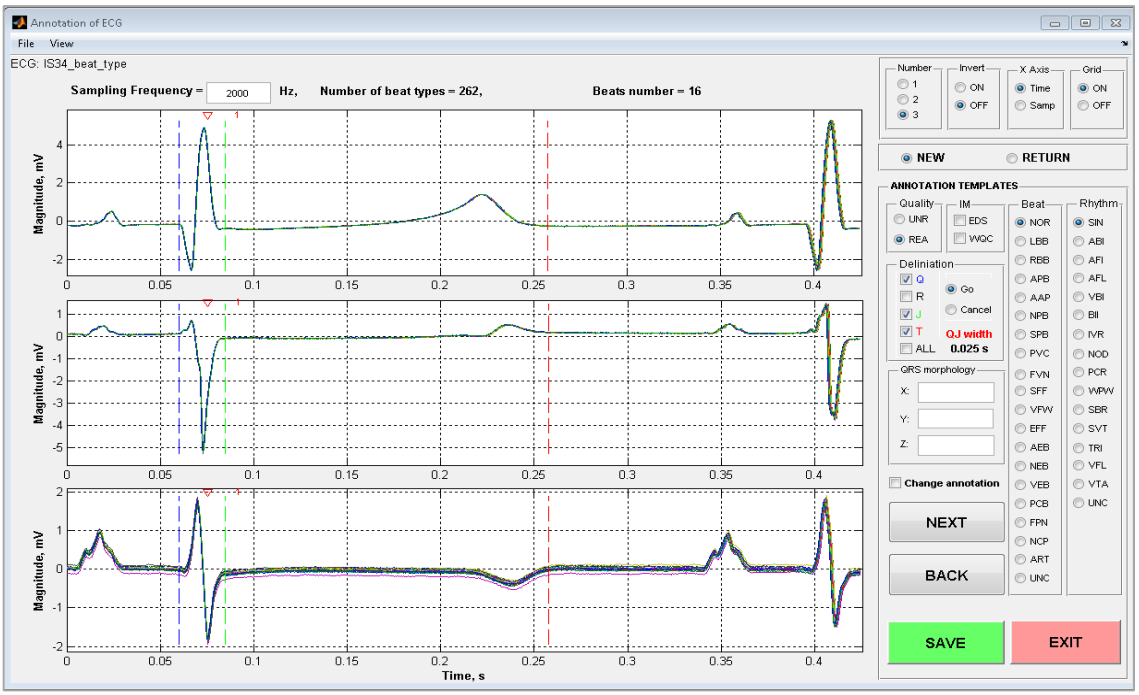

Figure 9. The main window of software for delineation and annotation of electrocardiographic data. Blue, green and red dashed lines indicate the beginning of Q wave, J point, and the end of T wave detected with the user in electrograms cluster. Here, the cluster includes 16 segments from rabbit isolated heart electrogram recorded during stabilization period.

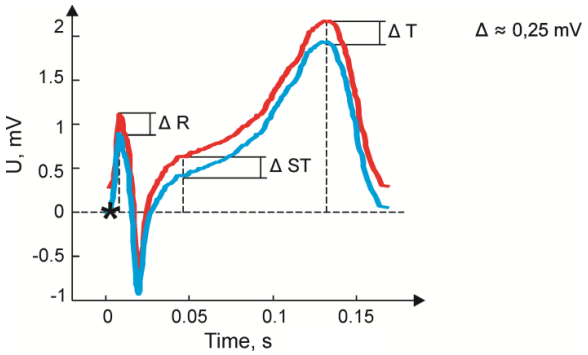

Figure 10. Example of QRS-T baseline correction.
QT part of lead II electrogram before (red) and after (blue) correction according to the beginning of QRS complex (black asterisk). Δ – difference in magnitude between the segment before and after correction.

3.3.2 PROCESSING OF ELECTROGRAMS RECORDED DURING HEART ROTATION

The processing of EG recorded in the rotated heart (corresponding parts of the first and the second experimental sessions in Fig. 3) is schematically shown in Fig. 11.

Figure 11. Flowchart of electrogram processing in case of data from rotated heart.

Baseline wander elimination and QRS complexes detection

Baseline wander elimination and QRS complexes detection were performed with the same way such as in previous case. The parts corresponding with the particular heart position were then selected from EGs. Each part included 8-20 segments depending on experimental period (in ischemia, the duration of fixed heart position was as short as possible due to rapid change of EG morphology) and actual heart rate.

Segments selection and averaging

QRS-T segments of 560 samples (or 280 ms) length were selected from EG parts based on the indexes of detected QRS complexes as 59 samples before and 500 samples after detected fiducial points. The first and the last segments were excluded from further analysis because of their morphology distortion due to transition effect during the change of heart orientation.

Each heart position was finally represented with group of QRS-T segments or the averaged QRS-T segment calculated generally from 10-15 segments from the middle of corresponding part of EG. Only highly correlated segments (Spearman's ρ higher than 0.95, for a few groups more than 0.99) were included in averaging procedure. Thus, the segments distorted by movement artefact mentioned above were excluded from the analysis.

It should be noted, that the stability of EG morphology within rotation session was verified by correlation analysis of the segments from the beginning (range 0° - 30°) of adjacent rotation sessions (see previous paragraph). According to the results, signal morphology was prominently changed only during rotation sessions performed in ischemic periods, especially in their middle part.

Segments delineation and post-processing

Delineation and post-processing of EG segments were then performed in the same way such as in previous case. Clustering of data was not required in this case. Thus, initial groups of highly correlated segments or averaged segments representing particular heart position were delineated individually.

Segments reconstruction

The rotation sequence described above is sufficient for reconstruction of EG in the range from -90° to 90° corresponding with the whole LV region using data recorded with horizontal leads during rotation of the heart within the range 0° - 90°. The reconstruction was performed according to Fig. 12. Each lead position from scheme in this figure was finally represented with the averaged QRS-T segment. Heart orientation changes did not affect EG from lead III. Correlation coefficient for QRS-T segments from this lead recorded for different heart orientations was more than 0.99. Therefore, all available segments from this lead were taken into account to define averaged one which was used to represent the positions in the range from -90° to -10°.

Indexes of fiducial points and delineation results were reconstructed besides the EG segments. Data from five rotation sessions performed during ischemia and reperfusion (experimental protocol from Fig. 3a) are available for analysis. These sessions are denoted as i1-i5 and r1-r5 for ischemia and reperfusion, respectively (see next chapter).

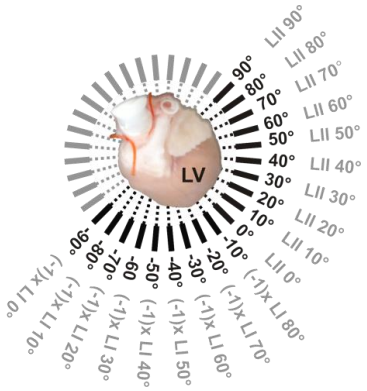

Figure 12. Scheme of EG reconstruction.
Reconstruction in the range from −90° to +90° (black font) using data recorded with two horizontal bipolar leads during the heart rotation from 0° to 90° (grey font). Opposite electrodes of the bipolar leads are depicted with grey boxes. Top view of the heart; LV – left ventricle; L – lead.

3.3.3 CALCULATION OF ELECTROGRAM PARAMETERS

Full list of EG and VCG parameters used for analysis of the heart electrical activity under different conditions can be found in Appendix A. Three main groups of parameters – namely, those representing interval and voltage characteristics of EGs, parameters based on areas under different parts of EGs and VCG-based parameters – were calculated in the study. The main reasons of including particular parameters in the study were: a) simple computation without the need of full EG delineation (such as detection of onset and offset of particular QRS peaks, beginning of T wave, etc.); b) use in similar experiments with the same and/or different species or in clinical praxes for comparative analysis; c) easy interpretation of parameters values obtained under different conditions.

Parameters calculated using delineation outcomes

1. The group is composed of *interval* and *voltage based* parameters which represent widespread used time intervals and maximal deviations calculated between the onset and the offset of particular identified EG patterns, respectively. The parameters are illustrated in Fig. 13a. Note, that ST20 was chosen empirically as an alternative to ST60 used in human ECG analysis, considering the differences in characteristics (mainly QT and ST-T duration) of human ECG and EG of rabbit isolated heart.

2. QRS-T segments were also represented by area under their particular parts, which is not usual approach. The *area under curve* (AUC) was calculated using trapezoidal method for evenly spaced points that approximates numerical integration procedure over the interval of interest defined using EG delineation results (such as the beginning and the end of QRS complex, etc.) or intermediate outcomes (such as position of maximal deviation of ST-T) as [78]:

$$AUC = \int_a^b f(x)dx \approx \frac{h}{2}\sum_{n=1}^{N}\left(f(x_n) + f(x_{n+1})\right) = \frac{h}{2}\sum_{n=1}^{N}\left(f(x_1) + 2f(x_2) + \cdots + 2f(x_N) + f(x_{N+1})\right), \quad (1)$$

where $f(x_n)$ are particular samples of EG within the interval [a, b] of length N+1; h=(b–a)/N is the space between consecutive samples.

Area below and above the x-axes gives negative and positive results, respectively. In case of pattern consisted of negative and positive parts with the same magnitudes, corresponding AUC may reach zero value (see Fig. 13b, left). To avoid this, modified AUC calculated *from absolute values of QRS-T* were used, too (see Fig. 13b, right). Additionally, the modification by dividing AUC of particular patterns by AUC calculated from the whole QRS-T or QRS (*relative AUC based parameters*) was performed to evaluate the pattern's fraction in the whole analysed segment.

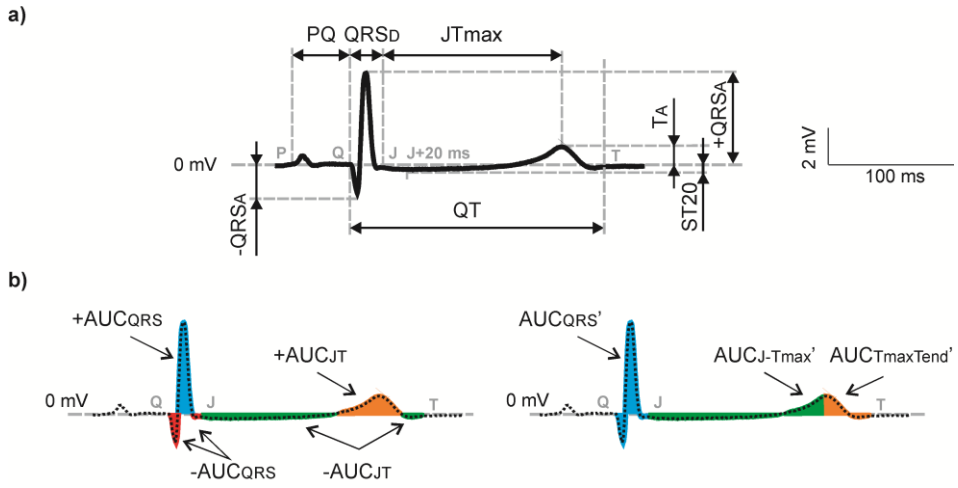

Figure 13. Illustration of interval and voltage based parameters.
Interval and magnitude parameters (a) and parameters based on areas under various parts of QRS-T (b). Electrogram from the end of stabilization period is shown.

3. Finally, VCG related parameters were calculated. In Fig. 14, conventional VCG [79] derived from experimental data is shown. The vertical axis (Y) stretching from top to down corresponds to lead III axis. For a rotating heart, axes extending from left to right (X) and from front to back (Z) were represented by EG recorded in positions -40° and 40° (Fig. 12), respectively. In protocols with fixed heart position, EG from lead I and lead II (Fig. 4, left and middle) were used as Z and X leads, respectively. In this case, XYZ coordinate system is rotated clockwise by approx. 45° relative to conventional one (Fig. 15). As a result, the parameters calculated from VCG reconstructed by two approaches are quite different (see below). Nevertheless, it can be acceptable given the experimental context of the study. Moreover, ischemia induced changes in such data are as much prominent as in case of conventional approach (see next chapter). Example of such VCG is shown in Fig. 17, left.

   As first, QRS and ST-T parts of EG loops were analysed individually using parameters representing maximal QRS and ST-T spatial vector magnitude and angles in frontal, horizontal and sagittal planes (α, β and γ, respectively). *Maximal spatial vector magnitude* was calculated from QRS loop as:

$$\mathrm{Lqrs} = \max_{i \in n} \|\mathbf{V}\mathrm{qrs}_I\|, \|\mathbf{V}\mathrm{qrs}_i\| = \sqrt{x_i^2 + y_i^2 + z_i^2}, n = \overline{1, N}, \quad (2)$$

where N is the number of point forming the loop. Similarly, L_{jt} was derived from ST-T loop. *Angles in three planes* were calculated between main vector (vector that gives maximal magnitude) and corresponding positively oriented axis according to Fig. 14.

3D perimeters and areas of 2D QRS and ST-T loops (in three planes) were then calculated to evaluate the shape of the loops. *3D perimeter* was estimated as:

$$P = \sum_{i=1}^{N-1} \sqrt{(x_{i+1} - x_i)^2 + (y_{i+1} - y_i)^2 + (z_{i+1} - z_i)^2}. \quad (3)$$

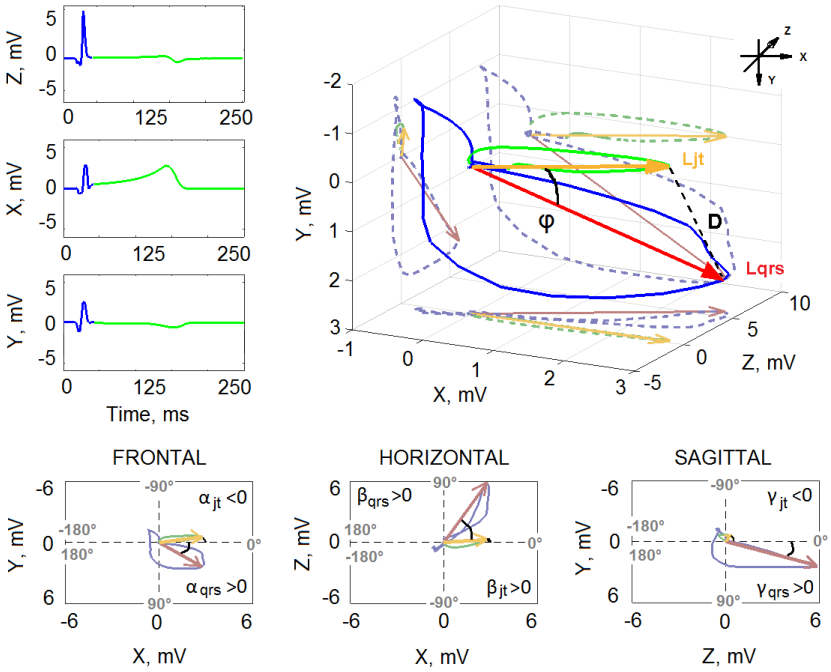

Figure 14. Illustration of VCG based parameters.
Conventional orthogonal leads (left), corresponding VCG (right) and three orthogonal planes (bottom) with parameters denoted. Data from the end of stabilization period are shown.

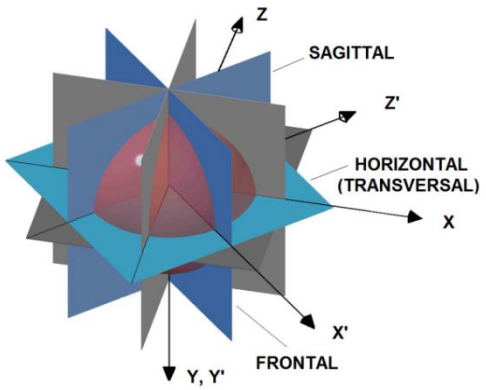

Figure 15. Coordinate systems used for VCG reconstruction.
XYZ (grey planes) and X'Y'Z' (coloured planes) are commonly used and shifted system, respectively.

Loop's areas calculation is rather difficult task due to the loops' values properties: a) the samples sequences forming the loops are not always strictly monotonic; b) in most cases, the

loops are self-intersecting, therefore particular parts of the same loop are traversed in a clockwise and counter clockwise sequences; c) data are scattered (i.e. values are not evenly distributed through the loop). These properties limit the use of simple method for calculation the area of irregular closed polygon made up of line segments between N vertices (x_i, y_i) [80]:

$$Axy = \frac{1}{2}\sum_{i=0}^{N-1}(x_i y_{i+1} - x_{i+1} y_i), \tag{4}$$

where the last vertex (x_N, y_N) is assumed to be the same as first. Above formula yields successful results in case of closed loops with simple boundary and fails otherwise, where there are various intersections and changes of the direction present in the loop, which is common for QRS loops from both stabilization and ischemia periods (see below).

Use of usual (linear, cubic or spline) interpolation methods is also complicated because of non-monotonic, scattered character of data. Therefore, the natural neighbour based method was applied to perform interpolation of data on a regular grid and calculate loops' areas from the projections of interpolated surface on particular planes. Briefly, this method is based on Voronoi tessellation constructed for initial discreet set with and without points where the interpolation have to be performed. Then values of added points may be estimated as the weighted sum of initial points. The weights are derived as the ratios of cell volumes from the Voronoi diagram calculated with added points to those from initial diagram. Only initial points about the point to be interpolated (so called natural neighbours) are taken into account. [80]

As a result, three surfaces $\mathbf{X}' = f(\mathbf{y}', \mathbf{z}')$, $\mathbf{Y}' = f(\mathbf{x}', \mathbf{z}')$ and $\mathbf{Z}' = f(\mathbf{x}', \mathbf{y}')$ were interpolated on equidistantly distributed samples $\mathbf{x}'$, $\mathbf{y}'$ and $\mathbf{z}'$ (pairs of them define so called grids of size $sp \times sp$) using scattered points involved in the QRS and ST-T loops with final distance between samples within the grid:

$$\Delta v = \frac{|V_{max} - V_{min}|}{sp - 1}, \tag{5}$$

where V_{max} and V_{min} is maximal and minimal value of corresponding initial data (X, Y or Z).

Then the areas of 2D loops were estimated considering the projections of all surfaces on corresponding planes. For all projections, values falling outside the initial data domain are not numerically defined (extrapolation were not performed), what is represented by 'NaN' value (not-a-number) in case of realization in MATLAB environment. It allows easy selecting the only samples from interpolated surface belonging to the projection. For two projections from three it is valid that their samples are equidistantly distributed in one dimension and are scattered in the other. For the third projection, the samples are distributed evenly in two-dimensional space (e.g. they form a grid). In first two cases, the area of the projection can be estimated as follows:

$$A_{proj} = \sum_{i=1}^{sp-1} \Delta h_i \Delta v, \tag{6}$$

where Δh_i is the length of i^{th} 1D slice of the projection:

$$\Delta h_i = \left|Proj^i_{max} - Proj^I_{min}\right|, \; i = \overline{1, sp-1}. \tag{7}$$

In last case, the area can be easily estimated by calculating the number of rectangles included in the projection:

$$A^{*}_{proj} = (N_{proj} - 2sp + 1)\Delta v_1 \Delta v_2, \tag{8}$$

where N_{proj} is the number of numerically defined samples (vertexes of the surfaces) in the projection, Δv_1, Δv_2 is the distance between the samples equidistantly distributed in two directions, respectively. Finally, the minimal area from three available for each plane was considered as the best estimation.

Different values of grid size were tested. Using sparse grid (sp of 50-70) leads to underestimation of loop area due to insufficient interpolation of the surface. Highly sampled grid (sp > 100) negatively affects the computational speed. Therefore, sp = 80 was used in the thesis as a compromise. Calculation of QRS loop area in sagittal plane is illustrated in Fig. 16. It is evident that the area of analysed QRS loop can be accurately estimated using the projection of interpolated Z′ surface (Z′zy). Use of Eq. 4 was insufficient in this case (calculated loop area 0.68 mV^2). For an example from Fig. 17, QRS loop areas in frontal, horizontal and sagittal planes calculated using Eq. 4 were similar to those obtained by proposed method (3.78 mV^2, 4.66 mV^2 and 7.63 mV^2, respectively).

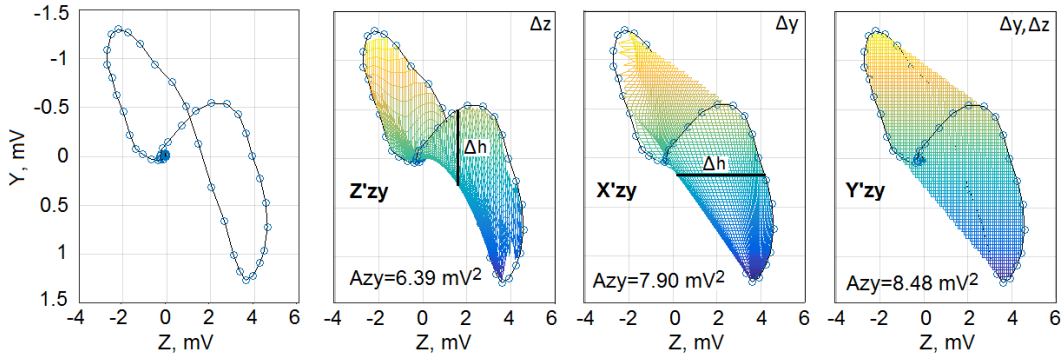

Figure 16. Illustration of 2D QRS loop area calculation.
QRS loop in sagittal plane (left); projections of surfaces Z', X' and Y' estimated via natural neighbour interpolation method on sagittal plane (right). Azy – loop area; Δ indicates equidistant distribution of projection values in corresponding dimension. Data from the end of stabilization period are shown.

VCG centroid based parameters were additionally proposed to evaluate the relationship between 'mean' and main electrical vectors. Uneven distribution of data within the loop resulted in inaccurate estimation of centroid coordinates as arithmetic means of loop samples, even if QRS and ST-T were selected according to the delineation results (Fig. 17).

Therefore, centroid coordinates **C** = [C_x; C_y; C_z] were estimated as mean values of corresponding surfaces X', Y' and Z' interpolated on evenly sampled grids. Then the angle and distance between main (QRS or ST-T) vector **V**xz = [V_x; V_z] and centroid vector **C**xz = [C_x; C_z] in horizontal plane are:

$$\varphi^{c}xz = \cos^{-1}\left(\frac{\mathbf{V}xz \cdot \mathbf{C}xz}{\|\mathbf{V}xz\|\|\mathbf{C}xz\|}\right), \tag{9}$$

$$D^{c}xz = \sqrt{(V_X - C_X)^2 + (V_Z - C_Z)^2}. \tag{10}$$

Parameters in other two planes were calculated in the same way.

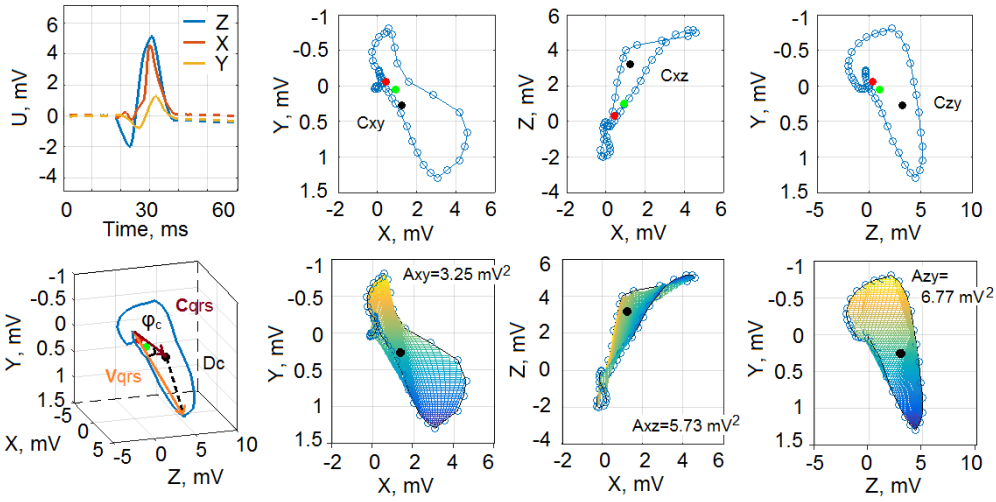

Figure 17. Illustration of QRS loops based parameters.
QRS complexes selected using (solid) and without (dashed) delineation outcomes (top left); corresponding orthogonal planes (right) and VCG (bottom left) calculated from lead I and lead II electrograms (shifted XYZ coordinate system) with parameters denoted. Green, red and black dots represent centroid derived from QRS loop (end of stabilization period) selected using and without delineation outcomes and interpolated loop surface, respectively (see text for more details).

Besides the parameters used for evaluation of depolarization and repolarization processes individually, two additional parameters – *the angle and the distance between main QRS and ST-T vectors* (see Fig. 14) – have been proposed to approximate the relationship between them:

$$\varphi = \cos^{-1}\left(\frac{\mathbf{V}\mathrm{qrs}\cdot\mathbf{V}\mathrm{jt}}{\|\mathbf{V}\mathrm{qrs}\|\|\mathbf{V}\mathrm{jt}\|}\right), \tag{11}$$

$$D = \sqrt{(\mathrm{Vqrs_X} - \mathrm{Vjt_X})^2 + (\mathrm{Vqrs_Y} - \mathrm{Vjt_Y})^2 + (\mathrm{Vqrs_Z} - \mathrm{Vjt_Z})^2}, \tag{12}$$

where **V**qrs = [$\mathrm{Vqrs_X}$; $\mathrm{Vqrs_Y}$; $\mathrm{Vqrs_Z}$]) and **V**jt = [$\mathrm{Vjt_X}$; $\mathrm{Vjt_Y}$; $\mathrm{Vjt_Z}$] are the main QRS and ST-T vector, respectively.

Interval and voltage based paraemtes proved in different studies to be suitable for ischemia detection (see last chapter). AUC based parameters are mainly used for classification of different types of arrhythmia (e.g. $\mathrm{AUC_{QRST}}$, $\mathrm{AUC_{QRS}}$, $+\mathrm{AUC_{QRS}}$, and $-\mathrm{AUC_{QRS}}$ [81]-[83]) and only rarely for ischemia detection (area between QRS offset and T-peak [84], ST area [85]-[86]). VCG parameters can also be found in both applications (2D QRS loop maximal vector and angle and 3D QRS loop parameters, such as maximum vector magnitude, volume, planar area, maximum distance between centroid and loop, angle between XY and optimim plane, perimeter, and area-perimeter ratio [36],[81],[87]). Such as in case of various arrhythmias, the morphology of experimental EG varies grately during progressing ischemia. Therefore, good discrimination ability of the parameters extensively used for arrhythmia classification may be expected in case of ischemia detection, too. The potential benefit of newly proposed parameters based on absolute and relative AUC values as well as VCG based descriptors might be in more detailed description of EG and VCG patterns and, consequently, higher capacity to indicate less and more pronounced changes caused by some pathologies.

Parameters not dependent on QRS-T delineation

All above EG parameters excepting interval characteristics can be calculated without delineation results. Regions for calculation of particular parameters ('artificial EG patterns') without use of delineation outcomes can be then chosen based on analysis of RR, QT and QRS_D calculated at the end of stabilization and ischemia (where the maximal deviation of parameters as compared to their control values is expected) from all available experiments (see Fig. 18). Inside band, top and bottom of boxes indicate median, 25^{th} and 75^{th} percentiles, respectively (valid for all boxplots presented in the thesis). The segments were finally selected from EGs as 59 and 500 samples before and after detected fiducial point, respectively. It results in 'artificial' QRS_D of approx. 60 ms (59 and 60 samples before and after fiducial point, respectively) and QT of approx. 280 ms. This has a minimal impact in case of AUC based parameters from stabilization period, where boundary parts of like-QRS or ST-T patterns usually lie on x-axes and, thus, do not affect resulting AUC value. On the contrary, poor match of boundaries with true onsets and offsets of patterns may lead to parameters distortion. Considering true RR and QT values, beginning of subsequent beat may appear at the end of artificial segments from stabilization period. On the other hand, the end of T wave may be missing in artificial data from ischemia. This may negatively affect parameters and their further analysis, too (see next chapter).

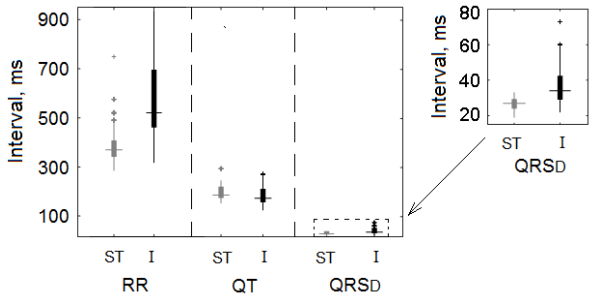

Figure 18. Main interval characteristics of electrograms.
Calculated from ten QRS-T at the end of stabilization (ST) and ischemia (I) for each experiment (n = 28).

Note that P wave was only analysed in experiments with di-4-ANEPPS administration (see next chapter). All computations and analysis were performed using Matlab R2014b (The MathWorks, Inc., USA).

4 ELECTRICAL ACTIVITY OF THE HEART UNDER NORMAL AND PATHOLOGICAL CONDITIONS

4.1 GENERAL CHARACTERISTICS OF ELECTROGRAM UNDER NORMAL AND ISCHEMIC CONDITIONS

The chapter is focused on quantitative and qualitative description of EG recorded in rabbit isolated hearts under non-ischemic conditions and characterization of the changes in EG caused by global ischemia (in absence of additional factors, such as changes in LV mass or effects of chemical agents). Some results were presented in the international conferences [88]-[90].

4.1.1 BACKGROUND

Interpretation of ECG is based on the describing of its main interval and amplitude characteristics which represent repolarization and depolarization processes in the heart. The characteristics of particular parts of ECG (such as polarity and shape of the waves and interweaves intervals) can vary based upon gender, activity, age, and used recording leads [91]. Many heart diseases are manifested in ECG, which makes the electrocardiography widespread powerful diagnostics tool.

As was mentioned above, electrocardiographic diagnostics of myocardial ischemia in human is mainly based on assessment of ST segment deviation (elevation or depression). Three grades of ischemia can be distinguished in ECG from leads facing the ischemic zone shortly after occlusion of a coronary artery [43],[92]: 1) tall, symmetrical and peaked T wave in at least two contiguous leads (grade I ischemia); 2) ST elevation without changes in QRS (grade II ischemia); 3) changes in the terminal portion of QRS complex, such as an increase of R wave amplitude and disappearance of S wave (grade III ischemia). The transient changes of QRS can be explained by [43],[93]: 1) ischemia of the conducting system; 2) prolongation of the electrical conduction in the Purkinje fibres in the ischemic region; 3) passive shift of the QRS deflections resulting from shift of the ST and TP segments. Transient changes associated with QRS duration prolongation or increase of Q wave amplitude may be observed during acute ischemic episode. These observations are not as frequent as above manifestations, but may allow achieving even greater sensitivity and specificity of ischemia detection than in case of ST segment criteria only and seem to be correlated with extent of ischemia [21],[92]. Among other ECG manifestations of ischemia during exercise test are a shortening QTc (i.e. QT interval corrected for heart rate) interval and shifting the mean QRS axis in frontal plane to the right. However, prolonged or non-changed QTc and leftward axis shift (in patients with narrowing of the LAD coronary artery) in presence of ischemia have also been reported [21]. Thus, it can be concluded that the diagnostics of the earliest phase of ischemia is traditionally based on the detection of repolarization changes in ECG (i.e. in ST segment and T wave), whereas the pronounced changes in ventricular depolarization (namely QRS complex morphology) are mainly associated with the onset of necrotic process.

The main electrophysiological characteristics of rabbit are very similar to those of human. Particularly, like in human ECG, there is a well distinguished isoelectric ST segment between QRS complex and T wave in rabbit ECG. It makes rabbit suitable for myocardial ischemia studies. Unlike human electrocardiography, there are no standardized guidelines to assess morphology of ECG/EG in animals (including rabbit), especially under pathological conditions. It is the most probably due to the high interspecies as well as intraspecies differences in anatomy of coronary

artery (and especially of collateral circulation) and conduction systems and, last but not least, in used methods for the recording of electrical activity (including such aspects as electrodes type and size and their placement). Furthermore, in case of recordings on isolated hearts, such factors as temperature, pressure, perfusion solution composition, and distance between the heart surface and recording electrodes may affect the heart function or/and morphology of recorded EG. Therefore, the describing of ECG/EG recorded in animal under normal or pathological conditions is rather difficult task, which can be solved by only comprehensive study covering all above aspects.

In this chapter, the results of data analysis for experiments on rabbit isolated hearts under non-ischemic and ischemic conditions (without additional factors, such as changed LV mass or effects of the chemical compounds) will be presented. The main aim of this part consists in the qualitative and quantitative description of rabbit EG under normal conditions and characterization of specific changes in its patterns caused by global ischemia including time and spatial distribution aspects. The quantitative description of EG morphology can be realized using specific parameters calculated from signal segments. The changes in heart electrical activity caused by ischemia are then reflected on the values of particular parameters and can be analysed using appropriate techniques. Based on the result of such analysis, some practical recommendations associated with the number and placement of recording leads (providing the highest quality of the signal and the most information about ischemic injury in preparation), distinguishable phases of ischemia and parameters suitable for ischemia (or particular degrees of ischemia) assessment can be defined.

4.1.2 METHODS

Data acquisition

The isolated hearts of sixteen New Zealand rabbits (both sexes, weight 2.26 ± 0.8 kg) were included in the study. Five and eleven experiments were carried out according to the protocols from Fig. 3a and Fig. 3c (bottom), respectively. As was mentioned above, the first protocol allows recording of EG from different areas of LV using only two orthogonal bipolar leads due to the rotation of the heart about its longitudinal axis during recording, when the electrodes are fixed in the same position. However, the cardiac electrical activity cannot be monitored continuously in this case. On the contrary, in second protocol, EGs are recorded from the heart which is fixedly placed relative to the electrodes. As a result, continuous EGs can be recorded during the whole experiment, which is required for detailed evaluation of ischemia-induced changes.

EG and VCG parameters calculation

Various morphological parameters (n = 32) were calculated from QRS-T selected from both types of EG. In the first case, they represented electrical activity of the heart in each recording position. In the second one, morphology of EGs recorded from the middle (lead II) and boundary region (lead I) of LV was analysed. In both cases, VCG parameters (n = 30) and those joint for all leads (RR, QT_D and QRS_D, n = 3) were also calculated. EGs recorded during rotation, where one horizontal lead represented the positions -90° to 90° (Fig. 12) and the second one was placed orthogonally, were used to reconstruct VCG. Horizontal leads' positions -40° and 40° and corresponding vertical lead III approximated the standard orthogonal electrode system (XYZ). In the second type of experiments, VCG was reconstructed from EGs recorded in initial position (Fig. 4, left and middle).

Data analysis

Firstly, correlation analysis was applied on different parts of EG (the whole QRS-T, QRS and ST-T) recorded in the first type of experiments. Spearman's rank correlation coefficients (Spearman's rho, ρ) were shown as 2D maps to evaluate the relationship between EGs: a) recorded in different positions within each rotation session; b) recorded during different rotation sessions (i.e. in different time moments of experimental periods) in a certain position. Secondly, each morphological parameter calculated from EG in different positions was analysed visually by 2D map constructed from: a) parameter values; b) differences between parameter values calculated for particular rotation session and stabilization (Δ); c) differences between parameter values calculated from adjacent rotation sessions (DIFF); d) differences between parameter values calculated from adjacent recording positions (DIFFpos). Finally, analysis of receiver operating characteristics (ROC) curve was performed to assess: a) the overall ability of particular parameters to distinguish among different phases of ischemia (i.e. different rotation sessions within ischemic period); b) the ability of different positions (i.e. recording leads) to provide EG suitable for ischemia detection. Namely, area under ROC curve (AUCROC) was calculated and analysed. AUCROC of 0.5-0.6 and 0.9-1 represents poor and excellent discrimination accuracy of the method, respectively [94].

Data from the second type of experiments were analysed statistically in more detail. According to the result of Shapiro-Wilk test (recommended for analysis of small data sets [95]), EG and VCG parameters are not normally distributed. Therefore, non-parametric methods were chosen for statistical data analysis. To compare the overall changes in each parameter at the end of particular ischemic (and reperfusion) periods relative to its level in stabilization (i.e. to compare changes induced by different ischemic periods), Friedman test for repeated measurement accompanied by Tukey-Kramer post-hoc test (e.g. [96]) was applied to the delta values defined as follows:

$$\Delta = p_E - p_S, \tag{13}$$

where p_E and p_S is averaged value of the parameter calculated from 20 last samples at the end of particular period (ischemic or reperfusion) and at the end of stabilization, respectively.

General trend of ischemia or reperfusion induced changes during the whole experiment was studied using the slope calculated from the line fitted through the normalized parameter's Δ. The standard scaling procedure to the range <0, 1> was applied to obtain the comparable ranges of slopes derived for different parameters:

$$\Delta_n = \frac{\Delta - \Delta_{min}}{\Delta_{max} - \Delta_{min}}, \tag{14}$$

where Δ_{max} and Δ_{min} are maximal and minimal value of Δ through three ischemic or reperfusion periods. Significance of slope values (comparing to the zero) was then verified by one-sample signed-rank test.

As in previous data set, ROC analysis was used to evaluate the discrimination ability of EG and VCG parameters. Besides AUCROC, sensitivity (Se), specificity (Sp) and optimal cut-off value of each parameter were estimated [94].

Finally, Mann-Whitney U-test (e.g. [96]) was applied to compare the parameters calculated using and without delineation outcomes.

For all abovementioned tests, $p < 0.05$ was considered as significant.

4.1.3 RESULTS

Electrogram recorded from different LV areas under normal conditions

Initial and averaged QRS-T segments from data recorded during stabilization period are shown in Fig. 19. The segments in range from -90° to approx. +60° have RS type of QRS complex with progressively decreasing S deviation. It changes at +60°, where RS type is replaced with QR with almost equal deviations of Q and R peaks. QR type of complex with increasing R deviation is characteristic for EG in range from +70° to +90°. In the whole range, the deviation of T wave changes from its maximal negative to maximal positive value. The latter is reached at approx. 0°. T wave at approx. -60° is mostly flat or biphasic.

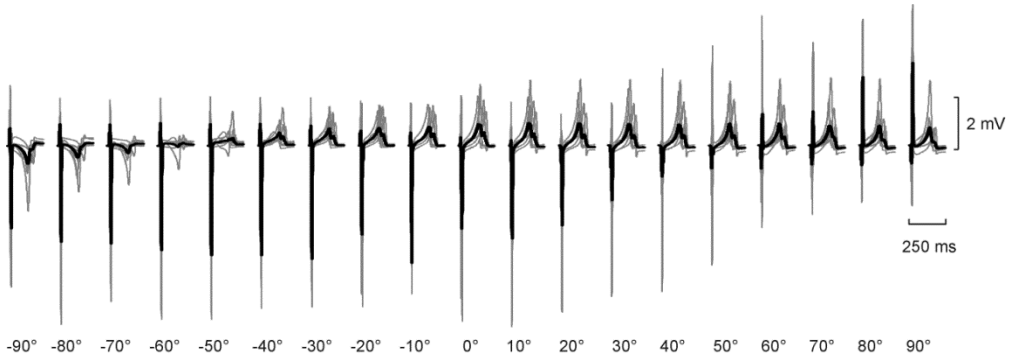

Figure 19. Example of QRS-T segments recorded during stabilization period.
Selected from electrograms in the positions from -90° to +90°; initial (grey) and averaged (black).

Above relation between recording position and the shape of obtained EG curve can be demonstrated using ρ map (Fig. 20) or distribution of morphological parameters values (Fig. 21) calculated from time-course of different part of EG. The change of QRS and ST-T polarity is represented with the change of ρ from positive to negative values at approx. +30° and -60°, respectively. The correlation map calculated from the whole QRS-T represents mainly the correlation between ST-T parts (compare left and right part in Fig. 20). Also the changes in QRS complex are reflected on +/-AUC_{QRS}. From Fig. 21a, this parameter reaches the positive values at +30° position. Boxplots for AUC_{JT} (Fig. 21b) it is evident that the parameter has the negative and positive value in range <-90°, -70°> and <-40°, +90°>, respectively, whereas it is close to zero at -60°. It corresponds to negative, positive and biphasic (or flat) T wave, respectively.

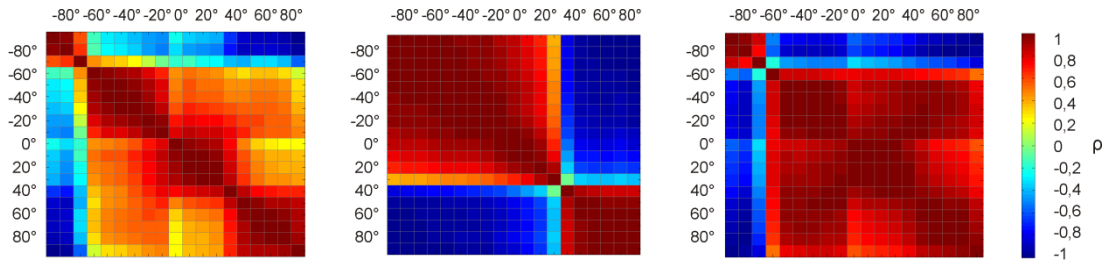

Figure 20. Correlation maps (Spearman's ρ) for data recorded in range from -90° to +90°.
QRS-T, QRS and ST-T (left, middle and right, respectively) from one experiment.

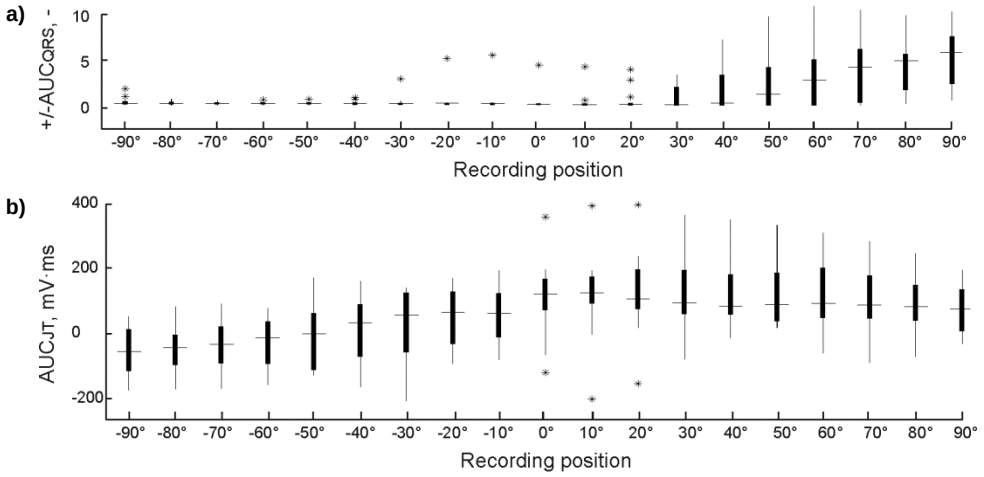

Figure 21. Distribution of +/-AUC_{QRS} (a) and AUC_{JT} (b) in stabilization period.

Electrogram recorded from different LV areas under ischemic conditions

Data from particular rotation sessions were analysed separately. Totally, five rotation sessions were performed during ischemia (i1-i5) and reperfusion (r1-r5). Reconstructed data represent heart electrical activity in approx. 2nd, 3rd, 5th, 7th, and 9th minute of ischemia (Table 1).

Table 1. Beginning of particular rotation sessions (i1-i5 and r1-r5) regarding the beginning of ischemic (I) and reperfusion (R) period.

I	**Session**	**i1**	**i2**	**i3**	**i4**	**i5**
	Mean±SD, min	1,61±0,10	3,24±0,26	4,84±0,38	6,86±0,39	8,51±0,53
R	**Session**	**r1**	**r2**	**r3**	**r4**	**r5**
	Mean±SD, min	0,20±0,13	2,25±0,40	4,04±0,45	5,87±0,51	8,48±0,61

An example of QRS-T in particular time moments of ischemia and reperfusion within the whole range of recording positions can be found in Appendix B. In Fig. 22, QRS-Ts are shown in selected positions only. As can be seen from the figures, the earliest changes (in i1-i2) are evident in QRS-T recorded from the middle of LV (where QRS changes its polarity), whereas the only slight widening of QRS can be found in EGs from LV boundary. From the middle of ischemia (i3 and later sessions), the changes are prominent in the whole recording range. All prominent changes are reversible and disappear during the first half of reperfusion.

Spearman's ρ maps for stabilization and the first, the middle and the last rotation session during ischemia (i1, i3 and i5, respectively) and reperfusion (r1, r3 and r5, respectively) calculated from one experiment (corresponds with that shown in Fig. 22) are shown in Fig. 23. At the beginning of ischemia (i1), there is a decrease of ρ in the whole map. From the second to the last rotation session, there are two characteristic types of QRS-T: with negative polarity of main patterns (in <-90°, -30°>) and positive deviation at other positions (see Fig. 22 and Appendix B). In late phase of ischemia, QRS is overlapped with ST-T interval; thus, all QRS-T belonging to the same type ('negative' or 'positive' one) are very similar to each other. It reflects in the maps, where two clearly separated regions with high positive and negative ρ can be distinguished. At the beginning of reperfusion (r1), there is a negative QRS in the range <-80°, -10°>, positive one in <+50°,+90°> and the transition QRS (not consistent, predominantly RS type) in <0°,+40°>. ST-T in this time moment is positive within the ranges <-80°,-20°> and <+70°, +90°> and negative in -90° and <-10°, +60°>. In the maps, high ρ (both positive and negative) is present in corresponding

areas. Since r2 (not shown), the maps are very similar to that of stabilization because of return of QRS-T morphology to initial one.

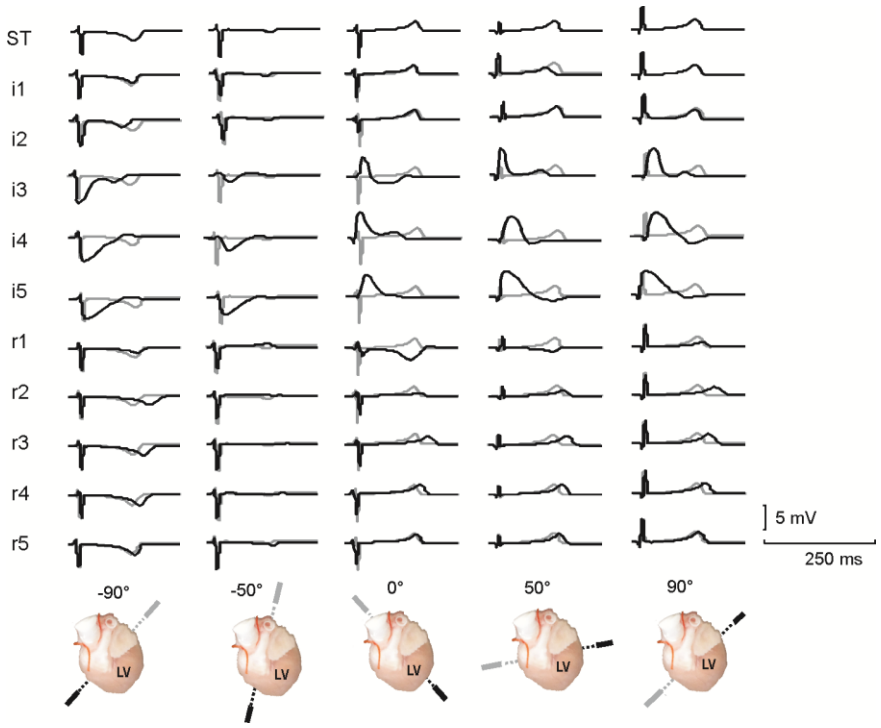

Figure 22. QRS-T (from one experiment) in selected recording positions for different rotation sessions. Top views of the heart illustrate the position of recording bipolar lead. ST – stabilization (corresponding QRS-T are depicted with grey otherwise); i, r – rotation session in ischemia and reperfusion, respectively.

For maps from Fig. 24, ρ between stabilization and other sessions were calculated. In i1, the decrease of ρ is characteristic for QRS correlation map. In ST-T map, low ρ appears in i2 only. Generally, ρ is low for both QRS and ST-T in the whole recording range during ischemia. Negative ρ around 0° and low positive ρ in boundary region of QRS map correspond to change of polarity and widening of QRS, respectively. In reperfusion, the return of ST-T morphology to initial one is faster in comparison with QRS morphology, where ρ reaches maximal positive values in the whole recording range in fourth rotation session only. ρ of all maps is maximal at the end of reperfusion. The correlation maps calculated from data of other experiments (not shown here) have very similar character.

Above changes in EG shape are reflected on the *values of morphological parameters*. For two-thirds of parameters (such as AUC_{QRST}, $+AUC_{JT}R'$, $+AUC_{QRS}$, etc.) the characteristic differences in their values between different recording positions remain almost the same during ischemia and reperfusion (see Fig. 25, top). In the rest (such as in ST20, AUC_{QRST}', AUC_{JT}', $-AUC_{JT}$, etc.), parameters calculated in various positions during stabilization are of similar value and differences between them appear during ischemia only (as in Fig. 25, bottom). In case of $+AUC_{JT}R'$, the parameter value increases by changing the recording position from -90° to +90°. This trend remains the same throughout the whole experiment. As for ST20, the position-related differences are present in ischemia only and they disappear to the end of reperfusion.

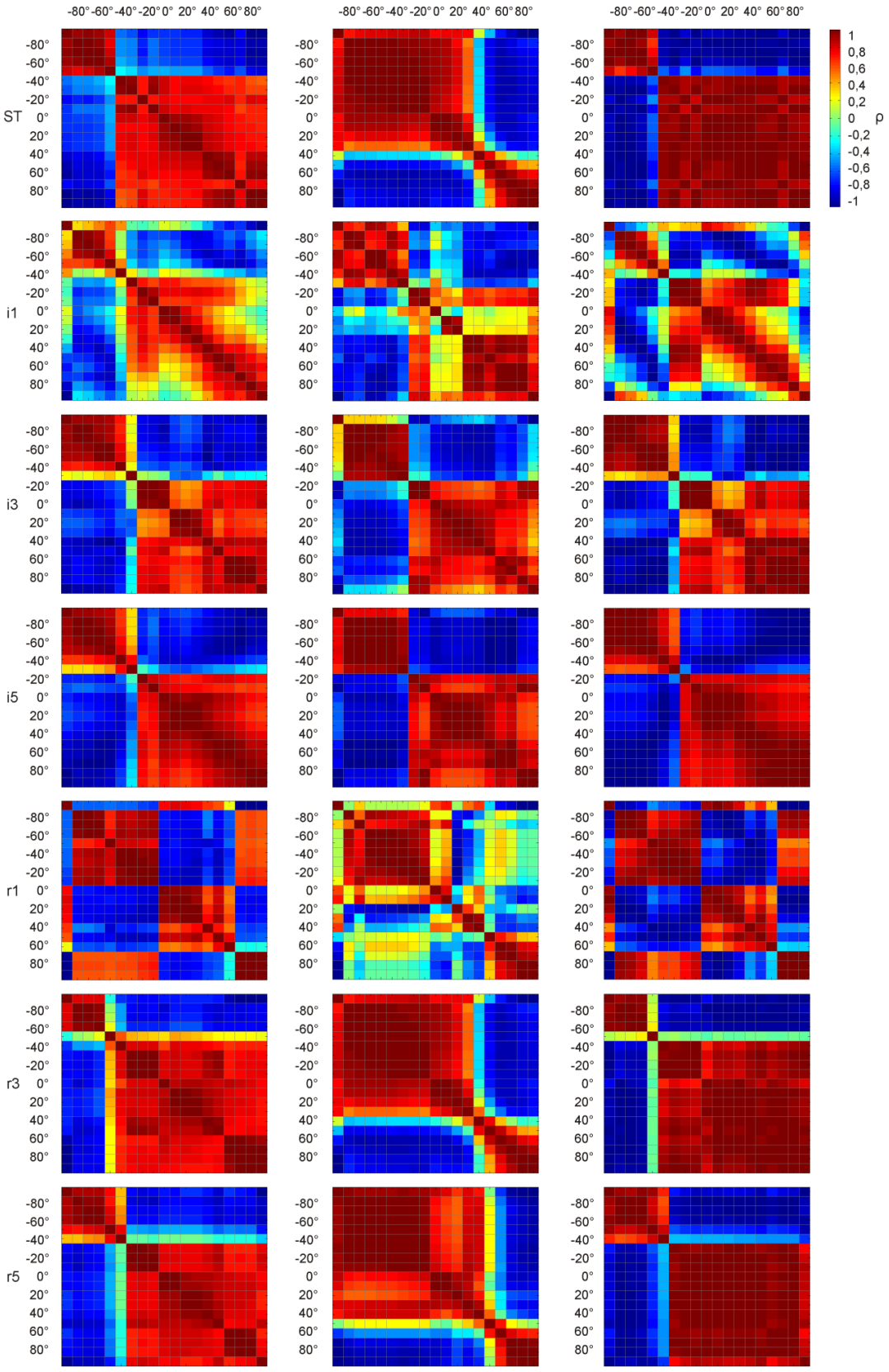

Figure 23. Correlation maps (Spearman's ρ) from data during various experimental periods. Calculated from QRS-T (left), QRS (middle), and ST-T (right) in different recording positions (-90° to +90°) (data from one experiment). ST – stabilization; i, r – rotation session in ischemia and reperfusion, respectively.

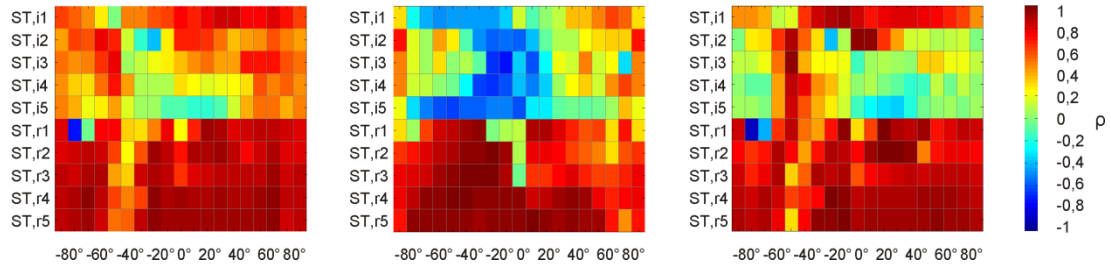

Figure 24. Correlation maps (Spearman's ρ) between data from stabilization and other rotation sessions. QRS-T (left), QRS (middle) and ST-T (right) in various recording positions (-90° to +90°) during one experiment. ST – stabilization; i, r – rotation session in ischemia and reperfusion, respectively.

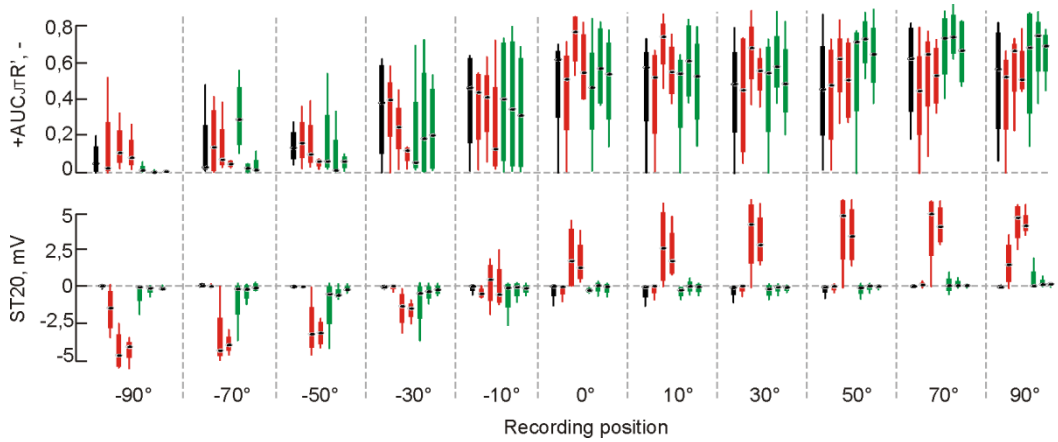

Figure 25. Boxplots of +AUC_{JT}R' and ST20 in different experimental periods and recording positions. Black, red and green boxes for stabilization, ischemia, and reperfusion, respectively. For ischemia and reperfusion, only data from the first, middle and last rotation session are shown.

All the parameters with evident changes during ischemia can be divided into two general groups. Parameters from the first one are increased after perfusion stopping. This groups is more frequent and includes for example ST20, QRS_D, QRS_A, T_A, AUC_{QRST}, AUC_{QRS}, $AUC_{TmaxTend}$', and +AUC_{QRS}Rq'. The second type of parameters is characterized by the decreasing trend in ischemia. It consists of JTmax, AUC_{JTmax}R', -AUC_{QRS}R' and other.

In some parameters (such as ST20, AUC_{QRST}, etc.), the prominent ischemia induced changes are present in the boundary region (<+80°, +90°>) only. On the contrary, in QRS_A, AUC_{JTmax}, +AUC_{QRS}R', etc.), ischemic changes are evident in middle of LV (around 0°) only. In some cases (such as +AUC_{JT}R', +AUC_{JT}R', AUC_{JT}R', and AUC_{QRS}R'), there are no prominent ischemic changes in any recording positions. Moreover, the changes do not occur in +QRS_A, -QRS_A, AUC_{QRST}, +AUC_{JT}, AUC_{QRST}', AUC_{QRS}', and +AUC_{QRS}Rq' calculated within the range <-70°, -10°>.

All ischemia induced changes are reversible regardless of the recording position. Moreover, in most parameters, return to the control values (i.e. the values in stabilization period) is complete immediately at the beginning of reperfusion (r1).

Above information can be demonstrated using map view of the parameter values calculated in various positions during different rotation sessions (i.e. different time of experiment). Such the maps for T_A, ST20, -AUC_{QRS}R', and –AUC_{QRS}Rq' are shown on left part of Fig. 26. Additionally, Δ, DIFF and DIFFpos were also illustrated as maps (middle and right parts of Fig. 26). It is evident that the earliest ischemic changes of T_A and ST20 appear in boundary region. In other positions, the

changes are time delayed (compare values of the parameters from these regions shown in the middle parts of the figure). It is also clear, that the return of T_A to stabilization level is slower comparing with ST20. In contrast to T_A and ST20, -AUC_{QRS}R' is characterized with almost constant values within region <+40°, +90°> during the whole experiment, whereas in other positions, ischemia caused the decrease of this parameter. –AUC_{QRS}Rq' calculated from the QRS samples only seems to be more sensitive to ischemia effects than –AUC_{QRS}R' which is depend on the shape of the whole QRS-T. From the right part of Fig. 26, the most prominent differences in each parameter were found between positions within the range <-30°, -20°> in ischemia. These changes correspond with the alterations of QRS-T morphology, mainly the change of QRS and ST-T polarity and magnitude.

Evaluation of the parameter ability to distinguish between EG recorded during stabilization and different rotation sessions during ischemia (i1-i5) can be performed using ROC curves, when AUCROC is considered as an index of discrimination. The overall discrimination ability of the parameter can be represented as the mean value calculated from AUCROC through all recording positions. Such values in particular time moments of ischemia are shown in Fig. 27. In case of the i1, none of the parameters has good discrimination ability (i.e. AUCROC in this time moment does not reach 0.8). Some of them have a fair, poor or even fail ability (area under ROC curve is in range 0.7-0.8, 0.6-0.7, and lesser than 0.6, respectively). For later sessions, the values are improved and some of them (e.g. JTmax and $AUC_{TmaxTend}$R') reach the excellent level higher than 0.9 or even 1. On the contrary, AUCROC of some parameters (e.g. AUC_{JTmax}, +AUC_{JT}R' and –AUC_{JT}R') remains poor, which is in concordance with above results. Percent of parameters with AUCROC reached certain levels is summarized in Table 2. It is obvious that the number of parameters with high discrimination ability increases from the beginning to the end of ischemia. It should be noted that these results give the information about the overall discrimination power of the parameters.

The suitability of each individual recording position to be used for discrimination between stabilization and ischemia was estimated using mean values of AUCROC calculated through all EG parameters for particular positions as shown in Fig. 28. It is evident that AUCROC in i1-i2 is higher near 0°. In the other hand, for last rotation session, overall discrimination ability is high enough almost whole recording range with maximal values characteristic for boundary region. Of course, as in the previous case, it is only overall assessment of recording positions suitability and low mean value of AUCROC for the position does not necessarily mean that data from this area cannot be used for ischemia manifestation. The number of recording positions with mean AUCROC calculated from all parameters reached high discrimination ability is summarized in Table 3. As was expected, AUCROC was high enough in the wide range of recording positions at the second half of ischemia. It should be noted that about 75 % of the positions with AUCROC>0.8 belongs to the range <0°, +90°>.

Similar analysis was performed for VCG parameters. Development of 2D EG loops in three planes during ischemia and corresponding main VCG parameters (for VCG reconstructed in standard coordinate system) are shown in Fig. 29. As can be seen, the main QRS and ST-T vectors change their orientation, mainly in horizontal and sagittal planes, in response to ischemia. The latter, furthermore, becomes longer. As a result, the orientation of these two vectors relative to each other changes, too. According to the results shown in Fig. 30, overall discrimination ability of various pairs of positions selected for reconstruction of VCG and calculation of corresponding parameters is quite similar in each rotation session. Particularly, AUCROC calculated for standard VCG parameters (i.e. for -40°) is comparable with that obtained for VCG reconstructed from 'shifted' axes (i.e. for 0°).

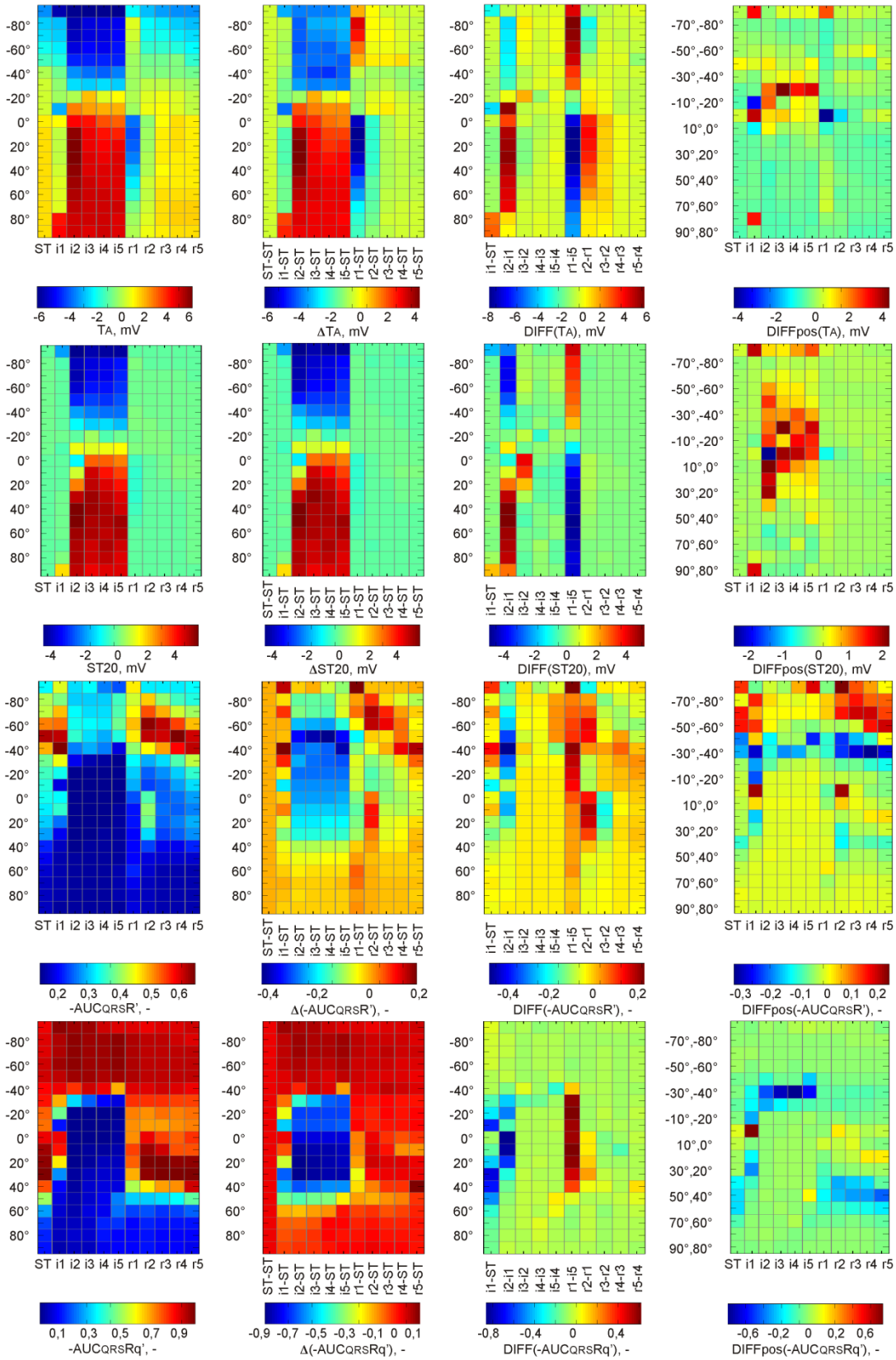

Figure 26. Values of T_A, ST20, -AUC_{QRS}R', and –AUC_{QRS}Rq' from one experiment. Difference between the parameter in stabilization and other periods (Δ), difference between parameter from adjacent periods (DIFF), and difference between parameter from adjacent positions (DIFFpos) (from left to right). ST – stabilization; i, r – rotation session in ischemia and reperfusion, respectively.

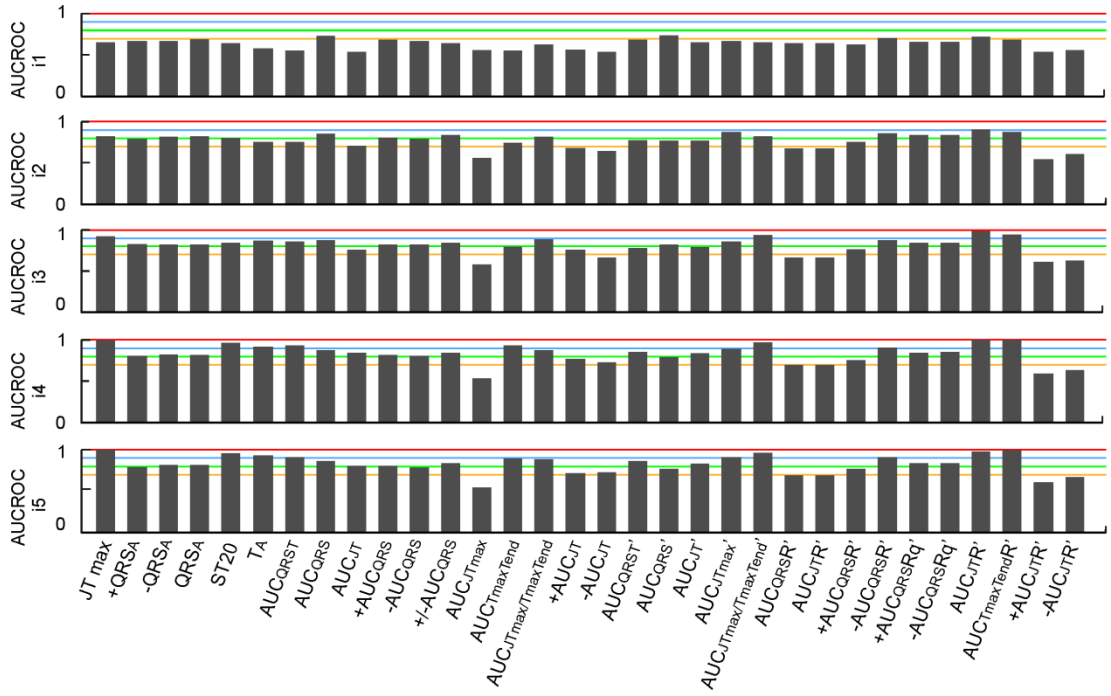

Figure 27. Mean values of AUCROC of various electrogram parameters.
Through all recording positions for different rotation sessions during ischemia (i1-i5). Orange, green, blue, and red lines indicate AUCROC of 0.7, 0.8, 0.9, and 1, respectively.

Table 2. Percent of parameters with averaged AUCROC (through all positions) higher than 0.7.

Ischemic period	**Mean AUCROC**		
	<0.7 – 0.8)	**<0.8 – 0.9)**	**<0.9 – 1)**
i1	14 %	0 %	0 %
i2	36 %	36 %	3 %
i3	17 %	50 %	11 %
i4	20 %	39 %	28 %
i5	17 %	39 %	28 %

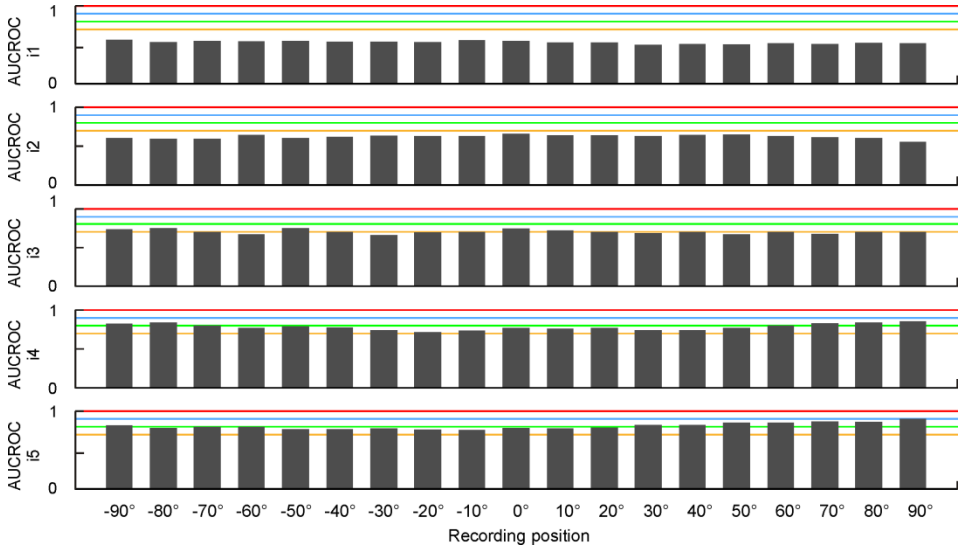

Figure 28. Mean values of AUCROC for EG parameters in different recording positions.
Calculated through all EG parameters for different rotation sessions during ischemia (i1-i5). Orange, green, blue, and red lines indicate AUC of 0,7, 0,8, 0,9, and 1, respectively.

Table 3. Number of recording positions with averaged overall AUCROC higher than 0.7.

Ischemic period	Mean AUCROC		
	<0.7 – 0.8)	<0.8 – 0.9)	<0.9 – 1)
i1	3	0	0
i2	13	3	0
i3	7	10	0
i4	3	15	0
i5	3	15	0

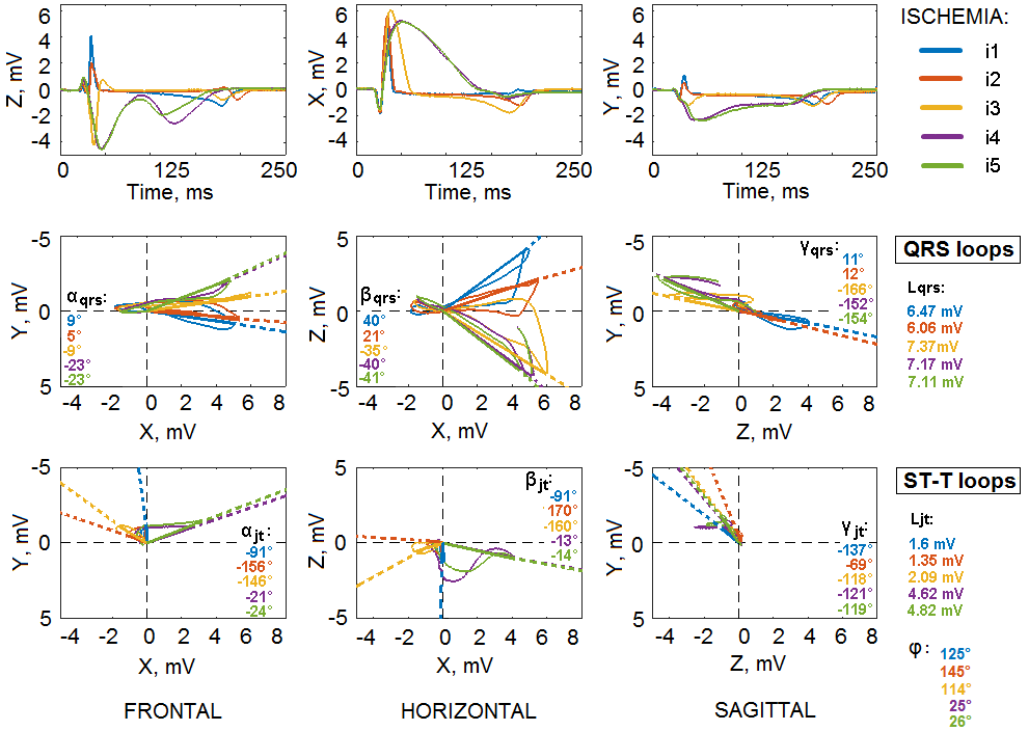

Figure 29. 2D EG loops and main VCG parameters during ischemia (standard VCG axes).

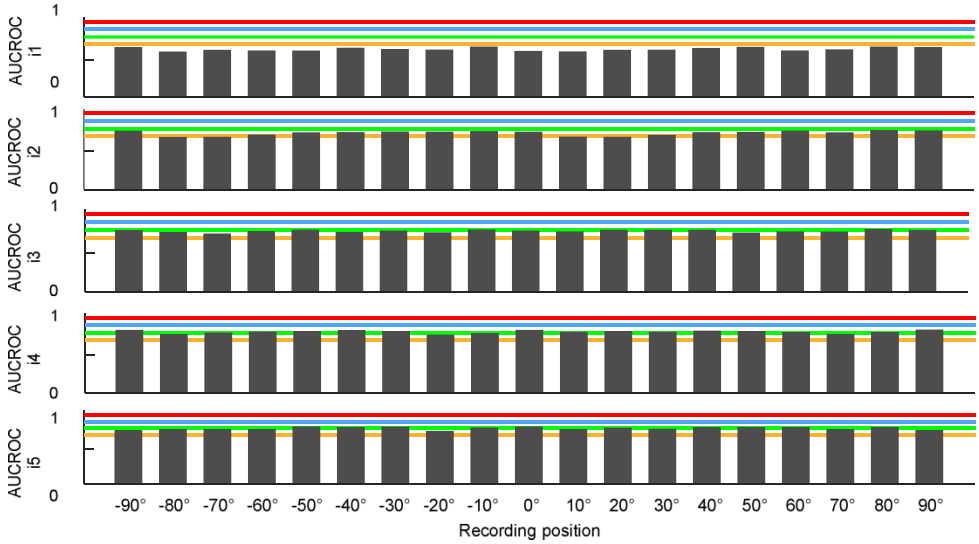

Figure 30. Mean values of AUCROC for VCG parameters in different recording positions. Calculated through all VCG parameters for different rotation sessions during ischemia (i1-i5). Orange, green, blue, and red lines indicate AUCROC of 0.7, 0.8, 0.9, and 1, respectively.

Electrogram recorded using fixedly placed electrodes under ischemic conditions

An example of typical time-course of orthogonal EGs recorded during ischemia and reperfusion (the first repetition after stabilization) and corresponding values of selected parameter are shown in Fig. 31 and Fig. 32, respectively. 3D and 2D QRS and ST-T loops reconstructed from EGs from Fig. 31 (i.e. for VCG reconstructed in shifted axis) can be found in Appendix B.

The most prominent visible changes in EGs and VCG during global 10 min long ischemia are summarized in Fig. 33. One of the earliest manifestations of ischemia is the change of QRS polarity in lead II, which begins in 2nd minute by the decrease of S peak deviation and results in positively oriented QRS (QR type) from the 3rd minute to the end of experiment. In 3rd minute, dramatic increase of R peak and T wave deviation are observed in lead I and lead II, respectively. These changes are accompanied by prominent QRS prolongation and deviation of ST-T loop vector in frontal and horizontal planes. Other phase with characteristics prominent changes in EG and VCG begin in 5th minute of ischemia, where ST elevation and decrease of S peak deviation are observed in lead I and lead III, respectively. This affects VCG, where ST-T loop parameters are altered dramatically. From the 6th minute, ST elevation is evident in all leads; QRS from lead I is covered by ST-T interval, thus QRS, ST segment and T wave cannot be easily distinguished in this EG. The late phase of ischemia is represented by the decrease of T wave deviation and slight decrease of QRS deviation. It should be noted, that ischemia affects T wave polarity (frequently observed inversion of T wave at the beginning and the end of ischemia) and PQ (lengthening), QT interval durations (shortening) and ST-T (shifting of T wave 'peak' towards QRS). After recovery of heart perfusion, QRS quite quickly (during first 2-3 min) returns to its non-ischemic shape in all leads. Inverted T wave from lead I becomes biphasic in the 2nd minute and positively oriented from the 3rd minute of reperfusion. In lead II, there is a significant increase of T wave deviation in the first minute and its slow changes up to 8th minute, where the control level is reached. In lead III, prominent increase of T wave in the 1st minute and its shifting to the right (according to the prolongation of QT interval) are found. Generally, the most significant changes of QT duration, T wave deviation and polarity are characteristic for first 3-4 minutes of reperfusion.

EG and VCG changes can be quantified by analysis of calculated parameters. Median values and 25th and 75th percentiles of all parameters from the beginning and the end of 2nd, 5th, 8th, and 10th minute of ischemia (from the first repetition) can be found in Appendix C. Ischemia leads to increasing or decreasing of particular parameters (or does not affect some of parameters et all). Above changes of are reflected on such parameters as QRS_D (QRS complex widening), QT_D (QT interval shortening), QRS_A and AUC_{QRS} (increasing QRS deviation and change of its polarity), T_A and $AUC_{TmaxTend}$' (increasing T wave deviation and change of its polarity), α_{qrs} and β_{qrs} (deviation of main QRS vector in frontal and horizontal planes, respectively), L_{jt} (lengthening of main vector due to the changes in voltage of ST-T), φ and D (same polarity of QRS and ST-T and significant overlapping between them in ischemia), etc. The changes of continuously monitored parameters are in accordance with those measured from signals recorded during rotation sessions (in recording positions 0° and 90° which correspond to initial placement of lead II and lead I in continuous recording, respectively). As was noted above, VCG parameters calculated in shifted axis differ from those derived in standard coordinate system. Therefore, VCG parameters from Appendix C belong to ranges different from those depicted in Fig. 29. For example, α_{qrs} derived from standard VCG at the end of stabilization is approximately within the range <0°, +90°>. In case of shifted coordinate system, this angle belongs to the range approx. <+65°, +182°>, which is due to the fact, that QRS main vector is projected on the plane rotated by 45° relative to the standard one.

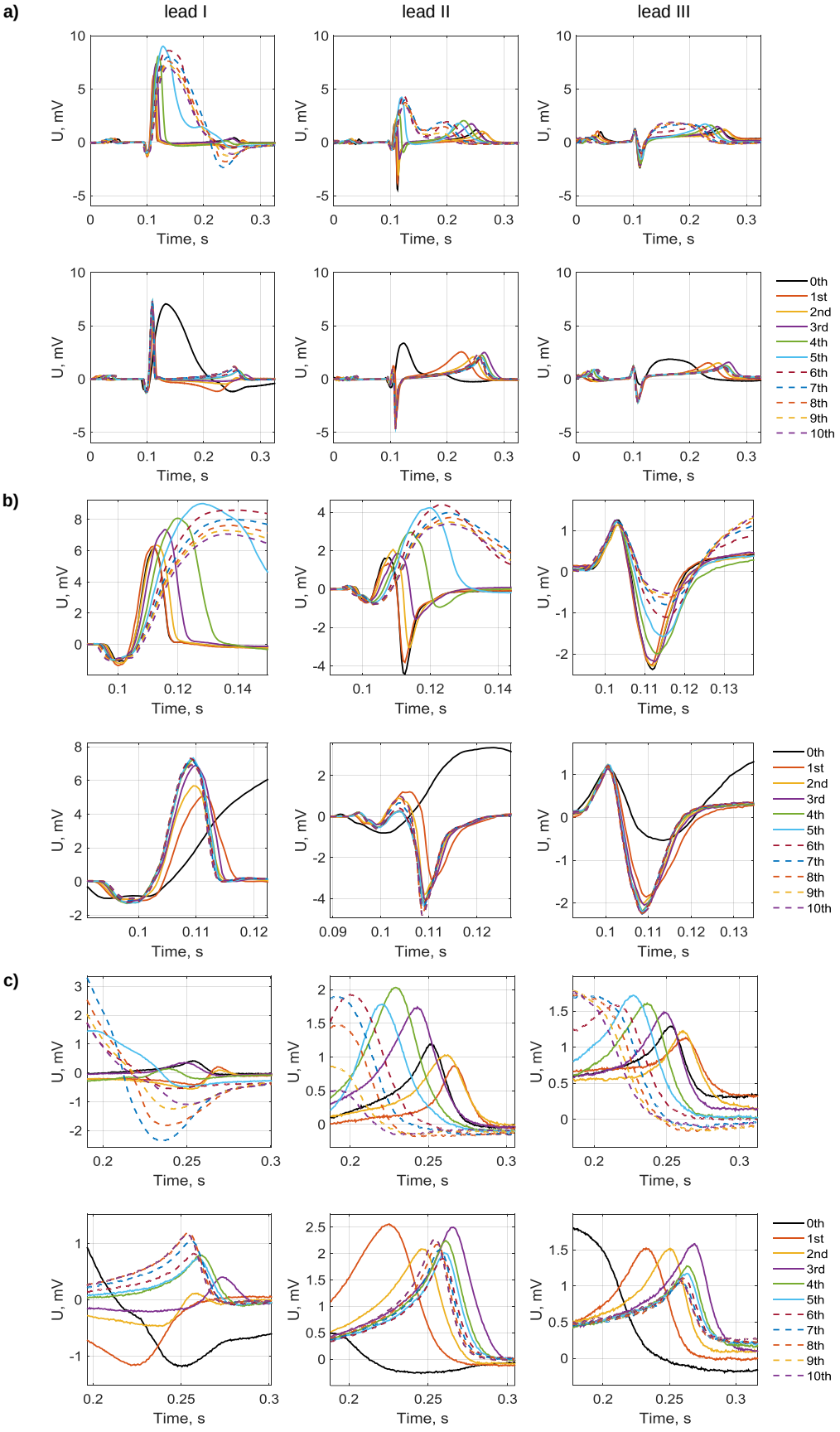

Figure 31. Typical time-course of electrogram recorded from rabbit isolated heart. P-QRS-T (a), QRS (b) and ST-T (c) during ischemia (top) and reperfusion (bottom). The segments are from the beginning (0^{th} minute) and from the end of each minute (1^{st} to 10^{th}) of particular experimental periods.

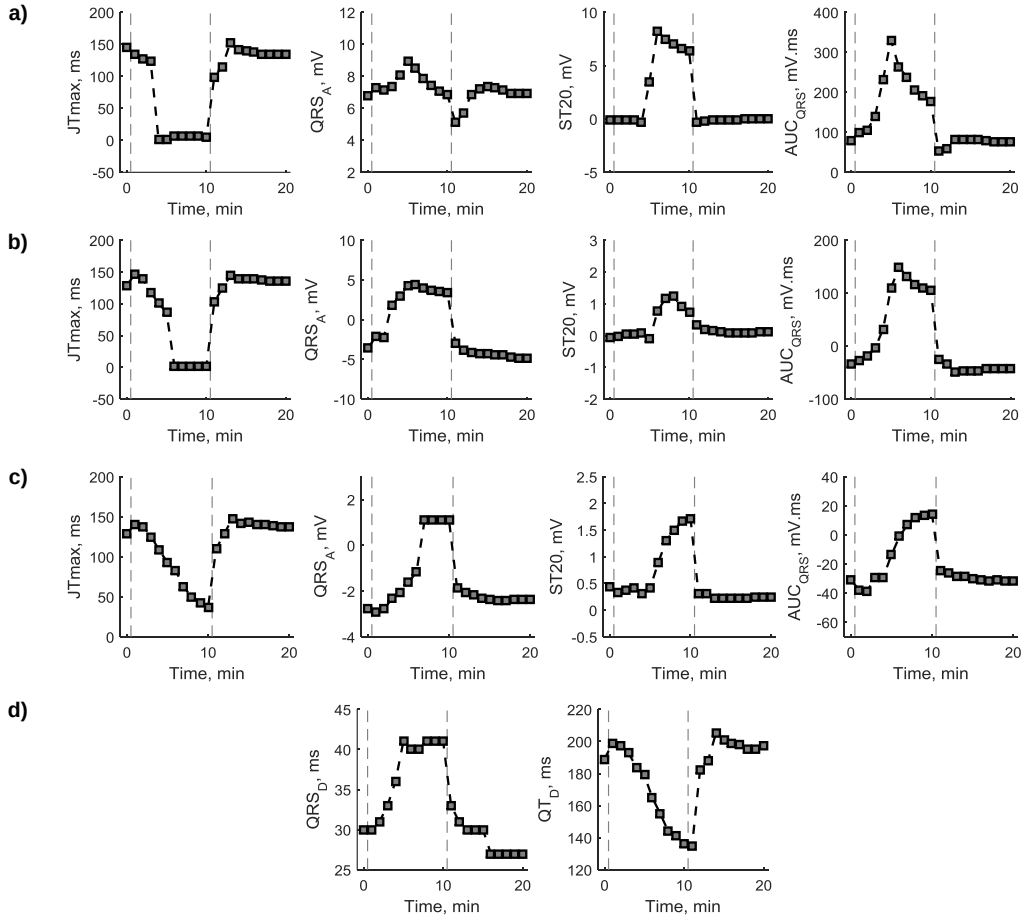

Figure 32. Time-course of the main parameters of rabbit isolated heart electrogram.
For lead I (a), lead II (b), lead III (c), and all leads (d). Data are shown for the beginning (0th minute) of ischemia to the end of reperfusion (20th minute). Second dashed line separates ischemia and reperfusion.

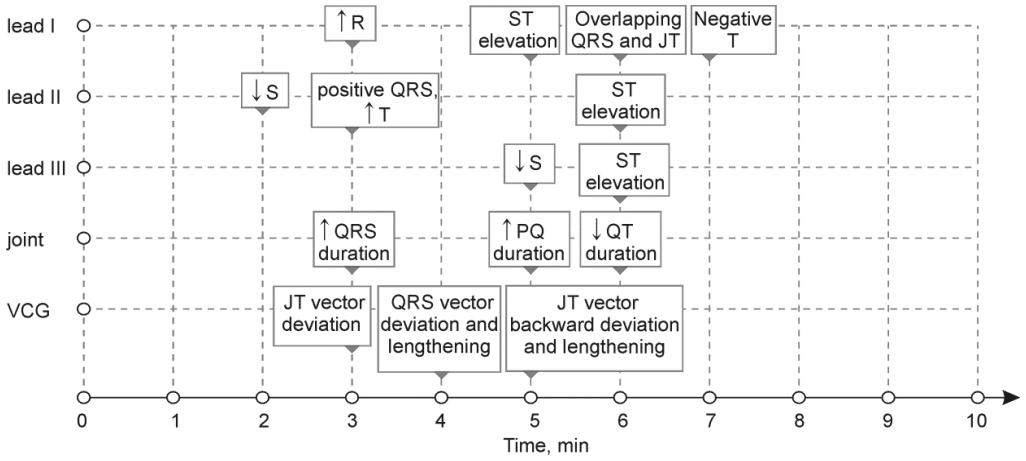

Figure 33. Time progress of the main visual changes in electrograms and VCG of rabbit isolated heart induced by 10 minutes long global ischemia.

Results of comparison of parameters in stabilization and each minute of ischemia are shown in Appendix D. The distribution of main indices describing overall (through various parameters) ability of different leads' parameters to discriminate between non-ischemic and ischemic data are shown in Fig. 34-35. The indices (including cut-off value) from time instances, where AUCROC of

parameter reaches the particular level (AUCROC > 0.7, 0.8 and 0.9) are summarized in Appendix E. Percent of lead I, lead II and joint&VCG (joint group includes interval characteristics calculated from all leads together) parameters with AUCROC of certain levels is shown in Fig. 36. Discrimination indices were also analysed separately for QRS and ST-T based parameters and, finally, within particular parameters' groups according to Appendix A.

As expected, *the earliest significant ischemia induced changes* appear in QRS-related parameters (from both EG and VCG) and there are more prominent in lead II data as compared to lead I data (see Appendix D, Appendix E and Fig. 37). Generally, there is an increasing trend for all discrimination indices from the beginning to the end of ischemia in lead I, lead II and joint&VCG data (Fig. 34-35). Furthermore, some parameters in the 1st minute of reperfusion do not recur to the control values, thus their AUCROC is quite high. It is valid mainly for the first and the second reperfusion.

Lead I and lead II parameters have better discrimination ability in comparison with *joint&VCG parameters* (where only a few parameters provide good discrimination – see top upper part of corresponding boxplots in Fig. 34-35). Se of lead I parameters decreases from the first to the third ischemia, whereas Se of lead II and joint&VCG parameters remains quite high. Sp is the highest in lead I parameters. Nevertheless, there is a lower variability in values of indexes (there is only few parameters with low values of indexes) in the second half of ischemia in case of lead II comparing to those from lead I and joint&VCG (Fig. 34-35 and Fig. 36). Despite the best overall discrimination ability, the number of lead I parameters reaching proper AUCROC is comparable or even lower than that of lead II parameters (where approx. 60% of parameters reach AUCROC > 0.8 in 6th minute of ischemia and half of parameters reach AUCROC > 0.9 in 8th minute of each ischemia) and only slightly exceeds this index in VCG parameters (see Fig. 36). About 20 % of lead II parameters reach AUCROC > 0.9 in the 4th min of the first ischemia. In case of lead I and VCG, it is valid for the 5th minute of the first ischemia. There is 1-2 minutes delay in courses calculated for the first and latest ischemic periods, respectively.

Indexes of *QRS-* and *ST-T-related parameters* are high in lead II and lead I, respectively, which is in concordance with above analysis of EG morphology. As regards joint&VCG group, all indexes are higher in ST-T-related parameters than in those based on QRS (see Fig. 37 and Appendix E). Nevertheless, there are a few QRS-related VCG parameters with perfect discrimination ability.

Finally, analysis results for *different groups of parameters* are summarized in Appendix F. Generally, AUCI and AUCII groups calculated from lead I and voltage based and AUCIII groups from lead II have good discrimination ability. Nevertheless, higher Se was obtained for voltage-based and AUCIII groups from lead I in comparison with that from lead II. Moreover, as compared to lead I, AUCI and AUCII groups from lead II give higher Sp and Se, respectively. As regard other parameters groups, all of them are characterized by high Se. Centroid based VCG parameters have poor Sp. Common and area based VCG parameters have good (and comparable) discrimination ability. The highest Se and Sp were found in case of 3D loop parameters and interval characteristics. Considering high variability in indexes of the latter group, 3D loop based parameters seems to be the most useful for non-ischemic and ischemic beats discrimination. According to the results of comparison of particular parameters groups between each other, AUCII parameters from lead I and 3D loop VCG parameters can be considered as the groups with the highest discrimination ability (and with comparable AUCROC, Se and Sp reaching high values in 5th-6th minute of ischemia).

Similar analysis of discrimination ability was performed for *lead III parameters*. Some results (including boxplots for AUCROC, Se and Sp in ischemia) can be found in Appendix G. Discrimination ability of the most proper lead III morphological parameters (such as JTmax, $AUC_{TmaxTend}R$' and other) is comparable to the corresponding parameters calculated from lead I and/or lead II. For most parameters, quite poor Se was observed even at the end of ischemia. Therefore, parameters from lead I and lead II were included to further analysis and lead III was only used to derive joint and VCG parameters.

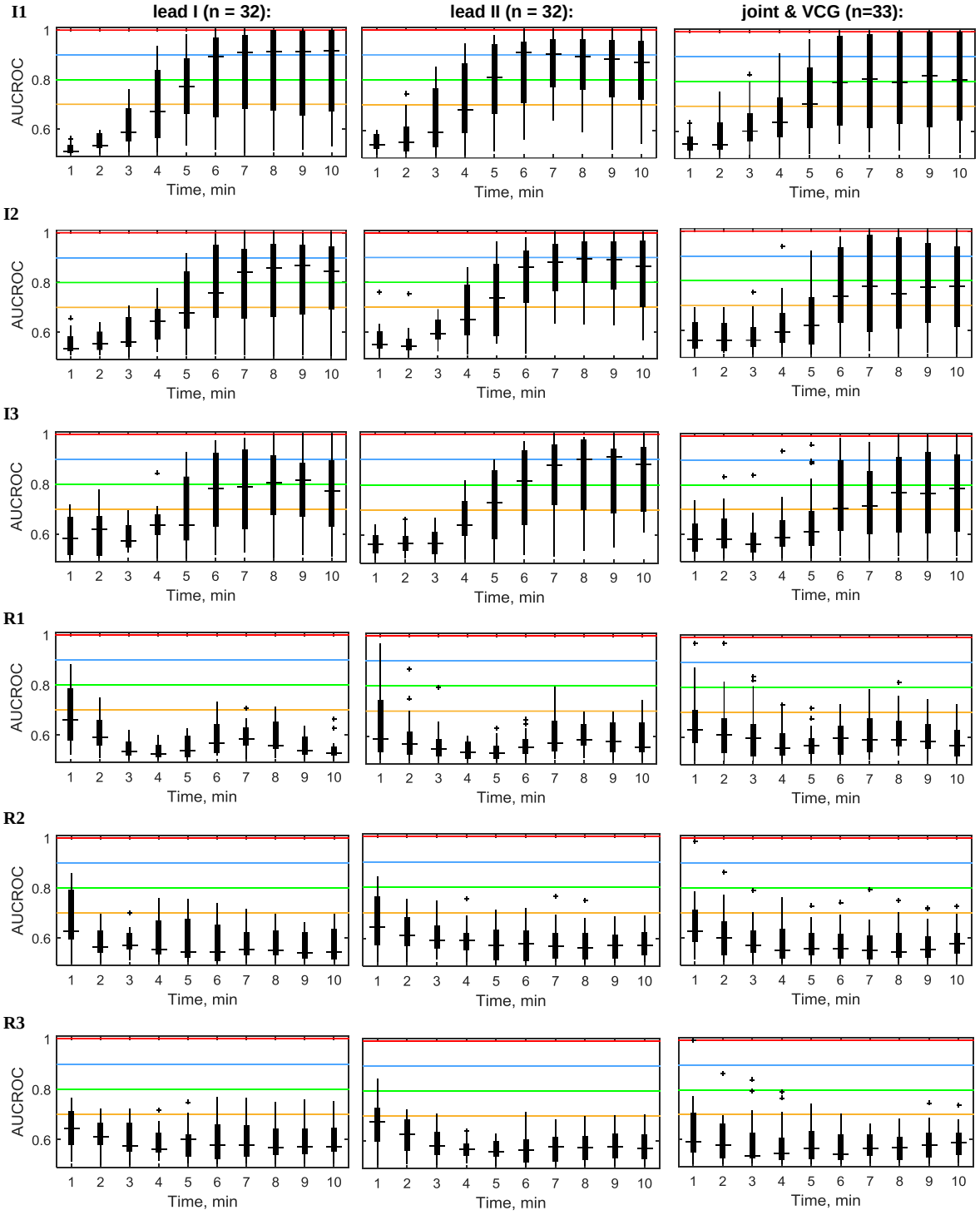

Figure 34. AUCROC of all lead I and lead II parameters and joint&VCG parameters during three ischemic (I) and reperfusion (R) periods.

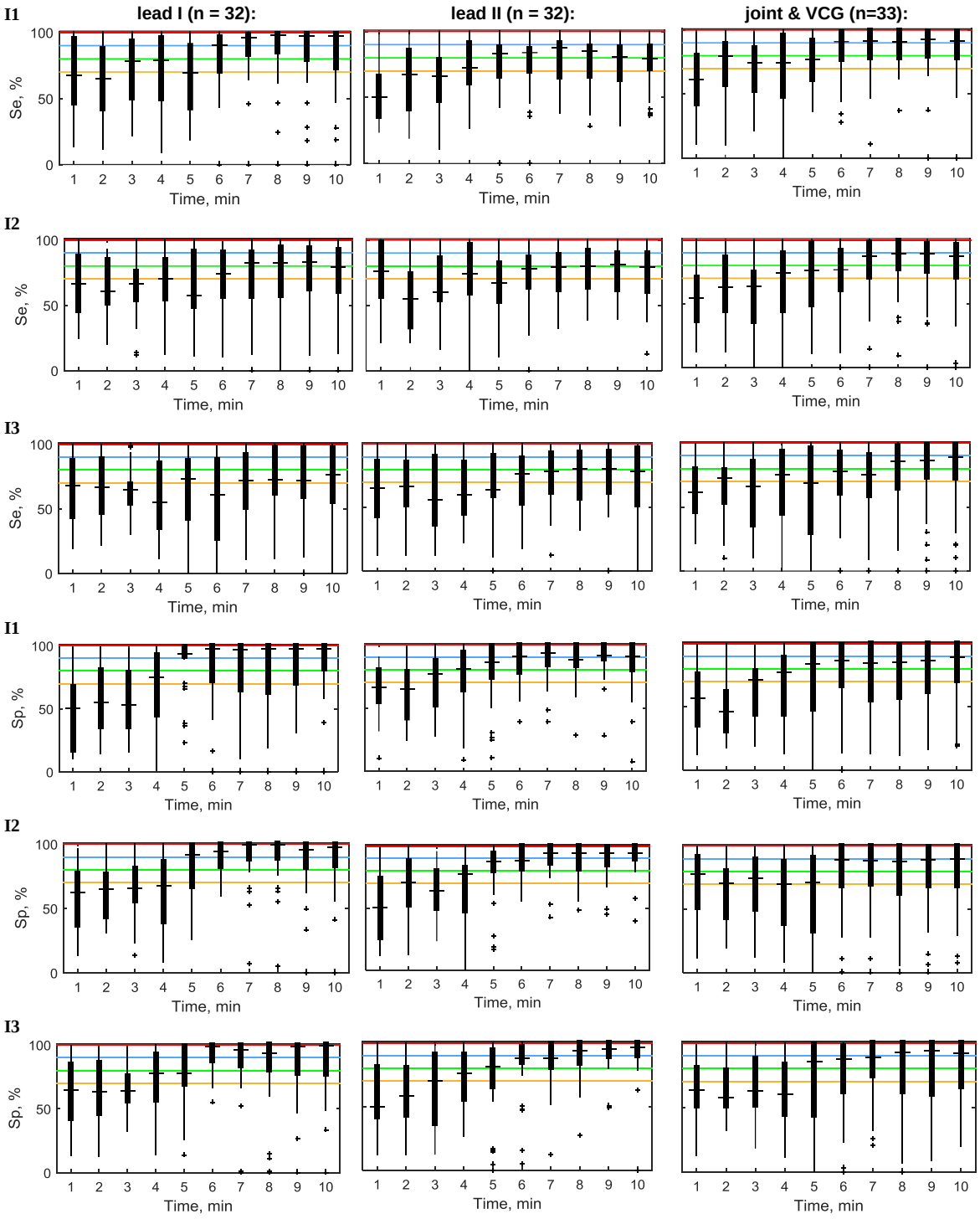

Figure 35. Se and Sp for all parameters from lead I, lead II and joint&VCG during particular ischemic (I) periods.

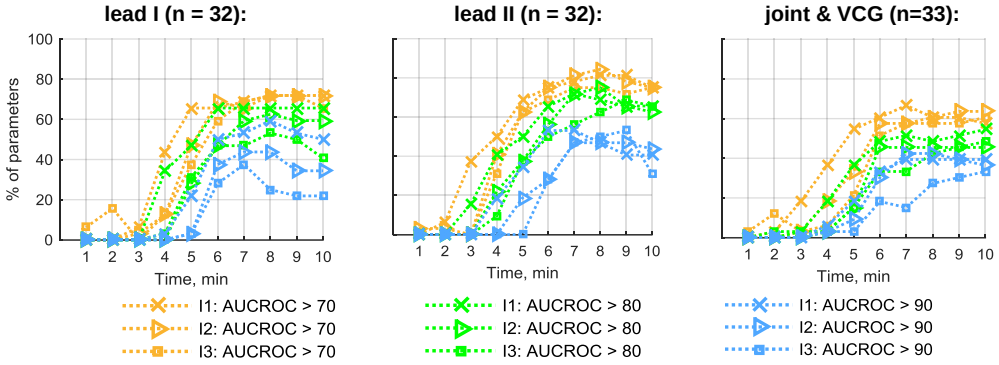

Figure 36. Percent of parameters with AUCROC > 0.7, 0.8 and 0.9 during particular ischemic (I) periods.

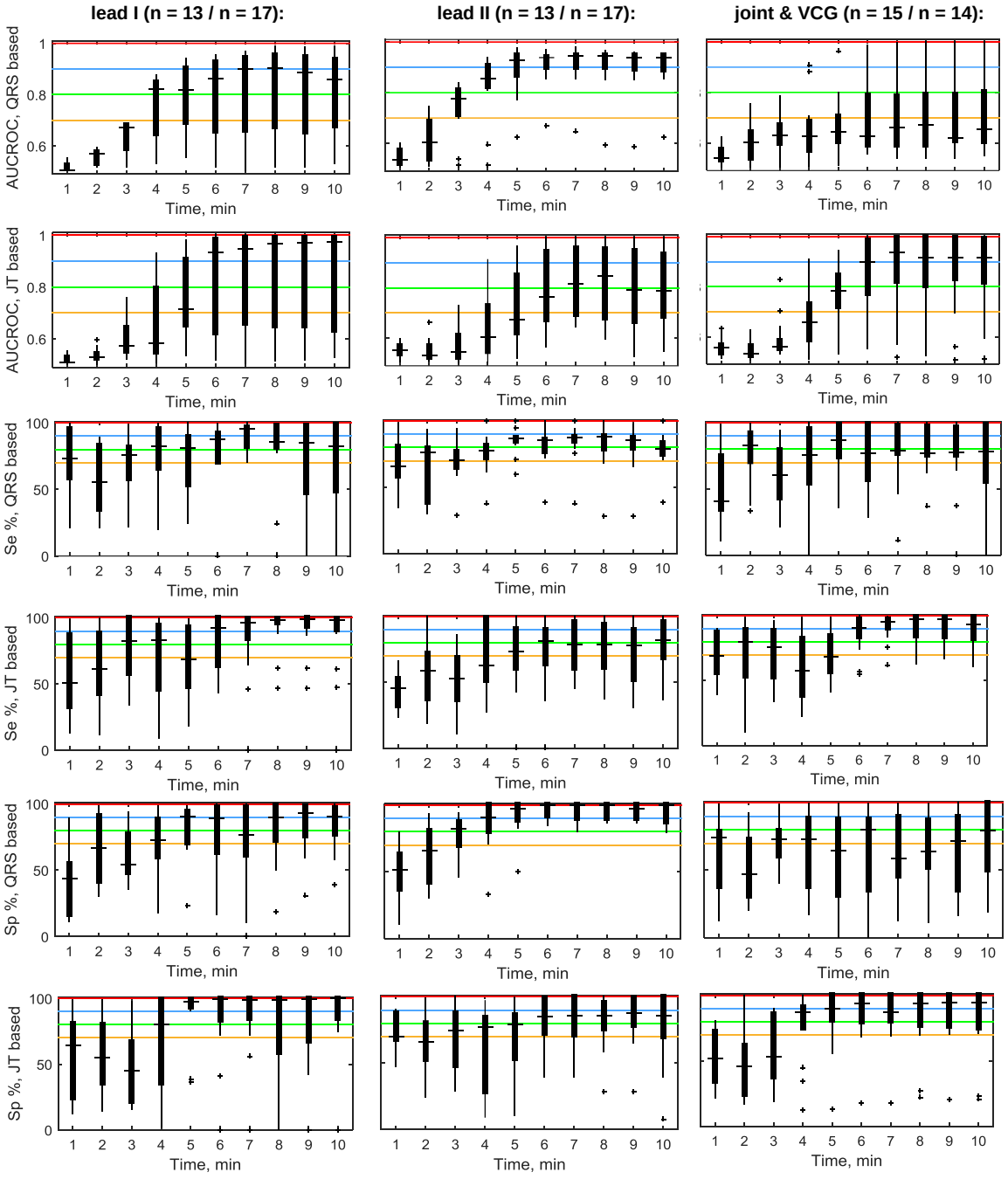

Figure 37. AUCROC, Se and Sp for QRS and ST-T (JT) based parameters during the first ischemia.

Time courses of AUCROC calculated for the most common EG and VCG parameters during the first ischemia are illustrated in Fig. 38. Among all parameters, AUCROC reached value higher than 0.9 in only AUC_{QRS} from both leads, T_A and ST20 from lead I, QRS_A from lead II, L_{jt}, β_{qrs}, QRS_D, RR and φ (generally in the 6th minute of ischemia). The earliest changes were characteristic for β_{qrs} and QRS_A from lead II (AUCROC > 0.9 in the 4th minute of ischemia), AUCROC of the latter parameter, furthermore, reached value higher than 0.7 already in the 2nd minute of ischemia. The most frequently used ischemia marker ST20 allows discriminating between non-ischemic and ischemic state in 5th minute of ischemic period (AUCROC is close to 0.8), whereas AUCROC for QRS_D reaches the value higher than 0.85 in the 4th minute of the period.

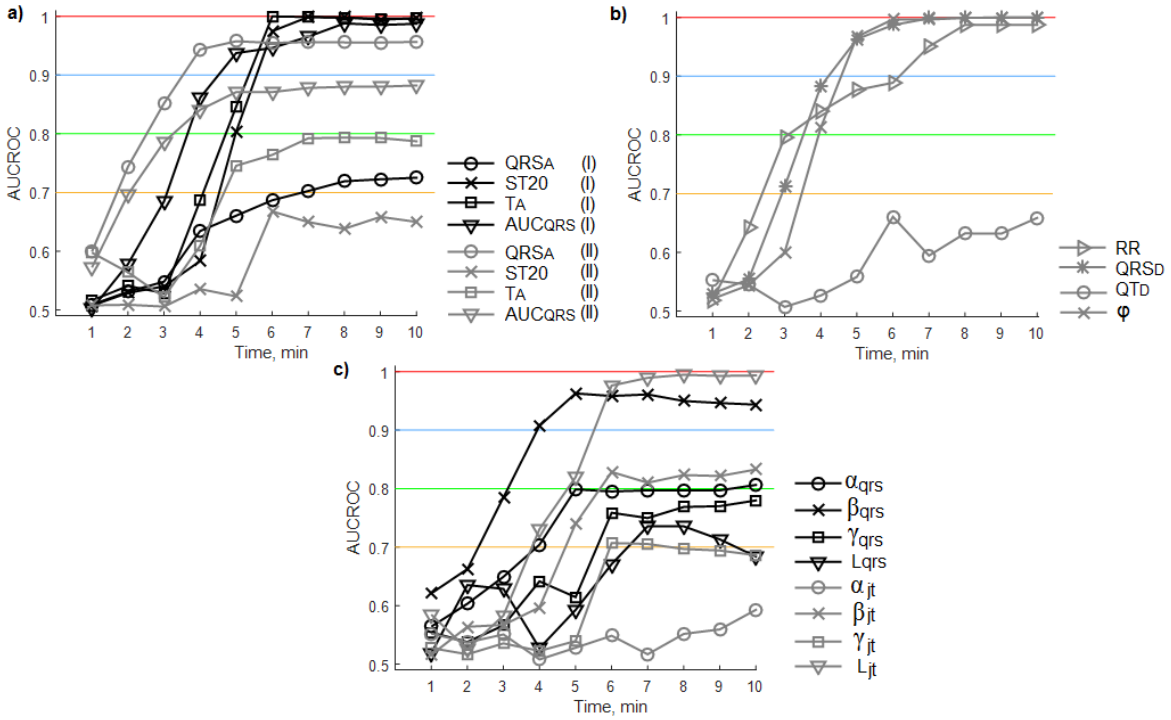

Figure 38. Time course of AUCROC of common parameters calculated from lead I and lead II (a) and joint&VCG (b-c) during the first ischemia.

Finally, parameters' Δ and slope values were analysed to test whether the development of EG and VCG shape alters significantly between particular ischemic (or reperfusion) periods. According to Friedman test results, Δ of only six lead I parameters differ between two particular periods (namely the first and the third reperfusion). Δ values of six lead II parameters calculated for the first ischemia differ significantly from those calculated for the second one. One of such parameters is AUC_{JT}. Significantly different values of ΔAUC_{JT} were found in case of ischemia as well as reperfusion (data from lead II and lead I, respectively). Corresponding results were obtained for slope derived from normalized ΔAUC_{JT}, where the slope for ischemic and reperfusion period reached values significantly different from zero (0.066 ± 0.071 and -0.039 ± 0.07, respectively). Normalized ΔAUC_{JT} and lines fitted for the slopes calculation are shown in Fig. 39. Despite the progressive decrease of AUC_{JT} through ischemic periods, this parameter in reperfusion tends to its stabilization value.

According to the results of analysis the parameters obtained using and without delineation outcomes, it can be concluded that significant difference between these two types of parameters was found in only $-AUC_{JT}$, $AUC_{TmaxTend}R'$, $-AUC_{JT}R'$, and P_{jt}. Thus, use of strictly determined

regions for calculation of QRS and ST-T based parameters does not lead to significant bias in their values as compared to convenient approach.

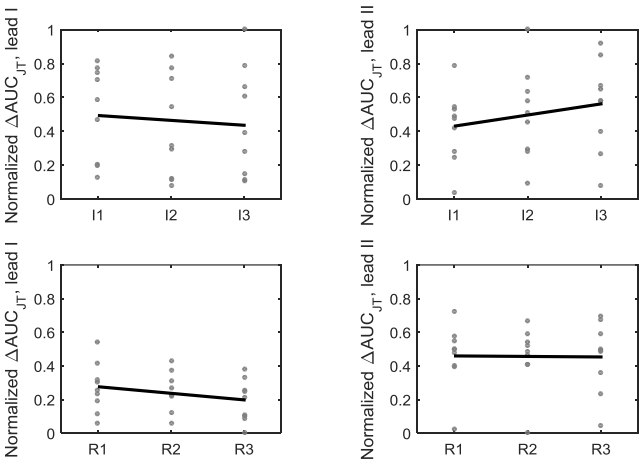

Figure 39. ΔAUC_{JT} from the end of ischemic (I, top) and reperfusion (R, bottom) periods and lines fitted through ΔAUC_{JT} from all experiments for slope calculation.

4.1.4 DISCUSSION

Recording and analysis of electrical activity of rabbit isolated heart under non-ischemic conditions

Generally, the shape of EG recorded from different areas of LV (during the heart rotation) corresponds to that of ECG recorded in human from precordial leads, particularly in terms of QRS complex configuration and the area of transition type of EG (where negatively polarized QRS becomes positively oriented), P and T wave polarity and the presence of isoelectric parts, such as ST segment (for human ECG refer for example to [11]).

Basic interval- and voltage-based parameters of ECG recorded in intact White New Zealand rabbit are summarized in Table 4. The values of ECG patterns of this rabbit breed are very similar (mostly the same) to those obtained in clinically normal pet rabbits [97],[98]. According to previous reports, the most outstanding features in ECG of White New Zealand rabbit are the high variability of QRS complexes and main QRS vector in frontal plane (α_{qrs}), P and T waves concordant with QRS in all leads and isoelectric P and T waves [99].

Corresponding parameters derived from EGs recorded in present study (orthogonal lead I with positively oriented QRS was chosen) are also shown in the table for comparison. It is evident, that heart rate obtained in isolated hearts is lower than that of intact rabbits. Consequently, QT_D is prolonged in isolated hearts. Other interval EG characteristics are similar or only slightly different from those of ECG. Compared to the commonly recorded ECG, the voltage-based characteristics in EG of isolated heart is several times higher. It can be explained by the specifics of used recording method, particularly: a) leads were oriented similarly to precordial ones and were placed around LV approx. in its middle area); b) short distance – of approx. 0.5-1.5 cm (up to 3 cm in case of lead III) only – between heart surface and electrodes; c) well conductive K-H solution in a space between the heart surface and the electrodes; d) absence of conduction inhomogeneities such as in torso (mainly lung, skeletal muscle and fat). The latter is of special importance as was proven in human, where the negative effect of the various torso compartments on the amplitude of epicardial potentials (without the effects on their patterns) was observed [100],[101]). As in intact rabbit

ECG, quite high variability of QRS complexes and isoelectric P wave (but not T wave) were observed in EG of isolated hearts.

Table 4. Basic ECG parameters of White New Zealand rabbit.

Basic characteristics and ECG parameters	**Studies on White New Zealand rabbits:**		
	Rezakhani et al 1995 [99]	Kour et al 2013 [102]	Present study (isolated heart)
Number of animals (sex)	119 (male & female)	12 (male & female)	10 (male & female)
Body weight, kg	-	2-3	2.26 ± 0.8
ECG lead*	standard Lead II	standard Lead II	orthogonal Z'
Heart rate, bpm	260 ± 41	204 ± 7	164 ± 19
P_A, mV	0.038 (mean)	0.059 ± 0.005	-
P_D, ms	24.9 ± 5.5	33 ± 3	23.9 ± 3.1
PR_D, ms	56 ± 6.6	60 ± 4	54.4 ± 7.9 (PQ_D)
QRS_A, mV	0.306 (mean)	0.214 ± 0.016	3.7 ± 1.8
QRS_D, ms	31.2 ± 5.0	52 ± 6	24.8 ± 3.3
T_A, mV	0.128 (mean)	0.149 ± 0.013	0.74 ± 0.49
T_D, ms	-	71 ± 4	-
QT_D, ms	144 ± 13.1	130 ± 7	182.6 ± 21.4
α_{qrs}, °	0° to 120°	-93° to +96°	33° to 82°

* lead used for calculation of voltage-related parameters, A – amplitude, D – duration

One of the factors influencing the quality and characteristics of ECG is the mutual orientation of electrode system and the heart which can be affected with the subject's body position or electrode placement during recording procedure. Various approaches focused on study of the ECG alteration caused by patient body position changes have been presented. Clinically significant ST segment deviation and changes of QRS complexes (polarity and relative size of Q, R and S) in standard ECG recorded at right and left-side lying position (comparing with supine) in both healthy and subjects with cardiac disease were reported [103]. Pseudo-ischemic alterations in VCG caused by changes in body position and their impact on monitoring during ischemia were discussed repeatedly [104],[105]. In the present study, longitudinal rotation of the heart placed in the bath filled with K-H solution was performed to record EGs from different heart areas. No significant pseudo-ischemic alterations such as deviation of ST segment (Fig. 25, bottom), change of polarity or increase of T wave amplitude, or widening of QRS complex (will be shown in next chapter) were found in EGs recorded during stabilization. It can be, therefore, concluded, that electrical activity can be successfully measured from different areas of isolated heart using fixed electrode leads, when the heart is rotated. Thus, detection of ischemia in this data should not be affected with the electrodes position relative to the heart surface. The effects of LV size on the main EG parameters recorded under non-ischemic conditions will be addressed in next chapter.

Recording and analysis of electrical activity of rabbit isolated heart undergoing repeated global ischemia

Generally, *ischemia manifestations* found in rabbit isolated heart are very similar to those in human. Particularly, during global ischemia, sinus bradycardia was observed in all experiments, which can be explained by impaired function of SA node. According to the results of the previous study on isolated rabbit SA node, pacemaker cells perfused by 'ischemic' solution (i.e. omission of glucose, pH 6.6 and additional upgrades for evaluation the role of increased serum [K]), reduction

of inward Na-Ca exchange current I_{NCX} and T-type Ca current $I_{Ca,T}$ contribute to ischemia-induced bradycardia [106].

Shortening of QT interval after short-term prolongation (immediately after the perfusion stopping), was also observed. This is a result of decreased APD, which was previously reported in the same animal model by Kolářová et al. [59]. In this study, MAPs were recorded by optical method using VSD di-4-ANEPPS. Pronounced shortening of APD recorded in rabbit isolated heart was also observed during first 10 minutes after LDA occlusion (regional ischemia) [65].

The *earliest* (and most prominent) manifestations of global ischemia were found in depolarization part (QRS complex), especially in EG recorded from anterolateral area (the middle of LV), where the change in polarity of QRS was observed besides the QRS widening. The changes in temporal part of QRS were evident in EG from boundary region, which is in accordance with observation in human (see above). QRS duration represents conduction of depolarisation through ventricles. Under ischemia, conduction velocity is decreased due to impaired metabolism in myocardium. In human, acute ischemic injury (myocardial infarction) is caused by significant reduction or even stopping of perfusion usually in one region of the heart. The changes in QRS are usually associated with the late phase of ischemia and ST deviation is used as early marker of injury. Nevertheless in global ischemia, QRS prolongation precedes changes in ST segment (elevation or depression), which are caused by some electric inhomogeneity in ventricles repolarization. In case of global ischemia, whole myocardium is affected in the same time, therefore the development of marked electric inhomogeneity (i.e. 'more' and 'less' ischemic regions) is not so fast and ST changes occur only in 5^{th}-6^{th} minute of ischemic period, whereas significant QRS prolongation ('global' marker) is observed 1-2 minutes earlier. Similar phenomenon associated with severe and global ischemia in human was previously reported by Takaki et al. [26]. Moreover, less steep R peak was observed in EG recorded during ischemia. The changes in these parts of EG are in accordance with the results of AP analysis in rabbits isolated hearts, where increased upstroke duration and decreased amplitude of AP (corresponding to the velocity of impulse conduction through ventricular tissue during depolarisation) were observed in both global and regional ischemia protocols [49],[59],[65].

In the *second half* of ischemia, when ST-T merges with the QRS, the transformation of QRS may be partially regarded as the passive response on the primary changes in repolarization part. In human, this finding is known as so called 'tombstoning pattern of ST segment' or 'monophasic pattern' which most often occurs because of proximal occlusion of LAD coronary artery (leads to the global ischemia of the whole anterior wall of the heart) and accompanies a large infarct [93]. Pronounced ST elevation and 'monophasic pattern' were observed in a broad region, when EG was recorded in different positions (see Appendix B). This is not unexpected because of global character of ischemia induced, where the whole myocardium (including both subendocardial and subepicardial regions) is affected at the same time (transmural ischemia). Thus, the most valuable manifestations in the second half of ischemic period are characteristic for ST-T.

Generally, none of EG and VCG parameters was able to detect successfully first two minutes of ischemia. It may be due to low sensitivity of evaluated parameters or EG itself to the earliest phase of ischemia. It might be also hypothesized, that the residual oxygen in the myocardium of the non-working heart (i.e. the heart does not pump against the load) is high enough to supply it for a limited time. However, this hypothesis cannot be easily verified. Nevertheless, it is in accordance with other studies on rabbit isolated hearts, where the first pronounced changes in the heart electrical activity were found at 3-5 minutes after the ischemia onset and 30-90-min perfusion stopping was used to induce myocardial infarct [53],[65],[107].

Horizontal *leads* facing LV wall are preferable for recording EG during ischemia, such as in human, where V3, aVF and V6 seem to be the most suitable for detection of ischemia presented in any territory [24]. Lead III is not as sensitive to ischemia as two others and the main manifestation in this lead data is ST elevation occurred 6 min after the perfusion stopping. Among the most common ischemia markers (ST20, QRS_A, QRS_D, and T_A), QRS_A from lead II is the most earliest. QRS_D, T_A and ST20 from lead I and QRS_A from led II have the best discrimination ability. Generally, AUC-based *parameters* (calculated from absolute values of QRS-T) from both horizontal leads, 3D loop parameters from VCG and interval characteristics (joint for all leads) can be considered as those with the highest ability to discriminate between non-ischemic and ischemic state (at 5^{th}-6^{th} minute after the onset). The most prominent manifestations of ischemia injury can be indicated in EG in the middle of ischemic period (i.e. approx. 4^{th}-6^{th} minute). After this period, only slight changes are presented in the most parameters. Thus, *three main degrees of isch*emia may be distinguished in data: 1) 1^{st}-3^{rd} minute, when the prominent changes can be identified mainly in QRS part of EG recorded from the middle of LV; 2) 4^{th}-6^{th} minute, when ischemia is manifested in pronounced ST-T changes in data from the whole LV (especially in its boundary); 3) 7^{th}-10^{th} minute, when marked alterations are present in EGs recorded from any area of LV. Therefore, recording EG in initial positions of lead I (posterolateral) and lead II (anterolateral) seem to be suitable for detection of various phases of ischemia. The issues associated with automatic detection of ischemia (or its different phases) and selection of the most relevant EG and VCG parameters will be addressed later.

The backward changes in *reperfusion* are carried out more quickly than those in ischemia. EG shape in the 3^{rd} minute of reperfusion is almost the same as at the end of stabilization. It is especially valid for QRS morphology. The EG (and VCG) alterations are very similar in all three ischemic-reperfusion repetitions. According to the results of delta and slopes analysis, the total changes in EGs morphology during three successive ischemia or reperfusion are the same. However, time moment, where significant alterations were achieved in the records, varies from the first to the third ischemic period.

It can be, therefore, concluded that, 10 minutes long ischemia is manifested in the pronounced modification of the whole QRS-T. These effects nonetheless vanish during the first minutes of reperfusion. 10 minutes of reperfusion is long enough to return the heart function to the control level. It is consistent with the results of biochemical analysis (not published yet), where no significant differences in three markers (e.g. [108]) – creatine kinase, lactate dehydrogenase (both are robust markers of direct myocardial injury and cell necrosis) and 4-hydroxynonenal (marker of lipid peroxidation occurring mainly in reperfusion) – measured at the end of stabilization, the first and the third reperfusion (see Fig. 3b) were observed.

Thus, ischemia-reperfusion injury can be successfully studied repeatedly in present animal model. It, in turn, allows studying the preconditioning effect, which is, in this case, characterized by delayed onsets of ischemia-related EGs and VCG changes during the second and the third ischemic periods relative to the first one. Preconditioning also results in the decreased number of detected VPBs (will be discussed later). The significant effect of ischemic preconditioning on the magnitude of the EG and VCG morphology changes was not confirmed.

4.2 EFFECTS OF LEFT VENTRICLE MASS ON ELECTROGRAM UNDER NON-ISCHEMIC AND ISCHEMIC CONDITIONS

This chapter is focused on the analysis of electrical activity of rabbit isolated heart with increased LV mass. The possible effects of increased LV mass on development of myocardial ischemia are described, too. The most important results were summarized in two conference manuscripts ([109],[110]) and two journal articles (Ronzhina M. et al. and Hlaváčová M. & Olejníčková V.) are under revision process at the moment.

4.2.1 BACKGROUND

Despite the intensive clinical and preclinical research, both morbidity and mortality associated with myocardial ischemia remain high. Diagnosis of myocardial ischemia might be complicated by co-incidence with other diseases, e.g. myocarditis, hypertension or LV hypertrophy. The association between myocardial ischemia and LV hypertrophy has been intensely discussed during the last few decades. Particularly, the studies elucidated such important aspects as mechanisms of development and prevalence of myocardial ischemia in LV hypertrophy patients, specific character of analysis of ECG with ischemia-like patterns recorded in LV hypertrophy patients with and without evidence of myocardial ischemia, and others [111]-[114]. Nevertheless, detailed quantitative analysis of effect of LV mass changes on myocardial ischemia manifestation in ECG is still missing. Perhaps the only study, where the need of development of special criteria for ST elevation myocardial infarction in patients with LV hypertrophy was addressed, is study of Armstrong et al. [115] Significantly different severity of ST elevation were obtained in LV hypertrophy patients (defined by standard voltage ECG criteria) with and without an angiographic culprit lesion. New diagnostic strategy based on standard criteria was proposed to improve specificity of ST elevation myocardial infarction (by decrease of false positive diagnoses) detection without loss of sensitivity.

In cardiovascular research, particular aspects can be successfully studied on animal models, frequently on isolated heart perfused according to Langendorff [4]. In contrast to human, in animal experiments the myocardial ischemia as well as LV hypertrophy can be simply induced. The development of ischemia in hypertrophic hearts can therefore be investigated and accuracy of its detection in ECG evaluated. Such investigation is, however, complicated since standard ECG criteria for both hypertrophy and ischemia assessment in animals are missing. As was mentioned above, rabbit is one of the most popular models in studies of cardiovascular system due to the similarity of electrophysiological parameters of rabbit hearts to those of human. Moreover, rabbit is characterized with the high sensitivity to spontaneous LV hypertrophy and myocardial coronary vasoconstriction [116].

Therefore, rabbit isolated heart model was used in this study to: a) find out electrogram (EG) parameters (as simple as possible in terms of computation) suitable for detection of even slightly increased LV mass; b) compare myocardial ischemia development in the hearts with normal and slightly increased LV mass (in terms of onset, magnitude and reversibility of the EG morphology changes) with aim to verify possible effect of moderate LV mass increase on the heart response to short ischemia; c) evaluate possible impact of LV mass on the EG criteria for ischemia detection. Besides the anatomical and electrical characteristics of the heart, the effect of mutual spatial orientation of the heart and electrode system on EG morphology was investigated, too.

4.2.2 METHODS

Experimental groups

Sixteen adult New Zealand rabbits (both sexes, weight 2.2-3.45 kg) were included to the study. Before anaesthesia, body weight (BW) of each animal was assessed. Immediately after the isolated heart experiment, the whole heart was weighted (heart weight, HW). Both atria and right ventricle were then separated and LV with septal wall was weighted (LV weight, LVW). Free lateral wall of LV was cut and the wall thickness (LVT) was measured.

Already during the preparation, visible enlargement of LV was observed in some hearts. Following indexes were calculated to assess the changed anatomical characteristics of the heart: the heart weight to body weight (HW/BW) ratio, the LV weight to body weight (LVW/BW) ratio and LV weight to heart weight (LVW/HW) ratio. According to the results of retrospective analysis, LVW/HW ratio – representing the LV fraction in the whole heart mass – was the only index suitable for dividing the animals into two groups. The discrimination threshold value of LVW/HW ratio (0.57) was found by analysis of ROC curve. Thus, animals with LVW/HW ratio below or equal threshold were assigned to group L and animals with the ratio above threshold to group H (LVW/HW 0.53 ± 0.03 and 0.61 ± 0.03, respectively; $p < 0.001$, Mann-Whitney U-test; $n = 8$ in each group).

Presence of the differences between the hearts from L and H groups was verified using histological analysis of myocardium performed immediately after the end of experiment. Briefly, heart tissue samples were collected from the left ventricular lateral wall, embedded in freezing medium, frozen in the liquid nitrogen, sliced on the sections (10 μm tick), dehydrated, stained by hematoxylin and eosin (both for general morphology) and Masson's trichrome (for the visualization of the extent of fibrosis), and analysed under light microscope. An example of the tissue samples from both experimental groups and the distribution of blue/red zones ratio are shown in Fig. 40. According to the results, the content of collagen differs between two groups, but the difference is not statistically significant (Mann-Whitney U-test, $\alpha = 0.05$). This is in agreement with the assumption that only slight changes in LV anatomy (in contrast to LV hypertrophy with significant changes in heart anatomy and function) are present in H group.

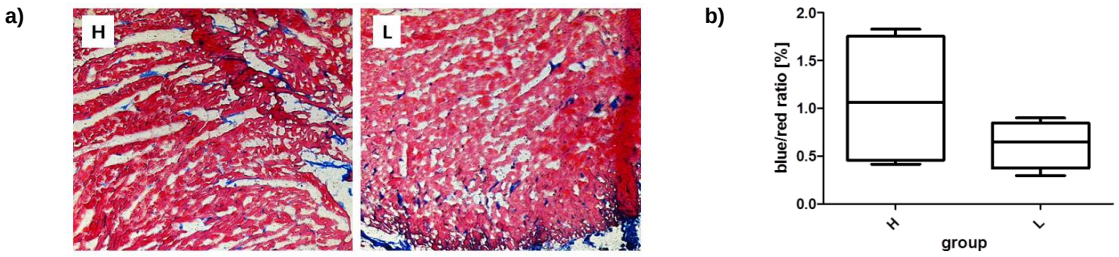

Figure 40. Results of histological analysis of myocardium tissue.
Examples of midventricular sections stained with Masson's trichrome (a) and the distribution of blue/red zones ratio (b) in hearts with low (L) and high (H) LV mass fraction.

Data acquisition

During the whole experiment, the heart was placed into the bath filled with the K-H solution and three EGs were recorded simultaneously according to the protocol from Fig. 3b. Thus, EGs were recorded from different sites of rotated heart in stabilization, whereas initial position of horizontal leads (corresponds with 0° and 90° in Fig. 12) was chosen for recording during ischemia

and reperfusion. According to the results from previous paragraph (see also [88]), this position of electrodes is suitable for monitoring the changes in EG morphology caused by global ischemia. The most important information about preparation phase of experiment, recording and processing of EG were described in previous chapter.

Electrogram parameters calculation

In order to study possible differences between both experimental groups, QRS- and ST-T-related parameters were evaluated in EGs recorded during rotation and during three repetitions of short-term global ischemia and reperfusion.

Following QRS-related parameters were analysed in each rotation position: QRS duration (QRS_D), absolute value of maximal QRS deviation (QRS_A), area under whole QRS (AUC_{QRS}), and area under positive ($+AUC_{QRS}$) and negative ($-AUC_{QRS}$) part of QRS. These parameters were also calculated from lead I and lead II EG recorded in ischemia and reperfusion.

Subsequently VCG was reconstructed for each experiment. In case of rotation session, QRS complexes from horizontal EGs at the positions -40° and 40° (Fig. 12) and corresponding EG recorded with lead III were used as Z, X and Y components of VCG, respectively. In case of ischemia and reperfusion, 3D QRS loop was reconstructed from EGs recorded in initial leads position. Following VCG-related parameters were assessed: the maximum of QRS spatial vector magnitude (L_{qrs}) and spatial angles in frontal, horizontal and sagittal planes (α_{qrs}, β_{qrs}, and γ_{qrs}, respectively).

Besides above mentioned parameters, level of ST segment at J+20 ms point (ST20) and maximal deviation of T wave (T_A) were calculated to study possible occurrence of ”pseudo-ischemic” EG patterns in stabilization period and ischemic and post-ischemic changes in ischemia/reperfusion.

Statistical analysis of data

It was found, that data are not normally distributed (Shapiro-Wilk test). The non-parametric Mann-Whitney U-test was then used to test the differences between L and H groups in following data sets: 1) EG parameters in different heart positions and VCG parameters, both calculated in stabilization, 2) EG and VCG parameters calculated from data recorded during ischemia and reperfusion, 3) parameters calculated using and without delineation outcomes. Additionally, Wilcoxon signed rank test was applied in L and H group separately in order to evaluate significant changes of all parameters at the end of each minute during ischemia and reperfusion in comparison with the values immediately before the ischemia onset. Correlation between anatomical characteristics was investigated using non-parametric Spearman’s correlation coefficient ρ. The diagnostic accuracy of different parameters at various cut-off points for the detection of the increased LV mass and also ischemia-induced EG changes was investigated by ROC curve. Se, Sp, AUCROC, and optimal cut-off point were used to quantify the accuracy. For all abovementioned tests, $p < 0.05$ was considered as significant.

4.2.3 RESULTS

Effects of LV mass fraction on EGs under non-ischemic condition

Mean courses of QRS complexes calculated for L and H group in various heart positions are shown in Fig. 41. In some positions, morphology of mean QRS evidently differs between the groups. It corresponds with the results of statistical analysis of QRS-related parameters.

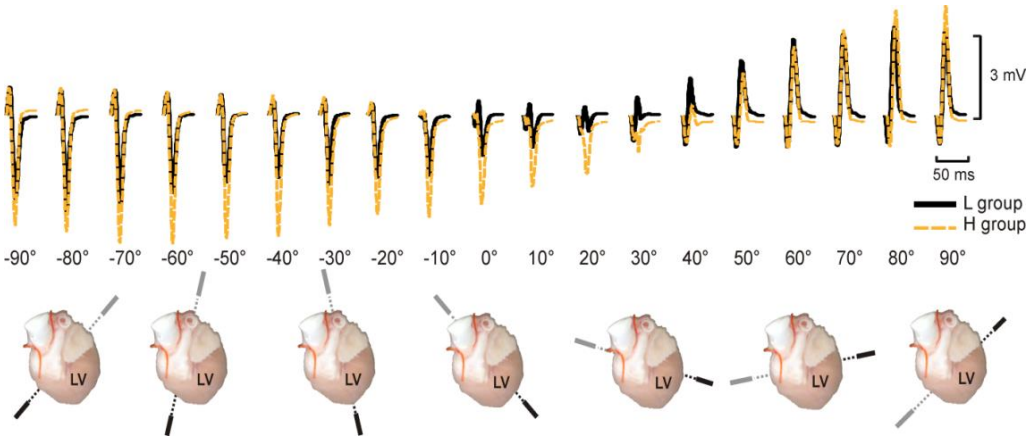

Figure 41. Averaged QRS complexes recorded in hearts with low (L) and high (H) LV mass fraction. Top views of the heart in the range from -90° to +90° illustrate the position of bipolar lead during electrogram recording (bottom). LV – left ventricle.

Significant differences between the groups were found in QRS_A in the range of <+0°, +20°> and in AUC_{QRS} in the range of <-60°, -30°> and <+10°, +20°> (see Fig. 42a,b). No significant differences were found in ST-T-related parameters. Slight deviation of ST segment was observed in H group in wide positional range (see Fig. 42c). There were no differences in polarity of T wave (see Fig. 42d).

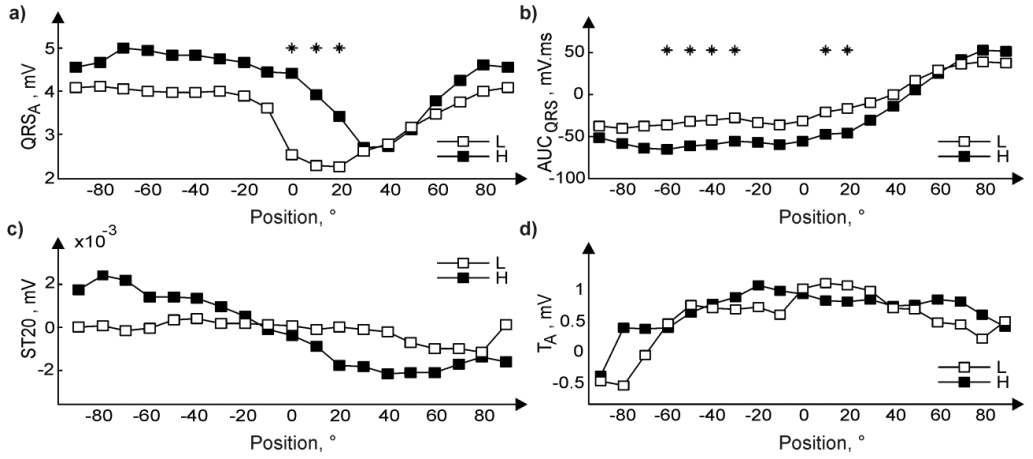

Figure 42. Median values of EG parameters recorded in hearts with low (L) and high (H) LV mass fraction. QRS_A (a), AUC_{QRS} (b), ST20 (c), and T_A (d) from electrograms in the range from -90° to 90° (* $p < 0.05$).

Mean 2D QRS loops in three planes are shown in Fig. 43. Corresponding median values of VCG parameters (for L and H group) were: 68° / 70°, 60° / 84°, 28° / 10°, and 5 mV / 6 mV for α_{qrs}, β_{qrs}, γ_{qrs}, and L_{qrs}, respectively. No significant differences were revealed in these parameters. It is in accordance with observations reported previously, where mean electrical vector of QRS in frontal plane calculated in New Zealand rabbits was located between 0°-120° and even -93° to +96° [99],[102]. It indicated that this parameter cannot be used satisfactorily for detection of vector deviation (right or left) in presence of ventricular hypertrophy.

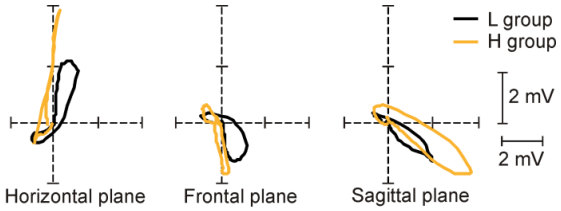

Figure 43. Mean QRS loops at horizontal, frontal, and sagittal plane calculated for hearts with low (L) and high (H) LV mass fraction.

Ability of EG parameters to detect increased LV mass fraction

The suitability of different parameters to detect increased LV mass was analysed by ROC curves. AUCROC calculated for EG parameters in different positions are shown in Fig. 44. Positions with high AUCROC (higher than 0.7, depicted with rectangles in Fig. 44) correspond with the positions, where the parameters' (AUC_{QRS}, $-AUC_{QRS}$ and QRS_A) differed significantly between L and H groups.

As seen in Fig. 45a,b, the best diagnostic accuracy of QRS_A and AUC_{QRS} indicated by the highest AUCROC was achieved in the position 0° and -30°, respectively. Corresponding accuracy characteristics for QRS_A (AUC_{QRS}) are: cut-off point 3.3 mV (-45.3 mV·ms), Se 82 % (75 %) and Sp 83 % (82 %). AUCROC, Se and Sp calculated for other parameters were significantly lower within the whole recording range (Fig. 45c,d). These findings are in accordance with the above results of statistical testing (see Fig. 42 for comparison).

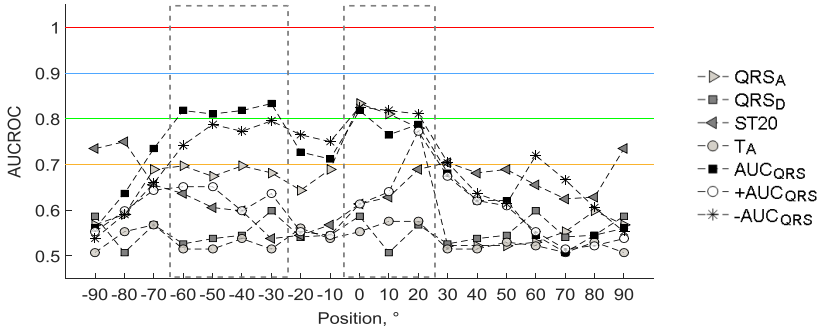

Figure 44. AUCROC for LV mass increase detection using parameters in the range from -90° to 90°.

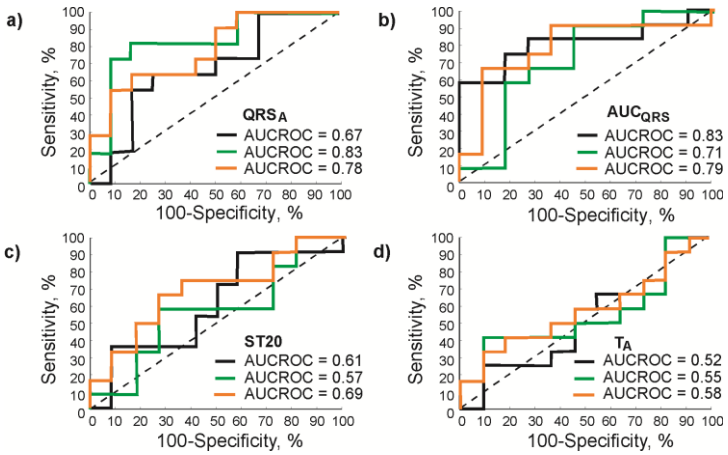

Figure 45. ROC curves of EG parameters proposed for the detection of LV mass increase.
QRS_A (a), AUC_{QRS} (b), ST20 (c), and T_A (d) calculated in the position -30°, 0°, and 20° (black, green and orange, respectively) . AUCROC – area under receiver operating characteristics curve.

Ischemia-induced changes in EGs of the hearts with low and high LV mass fraction

In this section, results of analysis of morphology changes appeared in EGs recorded in both experimental groups during ischemia-reperfusion repetitions are summarized. The values of the parameters measured at the end of each minute of ischemia were compared with those measured at the end of stabilization in L and H group separately using *paired test*. Onset of statistically significant changes of the most common EGs and VCG parameters during ischemic periods are summarized in Table 5. Results of the test are shown in Appendix H. In all cases, the increase of the parameters' values with maximal elevation at the end of ischemia was revealed. According to the results, the earliest significant changes (already in the 1st minute of ischemia) appear in values of QRS-related parameters (mostly derived from lead II) in both groups. Effects of ischemia indicated in EGs recorded with lead I appear with 1-2-minute delay; moreover, the changes in AUC-related parameters are revealed in H group 1-2 minutes earlier than in L group. In some parameters (QRS_A and $-AUC_{QRS}$), the alterations are present only in lead II data. In most QRS-related parameters, they are revealed already in the first half (the 3rd minute) of ischemia, whereas the values of ST-T-related parameters increase significantly only in the second half (the 5th minute or later) of ischemia. Regarding VCG parameters, the earliest changes (the 2nd minute of ischemia) are characteristic for β_{qrs} (both groups), whereas only sporadic alterations were observed in values of α_{qrs} and γ_{qrs} (L group) and L_{qrs} (both groups).

Generally, the character of EG morphology development through different ischemia periods is almost the same within experimental group (supported by the results of parameter slopes analysis via one-sample test, where it was found that the slopes of almost all parameters are close to zero).

Based on the results of statistical analysis, it can be nevertheless concluded that the significant changes of the most parameters appear in the second and third ischemic period with 2-minute delay in comparison with the first one. This finding is valid for both analysed groups and it is likely due to mentioned preconditioning effect, when a brief ischemic period protects the heart from more prolonged episodes of ischemia by reducing infarct size and by attenuating the incidence and severity of arrhythmias in reperfusion [117]. It also corresponds with related results (summarized by Hlaváčová M. and Olejníčková V., Masaryk University, Brno), where it was found that the hearts from H group were more susceptible to ischemic insults expressed both by higher total number of arrhythmias and their higher severity during the first and the second ischemia, whereas the effect of ischemic preconditioning was observed in the last ischemic period. This was represented with reduced total number of VPBs and their delayed onset. It may be explained by the fact, that the hearts with increased LV mass have different redox signalling in comparison with the hearts with unchanged LV. The hypothesis about different preconditioning effect due changed signalling in the heart with bigger LV mass was also supported by the results of heart rate analysis. No significant differences were found in the heart rate between L and H group. Nevertheless, the trends showed its better recovery after the second ischemia and lower decrease of heart rate in the last ischemia in group H.

Values of almost all parameters return to the control level immediately at the beginning of reperfusion. The exceptions are QRS_D and ST20 from H group, where ischemia-induced changes disappear after 3-4 minutes of perfusion recovery.

Table 5. Onset of significant ischemia-induced changes ($p < 0.05$) in EG and VCG parameters calculated for the hearts with low and high LV mass fraction.

Parameter	Onset, min		
	I1	I2	I3
QRS_A , AUC_{QRS}, and $-AUC_{QRS}$ (L&H, lead II) $+AUC_{QRS}$ (L&H, lead I)	1^{st}	3^{rd}	4^{th}
β_{qrs} (L&H)	2^{nd}	4^{th}	4^{th}
QRS_D (L&H) AUC_{QRS} (L&H, lead I)	3^{rd}	4^{th}	4^{th}
$+AUC_{QRS}$ (L, lead II)	3^{rd}	5^{th}	2^{nd}
$+AUC_{QRS}$ (H, lead II) α_{qrs} (H)	3^{rd}	5^{th}	6^{th}
ST20 and T_A (L&H, lead I) γ_{qrs} (H)	5^{th}	7^{th}	6^{th}
ST20 and T_A (H, lead II)	6^{th}	7^{th}	7^{th}
ST20 and T_A (L, lead II)	-	7^{th}	7^{th}
QRS_A and $-AUC_{QRS}$ (L&H, lead I) L_{qrs} (L&H) α_{qrs} and γ_{qrs} (L)	-	-	-

L, H – hearts with low and high LV mass fraction, respectively; I – ischemic; '-' – no significant changes

Additionally, the comparison of parameters calculated from L and H group data recorded during the ischemic and reperfusion periods was performed using *unpaired test*. Significant differences were mainly found between QRS_D calculated for L and H groups in the middle (4^{th}-7^{th} min) of ischemia. The differences were also observed in AUC_{QRS} and $+AUC_{QRS}$ (not shown) from 5^{th}-10^{th} minutes of ischemic periods. There were no differences in values of ST-T- and VCG-related parameters as well as in parameters calculated from reperfusion. In Fig. 46, the changes in distribution of values of QRS_D and AUC_{QRS} (the last was calculated from data recorded using lead I) are shown using box plots displayed at the end of each minute of corresponding experimental period.

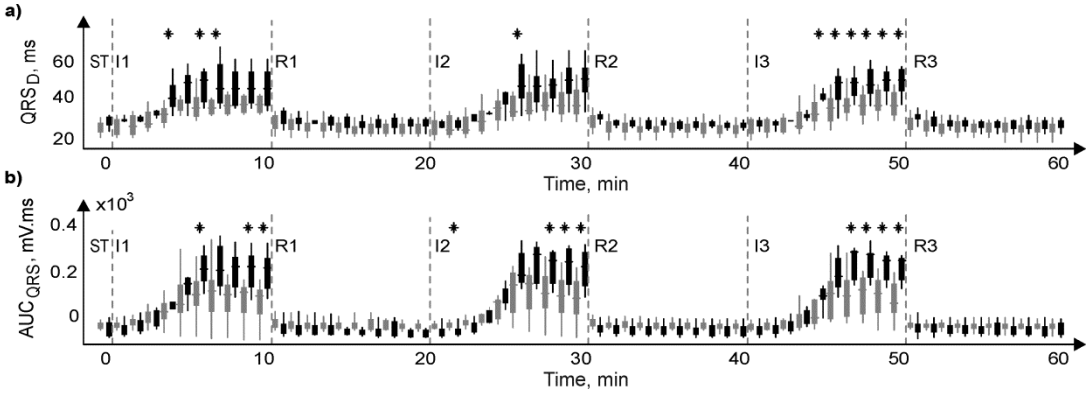

Figure 46. Distribution of QRS_D (a) and AUC_{QRS} (b) during experiments.
For the hearts with low (grey) and high (black) LV mass fraction during the end of stabilization (ST) and ischemic (I) and reperfusion I periods (* $p < 0.05$).

As in previous section, values of $-AUC_{JT}$, $AUC_{TmaxTend}R'$, $-AUC_{JT}R'$, and P_{jt} calculated using and without delineation outcomes were significantly different in the hearts with high LV mass fraction. Sporadic differences were also found in JTmax of H group during reperfusion periods.

Effect of LV mass fraction on myocardial ischemia detection

Above results of paired statistical test are in agreement with those of ROC analysis used for evaluation of overall ability of the parameters to discriminate between non-ischemic and ischemic state (for overall view of AUCROC analysis results refer to Appendix I). Distribution of AUCROC for lead II parameters (from Fig. 44) calculated for each 60 s of ischemic periods in L and H group individually is shown in Fig. 47a. From about the 4th minute of each ischemia, the median value of AUCROC is higher in H group than in L group. As in previous analysis, the delay between reaching of high AUCROC in adjacent ischemic periods is approx. 0.5-1 min. Similar AUCROC distribution was found in lead I data (not shown). Rapid return of parameters' to stabilization values corresponds with the decrease of AUCROC median from 0.72-0.76 to 0.55 during the first minute of each reperfusion (see Fig. 47b). It is evident from Fig. 47c, that the percent rate of parameters with AUCROC > 0.7 and 0.8 is almost the same in L and H group, whereas the number of parameters with AUCROC > 0.9 is higher in H group in comparison with L one (about 85 % and 35 % at the second half of the first ischemia, respectively). Both the percent of parameters with high AUCROC and the time to particular AUCROC thresholds (AUC > 0.7, 0.8, and 0.9) increase through the experiment in both groups. For lead I parameters, it is valid only for time to threshold and there is no difference in AUCROC course between L and H group. In joint parameters, there are not differences in AUCROC distribution during ischemia.

With regard to certain parameters, in case of those with delayed response to perfusion cessation (e.g. ST20), AUCROC reaches 0.8 in approx. 5th-8th minute of the first ischemia (see Fig. 47a). For parameters with the earliest response to ischemia (such as QRS_A and AUC_{QRS} derived from lead II in both groups), such a good discrimination between non-ischemic and ischemic data can be obtained in approx. 3rd-5th minute of ischemia (see Fig. 47b). In most parameters calculated in H group and in some parameters from L group, AUCROC increases up to 0.95-1 (perfect discrimination) at the end of ischemia with corresponding Se and Sp of approx. 75 % - 90 % (even 100 % in some cases) (see Fig. 47c).

The effect of LV mass on criteria and accuracy of myocardial ischemia detection can be illustrated by AUCROC, Se and Sp calculated for different experimental groups. As an example, the course of AUCROC for AUC_{QRS} calculated for L, H and joint (both groups together) group in the first ischemia is shown in Fig. 48b. It is evident, that the differences in parameter between different groups appeared in approx. 4th minute of the period (see Fig. 46b) are reflected in corresponding AUCROC. Results of ROC curve analysis for lead I AUC_{QRS} calculated at the end of ischemia in three groups are summarized in Table 6. As can be seen, the cut-off point used to distinguish between non-ischemic and ischemic data (also depicted with arrows in Fig. 48d) and corresponding AUCROC, Se and Sp (operating points with optimal cut-off value on ROC curves are also depicted with crosses in Fig. 48c) obtained in different groups are quite different. In particular, the cut-off value in H group is positive, whereas that of L group is negative. Se and Sp in H group reach maximal possible value (100 %). The cut-off value calculated for L and joint group is the same. If data from hearts with low and high LV mass fraction are analysed together, the slightly higher Se and lower Sp are obtained comparing with L group. Use of L group cut-off for detection of ischemia in the hearts with high LV mass fraction results in prominent decrease of Sp (by approx. 15 %). On the contrary, the cut-off previously calculated from H group data should not be used for ischemia detection in L group hearts because of low Se obtained in this case. Similar results were obtained for $+AUC_{QRS}$ and QRS_D.

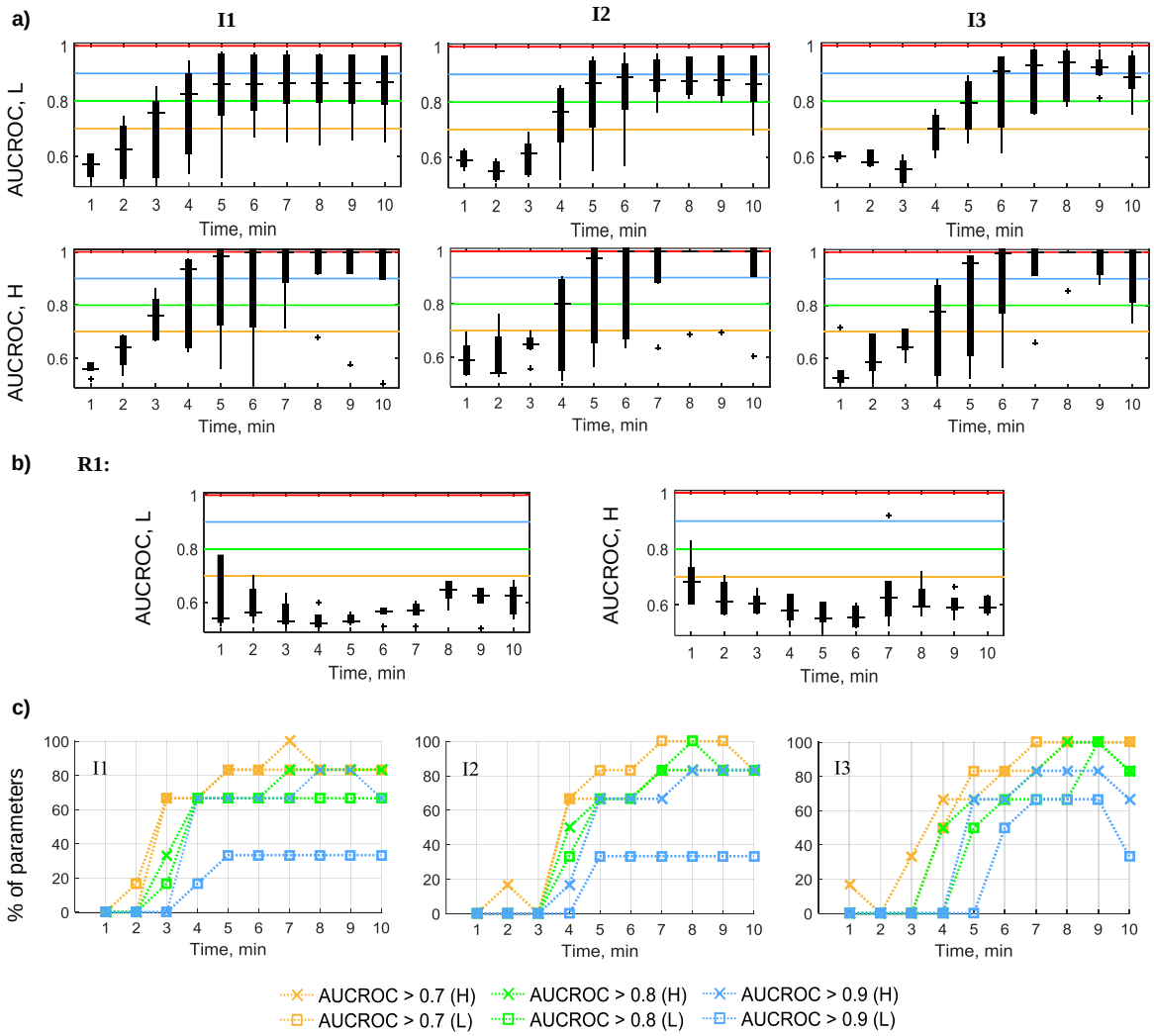

Figure 47. AUCROC of selected parameters from lead II EG.
AUCROC of parameters (N = 6) calculated during three ischemic periods (I1-I3) (a) and during the first reperfusion (R1) (b) and percentage rate of parameters with AUCROC > 0.7, 0.8, and 0.9 (c) calculated in groups with low (L) and high (H) mass fraction.

Table 6. Accuracy characteristics of myocardial ischemia detection.
For the 10th minute of the first ischemia using lead I AUC_{QRS} calculated for hearts with low (L) and high (H) LV mass fraction and both (L&H). AUCROC – area under receiver operating characteristics curve.

Data group	AUCROC, -	Sensitivity, %	Specificity, %	Cut-off, mV·ms
L	0.88	89	94	-8*
H	1	100	100	39*
L&H	0.94	94	90	-8*
L	0.88	79	98	39
H	1	100	85	-8
L&H	0.94	89	99	39

* Optimal cut-off value derived from receiver operating characteristics curve for corresponding group

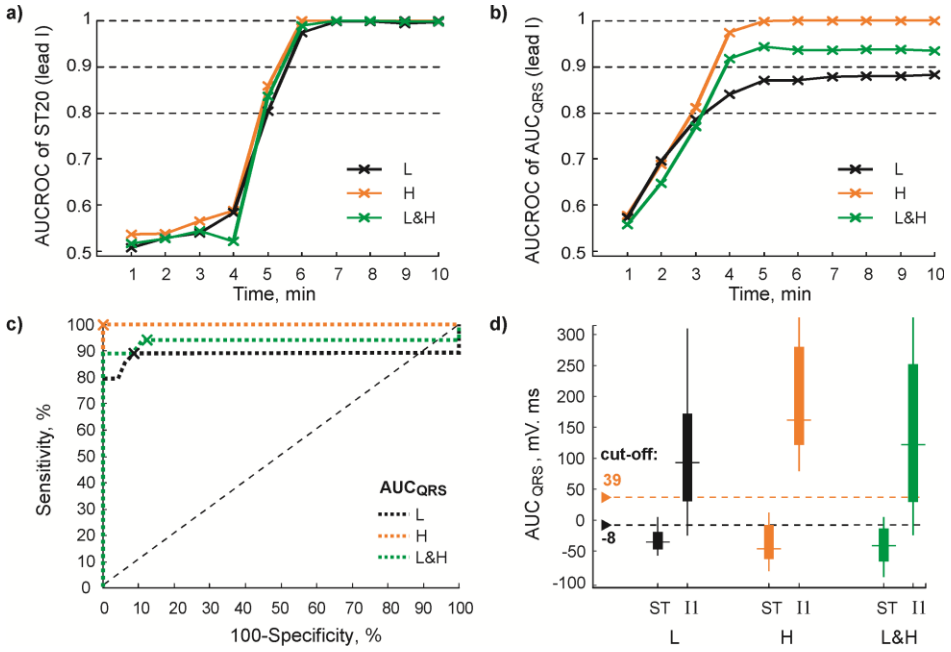

Figure 48. Discrimination ability of selected EG parameters.
AUCROC for ST20 (a) and AUC_{QRS} (b) during the 1st ischemia (I1), ROC curves for AUC_{QRS} at the end of I1 (c), distribution of AUC_{QRS} in stabilization (ST) and at the end of I1 and discriminating cut-off values (see text for details). L, H, L&H – hearts with low and high LV mass fraction and united group, respectively.

4.2.4 DISCUSSION

Evaluation of anatomical characteristics of the heart

In human, LV mass assessment is generally based on evaluation of LV volume parameters measured noninvasively by echocardiographic or magnetic resonance techniques [118]. Due to large inter-individual differences in body size and due to its close relation to LV mass, various formulas have been proposed for LV mass normalization. For this purpose, various parameters are used, such as body weight, body surface area, body mass index, or height [118]-[120]. However, none of these indexes is optimal. Associations between LV mass and various anatomical parameters and/or concomitant cardiac disorders should be taken into consideration when choosing an appropriate normalization method [118],[119].

In animal studies, LV mass and other anatomical parameters can be measured directly. LVW/BW ratio is frequently used to assess the LV mass increase [121]-[124]. In present study, the LVW/HW ratio was additionally proposed for evaluation of the mass fraction of LV in the whole heart mass. This ratio seems to be useful to assess the slight increase of LV mass which cannot be easily detected using abovementioned indexes. In the model used, LVW/BW ratio and LVW/HW ratio measured in hearts with high LV mass were higher on average by 5 % and 15 %, respectively, in comparison with the hearts with low LV mass. Other authors reported increase of LVW/BW ratio (comparing to sham-operated animals) by 20-30 % in different rabbit models of induced LV hypertrophy [122]-[124]. It is obvious, that the differences in this index between the hearts with unchanged and spontaneously increased LV mass obtained in present study are not as significant as in above observations. This is in agreement with the results of statistical analysis, according to which the LVW/HW ratio is the only index affected with slight increase of LV mass. Normalization of LVW by HW instead of BW seems to be reasonable because of high correlation

(Spearman's ρ) between HW and BW (0.72, $p < 0.05$), LVW and BW (0.86, $p < 0.05$) and LVW and HW (0.92, $p < 0.01$).

Reliability of EG recording in various heart positions

The dramatic worsening of detection of ischemia and LV hypertrophy caused by variation in the positioning of chest electrodes has been reported in human [125]. Therefore, as in previous chapter, the possible effect of mutual orientation of the heart and electrodes on EG patterns was verified in L and H groups. According to the results in both animal groups, no significant pseudo-ischemic alterations were found in EGs recorded during stabilization. Small alterations in ST20 in boundary LV area of H group data were negligible in comparison with ischemia-induced ST alterations observed in both groups. Thus, detection of increased LV mass or ischemia in this data should not be affected with the heart and electrodes orientation.

Assessment of increased LV mass by EG morphology analysis

This study reports that even slight change of LV size can be assessed by analysis of data derived from EG simply recorded with orthogonal electrode system. It is known that the anatomical changes of the heart such as LV hypertrophy produce the changes in ECG morphology including increased amplitude and duration of QRS, the left axis deviation, and QRS patterns associated with the defects of intraventricular conduction [112],[126],[127]. Despite relatively low Se of ECG-based LV hypertrophy detection (in the range of 40-60 %), electrocardiography is still frequently used for LV hypertrophy screening due to its low cost, easy performance and wide availability [128],[129]. Many electrocardiographic indexes have been proposed for diagnosis of LV hypertrophy in human. Most of them are based on the so called QRS voltage criteria [112],[129]. Thus, diagnostic performance of these indexes particularly depends on the precision of QRS complexes delineation. However, in experimental data, the detailed delineation of QRS is challenging task, especially in case of EG recorded under variable conditions [130],[131]. Moreover, standard indexes used for LV hypertrophy manifestation in human cannot be easily applied to experimental data due to lack of diagnostic criteria specific for different species. Considering the fact that various rabbit models of LV hypertrophy appropriate for studying the congestive heart failure, regional ischemia, LV hypertrophy regression and others, have been reported (e.g. [121],[123],[124]), it would be interesting to investigate this area in detail.

According to the results achieved in this study, easily calculated EG parameters (without the need of complete delineation of all parts of QRS complex) can be successfully used for detection of increased LV mass. As in human [112], one of such parameters is QRS_A. Nevertheless, AUC_{QRS} seems to be the most sensitive to the changes in electrical activity caused by LV mass increase (see Fig. 45). This is probably due to the method of parameter calculation, where all peaks within the whole QRS complex are taken into account including their polarity. As a result, minor changes in QRS morphology may cause significant change of AUC_{QRS} value (compare graphs in Fig. 41 and Fig. 42) that allows detecting increased LV mass with relatively high Se and Sp (both approx. 82 %). Above founding is in agreement with the results of study on 12-lead standard ECG recorded in healthy subjects and patients with LV hypertrophy, where voltage-duration product and true time-voltage QRS area were used instead of standard QRS voltages and duration to calculate Sokolow-Lyon criteria and the 12-lead sum of voltage criteria [132]. The diagnostic accuracy of each approach was then examined. Significant improvement of Se was achieved in case of criteria based on QRS area: 76 % for the 12-lead sum area and 65 % for Sokolow-Lyon area vs. 54 % for voltage-duration product and approx. 45 % for simple voltage criteria.

It should be noted that areas with high accuracy of increased LV mass detection in rabbit isolated heart electrogram (<-60°,-30°> and <0°, 20°>) correspond roughly with areas usually used for LV hypertrophy detection in human ECG (precordial leads V1, V2, V5, and V6 [112]).

Detection of myocardial ischemia in EGs from the hearts with low and high LV mass fraction

According to ESC/ACCF/AHA/WHF, the earliest ischemia-induced changes in human are reflected in ECG on T wave and ST segment and the changes in QRS complex are generally associated with severe myocardial ischemia (eventually myocardial infarction) [92]. These changes are linked to the region of myocardial ischemia and, thus, can be used to its localizing. In the present model of short-term global myocardial ischemia, the earliest ischemia-induced changes are associated with electrical activity during ventricular depolarisation. In both experimental groups, it is mainly reflected in the values of QRS-related parameters extracted from EG recorded with lead oriented approximately through the anterolateral wall of LV (lead II at initial position in Fig. 4, middle). Some data from this area, however, seem to be sensitive to LV mass increase, too (see Fig. 42a,b). If electrophysiological effects of LV mass increase on investigated phenomena are not desired, only EG and/or VCG parameters resistant to such effects should be included in the study (such as ST20, see Fig. 48a). Other possible approach is use of the data recorded from boundary LV areas (lead I in initial position in Fig. 4, middle), where no significant effect of LV mass on the parameters was found (see Fig. 42). However, ischemia-induced changes in such case can be revealed with some time delay compared to previous one (see Table 5). Thus, appropriate parameters and/or recording area should be carefully chosen depending on the study goal.

It is worth mentioning, that even recording with leads ‘insensitive’ to LV mass increase in stabilization period does not ensure that EG alterations indicated in ischemia are associated merely with this pathological condition. The influence of LV anatomical change on the heart electrical activity may appear during ischemia only, which can be seen e.g. on QRS_D and AUC_{QRS} extracted from lead I EG (see Fig. 46), where significant difference in parameters between L and H groups was revealed in the middle of ischemia. This may be explained by certain electrical dyssynchrony based on subtle metabolic changes in slightly increased LV. According to the results of ROC analysis, above phenomenon may have an impact on ischemia assessment, where the detection accuracy depends directly on discrimination threshold. Particularly, if no attention is paid to LV mass and AUC_{QRS} values from L and H groups are analysed together, than resulting Se overestimates by 5 % and underestimates by 6 % that obtained in L and H group, when the ‘joint’ cut-off value is used in all three cases (see Table 6). On the other hand, Sp calculated for joint group underestimates this index for L group by 4 % and overestimates that of H group by 5 %. Use of threshold ‘adapted’ for H group to detect ischemia in the hearts with high LV mass fraction results in excellent Sp (i.e. 100 %). Thus, the overall decrease of Sp due to unsuitable cut-off value reaches 15 % in this case. The source of such discrepancies is illustrated in Fig. 48d, where distributions of the parameter in different groups and corresponding thresholds are shown. It is obvious, that use of cut-off calculated from another group data results in increase of false positive or false negative detections and, consequently, in decrease of Sp or Se (or both). Thus, the cut-off value should be carefully set with regard to the type of analysed data. It is generally in agreement with the studies, where increase of false positive detections due to neglecting of various patient-related factors (e.g. gender, age, LV hypertrophy, etc.) affecting ECG morphology at rest was revealed and adaptation (arising) of ST-segment threshold was suggested to improve ischemia detection accuracy [92],[93],[115]. Analysis of anatomical peculiarities of the heart may help to reduce number of incorrect detections and avoid confusions in results interpretation.

4.3 EFFECTS OF VOLTAGE-SENSITIVE DYE DI-4-ANEPPS ON ELECTROGRAM UNDER NORMAL AND ISCHEMIC CONDITIONS

This chapter is focused on the evaluation of electrophysiological effects of voltage-sensitive dye di-4-ANEPPS on rabbit isolated heart under non-ischemic and ischemic conditions. Some preliminary observations and results related to optical recording method via fluorescent dyes were reported as the conference manuscripts ([133]-[136]) and journal papers ([67],[137]), respectively. The most important results were summarized in article which is under consideration by the journal (Ronzhina et al.).

4.3.1 BACKGROUND

As has been mentioned above, AP is often used in experimental studies to monitor electrical activity of the myocardium. Cardiac AP is generally recorded by two methods. The conventional one – with microelectrodes – is the gold standard for measuring electrical signals on the cellular level [138]. However, this method has one significant disadvantage: insertion of the electrode into the cell leads to its membrane disruption and may negatively affect cell function. Moreover, the procedure of electrode application is rather difficult. Thus, the experimental results depend on the experience and skills of the investigator. Optical method uses fluorescence properties of special chemical compounds, so called fluorescent dyes. Fluorescence of VSD molecules bound on the cell membrane is proportional to its transmembrane potential. Briefly, the procedure of AP measurement using VSD consists of: a) loading the heart with the for a definite time; b) washing the heart with perfusion solution to remove the unbound molecules; c) exposing the heart to excitation light (with halogen lamp, xenon/mercury arc lamp, LED or laser); d) detecting the emission light with some photodetectors (mostly photodiodes, photodiode arrays, photomultiplier tubes, and CCD cameras) [3],[60],[62],[67],[139]. Various fluorescent dyes with different properties are commercially available. The most commonly used VSDs are RH-237 and di-4-ANEPPS. Di-4-ANEPPS allows reaching a time resolution better than 1 ms [3] and exhibits changes in fluorescence of up to 10% per 100 mV [140]. VSD based approach allows noninvasive record of AP from a larger area of heart surface with high spatial resolution.

Despite such benefits, the application scale of optical method is generally limited because of the properties of available fluorescent dyes [67]. One of the most important disadvantages of VSDs is their possible effects on cardiac electrophysiology. Many authors reported various effects of di-4-ANEPPS in different experimental models, among which are the following: a) increasing contractility of cardiac muscle in isolated rabbit heart and human atrial preparation [141]; b) AP duration prolongation in guinea pig isolated ventricle myocytes [142] and in LV midmyocardial myocytes of beagle dog [143]; c) QRS duration prolongation [144], decrease of heart rate [145], and slowing cardiac impulse propagation [146] in guinea pig isolated heart; d) PQ interval prolongation, transient blocks of atrioventricular (AV) conduction, decrease of perfusion pressure due to dilation of coronary arteries [147], decrease of heart rate and slight prolongation of QRS and QTc duration [148] in rat isolated heart; e) vasoconstriction [149] and increase of total activation time [150] in mouse isolated heart. Some above effects are dose dependent [146] and some seem to be caused by phototoxic effect of the dye [143] or by other mechanisms associated with the binding of the dye to the cardiac cell membrane [142]. The most of above observations are the secondary outcomes obtained during experiments and there are only a few studies primarily focused on the evaluation of undesirable effects of VSD.

From above overview, it is evident that the response of myocardium to staining with di-4-ANEPPS is described mainly for small rodents such as mouse, rat and guinea pig. Nevertheless, as was mentioned above, the rabbit model is more suitable for cardiovascular studies due to the high similarity with human in cardiac electrophysiology parameters. One of the areas, where this model is intensively used, is the investigation of myocardial ischemia, infarction and ischemia-related arrhythmia, when the electrical activity is evaluated by conventional or/and optical method (e.g. [3],[5],[48],[49],[51],[61],[63]). In the second approach, unfortunately, the possible side effects of VSD are only briefly discussed or not addressed at all.

With regard to the results obtained for other species and some preliminary observations, various electrophysiological effects can be expected in case of rabbit myocardium. This chapter, therefore, introduces the results of electrical activity analysis in experiments on rabbit isolated heart after administration of di-4-ANEPPS.

4.3.2 METHODS

Data acquisition

The isolated hearts of twenty New Zealand rabbits (both sexes, average weight 2.65 ± 0.67 kg) were included in the study. Experiments were carried out according to two different protocols. In the first type of experiments (Fig. 3, c, top, n = 9), VSD di-4-ANEPPS (di-4-amino-naphthyl-ethenylparidiunium, Molecular Probes, Inc., USA) was added to the perfusing solution to the final concentration of 2 μmol/l (stock solution either in DMSO or DMF, 2 mmol/l) for recording AP from the middle of LV by optical method simultaneously with EG. Such a "slow" staining allows use low-concentrate dye solution and consequently reduces possible undesired effects of the dye on the heart. In contrast to frequently used injecting the dye as a bolus with a high concentration, "slow" method enables obtaining the preparation with quite high persistence of the dye in the heart tissue and, therefore, recording high-quality data (i.e. with quite high signal-to-noise ratio of AP) even in case of long-term experiments [151]. The recording of optical AP was performed in the dark to eliminate potential phototoxic effects of the dye.

The second protocol (Fig. 3c, bottom, n = 11) did not include VSD administration; thus, only EGs were recorded. In both cases, three consecutive periods of ischemia and reperfusion (each 10 min long) were carried out. Choice of control experimental group will be addressed more detailed in Discussion.

Electrogram parameters calculation

EG and VCG based parameters were calculated from data recorded during the whole experiment according to the procedure mentioned above. The duration of P wave (P_D), PQ interval (PQ_D) and ratio between QT and RR duration (QT/RR) were additionally derived from data recorded before ischemia. According to above results, many of the selected parameters are suitable for ischemia assessment. Furthermore, the changes in values of some parameters (such as QRS, PQ and QRS duration and other) induced by di-4-ANEPPS administration were observed by other authors in studies on other species (see above). Therefore, they were included in present study to verify potential effects of this VSD on rabbit myocardium.

Arrhythmia evaluation

Various types of arrhythmias such as junctional rhythm (NOD), and atrioventricular block (AVB) of the 2nd and 3rd degree were evaluated manually through the whole data set. P_D, PQ_D and

QRS_D were used to monitor the possible VSD-induced slowing of impulse conduction through the atria, atrioventricular (AV) node and the ventricles, respectively. QT_D was analysed to evaluate possible direct proarrhythmic effect of di-4-ANEPPS. Finally, ventricular premature beats (VPBs) and supraventricular extrasystols (SVES) were counted within particular experimental periods.

Whole-cell patch clamp experiments

It is well known that Ca^{2+} influx into the cell during '0' phase of AP (Fig. 1b) triggers the voltage-gated calcium channels in the cardiac sarcolemma which, consequently, induces the release of Ca^{2+} from the sarcoplasmic reticulum and causes muscle contraction [6]. Blocking of sodium current (I_{Na}) results in slow depolarization, reduced conduction velocity through the ventricles and widening of QRS interval. Experiments focused on the verification of the effects of di-4-ANEPPS (of 2 μmol/ml concentration) on sodium channels were carried out by team from collaborating institution (Institute of Molecular Physiology and Genetics, Slovak Academy of Sciences). Briefly, differentiated NG108-15 cells with sodium channels expression similar to those in cardiac myocytes were included in the study. Two experimental protocols – with acute application of the dye and 30 min long incubation of the cell in presence of this VSD – were used to test the response of sodium channels to the dye. Possible effect of DMSO (commonly used for dye dilution) was also evaluated in dye-free experiments. I_{Na} was measured in the whole-cell patch clamp configuration.

Statistical analysis

The statistical analysis was carried out for data recorded during two main parts of experimental protocol individually. The first part consisted of heart stabilization, loading with VSD and washout in case of the experiments with di-4-ANEPPS administration and the long stabilization period otherwise. The second part included three ischemia-reperfusion repetitions in both data groups.

Mean values calculated using twenty last samples of parameters at the end of each experimental period were used as an input for comparison tests. Additionally, Δ and the slope values were calculated as was mentioned previously.

The normality and homoscedasticity (where data from different groups have the same standard deviation) of different groups data were checked with Shapiro-Wilk test and Levene's test, respectively. It was confirmed, that both assumptions are not precisely hold. Wilcoxon signed rank paired test was applied to compare the parameters' values calculated at different experimental periods within one particular experimental group (i.e. stained or non-stained hearts). The significance of the slope values (comparing to the zero level) was verified via one-sample signed rank test. Unpaired Mann-Whitney U-test was used for comparison of data (namely, the parameters' values, their Δ and the slopes and the number of VPBs) calculated at corresponding periods from experiments with and without VSD administration. The above mentioned methods are nonparametric, thus they can be applied to unbalanced design (i.e. sample sizes of different groups are not the same, such as in case of data measured for experiments with and without VSD), when the assumption of normality of data distribution and homoscedasticity are not hold.

One-way analysis of variance (ANOVA) followed by Tukey test for pairwise multiple comparisons were performed to verify group statistical differences in patch-clamp data.

Finally, ROC analysis was performed as in previous sections to describe the capacity of the parameters to detect ischemic changes in both groups and, consequently, to prove the suitability of using VSD di-4-ANEPPS in study of ischemia in present animal model. ROC curves were

constructed for data from each minute of ischemia separately (where non-ischemic part of the set included samples from the end of washout or stabilization period for stained and non-stained hearts, respectively) for more detailed analysis of the parameters discrimination ability in different phases of ischemia. Additionally, the same analysis was carried out on ROC curve calculated from the whole ischemic period to estimate overall (and, consequently, less optimistic) discrimination ability of particular parameters. In all tests, p-value less than 0.05 was considered statistically significant.

4.3.3 RESULTS

Electrophysiological effects associated with dye loading

Changes in cardiac impulse conduction

Impact of di-4-ANNEPS to cardiac impulse conduction through atria, AV node and cardiac ventricles during dye loading and washout periods was evaluated by analysis of interval characteristics of EGs. Distribution of P wave, PQ interval and QRS complex durations during the first part of experimental protocols is shown in Fig. 49. In the non-stained hearts, there were no significant alterations in EG parameters compared to the end of 20th minute of stabilization (paired test). On the contrary, significant increase (transient in case of P_D and PQ_D and sustained in case of QRS_D) was observed in parameters from stained hearts. From comparison of both groups, it is evident that di-4-ANEPPS has no significant, long-term effect on the AP conduction through the atria and AV node. Though some increase of P_D and PQ_D in stained hearts can be seen, the significant differences in parameters between two groups were only sporadically observed in washout and dye loading period, respectively. QRS of stained hearts was significantly prolonged from approx. the 13th minute of dye loading. These changes persisted till the end of washout.

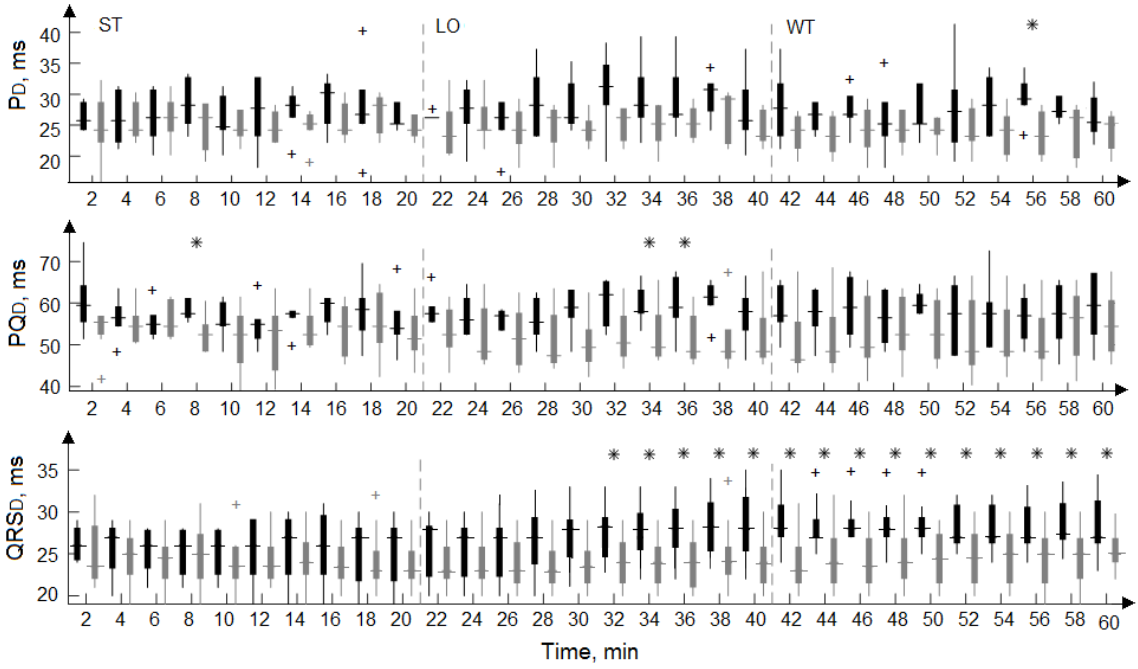

Figure 49. Duration of P wave, PQ interval and QRS complex in stained and non-stained hearts. Experiments with (black) and without (grey) di-4-ANEPPS administration. ST, LO, WT – stabilization, dye loading and washout, respectively. * for $p < 0.05$ (Mann-Whitney U-test). Data from every second minute of the period are shown.

Distribution of RR and QT interval duration is shown in Fig. 50 (top and middle, respectively). As in previous case, parameters computed in loading and washout vary from those measured at the end of stabilization in stained group only (according to the results of paired test, not shown here). It corresponds with the results of unpaired test, where the significant differences in RR and QT_D were found from the beginning of loading till the end of washout.

QT/RR ratio was additionally computed to evaluate the potential change in relation between QT_D and RR. As seen in Fig. 50 (bottom), QT/RR decreases from the loading till the end of washout in stained hearts. It, nevertheless, cannot be interpreted as a sign of direct VSD pro-arrhythmic effect on the myocardium. This phenomenon is most probably due to the changes in RR only, as illustrated in Fig. 51, where differences in QT_D and RR between adjacent minutes of loading and washout (i.e. approximation of the first derivative of these two parameters) are shown for both experimental groups. It is evident, that RR is changed continually during the whole period, whereas QT_D is quite stable excepting the first minute of dye loading. Obviously, both parameters are much more stable in control group than in stained hearts.

The values of parameters at the end of stabilization, dye loading and washout and the differences between last two periods and stabilization are summarized in Table 7. Besides more prominent changes in mean values of the parameters, higher variability is characteristic for stained hearts parameters in comparison with control group (see Δlo and Δwt in table).

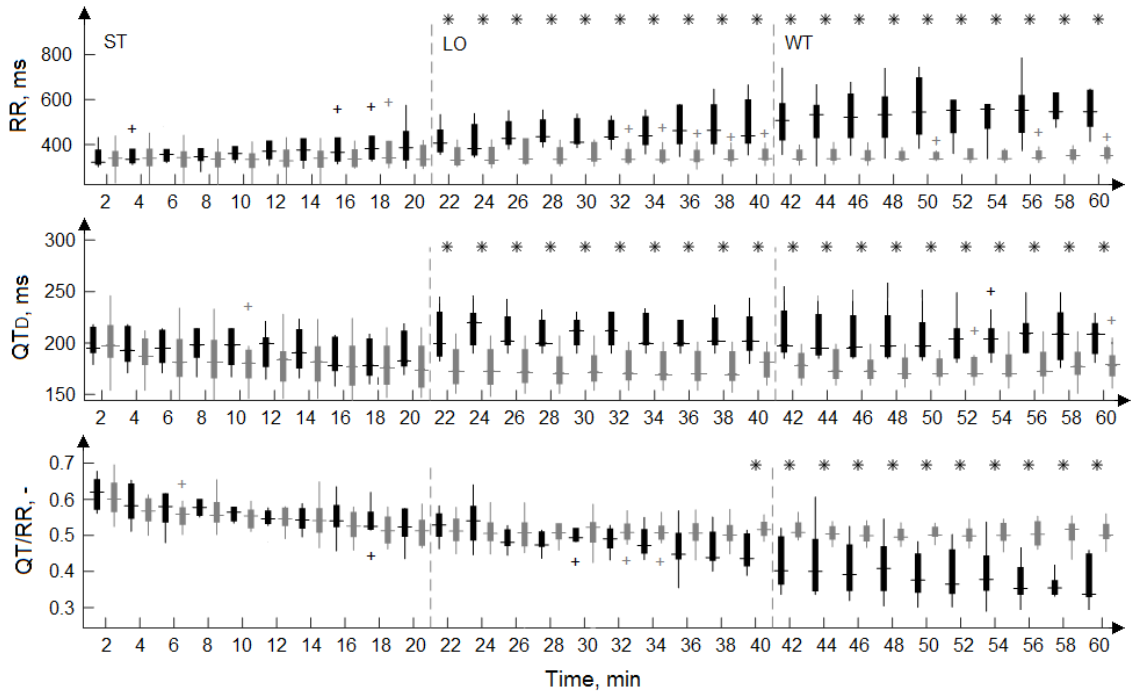

Figure 50. Duration of RR and QT interval and the ratio between them in stained and non-stained hearts. Experiments with (black) and without (grey) di-4-ANEPPS administration. ST, LO, WT – stabilization, dye loading and washout, respectively. * for $p < 0.05$ (Mann-Whitney U-test). Data from every second minute of the period are shown.

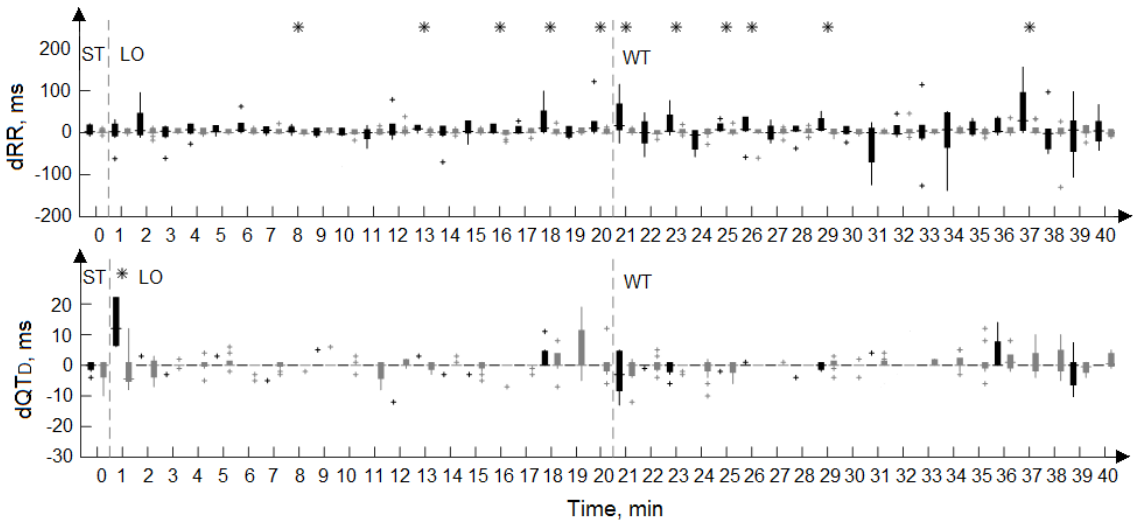

Figure 51. Distribution of differences between adjacent minutes for RR and QT interval duration. Calculated from the end of stabilization (ST), through the whole dye loading (LO) till the end of washout (WT) in two experimental groups. * for $p < 0.05$ (Mann-Whitney U-test).

Table 7. Main interval characteristics in two experimental groups.
Calculated at the end of stabilization (ST), dye loading (LO) and washout (WT) and differences between parameters derived at the end of loading or washout and the end of stabilization (Δlo and Δwt, respectively) in two experimental groups. Expressed as mean ± SD.

Parameter		ST	LO	WT	Δlo	Δwt
QRS_D	N	24.2 ± 4.2	25.1 ± 2.9	24.1 ± 3.2	-0.08 ± 2.1	0.9 ± 2.2
[ms]	S	25.1 ± 3.9	28.6 ± 4.6	27.8 ± 5.2	2.6 ± 3.2	3.4 ± 3.4*
RR	N	344.1 ± 46	358.8 ± 33	352.5 ± 41.39	8.4 ± 25.9	14.8 ± 45.1
[ms]	S	397.8 ± 96	582.1 ± 170	485.7 ± 116.3	87.9 ± 59.4*	184.4 ± 121*
QT_D	N	175.3 ± 21.9	181 ± 20.1	179.1 ± 13.7	4.1 ± 17.6	2.16 ± 18.32
[ms]	S	210.6 ± 43.4	204 ± 17.6	214.9 ± 35	9.3 ± 34	1.6 ± 29.9
QT/RR	N	0.53 ± 0.04	0.50 ± 0.03	0.51 ± 0.03	-0.0005 ± 0.03	-0.007 ± 0.02
[-]	S	0.54 ± 0.03	0.37 ± 0.08	0.45 ± 0.05	-0.09 ± 0.07*	-0.17 ± 0.08*

N, S – non-stained and stained hearts, respectively; * $p < 0.05$ for one-sample Wilcoxon signed-rank test

Arrhythmia incidence

Percentage duration of different types of cardiac rhythm regarding the total duration of particular experimental periods is shown in Fig. 52. In stabilization, none pathological episode was found in both groups. Short-term episodes of junctional rhythm (of total duration about 5 %) were detected during loading of the hearts with the dye. In washout, this type of arrhythmia was quite frequent (about 16 %).

AVB and SVES were only sporadically present in both experimental groups. VPBs were mostly observed at the beginning of stabilization, which is mainly due to manipulations with the heart during preparation. In experiments with the dye, insignificant increase of VPBs number was observed during washout (from 2-3 in dye loading up to 3-5 episodes in washout).

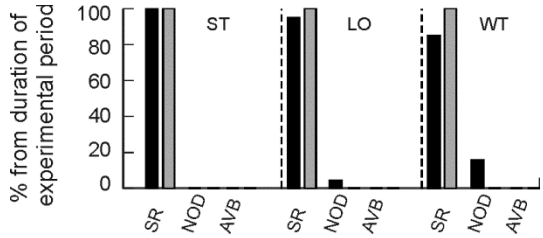

Figure 52. Distribution of most frequently observed types of cardiac rhythm in electrograms. Expressed as a percentage of total duration of corresponding experimental period in experiments with (black) and without (grey) di-4-ANEPPS administration. ST – stabilization; LO – dye loading; WT – washout; SR – normal sinus rhythm; NOD – junctional rhythm; AVB – atrioventricular block of the 2nd and 3rd degree.

Electrogram morphology and VCG parameters

Significant sustained increase of EG (mostly in both horizontal leads) and VCG parameters such as $AUC_{TmaxTend}$, $+AUC_{JT}$, AUC_{QRST}', AUC_{QRS}', AUC_{JT}', AUC_{JTmax}', $AUC_{TmaxTend}$', $AUC_{TmaxTend}R$', Lqrs, $D^{c}_{jt}xz$ was obtained during dye loading in stained hearts. In most cases, this change persisted during the first half of washout. *D* and angle parameters φ and β_{qrs} decreased significantly during loading and washout, respectively. Sporadic changes appeared in values of AUC_{QRS} (lead I), JTmax (both leads), and $-AUC_{JT}$ (lead II) during dye loading and washout. Parameters calculated for non-stained hearts remained stable from the end of stabilization till the end of washout. As a result, significant differences between experimental groups during loading and washout corresponded with time instances, where above changes were present in stained hearts. All mentioned changes disappeared by the end of washout.

Effect on sodium channels of differentiated NG-108-15 cells

In case of acute dye application, current density measured in the peak of I-V relation did not change (not shown here). On the contrary, consistent inhibition of sodium current density was observed at whole range of membrane voltages, if cells were incubated for 30 minutes in the presence of di-4-ANEPPS (see Fig. 53). No alterations of the sodium current were found in case of dye-free experiments with acute and slow application of DMSO.

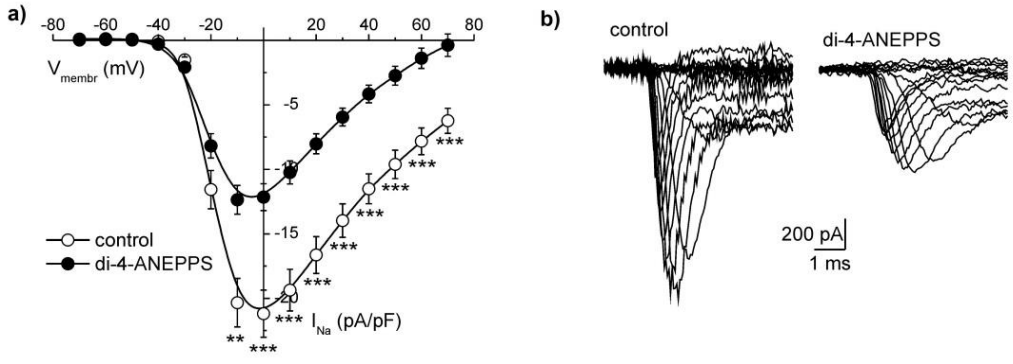

Figure 53. Results of patch clamp analysis of sodium channels in differentiated cells. Averaged current-voltage relations for sodium current recorded under the control conditions (○; n=27) or after 30 min long incubation of cells in the presence of 2 μM di-4-ANEPPS (●; n=31). Solid lines represent B-spline fit to the experimental data. ** - $p < 0.01$, *** - $p < 0.001$. b) Representative examples of current traces recorded under the control conditions or after 30 min long incubation of cells in the presence of 2 μM di-4-ANEPPS.

Repeated short global ischemia episodes in both experimental groups

Changes in cardiac impulse conduction

Onsets of significant changes observed in main interval characteristics calculated during three ischemic periods relative to the end of stabilization are summarized in Table 8. As seen, RR interval in stained hearts altered earlier in comparison with control group. The changes courses in QRS_D were similar in both groups, whereas QT_D revealed persistent significant changes in non-stained hearts only.

Table 8. Onset of significant ischemia-induced changes ($p < 0.05$, Wilcoxon signed-rank test) in EG and VCG parameters from experiments with and without di-4-ANEPPS administration.

Parameter	Onset, min					
	Non-stained hearts			Stained hearts		
	I1	I2	I3	I1	I2	I3
RR	4^{th}	2^{nd}	1^{st}	1^{st}	1^{st}	5^{th}
QRS_D	3^{rd}	4^{th}	4^{th}	3^{rd}	4^{th}	5^{th}
QT_D	6^{th}	7^{th}	8^{th}	-	tr	tr

I – ischemia; 'tr' – transient changes; '-' – no significant changes

Distributions of the parameters calculated in both experimental groups during three ischemia-reperfusion repetitions are illustrated in Fig. 54a,c (top). It is evident from the box plots and above results that significant differences between stained and non-stained hearts data – especially present in control and reperfusion – are likely due to the offset in values appeared in stained hearts before ischemia (direct and non-direct effects of the dye). The character of the parameters courses is very similar in both groups. To assess possible dye effects on the heart in ischemia and reperfusion regardless the changes appeared under non-ischemic condition, the same statistical test was applied on Δ values (calculated by subtracting value derived at the end of stabilization from corresponding values obtained for other experimental periods) of the parameters. Distributions of such corrected data are shown in Fig. 54a,c (bottom). The correction leads to diminishing (especially in reperfusion periods) or, on the contrary, emphasizing (in ischemia) of some differences between two groups. In QRS_D, the combination of both phenomena was observed; QRS prolongation in the middle of ischemia in non-stained hearts was higher (significantly in the first and second ischemia and non-significantly in the third one) than in hearts from the second group. The differences presented in RR and QT_D throughout whole experiment were almost completely eliminated by the correction; the magnitude of the parameters' changes relative to their non-ischemic level was the same for experiments with and without VSD administration.

Arrhythmia incidence

Percentage duration of different types of cardiac rhythm regarding the total duration of particular ischemic and reperfusion periods is shown in Fig. 55. In both groups, the incidence of arrhythmias was generally more prominent during ischemia-reperfusion repetitions than in previous experimental periods (see above). Moreover, arrhythmia episodes were more frequent in stained hearts as compared to the control group, where in approx. half of experiments, only normal sinus rhythm was detected throughout the whole time period. In experiments with dye administration, about 90 % and 70 % of ischemic and reperfusion periods, respectively, was represented with sinus rhythm and the most frequent pathology found was junctional rhythm (up to 7 % and 25 % in

ischemia and reperfusion, respectively). AVBs and SVES were only sporadically presented in both groups.

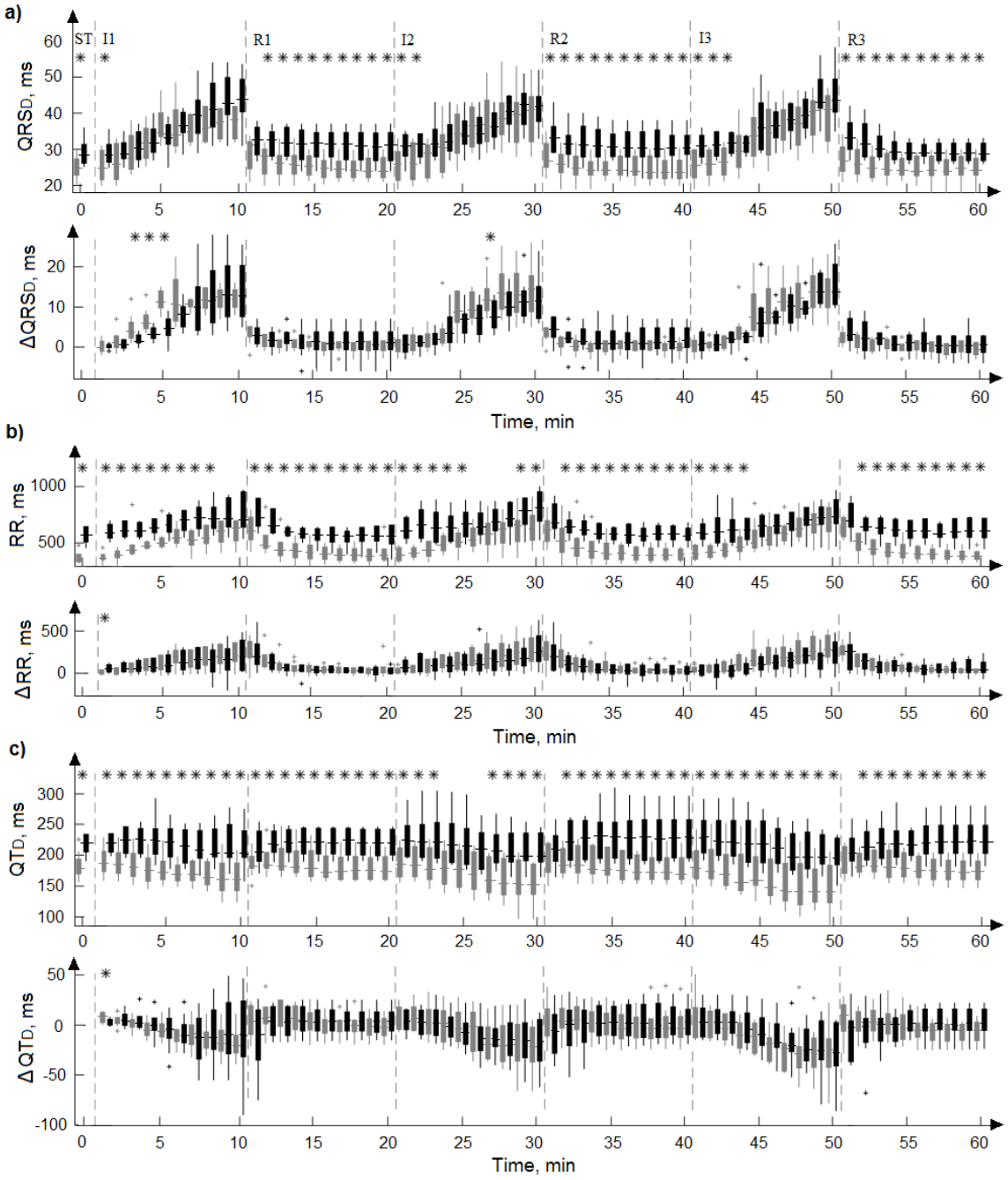

Figure 54. Main interval EG characteristics from stained (black) and non-stained (grey) hearts. Calculated for each minute (mean value) at the end of stabilization (ST) and during three ischemic (I) and reperfusion I periods: QRS, RR, and QT interval durations (top part of a, b and c, respectively) and difference (Δ) between actual value and value from the end of ST (bottom part of a, b and c, respectively).
* for $p < 0.05$ (Mann-Whitney U-test).

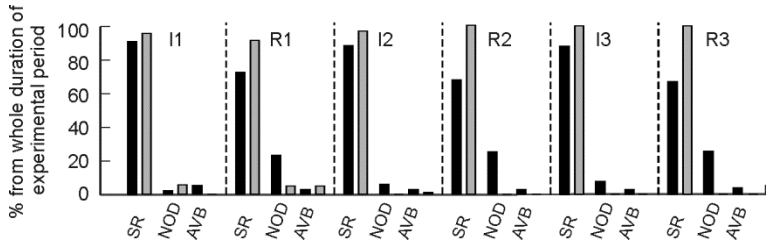

Figure 55. Distribution of different types of cardiac rhythm during ischemia and reperfusion. Expressed as percentage of total duration of corresponding experimental period in experiments with (black) and without (grey) di-4-ANEPPS. I – ischemia; R – reperfusion; SR – normal sinus rhythm; NOD – junctional rhythm; AVB – atrioventricular block of the 2nd and 3rd degree.

As regards VPB (see Fig. 56), there is the significant difference in their number between groups with and without dye administration in the second ischemia (Mann-Whitney U-test, $\alpha = 0.05$). In both groups, VPBs were predominantly observed in the middle of the first ischemia. Decrease of VPB number from the first to the last ischemia is evident in both groups. Little number of premature beats was also observed in the first reperfusion.

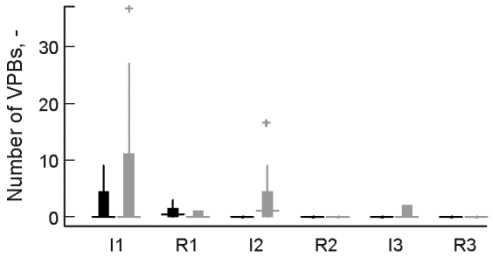

Figure 56. Total number of ventricular premature beats (VPBs) in ischemia and reperfusion. Experiments with (black) and without (grey) di-4-ANEPPS administration. I – ischemia; R – reperfusion.

Electrogram morphology and VCG parameters

Illustration of paired test results for all parameters from control and stained heart groups can be found in Appendix D and Appendix J, respectively. Onsets of significant changes observed in selected parameters (representing different parameters groups from Appendix A) calculated during three ischemic periods relative to the end of stabilization are listed in Table 9. Generally, significant alterations in parameters measured in stained hearts were time delayed (1 to 5 minutes) in comparison with corresponding changes in control group. In both groups, the most of changes appeared earlier in lead II data as compared to those from lead I. The earliest ischemia-induced changes are characteristic for QRS related parameters calculated from both EGs and VCG. In most parameters from both groups, the onsets in the second and third ischemia were approx. 1-3 minutes delayed regarding the onsets in the first one.

Above trends are also reflected in the results of ROC analysis which are summarized in Appendix K. It is clear that the number of parameters with the good discrimination ability is much smaller in stained hearts data than in control or H groups (Appendix E and Appendix I, respectively). AUCROC in each minute of the first ischemia calculated for the most common EG and VCG parameters are shown in Fig. 57 and the distributions of AUCROC, Se and Sp calculated from these parameters are graphically presented in Fig. 58.

Table 9. Onset of significant ischemia-induced changes ($p < 0.05$, Wilcoxon signed-rank test) in EG and VCG parameters from experiments with and without di-4-ANEPPS administration.

Parameter	Onset, min					
	Non-stained hearts			Stained hearts		
	I1	I2	I3	I1	I2	I3
JTmax (LI)	4^{th}	5^{th}	6^{th}	6^{th}	6^{th}	6^{th}
JTmax (LII)	3^{rd}	4^{th}	5^{th}	8^{th}	7^{th}	7^{th}
QRS_A (LI)	tr	tr	tr	5^{th}	7^{th}	8^{th}
QRS_A (LII)	1^{st}	3^{rd}	4^{th}	2^{nd}	3^{rd}	6^{th}
T_A (LI)	5^{th}	7^{th}	6^{th}	7^{th}	10^{th}	10^{th}
T_A (LII)	-	-	-	-	-	-
AUC_{QRS} (LI)	3^{rd}	4^{th}	4^{th}	8^{th}	7^{th}	10^{th}
AUC_{QRS} (LII)	1^{st}	3^{rd}	5^{th}	2^{nd}	9^{th}	9^{th}
$AUC_{JTmax}R'$ (LI)	3^{rd}	5^{th}	5^{th}	6^{th}	8^{th}	7^{th}
$AUC_{JTmax}R'$ (LII)	5^{th}	6^{th}	6^{th}	-	9	-
φ	3^{rd}	6^{th}	6^{th}	10^{th}	9^{th}	-
D	1^{st}	6^{th}	6^{th}	10^{th}	9^{th}	10^{th}
$A_{jt}xz$	4^{th}	5^{th}	4^{th}	tr	9^{th}	8^{th}

I – ischemia; LI, LII – lead I and lead II, respectively; 'tr' – transient changes; '-' – no significant changes

In both groups, lead I data have a good discrimination ability at the last phase of ischemia, whereas parameters from lead II allows discriminating between non-ischemic data and that obtained at earliest phase of ischemia. In stained hearts group, the best discrimination ability was observed for T_A and AUC_{QRS} from lead I EG and for AUC_{QRS} and QRS_A from lead II EG. Among VCG and joint parameters, QRS_D, L_{jt} and β_{jt} from both groups and β_{qrs} from non-stained heart group provide the best discrimination.

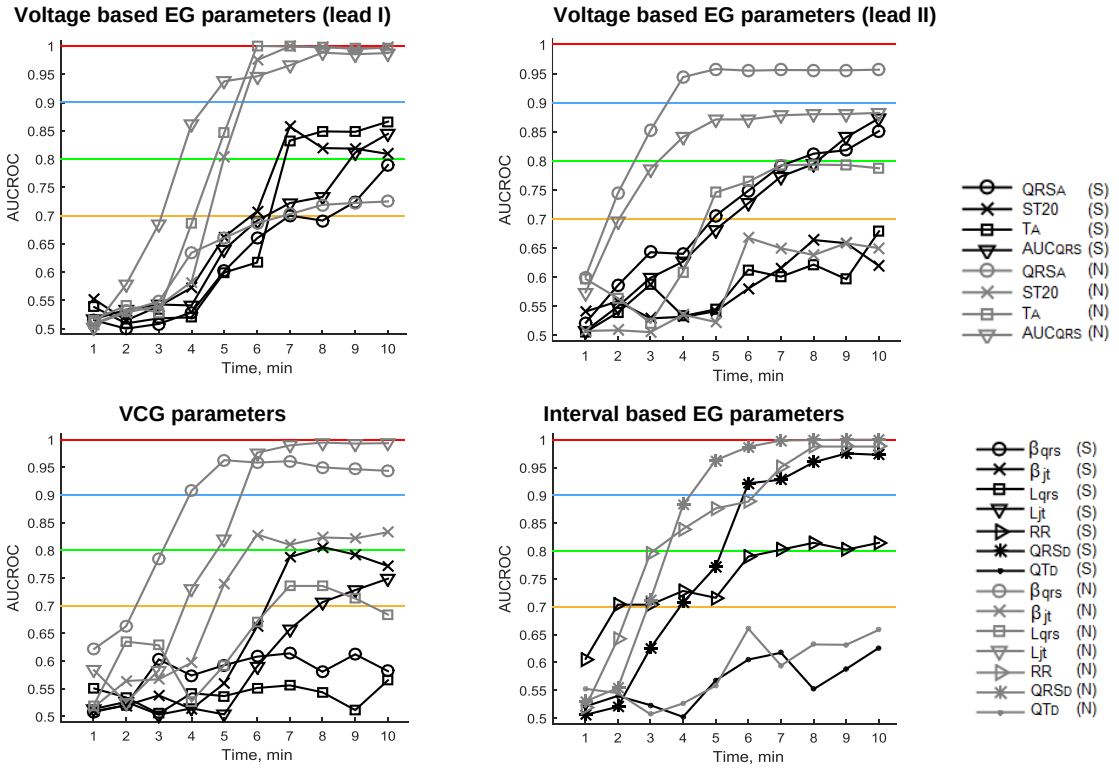

Figure 57. Course of AUCROC calculated for different groups of parameters during the first ischemia. S, N – stained and non-stained hearts, respectively.

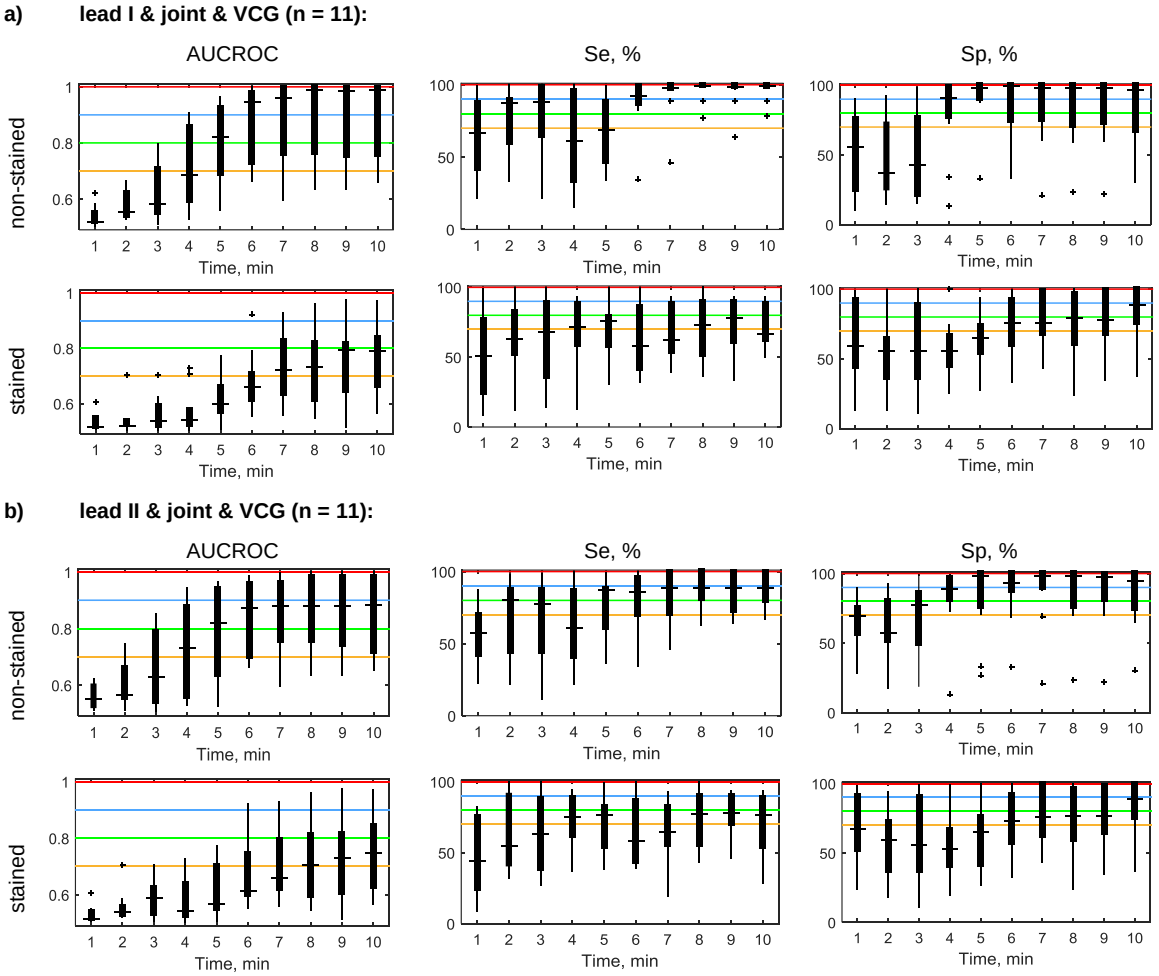

Figure 58. AUCROC, Se and Sp for main lead I & VCG (a) and lead II & joint & VCG (b) parameters calculated for stained and non-stained hearts.

Se, Sp, AUCROC, cut-off value, and time of detection corresponding to the optimal points on ROC curves constructed for the case, where the whole period of stopped perfusion is considered as 'true' ischemia, are summarized in Table 10 for various parameters selected from different parameters groups. Optimal point was determined using Se and Sp (both higher than 50 %) as a pair providing maximal sum Se + Sp. Three parameters – RR, JTmax (from lead I) and AUC_{QRS} (from lead II) – provide good discriminating between non-ischemic and ischemic state in both control and stained hearts groups. In control group, besides these parameters, good discrimination capacity was found in some other such as ST20 and T_A (lead I), JTmax and QRS_A (lead II) and α_{qrs}, β_{qrs}, φ, and D. In stained hearts, QRS_A and $AUC_{JTmax}R'$(from lead I) and QRS_D, L_{qrs}, $D^c_{qrs}xz$ and $A_{qrs}xy$ were suitable for data discrimination besides the parameters observed for both groups. In most cases (RR, JTmax, AUC_{QRS}, L_{qrs}, etc.), the cut-off values calculated for control and stained heart groups differ from each other. On the contrary, in some parameters (such as D), the cut-off values are very similar; nevertheless, Se and Sp obtained for stained hearts are dramatically lower (up to 47 % for Se) in comparison with the second experimental group.

Table 10. Discrimination ability indices of selected parameters in non-stained and stained hearts. The whole period of stopped perfusion is considered as 'true' ischemia.

Parameter	Performance indices (non-stained / stained)				
	T, min	Se, %	Sp, %	AUCROC, -	Cut-off
RR	**8/6**	**70/88**	**90/67**	**0.81/0.81**	398/535, ms
QRS_D	7/**7**	58/**63**	98/**74**	0.80/**0.68**	31/32, ms
QT_D	10/9	77/78	42/43	0.57/0.52	173/205, ms
JTmax (LI)	**2/5**	**95/82**	**60/62**	**0.77/0.71**	98/128, ms
JTmax (LII)	**2**/4	**99**/82	**60**/56	**0.77**/0.68	102/127, ms
QRS_A (LI)	1/**9**	63/**64**	59/**67**	0.61/**0.63**	4.1/2.4, mV
QRS_A (LII)	**3**/4	**64**/55	**99**/84	**0.87**/0.72	-1.8/-1.5, mV
ST20 (LI)	**10**/3	**60**/88	**86**/40	**0.73**/0.69	0.21/-0.50, mV
ST20 (LII)	7/5	44/42	68/58	0.50/0.53	0.14/-0.71, mV
T_A (LI)	**10**/2	**70**/65	**79**/50	**0.79**/0.62	0.9/0.6, mV
T_A (LII)	10/6	40/71	69/40	0.56/0.55	1.9/0.9, mV
AUC_{QRS} (LI)	**1**/1	**60**/40	**90**/98	**0.80**/0.67	74/65, mV·ms
AUC_{QRS} (LII)	**1/1**	**61/63**	**99/74**	**0.79/0.68**	-10/-35, mV·ms
$AUC_{JTmax}R'$ (LI)	8/**4**	94/**80**	50/**63**	0.73/**0.75**	0.1/0.5, -
$AUC_{JTmax}R'$ (LII)	3/7	87/76	48/46	0.75/0.59	0.36/0.43, -
L_{qrs}	1/**1**	48/**63**	57/**64**	0.52/**0.63**	5.6/2.3, mV
α_{qrs}	**3**/1	**79**/43	**77**/66	**0.72**/0.54	139/93,°
β_{qrs}	**4**/1	**99**/72	**66**/49	**0.85**/0.52	110/-81,°
γ_{qrs}	8/4	79/58	49/58	0.60/0.52	6.9/87,°
φ	**4**/1	**96**/73	**63**/46	**0.84**/0.54	75.0/6.2,°
D	**1**/3	**97**/50	**68**/52	**0.84**/0.51	5.1/5.7, mV
$D^c_{qrs}xz$	5/**1**	49/**63**	55/**64**	0.57/**0.63**	3.6/2.3, mV
$A_{qrs}xy$	10/**2**	61/**69**	56/**63**	0.60/**0.63**	3.9/13.0, mV^2

LI, LII – lead I and lead II, respectively

The examples of distributions of ΔJTmax, ΔQRS_A and ΔT_A in ischemia and reperfusion periods are presented in Fig. 59. Significant differences between ΔJTmax (in both leads) and ΔQRS_A (in lead II) were found in the middle part of ischemia. This trend represents the fact that ischemia-induced changes are time-delayed in stained hearts comparing to the non-stained ones. It is typical for approx. half of analysed parameters. Other trend, namely the difference at the second part of ischemia, was observed in ΔQRS_A (lead I) and other five parameters ($\Delta AUC_{JTmax}R'$ (lead II), $\Delta AUC_{TmaxTend}R'$ (lead II), Δφ, ΔD, and $\Delta\varphi^c_{jt}zy$). Only in ΔQRS_A, the values for non-stained hearts were higher than those for stained hearts. In other cases, inverse relation was valid. In the rest (e.g. ΔT_A), no differences between two groups were found. The variability of parameters values within stained group was often much higher in comparison with control group data, especially in ischemia (see Fig. 54c and Fig. 59). It can be concluded that staining of the heart with di-4-ANEPPS leads to the changes in its electrical activity which may affect ischemia manifestations in EG.

No significant differences were found in stained hearts group between parameters calculated using and without delineation results. The overall ischemia-induced changes (i.e. changes at the end of ischemia) of EG morphology were similar in three ischemic periods which was verified by the analysis of the parameters' slopes (see above). According to one-sample signed-rank test, the slopes were mostly closed to zero and the significant differences in slopes values between stained and non-stained hearts were found in only few cases.

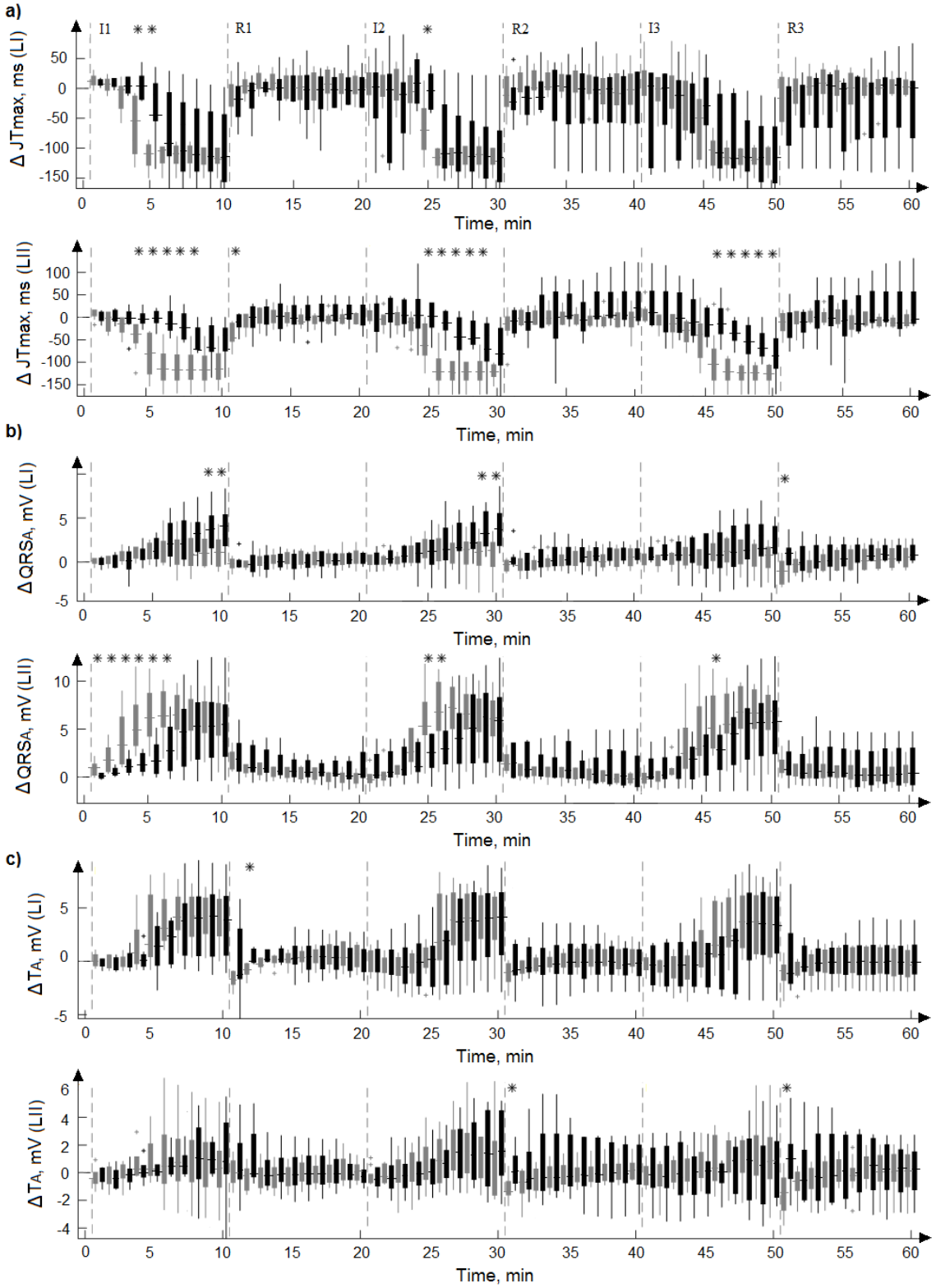

Figure 59. Distribution of the parameters' Δ in stained (black) and non-stained (grey) hearts groups. Δ is the difference between actual value and value from the end of stabilization; calculated for lead I (LI) and lead II (LII) data from three ischemic (I) and reperfusion I periods. * for $p < 0.05$ (Mann-Whitney U-test).

4.3.4 DISCUSSION

Choice of control experimental group

First off all, choice of control, non-stained group should be addressed in more detail. Unfortunately, basic characteristics such as LV thickness and LV weight were not available for experiments with VSD administration. According to the results from above chapter, LV size may dramatically affect electrophysiological parameters measured under non-ischemic as well as ischemic condition. Therefore, it was necessary to decide which hearts – with low (L) or high (H) LV mass fraction (or both) – should be included into control group (non-stained hearts).

As first, lead II AUC_{QRS} calculated at the end of stabilization in stained hearts was compared with that calculated in corresponding time instance approx. 20th minute from the beginning of experiment) of stabilization in non-stained hearts. According to Fig. 45, this parameter has good ability to discriminate between L and H group. Results of analysis are shown in Fig. 60. Kruskal-Wallis test combined with Tukey-Kramer post-hoc test revealed significant difference in AUC_{QRS} between H group and both stained and L group, whereas no difference was found between stained and L groups.

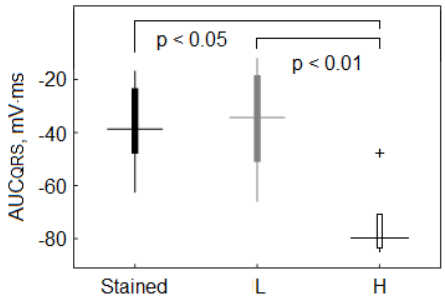

Figure 60. Distribution of AUC_{QRS} in different experimental groups.
Calculated for stained hearts and non-stained hearts with low (L) and high (H) LV mass fraction. P values are shown for Kruskal-Wallis test followed with Tukey-Kramer post-hoc test.

Taking into account the fact that only sporadic changes were observed in EG morphology during dye staining and washout (expecting QT_D and QRS_D), similar course of the most morphological parameters measured in stained hearts and "true" control group may be expected. Therefore, morphological parameters from stained hearts' EGs were retrospectively compared with those from L and H groups (data for stained vs. H group are not shown here). Significant differences were found between stained and H groups in almost all parameters measured before ischemia as well as during ischemia-reperfusion repetitions. On the contrary, ischemia-related changes in stained hearts were very similar to those in L group (as was shown above).

Considering all abovementioned, only the hearts with low LV mass fraction were included in control group.

Direct effects of di-4-ANEPPS on cardiac electrophysiology

Despite the fact that the impact of di-4-ANEPPS on electrophysiological parameters is disputable, it is the most widely used VSD for heart study. Previous studies as well as results presented in this thesis confirm the alteration of heart function in the presence of the dye.

Decrease of spontaneous heart rate and slowing impulse conduction through ventricles were found in stained isolated heart of almost all commonly used laboratory animal species

[66],[146],[147]. Decrease of the heart rate may be caused either by effect of di-4-ANEPPS on ion channels in sinoatrial (SA) node or by impairment of coupling between the nodal cells. The SA node is a heterogeneous complex of nodal cells and other tissue [152]. The heterogeneous ion channel expression in different parts of the node and the variation of ion channels within a single nodal cell make the experimental verification of the finding very difficult. Nevertheless, the effect of di-4-ANEPPS is very similar to the effect of specific ion channel blocker ivabradine. Ivabradine selectively inhibits an important sodium depolarization current (the "funny" current, I_f), which controls the rate of spontaneous firing in SA node. It was reported that administration of ivabradine decreases heart rate and reduces severity of ischemia [153]. However, the direct effect of di-4-ANEPPS on I_f has not been studied yet.

For our best of knowledge, evolution of cardiac impulse conduction through atria and AV node in rabbit isolated heart stained with di-4-ANEPPS was addressed for the first time in this study. Besides the rat heart [147], the slowing cardiac impulse conduction through AV node (manifested as increased PQ_D) was observed in rabbit heart. The effect was found in negligible time period during dye loading only.

For the staining of the isolated heart, perfusion with low concentration of the dye lasted approx. 20 min was used. In accordance with the results of patch clamp analysis, significant prolongation of impulse conduction through the ventricles (represented by widening of QRS complex) was observed at the middle of loading procedure. The cell experiment results indicate that the effect of the di-4-ANEPPS on ventricular conduction may depend on the staining procedure, namely on the duration of loading period. Significantly higher inhibition of sodium current density was obtained in case of 30 min staining compared to acute application of the dye in the same concentration. The change is caused by direct effect of the dye and is not a result neither of phototoxic effect nor an effect of DMSO used for dye dilution.

Only sporadic episodes of arrhythmias were detected in non-stained hearts during long stabilization. In stained hearts during washout, junctional rhythm was observed for almost the half of the period. Taking into account the absence of pathological episodes before staining (in stabilisation), the presence of impaired rhythm in following periods seems to be due to the dye. The di-4-ANEPPS may affect various ion channels as well as intracellular connections. Staining by the dye leads to decrease of conduction velocity and impairment of electrical homogeneity. Moreover, decreasing heart rate in stained hearts may lead to onset of junctional rhythm. Above observations were accompanied by the changes in shape of EG and VCG, which were found in repolarization part (ST segment and T wave). It can therefore be assumed that di-4-ANEPPS affects cardiac potassium channels. Since these alterations were fully washable, it was not necessary to verify the phenomenon via rather difficult, time-consuming patch clamp technique.

Some of presented results are in agreement with observations (QRS prolongation, slowing impulse propagation [144],[146]) in guinea pig isolated heart, despite the fact, that the hearts were stained by bolus of highly concentrated dye administered directly to the aorta (i.e. by "fast" staining procedure in contrast to "slow" staining by perfusion with low dye concentration used in present study on rabbit hearts). Similar phenomena caused by "fast" staining with di-4-ANEPPS might be expected in rabbit hearts, since the mechanism of AP propagation (in terms of depolarisation and repolarisation currents involved in the process [154]) in guinea pig and rabbit myocardium is similar. The changes in RR and QT interval duration accompanied staining the rabbit heart from the beginning of this experimental period. It may consequently be supposed that these effects would be present in case of fast dye application, too.

Hence the interpretation of data from the experiments with di-4-ANEPPS (regardless the staining procedure used) should be performed with caution and the results obtained in this case should be validated using different experimental tools if possible. Particularly, the assessment of drug effects in isolated heart stained by di-4-ANEPPS might be complicated due to confounding effects of the dye such as QT and QRS prolongation appeared in the beginning of loading procedure. It is especially important in studies where the rabbit heart is used for the study of the arrhythmogenic potential of drugs such as antipsychotics or antiarrhythmics [38].

The abovementioned observations are not the result of phototoxic effect of the dye. The heart tissue illumination (i.e. dye molecules excitation) was performed locally by 6 optical fibres with diameter of 200 μm after washout period only [59]. During the whole experiment, the heart preparation was kept in the dark. Thus, all the observations can be considered as direct effects of di-4-ANEPPS on the rabbit heart.

An important advantage of this study is that no excitation-contraction uncoupler was used. In other studies, uncouplers (such as 2,3-butanedione monoxime, cytochalasin D and blebbistatin) are frequently used to reduce the motion artefact in AP records. Possible side effects of such agents (e.g. [61],[155],[156]) may complicate the analysis of electrocardiographic data and may lead to incorrect interpretation of the results.

Above results were obtained in rabbit isolated heart; the effects of di-4-ANEPPS may be less (or more) pronounced in other species. It should be also noted that mentioned observations are valid for only di-4-ANEPPS and may not be simply applied in case of other VSD.

Electrophysiological evaluation of global ischemia in the hearts stained with di-4-ANEPPS

According to above observations, di-4-ANEPPS affects ECG interval characteristics (such as QT_D and RR). Nevertheless, the relative changes of these parameters in stained hearts during ischemia-reperfusion were almost the same as in controls.

In about half of evaluated parameters, onset of significant changes during ischemia was 1 – 3 min delayed in case of stained hearts. Moreover, in QRS_D (ventricular conduction) as well as in other parameters (such as ST20 from lead I, β_{qrs}, φ, and D) more pronounced changes were found in controls. The total number of VPBs was higher in control hearts, as well. It can therefore be concluded that di-4-ANEPPS affects the progress of myocardial ischemia: it delays the occurrence of significant ischemic changes and partially attenuates the severity of ischemia.

The progress of EG and VCG parameters in the first ischemia remained almost the same in later ischemic periods. In comparison with the first ischemia, the only difference was that the significant changes were delayed. VPBs number also decreased through three ischemic periods. Both phenomena can be explained by preconditioning effect.

In reperfusion, the values of parameters affected by ischemia gradually returned to their non-ischemic levels. In stained hearts the recovery was usually faster than in non-stained hearts, where the EG alterations caused by ischemia were vanished during approx. first two minutes of reperfusion, such as in case of ST-T related parameters (compare the results for lead I data from control and stained hearts in Appendix D and Appendix J, respectively).

Slower ischemia development in stained hearts may be explained by decreased resting heart rate (see above). It has been reported, that slowing heart rate significantly reduces cardiac energy consumption and therefore may reduce the severity of ischemia and enhance recovery at reperfusion [153],[157],[158]. In patients treated with drugs such as beta blockers and verapamil, which reduce heart rate and systolic arterial blood pressure, false-negative response to exercise test may be obtained due to decreased myocardial oxygen requirements [21].

Above findings complicate analysis and interpretation of data obtained in experiments with optical mapping by di-4-ANEPPS. Particularly, later and probably less pronounced response to ischemia should be expected in stained hearts. If response to ischemia is under investigation, the prolongation of ischemic period and increase of heart rate by pacing may be considered to achieve appropriate results.

To avoid possible discrepancies in results, stained hearts should be used as controls. If the results from experiments with di-4-ANEPPS are compared with those from control group without dye administration, special care should be taken. In this case, possible changes appeared during staining or washout should be identified and appropriate methodological correction (such as analysis of Δ values instead of initial parameters which was proposed in this study) should be performed to avoid wrong interpretation and conclusions.

5 AUTOMATIC DETECTION OF ISCHEMIA IN ELECTROGRAMS

This chapter is focused on the possibilities of using EGs and VCG parameters for automatic ischemia detection in three above mentioned experimental groups. Effect of type of data used for training the classification model on its resulting classification performance is also addressed. Related results were previously presented in international conferences ([159], [160]) and reported in the peer-reviewed journal [161], [162]. Two articles (Ronzhina M. et al. and Maršánová et al.) are being prepared for submission to the impacted international journals at the moment.

5.1 BACKGROUND

Rapid development of computer technologies leads to the intensive automation of various processes traditionally performed by human experts. One of the spheres characterized by the introduction of new highly intelligence tools substituting analysis performed by humans is detection of myocardial ischemic episodes in patients' data. Information about the duration and severity of cardiac ischemic episodes in patients are commonly obtained by monitoring ECG over a prolonged time. The long-term records obtain huge amount of data which have to be checked and analysed. Manual (or visual) analysis of the records is a difficult time-consuming process and use of computer interpretation tool can decrease the time required for data analysis by up to 28 % [163]. Moreover, scoring by human expert may not be absolutely correct due to the subjectivity of decision making and accuracy of ECG interpretation ranges approx. from 57 % to 95 % depending on interpretation skills (noncardiologist physicians *vs* more experienced electrocardiologists) and type of ECG abnormality detected [164]. Se and Sp of ST episodes (both elevations and depressions) detection in data from European ST-T Database (commonly used for assessment of algorithms for ST-T changes detection) by the independent cardiologists are in ranges 70-83 % and 85-93 %, respectively [165]. The interrater agreement (by using κ statistics) for identification of ST-segment elevation and depression was poor to moderate (κ = 0.05 and κ = 0.38) for local cardiologists and good in case of expert electrocardiographic consensus panel (κ = 0.58) [166]. Computer-based decision support system providing correct data analysis (relative to the gold standard) can generally improve the accuracy of physicians in ECG interpretation by up to 6.7 %; on the contrary, accuracy decreases by approx. 0.6 % when the computer advice is incorrect [167]. Therefore, there is an effort to design automated computer-based methods for reliable and timing myocardial ischemia detection.

The detection of myocardial ischemic episodes in ECG can be considered as a classification task, where various parameters derived from ECG (classification features, attributes) are used to discriminate between non-ischemic and ischemic segments by some computational algorithm. Main goal in classification is to assign input vector (feature vector) to one of discrete classes (two or more for binary and multi-class task, respectively). The feature space is divided into decision regions determined by decision boundaries (or decision surfaces). Generally, the classification algorithms differ from each other by the definition of the boundaries (e.g. linear, quadratic, logistic, etc.). Standards for myocardial ischemia detection in ECG have been proposed based on the potentials of human experts to recognize characteristics patterns of the records with no extra tools [2]. Thus, the results of machine detection are generally compared with those obtained by visual analysis to estimate the classifier performance. Results of human expert interpretation (gold standard) can be used as so called target (output) values defining the labels of particular classes. The majority of reported tools for automatic ECG analysis use so called supervised learning

techniques. In contrast to unsupervised approaches describing hidden structure from unlabelled data (similar to that used above for EG segments clustering), supervised algorithms are learned to map the input variables (feature vector) to the target value (class labels) [74]. The main goal is to approximate the high-quality mapping function that would correctly predict output value. Moreover, the classifier should be capable to response satisfactorily not only to data used for fitting the function (training data) but also to new instances (training data). This property – the generalization ability – is one of the most important characteristics which should be carefully tested in all newly designed approaches [75].

The generalization performance of the classification model (and consequently the precision of classification results) can be enhanced by using data set consisted of many different features. However, use of large feature set for training the classifier may result in its overfitting, which is the situation, when the overly complex model fails by classifying novel samples regardless of the perfect classification results achieved for the training samples [74]. Some features may be redundant or/and irrelevant with respect to the solved problem and can be, therefore, excluded from the analysis. Feature selection is widespread technique used for removing redundant classification features, which usually allows reducing the complexity of model and time required for its training and testing and, consequently, avoiding the model overfitting. In contrast to feature extraction (where the parameters transformed by some technique, such as principle or independent component analysis, are used as input instances), feature selection methods allow using initial variables without loss of their 'natural' sense which is important, if the results of the selection and classification should be interpreted in detail [75].

Generally, there are two main approaches for reducing of feature set by selecting, namely wrappers and filters. In wrapper methods (e.g. forward and backward selection, sequential floating forward selection, etc.), searching of the features and their selection is embedded into the classification procedure. Thus, the content of resulting feature set depends on the learning algorithm used. As a result, different features can be selected by different classification models and use of particular feature sets with other classifiers may lead to achieving poor results. Moreover, such a combination of feature selection and learning algorithms usually results in dramatic increasing the computational expenses of the method, which may by inappropriate in some applications. In contrast, filters are model-free and can be successfully applied if there is a need to design 'universal' feature set for testing the efficiency of different classification algorithms and comparing their performance with each other. In this case, some intrinsic properties of data are evaluated to select the most relevant features from the whole set, regardless the method used for further classification. Various filter approaches (using correlation or distance between features, mutual information, etc.) have been proposed recently. Combination of both methods – filter and wrapper – may be very useful for processing and analysis of large amount of data. [74],[75],[168],[169]

Some older and more recent approaches for automatic classification of ECG data including human-like decision rule-based systems and other supervised techniques are summarized in Table 11 and Table 12, respectively. Selected reports cover a wide range of various methods in terms of used ECG data (from short-term episodic to long-term Holter records), features (from simple use of ECG samples to parameters extracted from principle components of ECG), feature selection methods (from use of all calculated features to sequential floating forward selection), classification algorithms (from the simplest thresholding to more advanced artificial neural networks and support vector machines) and methods of performance validation (from simple separation of training and testing sets to leave-one-out cross-validation). Some of techniques will be addressed later.

Data recorded during experiments with induced ischemia include normal (non-ischemic) parts without ischemic patterns as well as those with manifestations of moderate (transitional state) and severe ischemia such as in case of ECG recorded in patients during PTCA available in STAFFIII database [170]. Furthermore, the effect of enlarged LV and drug intervention on properties of the classification approach (e.g. selected features, cut-off values, computational time, etc.) and ischemia detection accuracy can be studied using EG from different experimental groups. Thus, use of experimental data set allows more advanced testing the classification approaches.

Table 11. Decision rule-based and tree classification approaches.

Author	Features	Classification method	Performance
Goletsis et al. 2004 [86]	ST deviation and slope, T amplitude, normal amplitude and polarity, age	GA & DR	Se= 91.2%, Sp=90.9%
Murugan 2010 [171]	ST deviation, slope, area, T amplitude and normal amplitude, age	DR with ACO and pruning	Se=92.3%, Sp=94.3 %
Xu et al.2015 [172]	Difference between ST segment level and baseline	DR; 6-class (normal *vs* 5 types of ST)	Se from 76.5% for down-sloping depression to 98.9% for normal ST
Kumar et al. 2016 [173]	Isoelectric energy of ST	DR	Se=98.1%, Sp=98.2%
Garciá et al. 2000 [32]	Filtered RMS difference (for ST and ST-T)	DR & post-cross-correlation	Se=85%, Sp=85% (ST) Se=86%, Sp=76% (ST-T)
Smrdel et al. 2011 [174]	Third statistical moment of ST deviation histogram	DR; 3-class (positive deflection, CAD, other including normal and mixed)	Acc = 87.5% Acc = 85.5% Acc = 9%
Exarchos et al. 2007 [85]	ST deviation, slope and area, T amplitude, QT duration, age	Fuzzy ES & DT	Se=91.2%, Sp=92.2%
Dranca et al. 2013 [175]	J level, ST level and slope; R upslope and downslope; RMS of RS, QR, QRS, and ST; SNR; heart rate; QRS duration, etc.	DT with bagging	Se=81.2%, Sp=74.83%
Fayn 2011 [23]	Mean quadratic deviation of QRS, ST60, T amplitude and spatial orientation, angular deviation of first 30 ms of QRS	DT	Se=98%, Sp=98%

GA – genetic algorithms; DR – decision rule-based system; ES – expert system; DT – decision tree; ACO – ant colony optimization algorithm; CAD - coronary artery disease.

Table 12. Supervised classification approaches (not based on decision rules).

Author	Features	Classification method	Performance
Park et al. 2012 [84]	Area between QRS offset and T-peak, sum from QRS offset to baseline, the slope from QRS onset to offset	KDE SVM ANN	Se=93.9%, Sp=91.2% Se=94.1%, Sp=92.3% Se=87.6%, Sp=93.3 %
Papaloukas et al. 2002 [176]	ECG intervals (J,J+400 ms) transformed by PCA	ANN	Se=90%, Sp=90%
Correa et al. 2013 [36]	QRS loop: maximum vector magnitude, volume, planar area, maximum distance between centroid and loop, angle between XY and optimum plane, perimeter, area-perimeter ratio *vs* ST-vector magnitude	LDA	QRS loop volume: Se=64.5%, SP=74.6% All QSR-loop features: Se=88.5%, Sp=92.1% Common ST vector: Se=73.2%, Sp=73.9%
Murthy et al. 2015 [177]	Samples of ECG beats	ANN SVM k-NN	Acc = 96.6% Linear: Acc = 91.5% RBF: Acc = 95.3% Acc = 94.6% (All: Se<90%, Sp>90%)
Firoozabadi et al. 2016 [33]	QRS upward and downward slopes (V2, aVR)	LDA for slopes *vs* ST guidelines (> 100 μV)	Both: Se=24%, Sp=93%
Llamedo et al. 2013 [178]	QRS and ST-T features: WT, PCA transformation	LR	IM>5%: Se=77%, Sp=88% IM>10%: Se=76%, Sp=90%
Garciá et al. 1999 [179]	Local: ST60, T maximal deviation and position, QT and QRS duration Global: KLT of QRS, ST-T, ST, and T (6 features)	CDF; 3-class (LAD, RCA and LCX occlusion)	Local: Acc=76% (3 features) Acc=85% (all) Global: Acc=83% (3 features) Acc=90% (all)
Tseng et al. 2016 [180]	ST deviation, slope and area, J80 amplitude, T amplitude and magnitude, T/R ratio	SRC SVM	Se=96.6%, SP=96.6% Se=94.8%, SP=99.5%

KDE – kernel density estimation; SVM – support vector machine; ANN – artificial neural network; SRC – sparse representation-based classification; PCA – principle component analysis; ACO – ant colony optimization algorithm; LR – logistic regression model; WT – wavelet transform.; CDF – canonical discriminant function; LAD – left anterior descending artery; LCX – left circumflex; RCA – right coronary artery; KLT – Karhunen-Loève transform; RBF – radial basis function kernel; IM – ischemic myocardium.

5.2 METHODS

The general scheme of experimental data classification is shown in Fig. 61a. Parameters calculated from EGs and VCG were used as so called classification features. The part addressed in this chapter is depicted with dashed line and includes selection of relevant features from the whole set of parameters, distinguishing of particular classes (e.g. non-ischemic and ischemic) using some classification procedure and evaluation of classification performance. All approaches used for feature selection and classification were cross validated by two different way (according to leave-

one-out and 10-fold cross-validation, Fig. 61b,c) to obtain relevant estimate of their efficiency. Besides cross-validation within a particular experimental group, 'cross-group' validation (see below) was performed to asses possible effect of data type used for model training on classification performance achieved on different test data. Before analysis, the parameters were scaled to the range <0, 1> via the procedure used above to process slopes values (see Eq. 14). Processed parameters contribute to the calculations with the same weight regardless its type, scale and unit which allows obtaining less biased results.

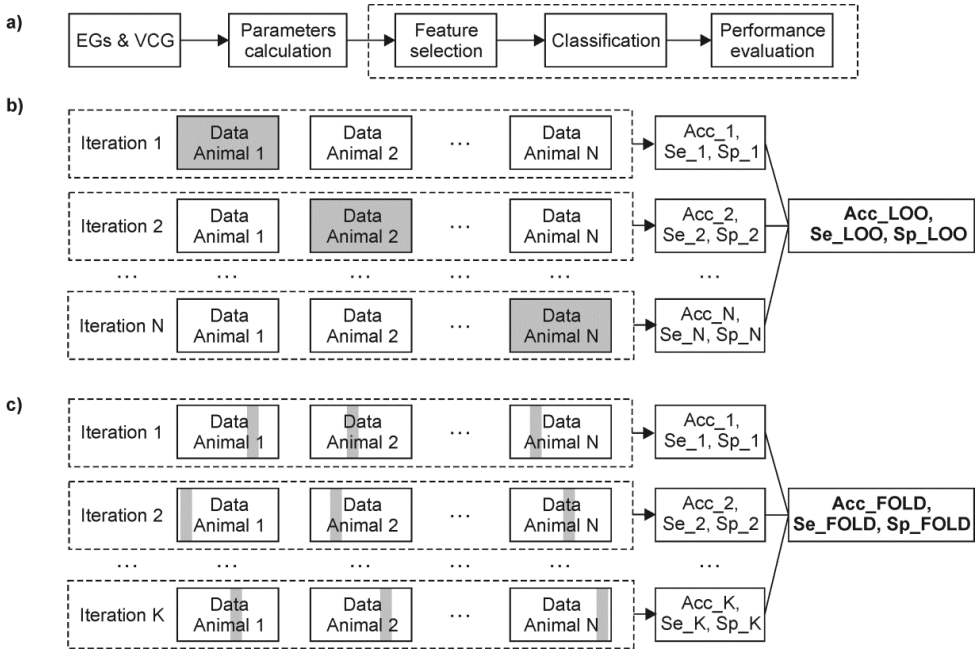

Figure 61. Classification of experimental data.
Classification framework (a) and block-diagrams illustrating leave-one-out (LOO, b) and k-fold (FOLD, c) cross-validation techniques (see text for more details).

5.2.1 FEATURE SELECTION

Three types of feature selection were realized. In all cases, parameters without statistical significance between non-ischemic and ischemic values (i.e. with $p \geq 0.05$ for Wilcoxon signed-rank test, see Appendix D, H and J) were removed from the data set before selection.

The first method is based on *correlation coefficient ranking* followed by *forward selection with LDF classification* (thus, hybrid method combining filter and wrapper approaches [168],[169]). Briefly, Spearman's ρ was computed for each pair of the parameters which were then sorted (ranked) according to their averaged (arithmetic mean values) correlation coefficients in ascending order. Non-significant ($p \geq 0.05$) ρ and those corresponding to the correlation of the parameters with themselves were excluded from the averaged value calculation. In contrast to Pearson correlation coefficient, Spearman's correlation coefficient may be used for evaluation of non-linear relationships between the features and it is robust to outliers (due to ranking procedure) [96],[181]. Parameters from the sorted sequence were then used to train the LDF in a stepwise manner, i.e. parameters from the first (less correlated with other) to the last (most correlated with other) were iteratively involved into the model and classification performance indices were calculated within each such iteration. Optimal feature number was then chosen according to the highest Se and Sp achieved. LDF – one of the simplest classifiers – was used as a basic approach

ensuring the classification performance depends mainly on features selected. Above analysis was performed for each experimental group and type of classification (i.e. binary and multiclass) separately. Example of averaged absolute values of correlation coefficients calculated for parameters from control group and correlation maps derived from the whole (n = 69) and selected (n = 15) set are shown in Fig. 62. It is evident that the inter-feature correlation of the initial data set is quite high. Application of above procedure allows both reducing the dimensionality of the final feature set and decreasing the inter-feature correlation in it.

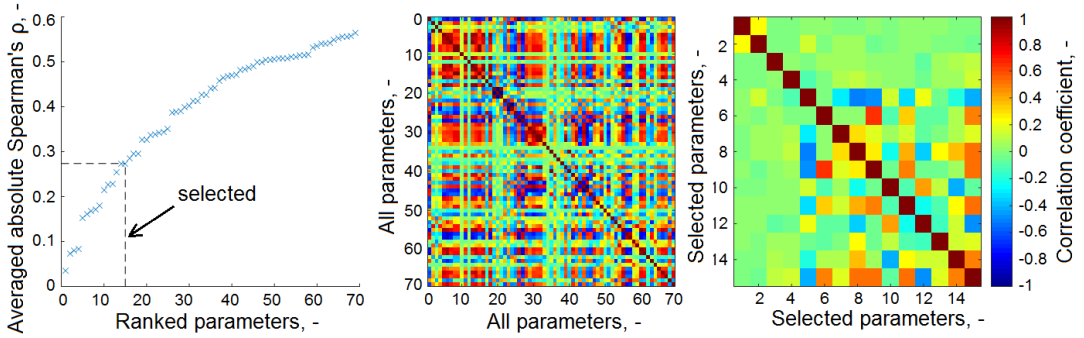

Figure 62. Correlation based feature selection.
Averaged absolute values of Spearman's ρ sorted in ascending order (left) and correlation maps for initial (middle) and selected (right) feature set; calculated from control group parameters.

The second feature set was selected using *PCA-based method*. Besides extraction new features, PCA allows selecting the only features containing the most relevant information (i.e. explaining the most variance in data). To do this, principal components (PCs) were calculated using the parameters and PC coefficients (so called loadings) were analysed such as described in [181]. Unfortunately, up to 12 PCs were required to explain more than 90-95 % of data variance. The first PC provided an explanation of about 33-48 % only and the distribution of loading values of different parameters was inhomogeneous in particular PCs. Thus, it was not possible to select the most relevant parameters unambiguously such as in case, when the first PC describes almost the whole variance in data. Some modifications of PC calculation or their further processing to avoid the discrepancies and facilitate interpretation (e.g. by modification of the most PC loadings to exactly zero values (Lasso method, sparse loading matrix [182],[183]) or by post-processing transformed features by k-means clustering algorithm to identify the most correlated features and remove those with redundant information [184], etc.) have been reported. However, one of the fastest and the most intuitive algorithms is based on simple ranking of the parameters according to the averaged values of their loadings calculated through all or several PCs [185]. This approach, however, does not consider the contribution of the PCs to explanation of the total variance in data and only takes into account the contribution of the parameters to particular PCs, which usually varies greatly. This may lead to incorrect results, where the feature with the high loading lo' in the PC moderately or even minimally contributing to the total variance explanation (usually 3rd-8th PC and later) is considered as more informative than that with the loading lo'': $lo'' < lo'$ from the first or second PC explaining the most of variance, as illustrated in Fig. 63. Therefore, the weighting of loading for k^{th} parameter was proposed as:

$$\overline{lo^k} = \frac{\sum_{i=1}^{M} w_i \cdot |lo_i^k|}{\sum_{i=1}^{M} w_i}, k = \overline{1,N} \qquad (15)$$

where w_i is weight defined as percent of total variance in data explained by corresponding i^{th} PC, $|lo_i^k|$ is the absolute value of loading of k^{th} parameter calculated for i^{th} PC, M is the number of PCs explaining together at least 70 % of the total data variance, N is the number of parameters with significantly different values measured under non-ischemic and ischemic conditions. Usually, 3-4 PCs explaining of about 70 % - 75 % from the total variance were used for parameters ranking to eliminate the bias of weighted mean loading estimation.

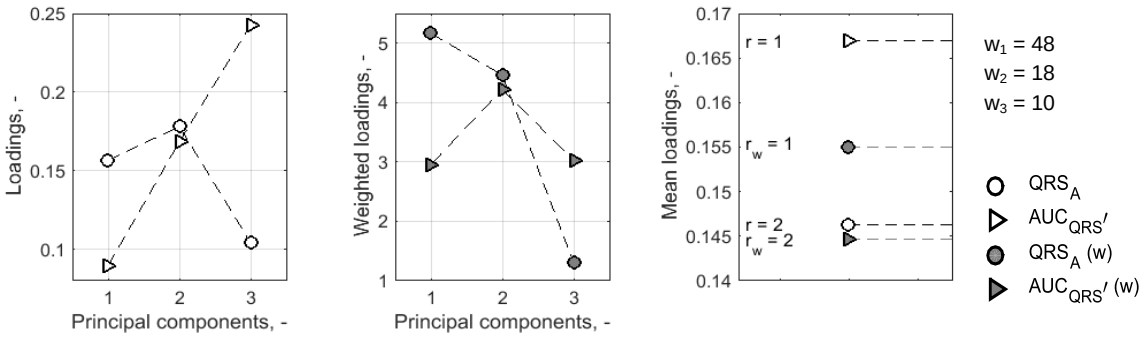

Figure 63. PCA-based ranking of the features.
Principal component (PC) loadings for QRS_A and AUC_{QRS}' for first three PCs (left); PC loadings weighted by the percentage of the total variance explained by particular PC (middle) and mean loading values calculated for each parameter through three PCs and corresponding ranks (r) of the parameters (right).

Then, the parameters were ranked according to their averaged loading $\overline{lo^k}$ sorted in descending order and optimal feature set was selected according to Se and Sp obtained by stepwise LDF based classification as in previous approach. Above two methods were applied for the selection of features from lead I (feature set F3), lead II (F4), joint & VCG (F5), and all parameters (F2), separately.

Finally, the parameters providing the best performance using *simple decision rule* (binary case) and *decision tree* (multiclass approach) were included into the feature set F7 (see next section).

Among the features selected by above methods, other sets were tested. The first one (F1) included the parameters with proven difference between their non-ischemic and ischemic values. The second one (F6) was formed by parameters commonly used for ischemia assessment, i.e. deviation of QRS complex, T wave and ST segment and QRS complex duration. All feature sets used for further classification are listed in Table 13 including their notation. Besides F1-F7, each parameter was also used as an input for decision rule based classifier and decision tree to assess its potential usability for single-feature classifier design.

5.2.2 DATA CLASSIFICATION

Two different classification approaches – binary and multiclass – were realized in the thesis. In first case, data from stabilization and ischemic period were used as non-ischemic and ischemic observations, respectively. In the second one, totally 4 (non-ischemic and beginning, moderate and severe ischemia, where ischemic data were selected from the 1^{st}-3^{rd}, the 4^{th}-6^{th} and the 7^{th}-10^{th} minutes of ischemia, respectively) or 11 different classes (non-ischemic and the 1^{st} to the 10^{th} minute of ischemia) were distinguished from each other. Target (known, desired output) values were coded by the sequence from zero to K, where K is the number of classification groups involved in the approach.

Table 13. List of feature sets selected by proposed approaches.

Feature set:		Description:
F1*		All with significant difference between non-ischemic and ischemic value
F2*:	F21	Selected from F1 according to Spearman's ρ
	F22	Selected from F1 according to principal component's (PCs) loadings
F3*:	F31	Selected from lead I based parameters (from F1) according to Spearman's ρ
	F32	Selected from lead I based parameters (from F1) according to PCs loadings
F4*:	F41	Selected from lead II based parameters (from F1) according to Spearman's ρ
	F42	Selected from lead II based parameters (from F1) according to PCs loadings
F5*:	F51	Selected from joint & VCG parameters (from F1) according to Spearman's ρ
	F52	Selected from joint & VCG parameters (from F1) according to PCs loadings
F6**:		Commonly used, i.e. QRS_A, T_A and ST20 (lead I and lead II) and QRS_D
F7*:		Five best parameters according to the results of DR or DT

* different for experimental groups; ** same for experimental groups; DR – decision rule; DT – decision tree

Five classification methods, namely *decision rule* (analogue of the method used in clinical practice, used for binary classification), *decision tree* (used for multiclass classification), *discriminant function* (linear and quadratic), *k-nearest neighbors* (with various *k*), and *support vector machine* (with linear and Gaussian kernel function) were tested in the study.

At first, the simplest binary non-metric technique – *rule based method* (decision rule, DR) – was tested using each parameter separately. Non-ischemic and ischemic observations were distinguished according to the simple rule applied on the parameter values p_i using corresponding cut-off c_p:

$$IF\ p_i \geq c_p,\ THEN\ output_i = 1,\ ELSE\ output_i = 0. \quad (16)$$

$$IF\ p_i \leq c_p,\ THEN\ output_i = 1,\ ELSE\ output_i = 0. \quad (17)$$

The first rule (Eq. 16) was used for data with upward trend during ischemia, whereas the second one (Eq. 17) was proposed for parameters characterized by decreasing values caused by ischemia. Cut-off values involved in rules were determined by analysis of ROC curves calculated from training data set. The optimal point on ROC curve was selected from all points ($Se_i > 50$ %, $Sp_i > 50$ %) as a pair providing maximal sum $Se_i + Sp_i$. Above two conditions allows eliminating the cases, when one index is extremely high and another is extremely low, and choosing the compromise, where both indexes are quite high. Then, optimal cut-off was applied on new testing data by LOO validation and average test performance indices, time moment of positive detection (ischemia) and the duration of one validation cycle (including both training and testing procedure) were calculated.

Use of above ROC-based technique is generally limited on binary cases. For multiclass task, the rules can be learned directly from the data extracted from hierarchical decision systems, so called *decision trees* (DTs) [186]. DTs used in the work were created by standard CART algorithm which is generally based on binary splitting the data according to the optimization criterion [74]. In each iteration, the split with the best optimization criterion is selected among all possible binary splits on every feature and imposed in the whole structure. Each node in the tree can be characterized by its impurity usually measured by Gini's diversity index [186]. Gini's index for node with observations belonging to just one class is zero; otherwise it is positive. This property of the nodes is used for selection of optimal feature in each iteration. One of the basic optimization criteria is so called gain of the feature which represents the expected reduction in impurity caused by partitioning the observations according to analysed feature.

Algorithm starts with all input data, where so called root node is selected according to above procedure. The choice of the best split (i.e. split providing the largest gain) is recursively repeated for the two child decision nodes created in previous step. The process usually stops if the node is pure, i.e. it contains only observations of one class. In this step, the observations are assigned (labelled) and the node becomes a leaf node. The algorithms employs a greedy strategy that grows the tree using the most appropriate (i.e. informative) feature at each step and does not allow backtracking. The classification of the test observation begins at the root node by asking for the value of a corresponding observation feature and following the appropriate branch to a subsequent node based on the answer. In the next step, the decision is made at the node and the process repeats until the leaf node is reached and the test observation (pattern) is assigned the category (label) of the leaf node. The size of tree (i.e. number of levels, nodes and branches) depends on the complexity of the problem. Large trees are predisposed to overfitting. One of the methods to avoid it is to reduce the tree size. In the thesis, the depth of tree (leafiness) was optimized by merging leaves on the some tree branch – tree pruning, as has been proposed in [74]. The main advantages of DTs are: a) DTs can be used with categorical data; b) very little computational expensive; c) easy application; d) obtained results are clearly interpretable due to natural and intuitive concept of the method.

Other tested methods – the statistical parametric approaches *linear* and *quadratic discriminant function* (LDF and QDF, respectively) – are based on the concept that different classes generate data based on different distributions. During training phase, the parameters of distribution for each class are estimated by the fitting function and used for calculation the model coefficients. During testing on new data, trained discriminant model finds the class with the smallest misclassification cost. [186]

In the feature space, regions with particular values of outputs (labels) are separated by straight lines (or hyperplanes in multidimensional case – LDF) or by conic sections (hyperspheres, hyperellipsoids, hyperhyperboloids, or hyperparaboloids – QDF). The boundaries between classes are determined by the coefficients of trained model. If classes can be accurately separated by linear decision surfaces, corresponding data set is considered as linearly separable. In case of linear problem, LDF is represented by linear function of the input vector so that [73]:

$$\mathrm{y}(\mathbf{x}) = \mathbf{w}^{\mathrm{T}}\mathbf{x} + b, \tag{18}$$

where $\mathbf{w}$ is a vector of linear function's coefficients, b is so called bias (constant term) of the model and $\mathbf{x}$ is a feature vector.

Consequently, a hyperplane discriminating between features is defined as:

$$\mathbf{w}^{\mathrm{T}}\mathbf{x} + b = 0, \tag{19}$$

and an input vector $\mathbf{x}$ is assigned to one class if $\mathrm{y}(\mathbf{x}) \geq 0$ and to another class otherwise. Coefficients $\mathbf{w}$ and bias b determine the orientation and the location of the decision surface, respectively.

In case of QDF (which is more general and flexible than LDF), the function is [73]:

$$\mathrm{y}(\mathbf{x}) = \mathbf{x}^{\mathrm{T}}\mathbf{W}\mathbf{x} + \mathbf{w}^{\mathrm{T}}\mathbf{x} + b, \tag{20}$$

where $\mathbf{W}$ is vector/matrix of quadratic coefficients of the function.

Discriminant analysis assumes that data comes from a Gaussian mixture model (i.e. have multivariate normal distribution) and estimate the model parameters mean value and covariance matrix. Generally, if this assumption is not satisfied, discriminant analysis cannot be expected to be

an appropriate classifier. In practice, however, sometimes discriminant functions are successfully used even if data are non-Gaussian. It seems to be due to the fact that linear or quadratic decision surfaces offer a reasonably good partition of feature space which results in good classification accuracy [75]. Linear discriminant analysis additionally assumes that the covariance matrices of all classes are the same (i.e. data can be successfully modelled by a single Gaussian covariance) and only the means vary. If it is not valid (i.e. both mean and covariance of each class vary), a Gaussian mixture could be more appropriate to model data; thus, quadratic discriminant analysis should be preferred. One of the widely used methods to examine the assumption is Levene's test (performed earliest to analyse EG parameters) which checks equality of the classes' covariance matrices [187]. Above procedures can be easily extended on multi-class approach [73]. For LDF, the performance indices were obtained as an outcome of feature selection procedure. Thus, only QDF was additionally tested on the feature sets.

The choice of inappropriate model of density (which is very limited) may lead to poor classification results, such as in case of simple Gaussian model used for capturing the data with multimodal distribution. In some cases, the classification accuracy can be improved by using of non-parametric approaches, such as histogram or kernel density estimator, approximating the density from data set itself. Another way is to avoid the estimation of probabilities and directly construct decision boundaries based on training data, such as in case of *k-Nearest Neighbor* method (k-NN). k-NN is very simple, intuitive algorithm assigning each testing observation to the corresponding class according to the labels of its nearest neighbors [186]. The neighbors are found by some distance metric (usually Euclidean distance [188]) and labelling of test point is provided by a majority vote of this samples. Thus, there is no essentially training in this case and above procedure is considered as lazy learning [73]. In the study, k-NN with varying *k* was tested.

Other non-parametric approach tested in this study was *support vector machine* (SVM). Briefly, SVM is the approach which constructs a separating hyperplane in a high dimension – typically much higher than the original feature space. Training of SVM consists of finding the optimal separating hyperplane, i.e. that with the maximal perpendicular distance across the hyperplane to the closest transformed training instances (so called support vectors) on either side of it. In case of linear problem, the hyperplane discriminating between features is defined in the same way such as in Eq. 19. Thus, the principle concept of this type of SVM is based on the inner (or dot) product between vector of model weights $\mathbf{w}$ and input vector $\mathbf{x}$. If $\mathbf{x}$ is replaced by the result of its transformation using some nonlinear kernel function ϕ (usually radial basis function RBF, or Gaussian kernel) as follows [73]:

$$\mathrm{y}(\mathbf{x}) = \mathbf{w}^{\mathrm{T}}\phi(\mathbf{x}) + b, \tag{21}$$

then SVM is able to map the nonlinearly separable data points to a high-dimensional space, where the problem usually becomes linear.

Both types of SVM – with linear and RBF kernel – were tested in the study. Basically, SVM is a binary classifier. Nevertheless, there are some techniques to enable its use for solving multiclass problems. One of them is so called one-against-all approach, when for *M*-class problem *M* binary discriminant functions are constructed to be the optimal hyperplane separating one class from all the others. The classification is then achieved according to the function providing maximal (positive) response. However, this procedure may lead to indeterminate regions, where more than one response is positive. Other disadvantage of the method is that training is carried out on highly asymmetric data set (with many more negative than positive observations). An alternative approach used in the thesis is one-against-one, where $M(M\text{-}1)/2$ binary classifiers are trained to separate a

pair of classes and the decision is made on the basis of majority vote. The drawback of the method is in its relatively high computational complexity due to a large number of binary classifiers has to be trained. SVMs are widely used in various areas due to their high classification accuracy and ability to work well with high-dimensional feature sets. [75]

Introduced methods represent different approaches – from the simplest to more advance – for data classification: parametric *vs* non-parametric, supervised *vs* semi-supervised, binary *vs* multi-class, single- *vs* multi-class. As was shown in Background, they are frequently used for automatic detection of ischemia episodes in ECG; thus results of some studies on different data sets are available in the literature. In contrast to artificial neural networks (which are also widespread in biomedical signal processing and analysis), they do not require setting of a big number of parameters (such as number of neurons in each layer, number of training epochs, learning rate, momentum, and many others in case of neural networks [189]) to reach sufficient classification performance. These are the main reasons of selection above methods for experimental data classification.

5.2.3 EVALUATION OF CLASSIFICATION PERFORMANCE

To assess the generalization ability of the classification approach on new data set, training of the classifier was performed on only some part of the whole feature set and the rest of data was used to test it. This so called cross-validation (CV) technique was performed during feature selection as well as classifier training and testing. To different CV approaches – one-leave-out (LOO) and k-fold (10-fold CV) were chosen in the study [73],[190]. Both methods are schematically illustrated in Fig. 61b,c, where the part of data used for training and testing of classifiers are depicted with white and grey colour, respectively.

In case of LOO, data from one experiment were used for testing only and the rest was included into the training set iteratively until each signal was used for testing. Resulting number of training and testing samples in each experimental group is summarized in Table 14.

Table 14. Average size of training and testing data sets in one cycle of LOO validation.

Experimental group	Number of animals	Number of training samples	Number of testing samples
Control	11	14268 ± 188	1585 ± 187
H group	8	10210 ± 167	1702 ± 166
Stained hearts	9	8201 ± 162	1165 ± 160

Because of quite high inter-subject data variability and low number of available experiments, classification results obtained using this cross-validation method may be very pessimistic. Moreover, since the test set contains data from only one record, the variance of estimated performance indices tends to be high [191].

The second approach is based on random partitioning of data from all experiments into *k* disjoint equal sized subsets, where one of them is then used for testing and rest k-1 subsets are used for training during *k* iterations (folds). An advantage of 10-fold CV over such methods as repeated random sampling, that it uses all observations for both training and testing. Moreover, each observation is involved in testing process exactly ones. In contrast to LOO, proposed 10-fold CV (where training and testing observations are selected from the same experiment, although not overlapped with each other such as in case of simple resubstitution, where the model is tested using training data) may have overly optimistic bias in estimation of classification performance. This

approach may, nevertheless, be helpful for assessment (at least rough) of the model performance, if LOO is not suitable due to small data set and large number of classes to be distinguished (see below).

Sensitivity (Se), specificity (Sp) and accuracy (Acc) were calculated to evaluate the classification performance of particular approaches as [87],[192]:

$$\mathrm{Se} = \frac{\mathrm{TP}}{\mathrm{TP} + \mathrm{FN}} \times 100\%, \tag{22}$$

$$\mathrm{Sp} = \frac{\mathrm{TN}}{\mathrm{TN} + \mathrm{FP}} \times 100\%, \tag{23}$$

$$\mathrm{Acc} = \frac{\mathrm{TP} + \mathrm{TN}}{\mathrm{TP} + \mathrm{FP} + \mathrm{TN} + \mathrm{FN}} \times 100, \tag{24}$$

where TP, FP is the number of correctly and incorrectly identified ischemic observations, respectively; TN, FN is the number of correctly and incorrectly identified non-ischemic observations, respectively.

In multiclass problem, Se and Sp for particular classification groups as well as overall (averaged through the groups) Se and Sp and total Acc (calculated using Eq. 22-24 extended to four or eleven classes) were calculated. TP and FP is the number of correctly and incorrectly identified observations belonging to i^{th} classification group, respectively; TN, FN is the number of correctly and incorrectly identified observations from all classification groups excepting i^{th} group, respectively.

Finally, the indices were averaged through all CV iterations which results in more accurate estimation of classification performance [73].

To evaluate possible effect of LV size and di-4-ANEPPS on efficacy of ischemia detection in these experimental groups, three different schemes were applied and tested ('cross-group' validation): 1) training of the classifiers on data from control experimental group (i.e. hearts with low LV mass fraction and with no di-4-ANEPPS administration) and testing them on observations including data from control group (not used for training) as well as groups with high LV mass fraction and VSD application; 2) training on H group data and testing on new observations from H group as well as control and dye-affected group; 3) training on data from experiments with the dye and testing on new observations from the same group as well as control and H group.

5.3 RESULTS

5.3.1 SELECTED FEATURE SETS

An example of the dependence of the LDF Se and Sp on the number of VCG parameters (ranked according to Spearman's ρ and weighted and non-weighted PC loadings) used for detection of ischemia in binary case in control experimental group is shown in Fig. 64. Performance indices achieved within each LOO iteration are shown as the boxplots and the optimal size of the feature set was chosen as the number of parameters corresponding to maximal Se and Sp obtained (global maximum through the whole validation) or the feature set size at the moment, where adding of new parameters did not improve performance. It can be seen that use of large feature set does not always allow obtaining high performance. Use of weighted PC loadings for ranking usually improved the classification performance.

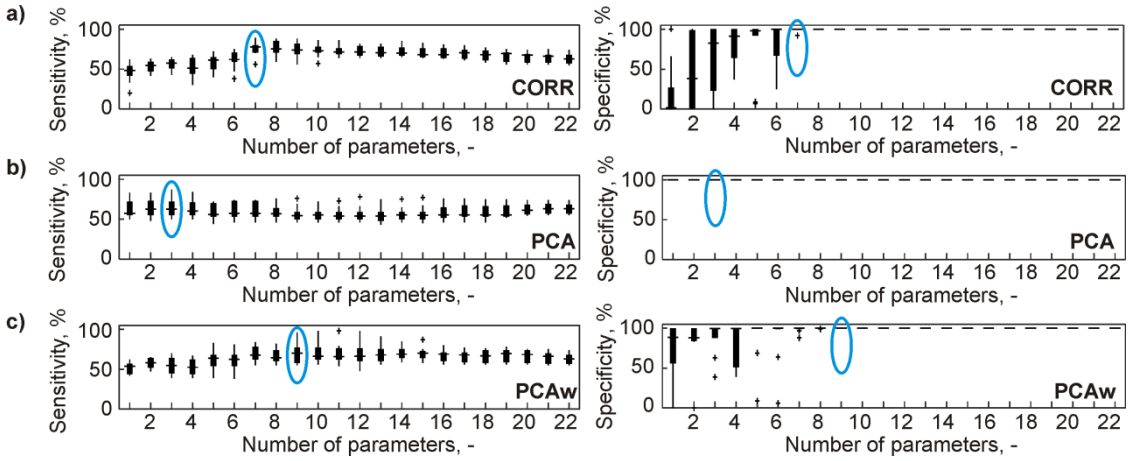

Figure 64. Selection of optimal feature number using linear discriminant function.
VCG & joint features ranked based on Spearman's ρ (a) and non-weighted (b) and weighted (c) principal components' loadings. Optimal feature number for detection of ischemia in control group is depicted with blue oval. Results are cross validated (LOO).

As regards 11-class classification, the best performance was obtained by using the whole parameters groups. Thus, the reduction of feature number was not possible in this case, which was expected considering the complexity of the task, the number of available experiments in each group and inter-animals variability of the data.

As a result, the number of features was significantly reduced (11 and 5 times as compared to the initial F1 set, for binary and 4-class classification, respectively) to avoid possible overfitting of classification models, especially in case of binary approach. Features selected by particular methods are listed in Appendix L.

If the selection was performed from the whole data set (F1), various features from both leads as well as joint&VCG were included by both selection methods in F2 sets. Among parameters selected according to averaged correlation coefficient, those based on AUC ratio calculation (namely +/-AUC_{QRS}, $AUC_{JTmax/TmaxTend}$) were presented in each experimental group. From lead I parameters, mostly QRS related features were selected by both methods to the set F3 for both binary and multiclass classification. In control and H group, both feature filters preferred ST-T parameters from lead II (F4 sets) for binary classification. The same trend was observed by using of correlation based filter for 4-class approach in both groups, whereas QRS related parameters were mainly presented in the feature set constructed by PCA method for 4-class procedure in H group. In stained hearts group, lead II set F4 for binary as well as multiclass approach was mostly represented by QRS parameters. The same type of parameters was involved in VCG set F5 in control and H group. In other cases, mostly ST-T related parameters were selected. For F7 (see below) for binary and 4-calss approaches, mostly QRS and ST-T parameters were chosen by correlation and PCA based methods in case of experiments without and with VSD administration, respectively. Thus, QRS related parameters predominated in control and H groups, whereas both types of parameters (both QRS and ST-T related) were equally important in stained hearts group.

In all groups, mostly AUC based features were involved in the feature sets from lead I and lead II data and different kinds of features were chosen from joint&VCG parameters.

The contents of the sets selected by correlation based method in control and H group were very similar for both types of classification. The sets for 4-class approaches were approx. two times larger (in term of features number) as compared to the binary case. Features preferred by

correlation and PCA based methods were generally different. Nevertheless, some features from VCG group were selected by both methods.

5.3.2 BINARY CLASSIFICATION: SINGLE-FEATURE DECISION RULES AND MULTI-FEATURE TECHNIQUES

Single-feature decision rule method

Best five results for each parameter group obtained by single-feature decision rule method are summarized in Table 15-17. Both QRS and ST-T related features were able to discriminate between non-ischemic and ischemic state. Some features such as JTmax and AUC_{QRST} (lead I), +/-AUC_{QRS} (lead I and lead II), QRS_D, D, and β_{qrs} were selected as one of the best features in at least two from three experimental groups. RR is presented in all groups. However, it is well known that RR is highly sensitive to many external factors (besides perfusion stopping) such as changes in the temperature of preparation, administration of some drugs, etc. Thus, it cannot be recommended as a feature for ischemia detection. It can be seen that the highest classification performance in control and H groups was achieved by using of features from VCG, where two (β_{jt}, β_{qrs}, $A_{jt}xz$, $A_{jt}xy$) or all three leads (QRS_D, D, L_{jt}) were used for calculation. High variability in data recorded in stained hearts (see previous section) results in the high variability of all performance indices as well as the time moment when ischemia can be successfully detected.

As was expected, Se of ischemia detection in all groups by simple single-feature decision rules is not high and reaches approx. 60 – 70 %. This can be explained by the fact that ischemia manifestations are not present in EG (and consequently its parameters) immediately after the perfusion stopping. Thus, the cut-off is usually chosen from the parameters values belonging to the beginning of the ischemic period. As a result, there are a lot of false negative observations in this time period and the moment of successful ischemia detection (TD in Table 15-17) is delayed relative to the beginning of ischemic period.

In control and H groups, the earliest detection of ischemia (approx. 1-2 min after the perfusion stopping) may be performed mainly using ST-T related parameters calculated from both leads and VCG. In stained hearts, QRS related parameters also play an important role and the average time of ischemia detection in this group is about 2-3 min after the perfusion stopping.

The most of the findings are in agreement with above results. Particularly, all kinds of AUC based features have evidently good capacity to detect ischemia in all experimental groups. However, according to the visual analysis of EG ischemia manifestations (Fig. 33) and ROC analysis performed separately for each minute of ischemic period (Fig. 37), the earliest ischemic changes usually occur in QRS complex of lead II EG. Nevertheless, if the whole period with stopped perfusion is considered as ischemia and the results are validated by LOO procedure, QRS related features are not able to provide the successful detection in the beginning phase of ischemia and relatively high Se may be obtained in only 3^{rd}-4^{th} minute of ischemic period.

It should be noted, that common ischemia markers ST20 and QRS_D do not provide successful detection in control group. Performance of QRS_D in H group is quite high. The same parameter in L group was among five best features (with still poor performance). It is in accordance with previously findings of visual and ROC analysis, where QRS prolongation was considered as better marker of ischemia than ST-segment deviations in present setup.

Five parameters providing the best single-feature classification (within each experimental group individually) were additionally included in the separate feature set (F7) for further testing using multi-feature approaches (see below).

Table 15. Best results obtained by decision rule method in control group.
Mean ± SD (through LOO cycles). Best results with both Se and Sp higher than 65 % are depicted with bold.

Feature	Cut-off	Acc, %	Se, %	Sp, %	TD, min	TC, s
Lead I						
ST20	0.21 ± 0.03 mV	63 ± 10	58 ± 23	83 ± 17	3.4 ± 2.4	0.36*
JTmax	99 ± 3 ms	65 ± 8	60 ± 15	86 ± 23	1.9 ± 1.9	0.11
AUC_{QRST}	143 ± 17 mV·ms	66 ± 13	63 ± 20	78 ± 19	2.6 ± 2.5	1.14
$AUC_{TmaxTend}$'	53 ± 13 mV·ms	67 ± 12	64 ± 22	78 ± 21	2.6 ± 2.5	1.14
+/-AUC_{QRS}	5 ± 0, -	**70 ± 20**	**67 ± 31**	**78 ± 20**	**2.9 ± 2.8**	**1.14**
+AUC_{QRS}Rq'	0.84 ± 0.00, -	**71 ± 21**	**69 ± 31**	**77 ± 23**	**2.9 ± 2.7**	**1.14**
Lead II						
ST20	0.08 ± 0.07 mV	31 ± 12	23 ± 20	62 ± 38	6.7 ± 2.1	0.78*
$AUC_{TmaxTend}$R'	0.22 ± 0.00, -	67 ± 13	62 ± 21	87 ± 13	2.0 ± 1.9	1.15
+AUC_{QRS}Rq'	0.36 ± 0.03, -	68 ± 20	61 ± 27	90 ± 8	3.7 ± 2.5	1.13
+/-AUC_{QRS}	0.56 ± 0.07,-	68 ± 20	61 ± 28	90 ± 10	3.7 ± 2.8	1.13
QRS_A	-1.86 ± 0.23 mV	**70 ± 20**	**66 ± 30**	**86 ± 13**	**3.2 ± 3.0**	**0.57**
$AUC_{JTmax/TmaxTend}$	1.84 ± 0.04 mV·ms	**72 ± 11**	**71 ± 19**	**78 ± 22**	**1.1 ± 1.0**	**1.88**
VCG & joint						
QRS_D	31 ± 1 ms	64 ± 15	58 ± 26	83 ± 15	3.4 ± 2.1	0.02*
β_{jt}	38 ± 3 °	68 ± 13	64 ± 17	84 ± 14	1.8 ± 1.7	1.15
β_{qrs}	111 ± 0 °	**72 ± 21**	**65 ± 28**	**98 ± 2**	**2.4 ± 2.1**	**2.28**
A_{jt}xy	0.34 ± 0.01 mV^2	**71 ± 10**	**69 ± 18**	**81 ± 19**	**1.5 ± 1.4**	**1.13**
RR	398 ± 1 ms	**74 ± 13**	**70 ± 18**	**89 ± 11**	**2.1 ± 1.5**	**0.09**
D	5.1 ± 0.0 mV	**74 ± 12**	**68 ± 17**	**96 ± 4**	**2.8 ± 1.9**	2.27

TD – time moment of ischemia detection; TC – average duration of one LOO iteration (training and testing);
* common parameter added to table for information.

Table 16. Best results obtained by decision rule method in H group.
Mean ± SD (through LOO cycles).

Feature	Cut-off	Acc, %	Se, %	Sp, %	TD, min	TC, s
Lead I						
ST20	0.38 ± 0.19 mV	58 ± 5	48 ± 7	95 ± 14	4.4 ± 2.1	0.28*
AUC_{JTmax}	-0.06 ± 0.13 mV·ms	63 ± 6	61 ± 12	70 ± 29	2.4 ± 2.4	0.55
+/-AUC_{QRS}	8 ± 1, -	65 ± 20	60 ± 30	86 ± 14	3.9 ± 3.0	0.82
AUC_{QRS}	108 ± 10 mV·ms	67 ± 21	62 ± 33	80 ± 20	2.6 ± 1.8	0.82
AUC_{QRS}'	142.2 ± 0.5 mV·ms	67 ± 21	62 ± 31	86 ± 13	2.6 ± 1.8	0.82
AUC_{QRST}'	181.2 ± 0.3 mV·ms	**81 ± 11**	**82 ± 16**	**80 ± 20**	**1.3 ± 1.2**	**0.82**
Lead II						
ST20	0.09 ± 0.01 mV	51 ± 21	44 ± 26	80 ± 20	4.9 ± 2.0	0.31*
AUC_{JTmax}R'	0.33 ± 0.02, -	66 ± 10	64 ± 15	76 ± 23	1.9 ± 1.8	1.26
-AUC_{QRS}R'	0.12 ± 0.05, -	69 ± 12	64 ± 21	86 ± 13	3.6 ± 1.9	1.64
$AUC_{JTmax/TmaxTend}$	1.9 ± 0.5 mV·ms	68 ± 5	69 ± 15	60 ± 40	1.2 ± 1.1	1.26
+AUC_{QRS}	22 ± 2 mV·ms	**69 ± 11**	**65 ± 11**	**86 ± 14**	**2.7 ± 2.1**	**0.82**
-QRS_A	-3.39 ± 1.17 mV	**75 ± 15**	**74 ± 25**	**75 ± 25**	**2.1 ± 1.6**	**0.30**
VCG & joint						
QRS_D	32 ± 1 ms	70 ± 9	64 ± 15	88 ± 12	2.1 ± 2.0	0.02
β_{qrs}	91 ± 27 °	**68 ± 11**	**66 ± 25**	**71 ± 29**	**3.1 ± 2.3**	**1.63**
D	6.4 ± 0.02 mV	**71 ± 15**	**64 ± 20**	**97 ± 3**	**3.3 ± 2.3**	**1.62**
RR	375 ± 9 ms	**77 ± 16**	**79 ± 21**	**73 ± 25**	**2.1± 2.0**	**0.07**
D^c_{jt}zy	0.63 ± 0.03 mV	**77 ± 12**	**75 ± 17**	**83 ± 16**	**1.3 ± 1.1**	**0.82**

TD – time moment of ischemia detection; TC – average duration of one LOO iteration (training and testing);
* common parameter added to table for information.

Table 17. Best results obtained by decision rule method in stained hearts.
Mean ± SD (through LOO cycles).

Feature	Cut-off	Acc, %	Se, %	Sp, %	TD, min	TC, s
Lead I						
ST20	-0.30 ± 0.1 mV	67 ± 29	72 ± 28	35 ± 30	3.1 ± 3.4	0.54*
AUC_{QRST}	-17 ± 19 mV·ms	53 ± 30	54 ± 45	54 ± 33	4.5 ± 4.5	0.65
$+QRS_A$	2.36 ± 0.09 mV	63 ± 24	66 ± 33	50 ± 38	3.5 ± 3.4	0.32
QRS_A	2.36 ± 0.08 mV	63 ± 23	66 ± 24	50 ± 35	3.5 ± 3.4	0.36
$AUC_{JTmax}R'$	0.37 ± 0.02, -	**65 ± 17**	**64 ± 26**	**64 ± 34**	**2.1 ± 2.0**	**1.09**
JTmax	128.5 ± 1.4 ms	**66 ± 13**	**63 ± 23**	**77 ± 23**	**2.6 ± 2.5**	**0.15**
Lead II						
ST20	-0.15 ± 0.07 mV	45 ± 30	50 ± 43	40 ± 31	3.2 ± 2.6	1.01*
JTmax	130 ± 11 ms	60 ± 18	56 ± 32	74 ± 26	2.8 ± 2.7	0.05
$+AUC_{QRS}Rq'$	0.80 ± 0.01, -	60 ± 24	58 ± 38	63 ± 24	3.6 ± 3.4	1.31
$+/-AUC_{QRS}$	0.24 ± 0.02, -	60 ± 25	58 ± 39	63 ± 37	3.2 ± 3.0	0.65
$-AUC_{QRS}$	-50 ± 15 mV·ms	65 ± 26	67 ± 32	51 ± 48	2.0 ± 2.0	0.66
AUC_{QRS}	-35.5 ± 0.8 mV·ms	**64 ± 27**	**62 ± 38**	**70 ± 29**	**3.8 ± 3.6**	**0.66**
VCG & joint						
$A_{jt}xy$	1.21 ± 0.77 mV^2	55 ± 25	55 ± 39	52 ± 45	3.6 ± 3.6	0.66
L_{jt}	7 ± 5, mV	68 ± 28	72 ± 25	36 ± 56	2.2 ± 2.1	1.31
QRS_D	60 ± 22 ms	50 ± 27	59 ± 37	60 ± 39	1.6 ± 1.4	1.22
$A_{jt}xz$	9 ± 7 mV^2	71 ± 29	75 ± 24	35 ± 48	2.5 ± 2.0	1.32
RR	31.9 ± 0.4 ms	**64 ± 23**	**64 ± 33**	**66 ± 24**	**3.6 ± 3.6**	**0.02**

TD – time moment of ischemia detection; TC – average duration of one LOO iteration (training and testing);
* common parameter added to table for information.

The efficacy of decision rule method was additionally evaluated on the features calculated without delineation outcomes (excepting QRS_D and QT_D which in this case have constant values during the whole experiment). According to the results summarized in Table 18, performance indices obtained in this case were similar (mainly in case of voltage features or VCG features based on voltage VCG characteristics) or slightly lower (mainly in case of AUC based – especially QRS related – features) as compared to the common method. In case of stained hearts, the only feature still providing detection accuracy of about 60 % is AUC_{QRS} calculated from lead II EG. Possible the strongest reducing of performance was obtained in case of $AUC_{JTmax}R'$ calculated from lead I EG. Despite the fact, that values of this feature calculated using and without delineation outcomes are not significantly different, there are some differences in its distribution before as well as during ischemia (see Fig. 65) which leads to different classification results obtained in both cases. Particularly, large number of false positive observations in feature calculated without delineation outcomes results in lower Sp (49 ± 39 %) as compared to common one (64 ± 34 %). Se obtained in both approaches is very similar (64 ± 26 % *vs* 62 ± 40 % in common and proposed method, respectively).

In most cases, slight, non-significant time delay (Mann-Whitney U test, $\alpha = 0.05$) in ischemic detection and prolongation of the time required for training and testing (TD and TC in Table 18, respectively) were observed as compared to above method.

Table 18. Results obtained by decision rule using features calculated without delineation outcomes. For best features from lead I (I), lead II (II) and joint&VCG. Mean ± SD (through LOO cycles).

Feature	Cut-off	Acc, %	Se, %	Sp, %	TD, min	TC, s
Control						
+/-AUC_{QRS} (I)	7.3 ± 1.4, -	67 ± 20	64 ± 13	79 ± 21	3.7 ± 3.1	1.39
+AUC_{QRS}Rq' (I)	0.13 ± 0.03, -	66 ± 19	64 ± 8	79 ± 20	3.7 ± 3.0	2.46
D	5.1 ± 0.0 mV	71 ± 14	64 ± 19	96 ± 4	2.9 ± 1.9	2.44
QRS_A (II)	1.86 ± 0.23 mV	**70 ± 20**	**66 ± 30**	**86 ± 14**	3.2 ± 3.0	0.70
β_{qrs}	111 ± 0 °	**72 ± 21**	**65 ± 28**	**98 ± 2**	2.4 ± 2.1	2.50
$A_{jt}xy$	0.34 ± 0.00 mV^2	**73 ± 12**	**71 ± 20**	**83 ± 16**	1.1 ± 0.9	1.33
$AUC_{JTmax/TmaxTend}$ (II)	2.44 ± 0.10 mV·ms	**75 ± 13**	**73 ± 17**	**83 ± 17**	1.3 ± 1.2	2.05
H group						
β_{qrs}	91 ± 27 °	**67 ± 12**	**65 ± 25**	**71 ± 27**	3.1 ± 2.3	1.89
D	6.7 ± 0.6 mV	**67 ± 9**	**66 ± 23**	**71 ± 28**	3.4 ± 2.4	1.82
+AUC_{QRS} (II)	24 ± 3 mV·ms	**69 ± 9**	**66 ± 13**	**82 ± 18**	2.7 ± 2.0	0.97
-QRS_A (II)	-3.39 ± 1.17 mV	**75 ± 15**	**74 ± 25**	**75 ± 25**	2.1 ± 1.6	0.45
$D^c_{jt}zy$	0.66 ± 0.03 mV	**77 ± 12**	**75 ± 17**	**85 ± 15**	1.4 ± 1.3	0.98
AUC_{QRST}' (I)	198 ± 1 mV·ms	**80 ± 11**	**80 ± 17**	**80 ± 20**	1.2 ± 1.1	1.11
Stained						
JTmax (I)	108 ± 13 ms	57 ± 22	52 ± 36	72 ± 37	3.2 ± 3.1	0.30
AUC_{JTmax}R' (I)	0.49 ± 0.11, -	60 ± 24	62 ± 40	49 ± 39	3.3 ± 3.2	1.36
AUC_{QRS} (II)	-50 ± 5 mV·ms	60 ± 25	60 ± 40	61 ± 50	3.2 ± 3.0	0.83

TD – time moment of ischemia detection; TC – average duration of one LOO iteration (training and testing)

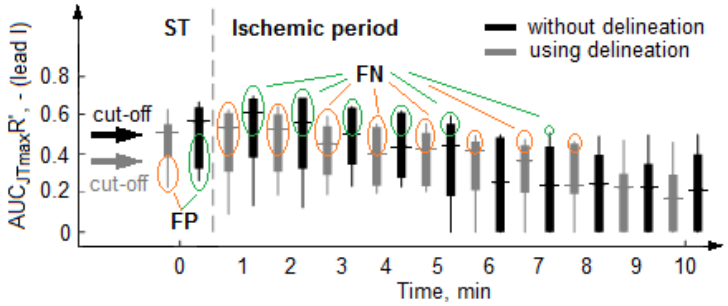

Figure 65. Distribution of AUC_{JTmax}R' values before and during ischemic period. Results for feature calculated using and without delineation outcomes; FP, FN – false positive and negative samples, respectively.

It should be noted that the high number of false negatives at the beginning of ischemic experimental period is in fact related to the definition of ischemic data group, mainly to the definition of the onset of myocardial ischemia injury in the heart preparation. This time moment cannot be strictly determined because of lack of the guidelines for ischemia detection in rabbit, especially in isolated heart model. In the absence of so called 'golden standard' and since the beginning of perfusion stopping was the only available reliable information, it was considered as the beginning of ischemia injury development in the heart. The effect of above methodological assumption on the detection results is illustrated in Table 19, where the performance indices and cut-off values obtained in case of differently defined beginning of ischemic period are summarized for three features from control and one feature from stained hearts groups.

In case of QRS_A (one of the best features from control group), the best performance was achieved if first three or four minutes of period with perfusion stopped were considered as non-ischemic period. This is in agreement with the course of QRS_A which changes its trend at approx.

middle of ischemic period (because of the change of QRS complex from type rS to qR, see Fig. 22 and Fig. 32). It results in prominent change (from the negative to the almost opposite positive value) of calculated cut-off and improves the detection outcome. Nevertheless, even better results were obtained by ST20, if more than first three minutes of ischemic period were considered as non-ischemic. If only first three minutes were indicated as non-ischemic, QRS_D provided better performance as compared to ST20. Thus, QRS_D seem to be a proper marker of early phase of ischemia, whereas ST20 is better for discrimination of moderate and severe ischemia. Obviously, the results obtained for ST20 in cases, where 5^{th}-10^{th} minutes of ischemia were considered as non-ischemic, should be accepted with caution. According to the minute-by-minute examination of some EG and VCG parameters by ROC curve, quite high Se and Sp were observed already in the 3^{rd} minute of ischemic period. Thus, such an optimistic performance of ST20 is much likely the result of overestimation due to incorrect definition of ischemia injury onset (too late in comparison with true beginning of ischemia). Quite similar results (with lower performance) were obtained for QRS_D and ST20 from H group and in stained hearts.

In case of one of the best single-feature approach for stained hearts (for characteristic trend of ΔJTmax – similar with that of JTmax – refer to Fig. 59), the best results were obtained when first four minutes of ischemic period were considered as non-ischemic one. In both cases, increasing Se (transient in QRS_A and sustained in JTmax) and concurrent decreasing (after short-term increasing) Sp were obtained. The latter is due to high number of false positives presented in last minutes of ischemic period, when they are considered (incorrectly) as non-ischemic ones. Similar trends are characteristic for other features in all experimental groups.

Table 19. Performance of decision rule method for various definition of ischemic period beginning.

Indices	**Minute/s of period with perfusion stopped considered as a non-ischemic period**								
	1^{st}	1^{st}-2^{nd}	1^{st}-3^{rd}	1^{st}-4^{th}	1^{st}-5^{th}	1^{st}-6^{th}	1^{st}-7^{th}	1^{st}-8^{th}	1^{st}-9^{th}
Control group: DR & QRS_A (lead II)									
Acc,%	78 ± 19	80 ± 16	85 ± 15	83 ± 13	81 ± 11	83 ± 10	80 ± 11	76 ± 14	74 ± 17
Se,%	76 ± 24	73 ± 27	80 ± 20	81 ± 19	73 ± 27	76 ± 24	78 ± 22	76 ± 24	70 ± 30
Sp,%	84 ± 16	91 ± 9	90 ± 10	85 ± 15	84 ± 14	84 ± 16	80 ± 18	76 ± 18	72 ± 20
Cut-off [mV]	-2.1±0.1	-1.1±1.0	-0.9±0.6	0.4±0.8	1.5±0.7	2.2±0.1	2.3±0.1	2.5±0.1	2.5±0.1
Control group: DR & ST20 (lead I)									
Acc,%	64 ± 8	71 ± 9	78 ± 13	85 ± 15	86 ± 14	87 ± 12	89 ± 7	83 ± 9	76 ± 11
Se,%	58 ± 22	60 ± 22	69 ± 20	80 ± 18	88 ± 12	96 ± 4	99 ± 1	88 ± 11	86 ± 14
Sp,%	82 ± 18	90 ± 25	90 ± 10	90 ± 10	87 ± 13	85 ± 15	87 ± 9	83 ± 12	79 ± 14
Cut-off [mV]	0.6±0.3	0.6±0.2	0.7±0.1	0.6±0.1	0.8±0.2	0.7±0.1	1.2±0.0	1.4±0.1	1.4±0.1
Control group: DR & QRS_D									
Acc,%	68 ± 8	72 ± 12	75 ± 18	77 ± 22	78 ± 22	78 ± 18	79 ± 15	74 ± 16	70 ± 15
Se,%	62 ± 23	65 ± 25	69 ± 22	77 ± 20	83 ± 18	81 ± 19	84 ± 16	85 ± 15	86 ± 14
Sp,%	76 ± 24	75 ± 25	74 ± 26	73 ± 27	74 ± 25	75 ± 25	77 ± 17	73 ± 17	69 ± 16
Cut-off [ms]	30±2	31±1	31±2	31±2	31±1	32±1	32±0	32±0	32±0
Stained hearts: DR & JTmax (lead I)									
Acc,%	70 ± 9	75 ± 10	80 ± 13	79 ± 14	76 ± 18	76 ± 21	76 ± 23	74 ± 21	71 ± 18
Se,%	68 ± 22	75 ± 21	81 ± 19	84 ± 17	81 ± 19	85 ± 15	89 ± 11	85 ± 15	88 ± 12
Sp,%	73 ± 27	73 ± 27	76 ± 24	75 ± 25	73 ± 27	72 ± 28	72 ± 28	72 ± 26	70 ± 21
Cut-off [ms]	128 ± 2	130 ± 2	129 ± 1	124 ± 3	119 ± 7	116 ± 7	110 ± 5	105 ± 4	104 ± 4

As a next step, cross-group validation of above approaches was performed to assess the effect of data type used for training (i.e. control, H or stained hearts group) on classification results and to select the most 'universal' method/s suitable for classification of data from any experimental group. Example of the performance indices of decision rule determined using the features from different groups obtained by testing on data from the other two groups are shown in Table 20. The only way to obtain successful performance in all three groups is to use features from lead II EG, namely QRS_A (or -QRS_A, same in lead II) and $AUC_{TmaxTend}R'$ or QRS_D from the control group. The best total performance (average through all groups) was obtained by using of QRS_A. When the cut-offs were determined from H group data, the successful performance was found in only one group from two others. The best total classification performance for training on stained hearts data was obtained in case of +/-AUC_{QRS}. However, Se calculated for stained hearts was even worse than in case of cut-off value determined for various features from the control group.

As obvious from Fig. 46, for given QRS_D cut-off (about 31-32 ms in control and H groups), less number of false negative results was obtained at the beginning of ischemic period in H group as compared to the control one. It is the reason of higher detection Se calculated for H group data. On the other hand, QRS_D in stabilization is insignificantly higher in H group than in control, which results in lower Sp for control group due to larger number of false positive outcomes in H group. QRS_D measured in stained hearts is significantly higher in stabilization (median value reaches approx. 27 ms which is close to cut-off calculated for control group, see Fig. 54) as compared to the control group, thus Sp obtained in stained hearts is even slower than that in H group.

Table 20. Results of cross-group validation of single-feature decision rule method.

Indices DR	**Training = QRS_A from lead II (control)** (cut-off: -1.9±0.2 mV)			**Training = $AUC_{TmaxTend}R'$ from lead II (control)** (cut-off: 0.216±0.004, -)			**Training = QRS_D (control)** (cut-off: 30.7±0.7 ms)		
	Test: Control	Test: H	Test: Stained	Test: Control	Test: H	Test: Stained	Test: Control	Test: H	Test: Stained
Acc,%	70 ± 20	74 ± 1	63 ± 2	67 ± 13	64 ± 1	66 ± 1	64 ± 15	77 ± 1	68 ± 1
Se,%	66 ± 30	72 ± 1	63 ± 3	62 ± 21	59 ± 1	67 ± 2	60 ± 26	78 ± 4	69 ± 3
Sp,%	86 ± 14	85 ± 0	65 ± 4	87 ± 13	83 ± 1	65 ± 2	83 ± 37	77 ± 11	64 ± 9
Indices DR	**Training = -AUC_{QRS} from lead II (H)** (cut-off: -30±15 mV·ms)			**Training = QRS_D (H)** (cut-off: 32.1 ± 0.9 ms)			**Training = +/-AUC_{QRS} from lead II (stained)** (cut-off: 0.24 ± 0.02, -)		
	Test: H	Test: Control	Test: Stained	Test: H	Test: Control	Test: Stained	Test: Stained	Test: Control	Test: H
Acc,%	69 ± 11	68 ± 11	56 ± 12	70 ± 9	60 ± 5	65 ± 3	60 ± 25	71 ± 0	75 ± 1
Se,%	64 ± 21	65 ± 19	51 ± 18	64 ± 15	50 ± 7	62 ± 4	58 ± 38	72 ± 1	75 ± 1
Sp,%	86 ± 38	78 ± 21	80 ± 14	88 ± 21	99 ± 1	73 ± 2	63 ± 37	70 ± 5	76 ± 7

Finally, the results obtained for the first ischemic period were verified using data from the other two ischemic periods. The results of such 'cross-ischemia' analysis for +AUC_{QRS}Rq' from the control group are shown in Table 21. The best performance of ischemia detection was obtained for testing on the feature from the first ischemic period regardless the period used to derive the training data set. As the cut-offs calculated for different cases are almost the same, this observation is most likely due to the above mentioned preconditioning effect, where appearance of ischemia manifestations in EG in the second and the third ischemic periods is time delayed in comparison with the first one. It leads to higher number of false negatives at the beginning and middle of these ischemic periods and, consequently, quite low Se obtained. It was also found that the indices

calculated for later ischemic periods are quite similar, which is probably due to the similarity between EG recorded during the second and third ischemia. Similar results were obtained for other parameters from all experimental groups.

Table 21. Results of cross-ischemia validation of single-feature decision rule method.

Indices DR	**Training = I1 control (+AUC_{QRS}Rq' lead I)** Cut-off: 0.84 ± 0.00, -			**Training = I2 (+AUC_{QRS}Rq' lead I)** Cut-off: 0.85 ± 0.03, -			**Training = I3 (+AUC_{QRS}Rq' lead I)** Cut-off: 0.84 ± 0.01, -		
	Test: I1	Test: I2	Test: I3	Test: I2	Test: I1	Test: I3	Test: I3	Test: I1	Test: I2
Acc,%	71 ± 21	68 ± 1	65± 1	60 ± 13	67 ± 7	61 ± 8	63 ± 17	70 ± 1	67 ± 1
Se,%	69 ± 31	65 ± 1	61 ± 1	55 ± 26	63 ± 12	55 ± 13	60 ± 29	68 ± 1	64 ± 1
Sp,%	77 ± 23	78 ± 1	78 ± 1	80 ± 20	82 ± 8	82 ± 8	77 ± 22	79 ± 0	79 ± 1

Multi-feature supervised techniques

Two types of discriminant function – linear and quadratic – were tested in this study. According to the results of Levene's test, the equality of the covariance matrices of the various classes was not confirmed in all feature sets. Nevertheless, the performance indices obtained by these methods using the same feature set were quite similar. QDF gave slightly lower Sp in all data groups. Therefore, *LDF* was chosen for further comparison with other classification approaches. It moreover enables the comparison of the results with those from the literature, where LDF is frequently used for ischemia detection in ECG (see above).

It is well known that the efficiency of *k-NN* may significantly vary depend on number *k* of the closest training examples used for assignment of training observations to the classes. Particularly, small value of *k* may lead to a very noisy density model, whereas a large value may result in too smooth classification boundary [73],[74]. For finite number of training observations, there is no theoretical guideline for choosing the optimum value of *k*. From the principles of k-NN, the number of features as well as the number of classes do not play important role in optimal *k* determining. Generally, the rule of thumb is based on choosing this value as squared root of the training samples number [74]. However, this value is not necessarily optimal and may lead to overfitting the model. The most frequently used strategy for searching optimal *k* is to apply cross-validation methods to estimate the misclassification rate of different *k* and choose the best one [188]. Number of training samples in this study reached approx. 8200-14300 depending on experimental group (see Table 14). Therefore, $k = 91$ (the closest odd value calculated as squared root of the smallest training samples number) was chosen as starting value for further search of optimal *k*. The sequence from 11 to 301 (with step of 20) was used to search the optimal *k* providing the best overall performance indices (through the whole cross-validation). Low values were excluded from the search because of the classifier overfitting (i.e. high number of misclassifications during testing, especially at the beginning of ischemia, despite zero resubstitution – or training, error) which was present in all groups in case of *k* chosen from 1 to 10. Odd values of *k* were chosen to avoid a tie, especially in case of binary classification [186]. Example of the dependence of mean performance for k-NN and F6 feature set (probably the simplest approach, the same for all experimental groups) on selected *k* is illustrated in Fig. 66, where the dashed rectangle depicts the most appropriate *k* for all experimental groups (mainly in terms of Se and Sp achieved). Finally, $k = 91$ was chosen as the value high enough to avoid the overfitting and low enough to keep the generalization ability of k-NN. This setting was applied in all experimental groups and feature sets.

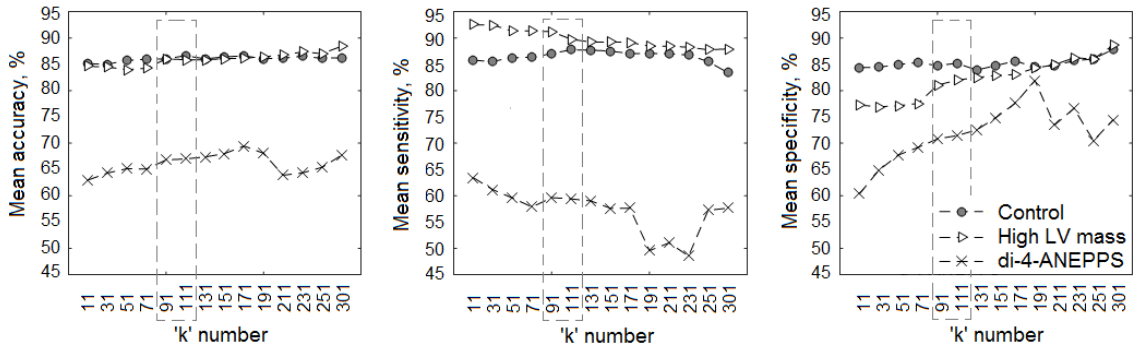

Figure 66. Selection of optimal 'k' parameter of k-NN classifier.
Mean performance indices (cross-validated) of k-NN used in three experimental groups (see text for more details).

Finally, two different types of *SVM*, namely regular (linear) one and that with Gaussian kernel (or radial basis function kernel), were evaluated on various feature sets. The performances of both methods were very similar. In case of high dimensional data (and especially binary classification), use of Gaussian kernel (quite flexible) often resulted in overfitting the SVM. Moreover, training process in this case was time-consuming. Therefore, regular SVM (with no kernel) was chosen for further analysis.

The best overall performance indices obtained by binary multi-feature supervised classification techniques using various feature sets are summarized in Table 22. Generally, use of multi-feature methods (even the simplest LDF based classifier) helped to improve the results of one-feature approach in terms of the classification performance (accuracy up to 87-89 %) and also time moment of successful detection of ischemia (approx. during the first minute after perfusion stopping). It is clear that SVM based approaches allow achieving high classification performance (and the best in control and H groups) in all experimental groups. One disadvantage of SVM is it's time-consuming as compared to LDF and k-NN. In most cases, k-NN model was overfitted, which resulted in poor classification Sp. In stained hearts, nevertheless, the best approach was based on k-NN classification.

Among all feature sets, F51 and F7 seem to be the most reliable for classification, even in case of H group, where F51 included only three uncommon features (QT_D, RR and $A_{qrs}xy$). Surprisingly, F32 set consisting of only three features (all of them are QRS related derived from lead I EG) provided quite good classification in H group by the simplest model – LDF. It should be noted that features commonly used for ischemia detection (F6 set with the same content for all experimental groups) provided quite good results by classification using SVM (Acc = 85 ± 10 %, Se = 85 ± 13 % and Sp = 88 ± 30 % in control group and Acc = 82 ± 9 %, Se = 87 ± 7 % and Sp = 61 ± 44 % in stained hearts) and LDF (Acc = 72 ± 5 %, Se = 64 ± 7 % and Sp = 100 ± 0 % in H group). An important advantage of these small feature sets (as compared to F1 or F2) is in lower computational complexity and lower probability of classifier overfitting.

It is evident, that the earliest detection of ischemia in control group is possible using F41 set, which is in agreement with above findings, where the earliest ischemia manifestations were presented mostly in lead II EG and corresponding parameters.

The usefulness of the best methods was also evaluated on the features calculated without delineation outcomes (see Table 22). Classification performance obtained in this case was slightly

lower (in terms of Se or Sp) in all cases than in common method. Nevertheless, the overall performance still remained higher in comparison with single-feature approach.

As was expected, the lowest indices belonged to approach for stained hearts data classification.

Table 22. Overall performance indices of the best binary multi-feature classification approaches. Mean ± SD through all cycles of LOO validation on test set.

Experimental group	Classifier & feature set	Overall performance indices			Time moment of ischemia detection, min	Computational time, s
		Acc, %	Se, %	Sp, %		
Control	LDF & F51	81 ± 7	76 ± 10	99 ± 1	1.4 ± 1.2	0.03
	k-NN & F41	77 ± 10	79 ± 13	68 ± 30	0.6 ± 0.4	5.22
	SVM & F7	**89 ± 8**	**90 ± 9**	**86 ± 14**	**0.8 ± 0.8**	**12.49**
		88 ± 8	88 ± 10	88 ± 11	1.3 ± 1.2	8.69*
High LV mass fraction	LDF & F32	74 ± 4	68 ± 3	93 ± 7	1.7 ± 1.4	0.02
	k-NN & F51	85 ± 9	92 ± 6	60 ± 39	0.4 ± 0.2	1.63
	SVM & F7	**87 ± 7**	**87 ± 7**	**90 ± 8**	**0.9 ± 0.8**	**5.87**
		81 ± 5	88 ± 9	64 ± 19	0.6 ± 0.5	5.78*
Stained hearts	LDF & F51	73 ± 9	69 ± 10	87 ± 13	1.4 ± 1	0.03
	k-NN & F7	**87 ± 8**	**91 ± 9**	**68 ± 30**	**0.8 ± 0.4**	**2.47**
		81 ± 5	100 ± 0	58 ± 34	0.1 ± 0.1	0.16*
	SVM & F21	85 ± 8	88 ± 8	66 ± 32	0.5 ± 0.2	6.86

* – results obtained using parameters calculated without manual delineation outcomes

The detailed distribution of correct and incorrect outcomes of the best single- and multi-features binary approaches for data from control group are shown in confusion matrices in Fig. 67. It can be seen, that in most testing sets (i.e. data from particular animals used within each LOO iteration), the number of misclassifications is lower in case of SVM detection as compared to corresponding DR-based approach.

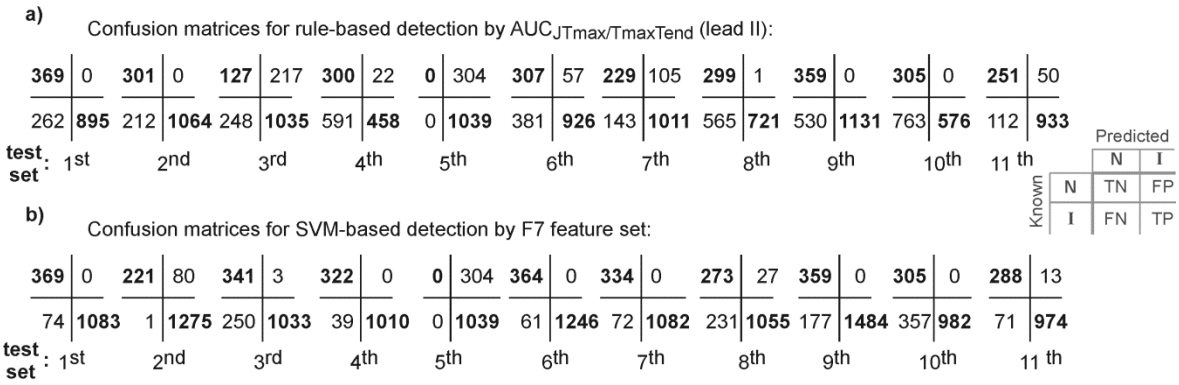

Figure 67. Confusion matrices for best single- and multi-feature binary ischemia detectors for control group data (LOO validation).

The dependence of detection performance in control group on definition of ischemia beginning is represented in Table 23. The best results were obtained in case, where observations from first four minutes of ischemic period were considered as non-ischemic (with improvement of about 5 % and 3 % for Se and Sp, respectively). As in previous case, shift of the moment which is considered as the beginning of ischemic injury in preparation results in increasing Se and on the same time decreasing Sp (from a certain moment). If samples from first 8-9 minutes of the period

were used as non-ischemic, the detection failed (all samples were classified as non-ischemic). Similar results were obtained for other classifiers and experimental groups.

Table 23. Dependence of performance of SVM trained on F7 (control group) on definition of ischemia beginning.

Indices	**Minute/s of period with perfusion stopped considered as a non-ischemic period**								
	1^{st}	1^{st}-2^{nd}	1^{st}-3^{rd}	1^{st}-4^{th}	1^{st}-5^{th}	1^{st}-6^{th}	1^{st}-7^{th}	1^{st}-8^{th}	1^{st}-9^{th}
Acc,%	89 ± 6	91 ± 6	90 ± 4	91 ± 7	88 ± 8	86 ± 6	83 ± 5	87 ± 2	94 ± 1
Se,%	87 ± 9	91 ± 8	91 ± 7	95 ± 5	98 ± 2	99 ± 1	99 ± 1	0 ± 0	0 ± 0
Sp,%	94 ± 14	92 ± 16	90 ± 12	89 ± 12	84 ± 12	82 ± 8	79 ± 6	100 ± 0	100 ± 0
TD [min]	2.1±1.2	2.4±1.4	2.0±1.7	2.4±1.9	2.6±2.0	3.9±1.9	4.2±1.9	10±0	10±0

TD – time of ischemia detection

According to the results of cross-group validation, LDF is the most appropriate for classification regardless the type of data (SVM was not able to generalize well on data from other experimental groups). In Table 24, the best results for multi-feature classifiers are shown. As can be seen, training LDF using data from stained hearts is the best choice. In this case, the performance calculated for control and H group is very close to those obtained by LDF trained on corresponding groups' data. Probably the main benefit of this approach is successful results achieved for stained heart group as compared to other methods. In two cases, F51 based classification was found as the best, which is probably due to the fact that parameters from VCG provided successful classification performance in all experimental groups (see Table 22).

Table 24. Best results of cross-group validation of binary multi-feature classifiers.
Mean ± SD through all cycles of LOO validation on test set.

Indices LDF	**Training = F6 (Control)**			**Training = F51 (H group)**			**Training = F51 (Stained)**		
	Test: Control	Test: H	Test: Stained	Test: H	Test: Control	Test: Stained	Test: Stained	Test: Control	Test: H
Acc,%	72 ± 8	72 ± 1	64 ± 2	73 ± 9	68 ± 2	67 ± 4	73 ± 9	74 ± 1	73 ± 3
Se,%	65 ± 10	65 ± 1	61 ± 1	67 ± 12	63 ± 2	67 ± 5	69 ± 10	71 ± 4	70 ± 4
Sp,%	100 ± 0	99 ± 1	75 ± 2	98 ± 2	88 ± 3	68 ± 1	87 ± 13	86 ± 13	84 ± 9

Results of cross-ischemia validation of SVM based classification in control group data are summarized in Table 25. As in single-feature method, the best performance was achieved for data from the first ischemic period regardless type of training data. Generally, the differences in Acc, Se and Sp obtained in different cases are not so prominent such as in previous case which is probably due to quite well generalization ability and flexibility of SVM as compared to simple decision rule application.

Table 25. Results of cross-ischemia validation of the best binary multi-feature classifier in control group.
Mean ± SD through all cycles of LOO validation on test set.

Indices SVM	**Training = I1 (F7)**			**Training = I2 (F7)**			**Training = I3 (F7)**		
	Test: I1	Test: I2	Test: I3	Test: I2	Test: I1	Test: I3	Test: I3	Test: I1	Test: I2
Acc,%	89 ± 8	74 ± 1	73 ± 2	73 ± 7	79 ± 1	76 ± 1	74 ± 4	83 ± 1	74 ± 1
Se,%	90 ± 9	69 ± 1	68 ± 1	64 ± 7	78 ± 1	67 ± 1	64 ± 6	76 ± 1	65 ± 1
Sp,%	86 ± 14	88 ± 1	88 ± 1	86 ± 13	97 ± 2	90 ± 2	99 ± 1	100 ± 0	99 ± 1

5.3.3 MULTICLASS CLASSIFICATION RESULTS: SINGLE-FEATURE DECISION TREE AND MULTI-FEATURE TECHNIQUES

Single-feature decision tree

The *decision tree* (DT) was applied for multiclass single-feature classification. As was mentioned above, large DTs constructed from the whole training set and including all features are usually redundant and predisposed to overfitting. One of the widely used approaches for eliminating this factor is based on pruning the tree to some level and monitoring reached accuracy [186]. This method combined with LOO cross-validation was used in the study. The optimal number of levels used to prune the tree was defined by calculation of the sum Se + Sp provided by pruned tree and searching the maximal value among all of them. Use of this technique for construction an optimal tree for AUC_{QRST} from H group is illustrated in Fig. 68. Surprisingly, removing of almost all levels (and consequently nodes, see Fig. 68d) from initial tree resulted in significant improvement of classification performance on testing data (can be seen in graphs of performance indices in Fig. 68a as well as outcomes of the tree relative to the target values in Fig. 68b), whereas the tree with 60-65 levels in it was clearly overfitted (high performance on training set corresponded with poor results on testing one). This was valid for all features to some degree. Resulting, very simple tree (Fig. 68c) was able to response on new, testing data with overall accuracy (through all classes) of about 70 % (results for one LOO cycle). It can be seen, that probably the largest number of misclassifications belonged to the middle of ischemia, which has a transient character similar to both beginning and severe ischemia states.

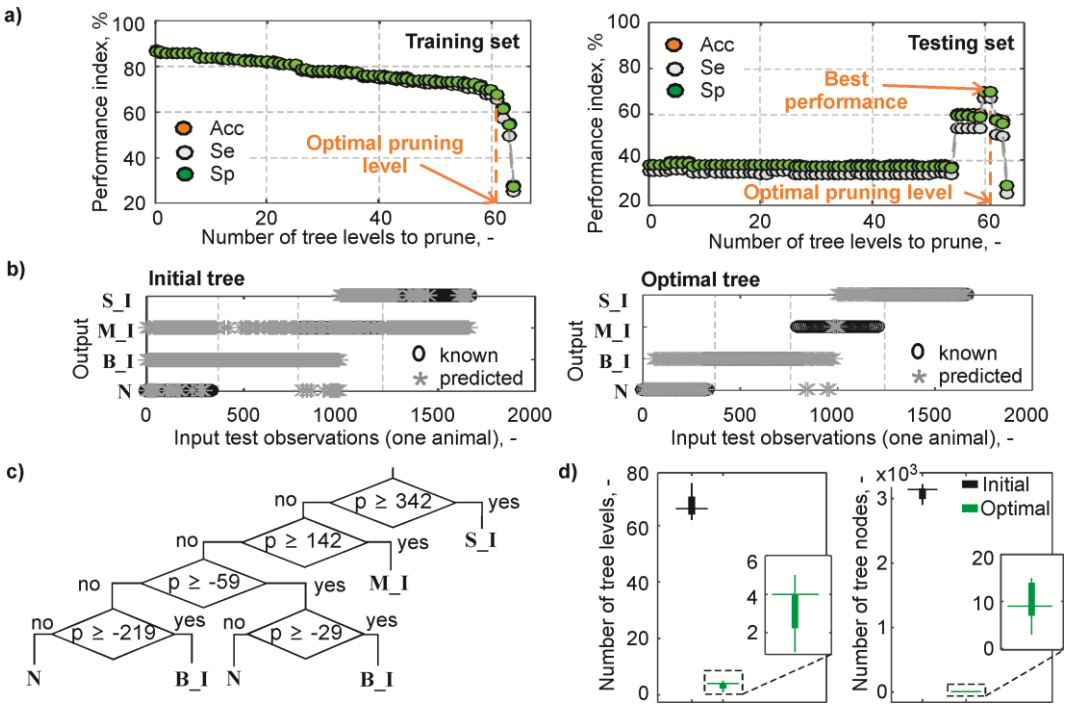

Figure 68. Selection of optimal decision tree for 4-class single-feature classification. Tree for AUC_{QRST} (lead I) from H group. Dependence of performance indices obtained by tree from one cycle of LOO validation on number of pruning levels (zero level means no pruning) evaluated on training (left) and testing (right) set (a) and corresponding trees' outputs (b) and optimal decision tree structure (c); size of initial and optimal (pruned) trees (LOO validation).

The best results obtained by DTs constructed for various features calculated using and without delineation outcomes are summarized in Table 26. As compared to binary decision-rule method (Table 15-17), the performance of 4-class classification by DT is generally lower by 5-15 %. Some of present features, such as QRS_A, $D^c_{jt}zy$ and JTmax (for control, H and stained hearts groups, respectively), are the same as in binary approach which confirms their capacity to detect myocardial ischemia. Unfortunately, none of feature measured in stained hearts gave accuracy higher than 52-55 %. In most features (from all experimental groups), such a low overall performance is due to very low Se obtained for non-ischemic and middle ischemic data and very low Sp in case of other two classes (both indices less than 30 %). Only those included in Table 26 provided Se and Sp higher than 60 % for three (non-ischemic, beginning and severe ischemia) from four classes, such as in case of AUC_{QRST} (see Fig. 68). It can be seen that the optimal trees consisted of relatively low number of levels which resulted in short duration of one validation cycles including training and testing (mostly shorter than 1 s) which is similar or even less than in cut-off determination using ROC curve analysis. In all cases except for φ, the decrease of performance was observed by using of the features calculated without delineation outcomes, especially in AUC_{QRST} which is strongly depend on the definition of the beginning and the end of QRS-T segments.

Table 26. Best results obtained by single-feature decision tree method.
Test results shown as mean ± SD (through all classes and LOO cycles).

Feature	Acc, %	Se, %	Sp, %	Computational time, s	Tree levels number
Control					
QRS_A (lead II)	61 ± 15	60 ± 14	60 ± 16	0.98	4 ± 2
	61 ± 15	59 ± 16	60 ± 16	1.08	6 ± 4*
φ	65 ± 10	63 ± 10	65 ± 10	1.27	20 ± 19
	66 ± 11	64 ± 11	65 ± 11	1.33	7 ± 7*
H group					
AUC_{QRST} (lead I)	62 ± 10	60 ± 9	61 ± 10	0.78	3 ± 1
	59 ± 2	54 ± 2	58 ± 2	0.98	5 ± 3*
$D^c_{jt}zy$	63 ± 5	62 ± 6	63 ± 5	0.85	5 ± 1
	62 ± 5	60 ± 6	61 ± 5	0.94	6 ± 2*
Stained					
JTmax (lead I)	52 ±12	48 ± 13	51 ± 13	0.19	6 ± 4
	48 ± 12	45 ± 12	48 ± 13	0.28	4 ± 2*
JTmax (lead II)	50 ± 18	45 ± 17	49 ± 18	0.13	10 ± 5
	45 ± 14	40 ± 13	44 ± 14	0.13	8 ± 6*

* – results obtained using parameters calculated without manual delineation outcomes

Cross-group validation of all features resulted in poor (lower than 55 %) overall performance obtained in different experimental groups. Thus, the 4-class classification model should be trained and applied on the same data.

As in case of testing DT on data from experimental group different from that used for training set definition, use of DT trained on features from the first ischemic period to classify data from other periods resulted in poor classification performance such as illustrated in Table 27 and Fig. 69a for φ (best feature for 4-class classification in control groups). This finding seems to be due to the differences in feature value measured in particular ischemic periods, mainly in their beginning (where higher values were obtained in the latest ischemic periods as compared to the first one) and ending (where because of preconditioning effect, higher values were obtained in 7^{th} -

8th minutes of the third ischemia as compared to the previous ones) phases (see Fig. 69b). As in cross-group approach, the best performance (according to SD values, quite well results were obtained in some animals) can be achieved only by tree trained on data from corresponding ischemic period.

Table 27. Results of cross-ischemia validation of single-feature decision tree method in control group. Test results shown as mean ± SD (through all classes and LOO cycles).

Indices DT	**Training = I1 (φ)** Tree level number: 21 ± 19			**Training = I2 (φ)** Tree level number: 3 ± 1			**Training = I3 (φ)** Tree level number: 18 ± 11		
	Test: I1	Test: I2	Test: I3	Test: I2	Test: I1	Test: I3	Test: I3	Test: I1	Test: I2
Acc,%	65 ± 10	54 ± 1	54± 2	59 ± 18	51 ± 10	52 ± 10	59 ± 12	54 ± 4	56 ± 2
Se,%	63 ± 10	53 ± 3	53 ± 2	59 ± 16	50 ± 11	51 ± 12	59 ± 10	53 ± 3	56 ± 2
Sp,%	65 ± 10	54 ± 2	53 ± 1	59 ± 17	51 ± 10	52 ± 10	59 ± 12	53 ± 4	56 ± 1

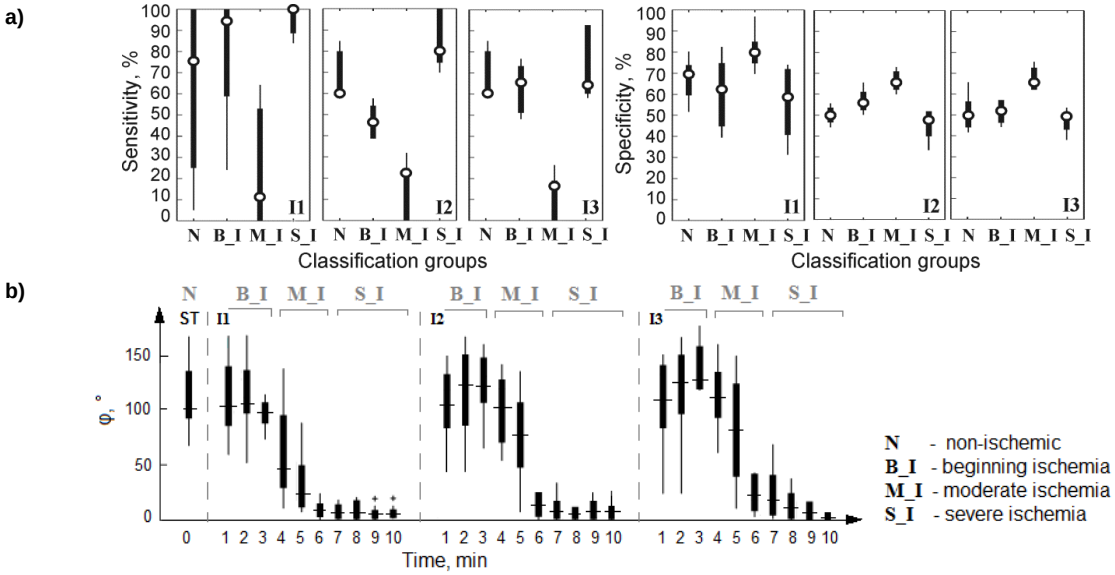

Figure 69. Cross-ischemia validation of decision tree 4-class classification using φ. Se and Sp (LOO) of tree (trained on data from the first ischemic period I1) tested on φ from the second (I2) and the third (I3) ischemia (a) and φ during corresponding periods (b).

Multi-feature supervised techniques

The best 4-class classification results obtained using different supervised approaches and feature sets are listed in Table 28. Except for H group, F51 based on VCG parameters seems to be suitable for classification by all models. In all groups, resulting performance indices are slightly higher than in DT method. The largest improvement (up to 5 %) was obtained in control group. SVM is evidently the best classification technique among three presented. The computational time is similar to that of multi-feature binary method (Table 22). Distribution of Se and Sp obtained by best approaches in particular classes is shown in Fig. 70. There are a large number of experiments, where the classification failed, even in the middle and ending phase of ischemia. On the contrary, high performance was achieved in some signals. This can be also illustrated as a graph of desired and 'real' outcomes and confusion matrixes showing a detailed distribution of the misclassified observations (Fig. 70b and Fig. 70c, respectively). According to the latter, the greatest number of incorrectly assigned samples given by SVM in the control group corresponded to those belonging to the transitional time periods (i.e. the beginning and the ending phases of particular classes).

It should be noted that the best approaches provide mentioned results despite utilizing of sets with only 7, 10 and 5 features in case of F6 (control group), F32 (H group) and F51 (stained hearts). For comparison, best classification accuracy achieved using the largest set F1 was 55 ± 11 % in control group (SVM), 56 ± 11 % in H group (LDF) and 46 ±13 % in stained hearts (SVM) which is even worse than that obtained by small sets.

In control group, use of F6 consisted from parameters calculated without delineation outcomes resulted in only slight performance decreasing despite the fact that QRS_D was removed from the feature set in this case. On the contrary, pronounced decrease in performance indices was observed in stained hearts group, where only three features remained in the set F51 after removing QRS_D and QT_D from it.

Table 28. Overall performance indices of the best 4-class multi-feature approaches. Shown as mean ± SD.

Experimental group	Classifier & feature set	Overall performance indices			Computational time, s
		Acc, %	Se, %	Sp, %	
Control	LDF & F51	62 ± 7	62 ± 8	62 ± 7	0.05
	k-NN & F51	60 ± 18	60 ± 18	60 ± 18	13.29
	SVM & F6	**68 ± 10**	**67 ± 11**	**68 ± 11**	**7.58**
		64 ± 8	63 ± 8	64 ± 8	8.20*
High LV mass fraction	LDF & F21	59 ± 16	57 ± 16	59 ± 15	0.06
	k-NN & F52	57 ± 12	55 ± 12	57 ± 11	10.39
	SVM & F32	**62 ± 22**	**63 ± 21**	**63 ± 22**	**6.71**
		59 ± 16	58 ± 15	59 ± 16	6.67*
Stained hearts	LDF & F51	50 ± 17	49 ± 15	50 ± 16	0.03
	k-NN & F51	48 ± 17	46 ± 15	48 ± 16	2.30
	SVM & F51	**57 ± 15**	**52 ± 12**	**56 ± 14**	**6.14**
		35 ± 21	33 ± 18	35 ± 21	7.79*

* – results obtained using parameters calculated without manual delineation outcomes

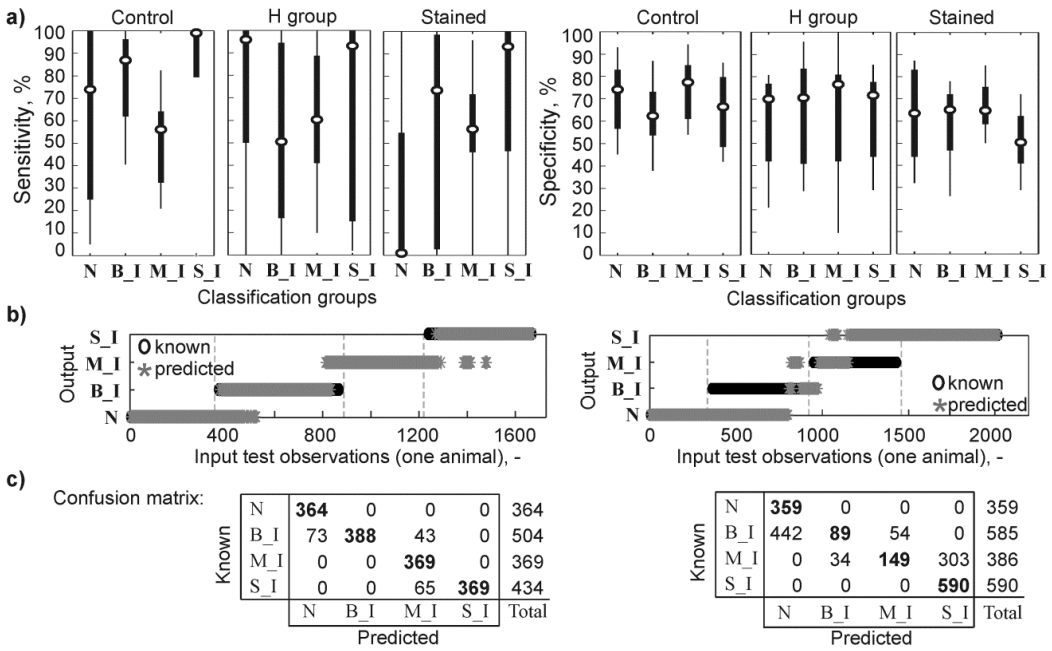

Figure 70. Outcomes of the best 4-class SVM based classifiers.
Se and Sp (LOO validation) of the best approaches for three experimental groups (a). Example of SVM response on control group testing data from two different animals (b) and corresponding confusion matrixes (c). N – non-ischemic; B_I, M_I and S_I – beginning, moderate and severe ischemia, respectively.

As in previous case, no approach was able to provide proper classification regardless the type of testing data.

As for cross-ischemia validation, the best results for control and H group were obtained by LDF trained on F51 from control data, whereas the only useful method for stained hearts data classification was LDF trained on F51 derived from corresponding experimental group (Table 29). According to Se and Sp calculated for particular classes (Fig. 71), the most difficult task (in terms of correct detection of ischemic samples, i.e. Se) was the recognition of the beginning and middle phases of ischemia.

Table 29. Results of cross-ischemia validation of the best 4-class multi-feature classifier in control group. Test results shown as mean ± SD (through all classes and LOO cycles).

Indices LDF	**Training = I1 control (F51)**			**Training = I2 control (F51)**			**Training = I3 control (F51)**		
	Test: I1	Test: I2	Test: I3	Test: I2	Test: I1	Test: I3	Test: I3	Test: I1	Test: I2
Acc,%	62 ± 7	59 ± 1	57 ± 1	55 ± 8	56 ± 3	61 ± 4	60 ± 16	59 ± 1	58 ± 2
Se,%	62 ± 8	60 ± 1	57 ± 1	57 ± 10	57 ± 3	62 ± 3	60 ± 16	60 ± 1	58 ± 1
Sp,%	62 ± 7	60 ± 1	57 ± 2	55 ± 8	57 ± 4	61 ± 3	60 ± 14	59 ± 1	59 ± 1

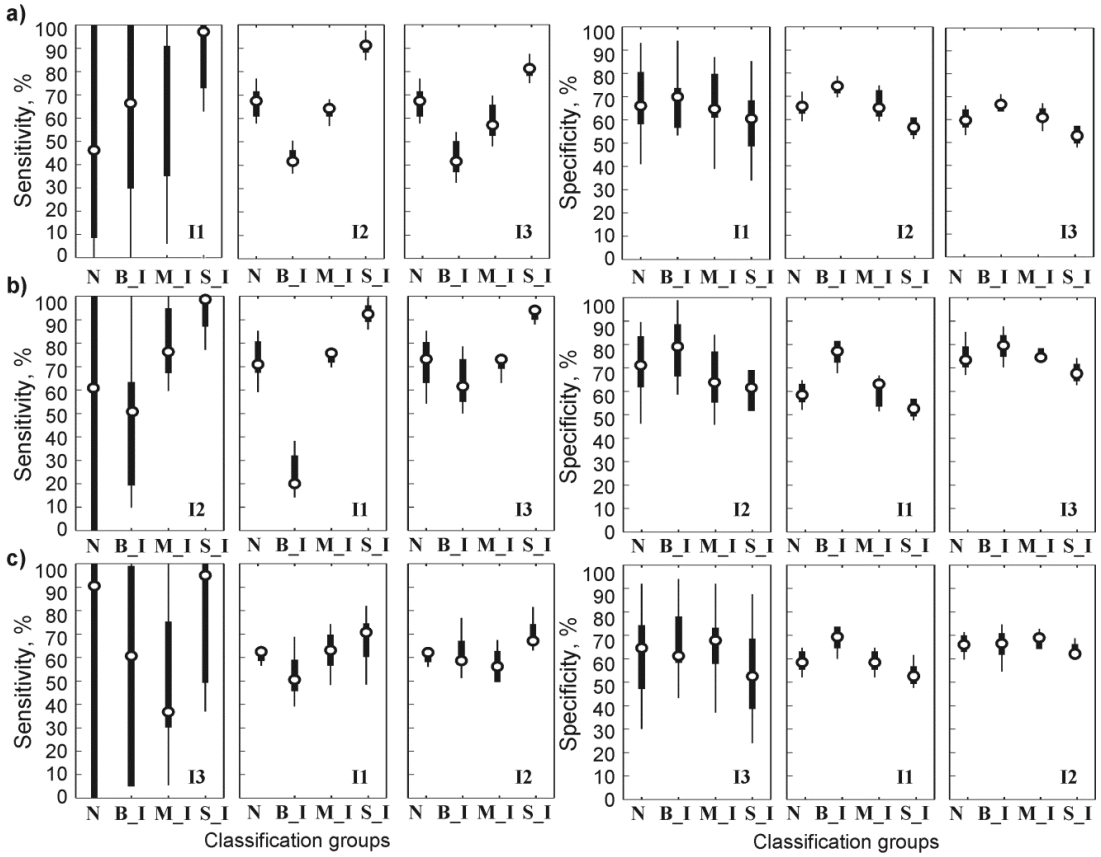

Figure 71. Cross-ischemia validation of 4-class LDF classification using F51 feature set. Distribution of Se and Sp obtained by testing (LOO) of LDF (trained on data from the 1st (a), 2nd (b) and 3rd (c) ischemic period) on F51 from two other periods. N – non-ischemic; B_I, M_I and S_I – beginning, moderate and severe ischemia, respectively.

As regards *11-class approach*, it can be, unfortunately, concluded that no technique was able to provide successful classification in particular experimental groups, which is most probably due to the small data set (in terms of number of available experiments). Thus, poor results were achieved by LOO validating procedure (see Se and Sp distribution for the best approach based on SVM in Fig. 72) even using the largest feature set F1.

Highly optimistic and nonetheless not perfect results were obtained by 10-fold CV (Fig. 72). In control and H groups, low Se at the end of ischemia can be explained by misclassifications between particular minutes within this part of experiment (i.e. between 7^{th} – 10^{th} minutes of ischemia). This performance index in approx. three first minutes of ischemia in all experimental groups is also quite low, because the most of testing samples were incorrectly classified as non-ischemic. As expected, these results are poorer in comparison with binary as well as 4-class approaches. Performance indices of method based on use the parameters calculated without delineation outcomes reached slightly lower values (up to 5 % reduction, not shown here).

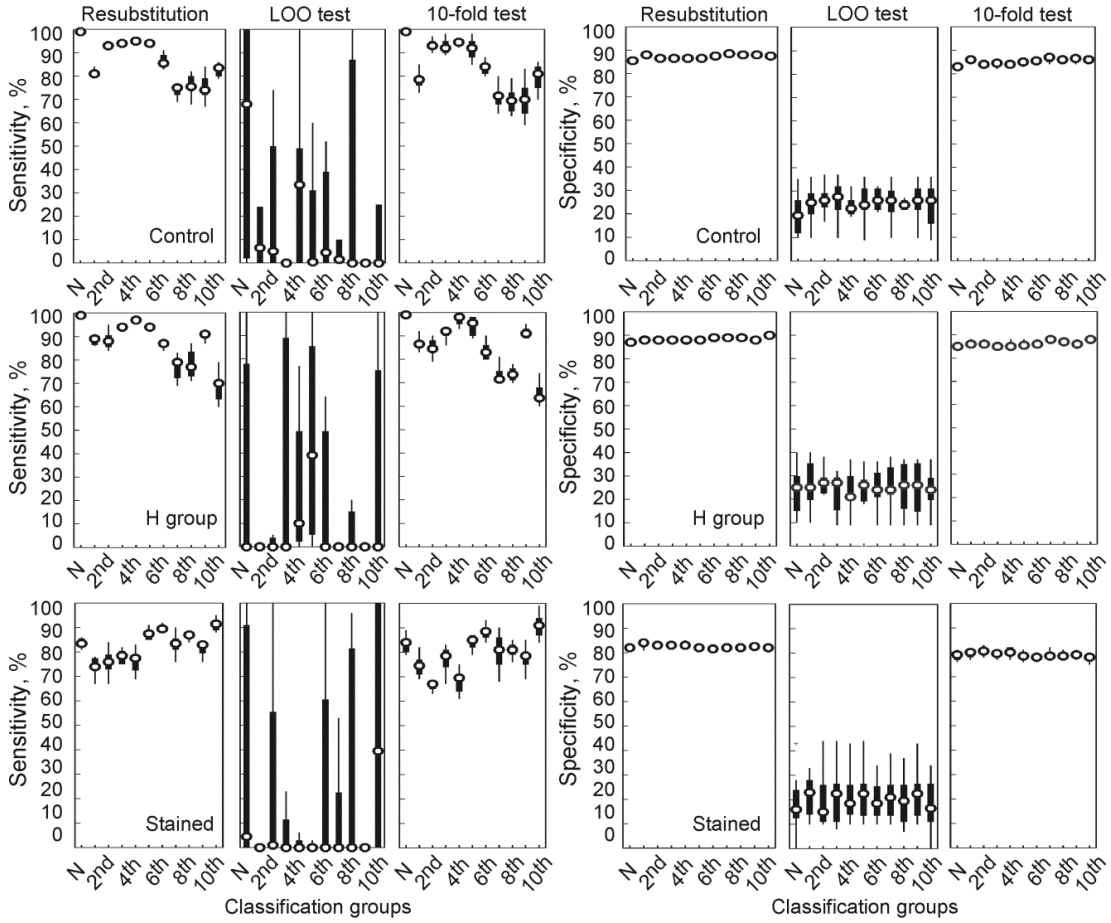

Figure 72. Sensitivity and specificity distribution for the best 11-calss SVM classifier.
SVM trained using F1 validated by LOO and 10-fold approaches. Results for control (top), H (middle) and stained hearts (bottom) groups. N – non-ischemic; 1^{th} - 10^{th} minutes of ischemic period.

5.4 DISCUSSION

The efficacy of simple single-feature ischemia detection by the decision rules is strongly dependent on the distribution of feature values. Although statistically significant ischemia-induced changes were found in some parameters in first two minutes of ischemic period (AUC_{QRS} and QRS_A from lead II, P_{qrs}, D, β_{qrs} in control group; +/-AUC_{QRS} from both leads, $A_{jt}xy$, P_{jt}, D in H

group; QRS_A and AUC_{QRS} from lead II in stained hearts), the high inter-subject variability in data does not allow providing good detection of early ischemia using these parameters.

Above phenomena is not so pronounced in case of multi-feature approaches, where only parameters selected by correlation- or PCA-based feature filter are taken into account. Forward selection proposed for feature selection by LDF is the simplest algorithm among all wrapper techniques. However, this method may fail and select redundant feature because of the principle used: once a feature is added to the feature set it cannot be removed later. Both correlation- and PC-based ranking may result in non-optimal selection. Estimation of the contribution the feature to the result is rather difficult task and selection of features with small contribution to the PCs or relatively high averaged correlation relative to other parameters would lead to performance enhancement. On the other hand, the feature set identification by this way is rapid and seems to be sufficient for the task addressed in the dissertation according to the results obtained using feature sets F51, F21, F41 and F32. Similar method was used by Tseng et al. [180], when four features were sequentially added to initial feature set consisted of three main features and accuracy was monitored to find out the best feature number. Selection of feature from only leads with minimal p-value of t-test comparing non-ischemic and ischemic data was proposed in [33]. More advanced techniques such as step-wise discrimination with LOO validation (3 to 6 features in final set [179]), sequential forward floating selection with 10-fold cross-validation (37 features [178]) and correlation-based feature subset selection (28 features [175]) or even feature extraction by PCA [176] were used to select more relevant features for ischemia detection. Nevertheless, some fixed number (in most cases relatively low) of features chosen in accordance with some empirical information or guidelines is usually used for ECG data classification.

It was found, that the features calculated from VCG are very promising, as was represented by the quite high performance obtained using VCG parameters (single-feature approach) and F51 feature set (multi-feature approach) in case of binary as well as 4-class classification in all groups. It was also supported by the results of cross-group classification, when the best overall performance was observed by LDF trained using F51 set. Various classification systems based on VCG parameters alone (such as QRS loop and spatial T wave parameters) or in combination with some others have been previously reported (e.g. [2],[23],[36],[37]). Particularly, it was found that uncommon QRS loop parameters combined with standard ST-change vector magnitude, QRS vector difference and spatial ventricular gradient may provide good detection of ischemia (Se = 95.4 % and Sp = 95.2 %) in data from the PTCA procedure. These indices are better than those obtained in thesis for binary classification using F51 (median values in control group: Se = 76 %, Sp = 99 %). It should be, nevertheless, noted that in above case ischemia was detected by minute-by-minute way and mentioned results were obtained for data from the 4^{th} minute of PTCA, whereas in present work data from the whole period of perfusion stopping was considered as ischemic.

VCG parameters include the information from two or three orthogonal leads. This approach can be replaced by using parameters calculated from several standard leads data. Such multi-lead method may be useful, if different phases of ischemia (from the earliest to the severe one) are manifested in signals recorded from different sites of the heart wall. According to the content of F2 and F7 feature sets observed by both correlation- and PC-based ranking in all experimental groups, both horizontal leads obtain information valuable for ischemia detection. Data from both leads (e.g. F3 and F4 sets) provide similar classification performance within the same experimental group, if they are used alone. Nevertheless, combination of common parameters (ST20, T_A and QRS_A) from both leads into one set results in enhancement of detection results as compared to methods based on

features from one lead (up to 15 % for Se and Sp, depending on experimental group). Classification methods reported in the literature are mostly based on two- ([33],[86], [171], [174],[179]), three- ([23],[174]) or even 12-lead ([87]) features.

According to present results and reports by other authors, multi-feature approaches have larger capacity to detect ischemia as compared to single-feature methods, which are, however, less computationally expensive and, consequently, more suitable for real-time applications. In experimental data, accuracy of multi-feature binary detectors was higher by 9-25 % (depending on experimental group) than that of the best single-feature methods. Similar improvement was achieved by Correa et al. by using 7-feature-based LDF model (Se = 88.5 %, Sp = 92.1 %) instead of single-feature method (Se = 73.2 % and Sp = 73.9 % for ST-vector magnitude or Se = 64 % and Sp = 74.6 % for QRS loop volume) [36]. In other report [179], use of six features (commonly used ST60, T amplitude, QRS duration as well as their KLT-based modifications) instead of three resulted in increasing accuracy of occlusion type classification by approx. 9 %. Number of classification features used in different studies vary from 2-7 ([23],[33],[36],[84]-[86],[171], [172], [180]) to several tens ([87],[175]) or even hundreds ([176],[177]) of parameters. However, large feature number does not ensure accurate classification outcome. For example, Se of classification by SVM trained on 150-feature-long vectors (corresponding to samples of RT interval) does not exceed 90 % [177], such as in case of ANN trained on feature vectors consisted of 100 samples of ECG beats transformed by PCA [176]. In all approaches from present study, the largest feature set F1 was not chosen as the best one, mostly because of overfitting the models.

The majority of features selected to the sets providing best ischemia detection in experimental data are probably represented by those based on calculation of area under various parts of QRS-T. In accordance with the results of analysis of parameters' discrimination ability (see above), QRS related features play important role (at least similar to ST-T related ones) in classification. Both findings are not common in ischemia detection in human ECG, although there are a number of studies, where the suitability of uncommon features such as third moment of ST deviation histogram [174], ECG samples simply transformed by PCA [176], features based on QRS loop [36], slopes of QRS [33], PCA-based features analogues to conventional [87],[179] has been proven. In the latter case, it was moreover shown that detection using PCA-transformed features is more sufficient as compared to use of common QRS and ST-T based features. Among other parameters, which are not convenient for ischemia detection, are heart rate ([175],[178]), QT duration [85], age and gender ([85]-[87],[171]), samples of ECG without any transformation [177] or directly transformed by PCA [176], etc.

The main advantage of using the single-feature approaches or/and easily calculated features (or using directly samples of ECG) is low computational expensive of the method. All methods employing the parameters derived from QRS and/or ST-T requires ECG delineation (or at least J point and/or T wave peak detection, if only ST is considered), which is a challenge itself. Both automatic and manual detection of J point and the end of T wave (fundamental for calculation of the most parameters used for ischemia detection) is especially difficult in a progressively changing signal, such as in that recorded during PTCA procedure or developed ischemia induced in isolated heart by perfusion stopped for a certain minutes. Incorrect delineation may be the source of the errors obtained during classification. In present work, method of parameters calculation without delineation outcomes (required only detection of QRS complexes) is proposed. Obviously, values of some parameters are biased (in most case non-significantly) as compared to those derived using manually detected beginning of QRS, J point and the end of T wave. It is shown that such parameters may be successfully used to detect ischemia, especially in control and H group, where

the variability in data is not so prominent such as in stained hearts. Use of this procedure allows significant reducing the time-consuming of the method and avoiding uncertainty characteristic for automatic and manual delineation. The results could be probably further improved by using 'artificial' regions determining QRS, QRS-T and ST-T, adapted for each separate experimental group.

One of the best published results for binary single-feature classification is that obtained by using so called isoelectric energy for ST and corresponding decision rule-based system [173], where Se and Sp reached 98.1 % and 98.2 %, respectively. Among multi-feature methods, one of the best is based on SVM trained on 7-feature-long vectors providing Se = 94.8 % and Sp = 99.5 % [180]. Generally, use of discriminant function yields poorer results as compared to more advanced supervised techniques. In experimental data, one of the highest performance with Se = 71 % and Sp = 78 % (median values) were found in case of thresholding $AUC_{JTmax/TmaxTend}$ from lead II (control group) and Se = 90 % and Sp = 86 % (median values) in case of multi-feature SVM based detection by 5-feature-length set F7. Thus, performance indices are not so high such as in published approaches. Nevertheless, the direct comparison of the results obtained for binary classification in thesis and reported by other authors is rather difficult which is associated not only with origin of data classified (from human *vs* animal isolated heart), but also with the concept used for definition of data set representing ischemic state. In most studies ([32],[84]-[86],[171]-[173],[176],[177], [180]), the efficiency of classification algorithm was tested using data from European ST-T Database containing ECGs and the results of their labelling by scorers according to ST-based guidelines [165]. Thus, ECG beats labelled by scorers as ischemic and consequently included into the corresponding data group for further classification show quite prominent, visible manifestations of myocardial ischemia, such as ST elevation or depression higher than standardized threshold. Moreover, in some cases, several parts of ECG (10 seconds from each side of the boundary) were excluded from the study to avoid ambiguous region between ischemic ST episode and normal beats [84].

On the contrary, in experimental data, the standardized ECG-based criteria for ischemia detection are missing and there are no available results of some other diagnostics method ('gold standard' such as SPECT or echocardiography). Moreover, in global ischemia model, the severity of ischemia cannot be regulated by adjustable percentage restriction of coronary supply such as in case of regional ischemia. Thus, the only reliable information about ischemia (or potential ischemic injury in preparation) is the beginning of perfusion stopping during experiment. This time moment was therefore considered as the beginning of 'true' ischemia. As was shown above, it results in more pessimistic Se due to large number of false negatives at first 2-3 minutes of ischemic period (transitional period between stabilization and middle phase of ischemia, where some changes can be found in EGs). The 'shift' of ischemia beginning to the 3^{rd}-4^{th} minute of this period allows reaching more advanced performance. This is in agreement with the results reported for ischemia detection in data recorded during PTCA procedure in ischemic patients from STAFFIII database. In this case, the successful performance of ischemia detection (relative to data of healthy subjects from other group) was obtained in only the 4^{th} minute of ischemia [37]. The results were depend on features used for detection by LDF and, when using only three conventional VCG parameters, values of indices were Se = 90.1 % and Sp = 89.9 % at the end of the 5-min-long occlusion (whereas results from Table 11 were achieved using seven VCG parameters including those calculated from QRS loop). In other study, the detection was performed on data from 'Exercise testing and imaging perfusion database' from THEW, where ECG beats were scored by the experts according to the manifestations on patients' SPECT images [33]. According to the results, ST

depression was presented in ECG only around the end phase of the 16-min-long exercise test and Se of the detection by LDF trained on QRS slopes reached only 24 %, despite the fact that only samples from peak exercise (i.e. at the time, at which the maximum heart rate was detected) – and not the whole test – were considered as 'ischemic'. On the same data, Llamedo et al. achieved more advanced results (Se = 77 % and Sp = 84 % for mild ischemia with ischemic myocardium ≥ 5 % and Se = 76 % and Sp = 90 % for severe ischemia which ischemic myocardium ≥ 10 %, respectively) by logistic regression model trained on large feature set including parameters from principle components and basic characteristics (age, systolic blood pressure, heart rate, gender, infarction, etc.) [87]. Thus, better results were obtained for more severe ischemia.

Other factor dramatically affected the results of classification and their validity is the size of data set and type of used cross-validation. In most reported cases ([84],[176] and other studies based on European ST-T database data), data for training and testing sets were selected from each patient as e.g. 2.5 % and rest of the final dataset, respectively (so called hold-out validation). In this case, the results were not cross validated. Despite relatively small training set, the results may be overestimated in comparison with those which could be obtained by LOO scheme of validation used in dissertation. It was validated on 11-class approach, where classification results obtained by 10-fold cross-validation were highly optimistic, whereas LOO procedure failed. Tseng et al. performed similar selection of training set and tested the model by 10-cross validation, but using only 462 beats [180], whereas Murthy et al. trained and tested the classifier on 297 and 296 observations, respectively [177]. Results obtained by Correa et al. by 100-fold cross-validation (i.e. by training and testing 100 different LDFs for data from 52 healthy and 80 ischemic patients [36]) seem to be the most reliable.

Considering the aforementioned, efficacy of binary approaches proposed in the thesis (mainly in terms of calculated parameters and used feature selection techniques) is generally comparable with those published in the literature. Binary classification by LDF – the simplest from all proposed methods – seems to be the most promising (low computational time but relatively good performance), which is in agreement with the literature [36],[179].

To the best of our knowledge, none of reported methods (multi-class) provide the discrimination between particular phases of ischemia. There are only studies, where the binary models for classification of data with ischemia manifestations developed during PTCA were trained for each minute of ischemia separately (minute-by-minute approach, [36]) or two separate models were trained for data from middle and severe ischemia phase [87]. Available multi-class approaches, on the other hand, enables discrimination between various types of ST deviations (normal *vs* concave or convex elevation, up-sloping, down-sloping, or horizontal depression [172]), types of disorder (Prinzmetal's angina, coronary artery disease or other including no episodes of ischemia or mixed deviations [174]) or types of culprit (LAD, RCA or LCX [179]).

OVERALL CONCLUSIONS

Results achieved in proposed dissertation mainly contribute to the field of basic electrophysiological research with methodological suggestions associated with the acquisition, analysis and interpretation of data from experiments on rabbit isolated heart undergoing global ischemia. Particularly, the main patterns of EGs and VCG recorded in the hearts under non-ischemic conditions are described in detail by various parameters derived from the records. These parameters are then used to quantify the heart response to short-term repeated global ischemia. It is shown, that electrical activity from different areas of the heart can be accurately recorded by touch-less way using three-lead orthogonal electrode system during longitudinal rotation of the heart. One of the most valuable results in this part is that the earliest global ischemia is mostly manifested in the depolarization phase, in contrast to the regional ischemia induced by occlusion of some coronary artery, when the pronounced changes are usually observed in repolarization period. Nevertheless, moderate and severe global ischemia results in marked changes of ST-T part of EG. As regards the spatial organization of global ischemia, the beginning and moderate phase are distinguishable mainly in EG from middle part of LV (anterolateral region), whereas the severe degree is represented in the records from any site of LV wall, with most pronounced manifestations in boundary part of LV (posterolateral region). Therefore, recording of EG by at least two leads facing above LV regions or three-lead VCG is suggested for accurate and timely assessment of all grades of ischemia.

Next contribution is associated with the evaluation of the effect of increased LV mass (which is relatively frequently seen in rabbits because of their high sensitivity to spontaneous LV hypertrophy) on cardiac electrical activity under both non-ischemic and ischemic conditions. Area under QRS complex (AUC_{QRS}) calculated for leads facing anterior or anterolateral area of the heart is proposed as electrophysiological marker of increased (even slightly) LV mass providing Se = 75 % and Sp = 82 %. In contrast to ECG indices commonly used in clinical practice for detection of LV hypertrophy (such as Sokolow-Lyon criteria, etc.), AUC_{QRS} does not require detection of particular peaks in QRS, which is a challenging task in case of experimental EG. Thus, increased LV mass mainly affects ventricular depolarization phase, which may lead to QRS patterns similar to those caused by ischemia. Manifestations of both phenomena are lead-dependent, which makes it possible to select data from lead 'insensitive' to LV mass changes, if study is focused on impact of ischemia itself and effects of LV mass on EG should be eliminated. However, it is shown, that some electrophysiological effects of increased LV may appear in ischemia only, which may negatively affect the accuracy of ischemia detection due to unsuitable discrimination criteria. For example, use of AUC_{QRS} cut-off calculated in the heart with normal LV (from 'insensitive' lead) results in perfect Se (100 %), but reduced Sp (85 % against 100 % in case of cut-off calculated for corresponding group of hearts with increased LV mass). Use of cut-off calculated for the hearts with changed LV leads to decrease of Se (by 10 %) and increase of Sp (by 4%) by discriminating ischemia in data from control group. ST-T based parameters (such as ST20 and others) seem to be more robust to changes of LV and, consequently, more suitable for ischemia detection in studies on the hearts with increased LV or if no information about LV mass is available. However, as was mentioned above, these parameters have less capacity to detect early phase of ischemia, as compared to those derived from QRS.

In recent animal studies, VSD di-4-ANEPPS is widely used for recording cardiac MAP. Nevertheless, the side-effects of the dye on cardiac electrical activity have been described mainly in small animals, such as rat, mouse and guinea pig. According to the results of previous studies,

the electrophysiological effects of the dye are mainly present in EGs recorded during staining and washout periods of experiment. Ideally, these changes are reversible and disappear by the end of washout. Results addressed in thesis show, nevertheless, that some changes in heart activity caused by the dye are irreversible. This may affect the results obtained during the part of experiment following the washout. Among the most significant direct effects (not associated with dye phototoxicity) of di-4-ANEPPS observed in rabbit myocardium are: a) decrease of spontaneous heart rate manifested in EG as RR interval prolongation, which, in turn, results in increased QT duration; b) slowing impulse conduction through the ventricles represented by significant QRS prolongation, which can be explained by the inhibition of I_{Na} in presence of the dye (validated by patch-clamp experiments); c) non-sustained slowing cardiac impulse conduction through AV node manifested as increased PQ duration during staining procedure. Prolongation of QT and QRS should be taken into account especially in cases, where the rabbit heart is used for the study of the arrhythmogenic potential of drugs. First two above mentioned phenomena are not reversible and, therefore, the progress of ischemia in stained preparations differs from that in control group (non-stained hearts). Namely, the dye delays the occurrence of significant ischemic changes, partially attenuates the severity of ischemia and enhance recovery at reperfusion in rabbit isolated heart, most likely due to reduced cardiac energy consumption caused by decreased resting heart rate. It is reflected in slower and less pronounced progress of EG and VCG parameters in stained hearts during 10-min long ischemia, as compared to the controls. This finding complicates analysis and interpretation of data obtained in experiments with di-4-ANEPPS. Particularly, significant ischemia-induced changes in EG and VCG can be expected by 1-3 min later than in controls and the number of parameters with the good ability to discriminate ischemia is much smaller in stained hearts. Among the parameters capable to detect ischemia in stained hearts, there are AUC_{QRS} and QRS_D, which, however, should be used with special care because of their sensitivity to LV enlargement. Therefore, other parameters should be preferred to avoid undesirable cross-effects of three factors – myocardial ischemia, VSD, and increased LV mass. The morphology of EG recorded in stained hearts varies quite widely among the preparations, which results in high variability of parameters values and, consequently, worsening of their discrimination ability. This additionally complicates the diagnosis of ischemia. Generally, to achieve appropriate results in ischemia studies, the prolongation of ischemic period or increase of heart rate by pacing may be considered. Possible discrepancies in results may be eliminated by using stained hearts as controls if possible; if not, appropriate methodological correction of evaluated parameters, such as analysis of values corrected by their stabilization levels instead of initial ones, should be performed to avoid wrong interpretation.

Finally, the dissertation contributes to the recent state-of-the-art in computer-based detection of myocardial ischemia by proposing of several classification approaches and validating them on data recorded during progressing ischemia. The effects of increased LV mass, VSD and preconditioning on efficacy of ischemia detection in electrophysiological data are quantified for the first time. Some methodological aspects, such as definition of the beginning of ischemic injury, method of feature calculation (using or without previous detailed delineation of EG), number (single- *vs* multi-feature approach) and type of the features (common – such as ST20, QRS_A and QRS_D, *vs* uncommon, such as those used recently for classification of different types of arrhythmias rather than ischemia and newly proposed, based on relative AUC values of EG and VCG patterns), number of classes (common binary *vs* non-conventional 4- or 11-class for more detailed analysis of particular grades of ischemia), type of algorithms for feature selection (correlation- vs PCA-based ranking) and classification (simple thresholding, decision tree,

discriminant functions, k-NN, and SVMs), and method for cross-validation (LOO *vs* 10-fold) are also addressed (some of them for the first time). The most interesting and useful observations are summarized below. According to the content of feature sets obtained by correlation- and PCA-based selection methods, parameters calculated as relative AUC values are the least correlated with others; QRS-related parameters explain the most variance in data (i.e. they are potentially the most informative for further classification). AUC- (calculated from QRS and ST-T) and VCG-based features (representing information about spatial orientation of cardiac electrical vectors) seem to be the most promising. Both feature types belong to uncommon group and allow obtaining similar or even better results in comparison with conventional ST20 and QRS_D. Small sets (7 and less features) provide good classification results, whereas large sets are not suitable for binary as well as multi-class approaches mainly due to model overfitting. Besides the elimination of overfitting, use of small feature sets significantly reduces computational complexity of the method, which is important in both off-line and real-time applications. Other technique allowing dramatic decrease of time-consuming of EG interpretation (by several times) consists in calculation of the parameters using empirically defined the beginning and the end of QRS complex and T wave. It is shown that classification performance achieved using such parameters is usually similar or only slightly reduced as compared to the conventional features. Nevertheless, the estimation of some features (such as AUC-based from QRS) via this method may be quite biased, which results in worsening of classification accuracy. Thus, more robust features (e.g. representing EG or electrical vectors deviation, etc.) should be preferred to avoid this effect. As in many previous reports, linear types of both discriminant function and SVM have better discrimination ability as compared to their non-linear alternatives (quadratic discriminant and SVM with Gaussian kernel). Along with k-NN, these types of classifier seem to be predisposed to overfitting, even in case of small feature sets. In most cases, SVM provides the best results. Nevertheless, if the low computational time is desirable, LDF may be used instead, without significant loss of detection quality. Besides all above factors affecting the efficacy of ischemia detection, there is other one, may be the most important, that is related to the heart condition itself. This is associated with above mentioned changes in cardiac electrical activity caused by increased LV mass or side-effects of chemical agents, such as VSD di-4-ANEPPS. According to the results, the most accurate ischemia detection can be performed in control group and hearts with changed LV, whereas slowed ischemia progress and high intra- and inter-subject variability in data results in quite poor detection performance in stained hearts. Thus, if there is a need to build the universal tool providing successful detection regardless data type, features from the group with the most complicated classification (and as a result the lowest performance achieved, such as in stained hearts) are suggested for training the model. Generally, such a tool can be suitable, if no information is available about LV anatomy or if classification is provided for hearts undergoing some chemical intervention, that changes (attenuates) the severity of ischemia. Preconditioning effect presented in all experiments should be also taking into account, when heart response to different subsequent ischemic periods is evaluated. Occurrence of ischemia manifestations in EG in the second and third ischemic periods is time delayed in comparison with the first one. As a result, low Se is obtained in second and third ischemia because of high number of false negative answers at the beginning and middle of these periods. Classifier trained on data from the first ischemic period provides quite good performance for data from subsequent ischemic episodes. Generally, in comparison with the reported results achieved in studies with PTCA data (where progressing ischemia is represented, such as in case of experimental data used in the thesis), the performance of proposed classification approaches is comparable or slightly better, even when data recorded immediately after perfusion stopping were considered as ischemic. In present setup

employing simple thresholding (analogue to the decision in clinical practice), ischemia detection is possible at 2^{nd}-3^{rd} minute after perfusion stopping (with Se and Sp of approx. 68 % and 85 %, respectively) in control hearts and those with increased LV mass and at 3^{rd}-4^{th} minute after ischemia onset (with Se and Sp of approx. 63 % and 70 %, respectively) in stained hearts. Use of more advanced classifier – SVM – improves the time (detection in 1^{st}-2^{nd} minute of ischemic period in all experimental groups) and the performance (approx. Se and Sp are 89 % and 81 %, respectively) of the detection. In case of 4-class approach, the most difficult task is distinguishing of moderate ischemia, where the first part of this period is usually assigned as the beginning grade and the latter as the severe grade of ischemia.

The study limitations are associated with various its aspects. Data clustering performed at the beginning affects the time resolution of the method, where the real courses of parameters during experiment are smoother than those obtained by the proposed procedure. On the other hand, this technique allows significant reducing of time required for manual delineation of EG (by several hours). Other possible source of distortion is in the delineation itself, where the main difficulty is associated with J point detection (especially in progressing ischemia), which is crucial for accurate calculation of important parameters. The delineation was, nevertheless, provided by one reader and possible systematic error in detection of particular points is nearly constant. Proposed approach for estimation of parameters without outcomes of manual delineation allows avoiding above errors; however, important interval characteristics, such as QRS_D and QT_D representing electrical depolarization and repolarization of the ventricles, are not informative in this case (constant during the whole experiment). Classification results are negatively affected by the concept used for determining the beginning of ischemic injury. According to this concept, data recorded immediately after perfusion stopping are considered as ischemic because of lack of gold standard for accurate assessment of ischemia in present experimental setup. It can be assumed, that the onset of ischemic injury in preparation is actually delayed due to reserve of oxygen in heart tissue. Thus, enhancement of the detection performance (due to less number of false negatives at the beginning of ischemic period) might be expected, if results of some other test would be available.

Further research might be focused on the verification of above results in subjects with evident LV hypertrophy (with significant changes in anatomy and/or function of LV) and on the investigation of gender and age dependence of phenomena associated with progressing ischemia in the hearts with unchanged and increased LV, which would be useful for support of ischemia diagnosis in patients with one or both these disorders. Validation of the dose-dependence of di-4-ANEPPS effects in the same heart model could be informative for effective experimental setup, reliable data acquisition and accurate interpretation of the results. Further development of ischemia detection methods can be based on other features, which seem to be promising according to published results. One of possible choices is investigation of high-frequency content of experimental QRS. However, there is no standardized method for quantification of the components even in human; moreover, signal averaging is required to obtain successful results, which may negatively affect the analysis of progressing ischemia. As shown in pilot study (see [193]), there is a high inter-subject variability in HF-QRS parameters. Thus, more experiments are needed to validate the findings and to appreciate the potential practical usefulness of this approach.

In view of aforementioned, comprehensive approach taking into account both anatomical and electrical characteristics of the heart and its orientation within the electrode system is required for proper analysis of heart electrical activity under normal and pathological conditions. Computer-based methods may be useful adjuncts in processing and analysis of ECG/EG and detecting various electrophysiological abnormalities.

REFERENCES

[1] Townsend N, Wilson L, Bhatnagar P, et al. Cardiovascular disease in Europe: epidemiological update 2016. Eur Heart J 2016.

[2] Wagner GS, Macfarlane P, Wellens H, et al. AHA/ACCF/HRS recommendations for the standardization and interpretation of the electrocardiogram: part VI: acute ischemia/infarction: a scientific statement from the American Heart Association Electrocardiography and Arrhythmias Committee, Council on Clinical Cardiology; the American College of Cardiology Foundation; and the Heart Rhythm Society: endorsed by the International Society for Computerized Electrocardiology. Circulation 2009; 119: e262–70.

[3] Dhein S, Mohr DW, Delmar M. Practical methods in cardiovascular research. Springer Berlin Heidelberg, 2005, p. 997, ISBN 978-3-540-40763-8.

[4] Olejnickova V, Novakova M, Provaznik I. Isolated heart models: cardiovascular system studies and technological advances. Med Biol Eng Comput 2015; 53: 669-678.

[5] Kang C, Brennan JA, Kuzmiak-Glancy, et al. Technical advances in studying cardiac electrophysiology – role of rabbit models. Prog Biophys Mol Biol 2016: 121: 97-109.

[6] Bers DM. Excitation-contraction coupling and cardiac contractile force (2nd edition). Dordrecht: Kluwer Academic Publisher, 2001, p. 427, ISBN 0-7923-7157-7.

[7] Lee HC, Mohabit R, Smith N, et al. Effect of ischemia on calcium-dependent fluorescence transient in rabbit hearts containing indo 1. Correlation with monophasic action potentials and contraction. Circulation 1988; 78: 1047-1059.

[8] Bers DM, Perez-Reyes E. Ca channels in cardiac myocytes: structure and function of Ca influx and intracellular Ca release. Cardiovasc Res 1999; 42: 339-360.

[9] Takahashi A, Camacho P, Lechleiter JD, et al. Measurement of intracellular calcium. Physiol Rev 1999; 79: 1089-1125.

[10] Leirner AA, Cestari IA. Monophasic action potential. New uses for an old technique. Arc Bras Cardiol 1999; 72: 237- 242.

[11] Kusumoto F. ECG interpretation: from pathophysiology to clinical application. Springer, 2009, p. 298, ISBN 978-0-387-88879-8.

[12] Nasario Junior O, Benchimol Barbosa PR, Trevizani GA, et al. Effect of aerobic conditioning on ventricular activation: a principal components analysis approach to high-resolution electrocardiogram. Comput Biol Med 2013; 43: 1920-1926.

[13] Riera AR, Uchida AH, Filho CF, et al. Significance of vectorcardiogram in the cardiological diagnosis of the 21st centrury. Clin Cardiol 2007; 30: 319-323.

[14] Carmeliet E. Cardiac ionic currents and acute ischemia: from channels to arrhythmias. Physiol Rev 1999; 79: 917-1017.

[15] Shaw RM, Rudy Y. Electrophysiologic effects of acute myocardial ischemia: a theoretical study of altered cell excitability and action potential duration. Cardiovasc Res 1997; 35: 256-272.

[16] Sulkin MS, Boukens BJ, Tetlow M, et al. Mitochondrial depolarization and electrophysiological changes during ischemia in the rabbit and human heart. Am J Physiol Heart Circ Physiol 2014; 307: H1178-H1186.

[17] Dekker LRC, Coronel R, Van Bavel E, et al. Intracellular Ca^{2+} and delay of ischemia-induced electrical uncoupling in preconditioned rabbit ventricular myocardium. Cardiovasc Res 1999; 44: 101-112.

[18] Kalogeris T, Baines CP, Krenz M, et al. Cell biology of ischemia/reperfusion injury. Int Rev Cell Mol Biol 2012; 298: 229-317.

[19] Gorgels APM. ST-elevation and non-ST-elevation acute coronary syndromes: should the guidelines be changed? J Electrocardiol 2013; 46: 318-323.

[20] Gibbons RJ, Balady GJ, Bricker JT, et al. Acc/AHA 2002 guideline update for exercise testing: summary article: a report of the American College of Cardiology/American Herat Association Task Force on Practice Guidelines. Circulation 2002; 106: 1883-1892.

[21] Surawicz B, Tavel M. Stress test. In: Surawicz B, Knilans TK, editors. Chou's electrocardiography in clinical practice, Philadelphia: Saunders Elsevier, 2008, p. 221-255, ISBN 978-1-4160-3774-3.

[22] Man S, Haar CC, Schalij MJ, et al. The dependence of the STEMI classification on the position of ST-deviation measurement instant relative to the J point. In Computing in Cardiology 2015; 42: 837-840.

[23] Fayn J. A classification tree approach for cardiac ischemia detection using spatiotemporal information from three standard ECG leads. IEEE Trans Biomed Eng 2011; 58: 95-102.

[24] Haeberlin A, Studer E, Niederhauser T, et al. Electrocardiographic ST-segment monitoring during controlled occlusion of coronary arteries. J Electrocardiol 2014; 47: 29-37.

[25] Michaelides AP, Dilaveris PE, Psomaraki ZD, et al. QRS prolongation on the signal-averaged electrocardiogram versus ST-segment changes in the 12-lead electrocardiogram: which is the most sensitive electrocardiographic marker of myocardial ischemia? Clin Cardiol 1999; 22: 403-408.

[26] Takaki H, Tahara N, Miyazaki, et al. Exercise-induced QRS prolongation in patients with mild coronary artery disease. J Electrocardiol 1999; 32: 206-211

[27] Goldberger AL, Bhargava V, Froelicher V, et al. Effect of myocardial infarction on high-frequency QRS potentials. Circulation 1981; 64:3 4-42.

[28] Abboud S, Cohen RJ, Selwyn A, et al. Detection of transient myocardial ischemia by computer analysis of standard and signal-averaged high-frequency electrocardiograms in patients undergoing percutaneous transluminal coronary angioplasty. Circulation 1987; 76: 585-596.

[29] Amit G, Granot Y, Abboud S. Quantifying QRS changes during myocardial ischemia: Insights from high frequency electrocardiography. J Electrocardiol 2014; 47: 505-511.

[30] Sharir T, Merzon K, Kruchin I, et al. Use of electrocardiographic depolarization abnormalities for detection of stress-induced ischemia as defined by myocardial perfusion imaging. Am J Cardiol 2012; 109: 642-650.

[31] Pueyo E, Sörnmo L. QRS slopes for detection and characterization of myocardial ischemia. IEEE Trans Biomed Eng 2008; 55: 468-477.

[32] Garciá J, Sörnmo L. Autimatic detection of ST-T complex changes on the ECG using filtered RMS difference series: application to ambulatory ischemia monitoring. IEEE Trans Biomed Eng 2000; 47: 1195-1201.

[33] Firoozabadi R, Gregg RE, Babaeizadeh S. Identification of exercise-induced ischemia using QRS slopes. J Electrocardiol 2016; 49: 55-59.

[34] Matveev M, Naydenov S, Krasteva V, et al. Assessment of the infract size in high-resolution electrocardiograms. In Computing in Cardiology 2006; 3: 461-464.

[35] Treskes RW, Cato Ter Haar C, Man S, et al. Performance of ST and ventricular gradient difference vectors in electrographic detection of acute myocardial ischemia. J Electrocardiol 2015; 48: 498-504.

[36] Correa R, Arini PD, Valentinuzzi ME, et al. Novel set of vectorcardiographic parameters for the identification of ischemic patients. Med Eng Phys 2013; 35: 16-22.

[37] Correa R, Arini PD, Correa L, et al. Acute myocardial ischemia monitoring before and during angioplasty by a novel vectorcardiographic parameter set. J Electrocardiol 2013; 46: 635-643.

[38] Kaese S, Frommeyer G, Verheule S, et al. The ECG in cardiovascular-relevant animal models of electrophysiology. Herzschr Electrophys 2013; 24: 84-91.

[39] Gralinski MR. The Dog's role in preclinical assessment of QT interval prolongation. Toxicol Pathol 2003; 31: 11-16.

[40] Pogwizd SM, Bers DM. Rabbit models of heart desease. Drug Discovery Today: Disease Models 2008; 5: 85-93.

[41] Bell RM, Mocanu MM, Yellon DM. Retrograde heart perfusion: the Langendorff technique of isolated heart perfusion. J Mol Cell Cardiol 2011; 50: 940-950.

[42] Verdow P, Doel MA, Zeeuw S, et al. Animal models in the study of myocardial ischaemia and ischaemic syndromes. Cardiovasc Res 1998; 39: 121-135.

[43] Birnbaum Y, Drew BJ. The electrocardiogram in ST elevation acute myocardial infarction: correlation with coronary anatomy and prognosis. Postgrad Med J 2003; 79: 490-504.

[44] Podesser B, Wollenek G, Seitelberger R, et al. Epicardial branches of the coronary arteries and their distribution in the rabbit heart: the rabbit heart as a model of regional ischemia. Anat Rec 1997; 247: 521-527.

[45] Abarbanell AM, Herrmann JL, Weil BR, et al. Animal models of myocardial and vascular injury. J Surg Res 2010; 162: 239-249.

[46] Cascio WE, Yang H, Muller-Borer BJ, et al. ischemia-induced arrhythmia: the role of connexions, gap junctions, and attendant changes in impulse propagation. J Electrocardiol 2005; 38: 55-59.

[47] Garg V, Taylor T, Warren M, et al. β-Adrenergic stimulation and rapid pacing mutually promote heterogeneous electrical failure and ventricular fibrillation in the globally ischemic heart. Am J Physiol Heart Circ Physiol 2015; 308: H1155-H1170.

[48] Mandapati R, Asano Y, Baxter WT, et al. Quantification of effects of global ischemia on dynamics of ventricular fibrillation in isolated rabbit heart. Circulation 1998; 98: 1688-1696.

[49] Matiukas A, Pertsov AM, Cram KP, et al. Optical mapping of electrical heterogeneities in the heart during global ischemia. Conf Proc IEEE Eng Med Biol Soc 2009; 6321-6324.

[50] Kazbanov IV, Clayton RH, Nash MP, et al. Effect of global cardiac ischemia on human ventricular fibrillation: insights from a multi-scale mechanistic model of the human heart. PLoS Comput Biol 2014; 10: e1003891.

[51] Qian YW, Sung RJ, Lin SF, et al. Spatial heterogeneity of action potential alternans during global ischemia in the rabbit heart. Am J Physiol Heart Circ Physiol 2003; 285: H2722-H2733.

[52] Ferdinandy P, Hausenloy DJ, Heusch G, et al. Interaction of risk factors, comorbidities, and comedications with ischemia/reperfusion injury and cardioprotection by preconditioning, postconditioning, and remote conditioning. Pharmacol Rev 2014; 66: 1142-1174.

[53] Bernardo NL, D'Angelo M, Okubo S, et al. Delayed ischemic preconditioning is mediated by opening of ATP-sensitive potassium channels in the rabbit heart. Am J Physiol 1999; 45: H1323-H1330.

[54] Botsford MW, Lukas A. Ischemic preconditioning and arrhythmogenesis in the rabbit heart: effects on epicardium versus endocardium. J Mol Cel Cardiol 1998: 30: 1723-1733.

[55] Dickson EW, Lorbar M, Porcaro WA, et al. Rabbit heart can be 'preconditioned' via transfer of coronary effluent. Am J Physiol 1999; 277: H2451-H2457.

[56] Walker DM, Walker JM, Yellon DM. Global myocardial ischemia protects the myocardium from subsequent regional ischemia. Cardioscience 1993; 4: 263-266.

[57] Zhang X, Xiano Z, Yao J, et al. Participation of protein kinase C in the activation of Nrf2 signaling by ischemic preconditioning in the isolated rabbit heart. Mol Cell Biochem 2013; 372: 169-179.

[58] Gutbrod SR, Sulkin MS, Rogers J, et al. Patient-specific flexible and stretchable devices for cardiac diagnostics and therapy. Prog Biophys Mol Biol 2014; 115: 244-251.

[59] Kolářová J, Fialová K, Janoušek O, et al. Experimental methods for simultaneous measurement of action potentials and electrograms in isolated heart. Physiol Res 2010; 59: S71-S80.

[60] Attin M, Clusin WT. Basic concepts of optical mapping techniques in cardiac electrophysiology. Biol Res Nurs 2009; 11: 195-207.

[61] Brack KE, Narang R, Winter J, et al. The mechanical uncoupler blebbistatin is associated with significant electrophysiological effects in the isolated rabbit heart. Exp Physiol 2013; 98: 1009-1027.

[62] Efimov IR, Nikolski V, Salama G. Optical imaging of the heart. Circ Res 2004; 94: 21-33.

[63] Holcomb MR, Woods MC, Uzelac I, et al. The potential of dual camera systems for multimodel imaging of cardiac electrophysiology and metabolism. Exp Biol Med 2009; 234: 1-34.

[64] Kelly A, Ghouri IA, Kemi OJ, et al. Subepicardial action potential characteristics are a function of depth and activation sequence in isolated rabbit hearts. Circ Arrhythm Electrophysiol 2013; 6: 809-817.

[65] Martišiene I, Jurevičius J, Vosyliute R, et al. Evolution of action potential altrenans in rabbit heart during acute regional ischemia. Biomed Res Int 2015: 1-12.

[66] Novakova M, Bardonova J, Provaznik I, et al. Effect of voltage sensitive dye di-4-ANEPPS on guinea pig and rabbit myocardium. Gen Physiol Biophys. 2008; 27: 45-54.

[67] Ronzhina M, Čmiel V, Janoušek O, et al. Application of the optical method in experimental cardiology: action potential and intracellular calcium concentration measurement. Physiol Res 2013; 62: 125-137.

[68] Curtis MJ, Hancox JC, Farkas A, et al. The Lambeth Conventions (II): Guidelines for the study of animal and human ventricular and supraventricular arrhythmias. Pharmacol Ther 2013; 139: 213-248.

[69] Kolářová J, Nováková M, Ronzhina M, et al. Isolated Rabbit Hearts – Databases of EGs and MAP Signals. In Computing in Cardiology 2013: 551-554.

[70] Kozumplík J., Smital L., Vítek M. Software for correction of baseline drift in ECG signal, 2011.

[71] Kaur M, Singh B, Seema. Comparison of different approaches for removal of baseline wander from ECG signal. ICWET 2011: 30-36.

[72] Vítek M., Kozumplík J. QRS SEEKER: Software for QRS complexes detection, 2010.

[73] Bishop CM. Pattern recognition and machine learning. Springer, 2006, p. 738, ISBN-10: 0-387-31073-8.

[74] Duda RI, Hart PE, Stork DG. Pattern classification (2nd edition). Wiley-Interscience, 2000, p. 680, ISBN 0-471-05669-3.

[75] Theodoridis S, Koutroumbas K. Pattern recognition (4th edition). Elsevier, 2009, p. 961, ISBN 978-1-59749-272-0.

[76] Tibshirani R, Walther G, Hastie T. Estimating the number of clusters in a data set via the gap statistics. J R Statist Soc 2001; 63: 411-423.

[77] Ronzhina M., Potočňák T., Kolářová J., et al. Software for annotation of heart beats ANEG, 2011.

[78] Burden R, Faires JD. Numerical analysis (7th edition). Example Product Manufacturer, 2001, p. 100, ISBN-10 0534382169.

[79] Drew BJ, Califf RM, Funk M, et al. Practice standards for electrocardiographic monitoring in hospital settings. Circulation 2004; 110: 2721-2746.

[80] Berg M, Cheong O, Kreveld M, et al. Computational geometry: algorithms and applications (3rd edition). Springer, 2008, p. 368, ISBN-10 3540779736.

[81] Christov I, Gomez-Herrero G, Krasteva V, et al. Comparative study of morphological and time-frequency ECG descriptors for heartbeat classification. Med Eng Phys 2006; 28: 876-887.

[82] Doquire G, Lannoy G, Francois D, et al. Feature selection for interpatient supervised heart beat classification. Comput Intell Neurosci 2011: 1-9.

[83] Mar T, Zaunseder S, Martínez JP, et al. Optimization of ECG classification by means of feature selection. IEEE Trans Biomed Eng 2011; 58: 2168:2177.

[84] Park J, Pedrcycz W, Jeon M. Ischemia episode detection in ECG using kernel density estimation, support vector machine and feature selection. Biomed Eng Online 2012; 11: 1-22.

[85] Exarchos TP, Tsipouras MG, Exarchos CP, et al. A methodology for the automated creation of fuzzy expert systems for ischaemic and arrhythmic beat classification based on a set of rules obtained by a decision tree. Artif Intell Med 2007; 40: 187-200.

[86] Goletsis Y, Papaloukas C, Fotiadis DI, et al. Automated ischemic beat classification using genetic algorithms and multicriteria decision analysis. IEEE Trans Biomed Eng 2004; 51: 1717-1725.

[87] Llamedo M, Martínez JP. Heartbeat classification using feature selection driven by database generalization ctireria. IEEE Trans Biomed Eng 2011; 58: 616:625.

[88] Ronzhina M, Olejníčková V, Janoušek O, et al. Effects of heart orientation on isolated hearts electrograms. In Computing in Cardiology 2013: 543-546.

[89] Ronzhina M, Olejníčková V, Stračina T, et al. Evaluation of repeated global ischemia in isolated rabbit heart. In Proceedings of the 41st International Congress on Electrocardiology 2014: 175-178.

[90] Janoušek O, Ronzhina M, Kolářová J, et al. Comparison of RR-intervals in rabbit heart in-vivo, ex-vivo, and under ischemia. In Proceedings of the 40th International Congress on Electrocardiology 2014: 72-77.

[91] Clifford DG, Azauaje F, McSharry PE. Advanced methods and tools for ECG data analysis. Artech House, Inc., 2006, p. 384, ISBN-10 1-58053-966-1.

[92] Thygesen K, Alpert JS, Jaffe AS, et al. Third universal definition of myocardial infarction. JACC 2012; 60:1581-1598.

[93] Surawicz B, Knilans T. Acute ischemia: electrocardiographic patterns. In: Chou's electrocardiography in clinical practice (6th edition). Philadelphia: Saunders Elsevier, 2008, p. 124-161, ISBN 978-1-4160-3774-3.

[94] Fawcett T. An introduction to ROC analysis. Pattern Recogn Lett 2006; 27: 861-874.

[95] Saculinggan M, Balase EA. Empirical power comparison of goodness of fit tests for normality in the presence of outliers. J Phys Conf Ser 2013; 435: 1-11.

[96] Sheskin DJ. Handbook of parametric and nonparametric statistical procedures (2nd edition). Chapman&Hall, 2000, p. 1016, ISBN 1-58488-133-X.

[97] Lord B, Boswood A, Petrie A. Electrocardiography of the normal domestic pet rabbit. Vet Rec 2010; 167: 961-965.

[98] Quesenberry K, Carpenter JW. Ferrets, rabbits and rodents: clinical medicine and surgery. Elsevier Health Sciences, 2011, p. 608, ISBN: 978-1-4160-6621-7.

[99] Rezakhani A, Rezaian G. Clinical electrocardiogram of laboratory White New Zealand rabbits. J Appl Anim Res 1995; 7: 63-68.

[100] Ramanathan C, Rudy Y. Electrocardiographic imaging: II. Effect of torso inhomogeneities on noninvasive reconstruction of epicardial potentials, electrograms, and isochrones. J Cardiovasc Electropysiol 2001; 12: 241-252.

[101] Rudy Y. The forward problem of electrocardiography revisited. Circ Arrhythm Electrophysiol 2015; 8: 526-528.

[102] Kour J, Ahmed JA, Aarif O. Impact of heat stress on electrocardiographic changes in New Zealand White rabbits. J Stress Physiol Biochem 2013; 9: 242-252.

[103] Adams MG, Drew BJ. Body position effects on the ECG. J Electrocardiol 1997; 30: 285-91.

[104] García J, Åström M, Mendive J, et al. ECG-based detection of body position changes in ischemia monitoring. IEEE Trans Biomed Eng 2003; 50: 677-685.

[105] Norgaard BL, Rasmussen BM, Dellborg M, et al. Positional changes of spatial QRS- and ST-segment variables in normal subjects: implications for continuous vectorcardiography monitoring during myocardial ischemia. J Electrocardiol 2000; 33: 23-30.

[106] Du Y-M, Nathan RD. Ionic basis of ischemia-induced bradycardia in the rabbit sinoatrial node. J Mol Cell Cardiol 2007; 42: 315-325.

[107] Feng Y, Cona MM, Vunckx K, et al. Detection and quantification of acute reperfused myocardial infarction in rabbits using DISA-SPECT/CT and 3.0 T cardiac MRI. Int J Cardiol 2013; 168: 4191-4198.

[108] Eaton P, Li JM, Hearse DJ, et al. Formation of 4-hydroxy-2-nonenal modified proteins in ischemic rat heart. Am J Physiol – Heart C 1999; 276: H935-H943.

[109] Olejníčková V, Ronzhina M, Paulová H, et al. Susceptibility of isolated rabbit hearts with various left ventricular mass to short ischemic periods. In Computing in Cardiology 2014; 1097-1100.

[110] Ronzhina M, Olejníčková V. Evaluation of QRS in electrograms recorded from rabbit isolated hearts with normal and enlarged left ventricle. Abstract book SMIT 2015: 64-64.

[111] Dunn FG, Pringle SD. Left ventricular hypertrophy and myocardial ischemia in systemic hypertension. Am J Cardiol 1987; 60: 19 I-22 I.

[112] Hancock EW, Deal BJ, Mirvis DM, et al. AHA/ACCF/HRS recommendations for the standardization and interpretation of the electrocardiogram. Part V: Electrocardiogram changes associated with cardiac chamber hypertrophy. JACC 2009; 53: 992-1002.

[113] Otterstad JE. Ischaemia and left ventricular hypertrophy. Eur Heart J 1993; 14: 2-6.

[114] Zehender M, Faber T, Koscheck U, et al. Ventricular tachyarrhythmias, myocardial ischemia, and sudden cardiac death in patients with hypertensive heart disease. Clin Cardiol 1995; 18: 377-383.

[115] Armstrong EJ, Kulkarni AR, Prashant DB, et al. Electrocardiographic criteria for ST-elevation myocardial infarction in patients with left ventricular hypertrophy. Am J Cardiol 2012; 110: 977-983.

[116] Weber HW, Van der Walt JJ. Cardiomyopathy in crowded rabbits: a preliminary report. S Afr Med J 1973; 47: 1591-1595.

[117] Kloner RA, Rezkalla SH. Preconditioning, postconditioning and their application to clinical cardiology. Cardiovasc Res 2006; 70: 297-307.

[118] Armstrong AC, Gidding S, Gjesdal O, et al. LV mass assessed by echocardiography and CMR, cardiovascular outcomes, and medical practice. JACC: Cardiovascular Imaging 2012; 5: 837-848.

[119] Foppa M, Duncan BB, Rohde LEP. Echocardiography-based left ventricular mass estimation. How should we define hypertrophy? Cardiovascular Ultrasound 2005; 3:17.

[120] Lorell BH, Carabello BA. Left ventricular hypertrophy. Pathogenesis, detection, and prognosis. Circulation 2000; 102: 470-479.

[121] Corno AF, Cai X, Jones CB, et al. Congestive heart failure: experimental model. Front Pediatr 2013; 1:33.

[122] McIntosh MA, Hicks MN, Kane KA, et al. A characterized model of left ventricular hypertrophy in the rabbit. Cardioscience 1994; 5: 95-100.

[123] Wolk R, Sneddon KP, Dempster J, et al. Regional electrophysiological effects of left ventricular hypertrophy in isolated rabbit hearts under normal and ischaemic conditions. Cardiovasc Res 2000; 48: 120-128.

[124] Zhao Z, Chen L, Xiao Y-B, et al. A rabbit model to study regression of ventricular hypertrophy. Heart Lung Circ 2013; 22: 373-382.

[125] Schijvenaars BJA, Kors JA, Herpen G, et al. Effect of electrode positioning on ECG interpretation by computer. J Eectrocardiol 1997; 30: 247-256.

[126] Bacharova L, Szathmary V, Kovalcik M, et al. Effect of changes in left ventricular anatomy and conduction velocity on the QRS voltage and morphology in left ventricular hypertrophy: a model study. J Electrocardiol 2010; 43: 200-208.

[127] Estes EH, Jacksin KP. The electrogram in left ventricular hypertrophy: past and future. J Electrocardiol 2009; 42: 589-592.

[128] Budhwani N, Patel S, Dwyer EM. Electrocardiographic diagnosis of left ventricular hypertrophy: the effect of left ventricular wall thickness, size, and mass on the specific criteria for left ventricular hypertrophy. Am Heart J 2005; 149: 709-714.

[129] Schillaci G, Battista F, Pucci G. A review of the role of electrocardiography in the diagnosis of left ventricular hypertrophy in hypertension. J Electrocardiol 2012; 45: 617-623.

[130] Hejč J, Vítek M, Ronzhina M, et al. A wavelet-based ECG delineation method: adaptation to an experimental electrograms with manifested global ischemia. Cardiovasc Eng Technol 2015; 6: 364-375.

[131] Kozumplík J, Ronzhina M, Janoušek O, et al. QRS complex detection in experimental orthogonal electrograms of isolated rabbit hearts. In Computing in Cardiology 2014: 1085-1088.

[132] Okin PM, Roman MJ, Devereux RB, et al. Time-voltage QRS area of the 12-lead electrocardiogram: detection of left ventricular hypertrophy. Hypertension 1998; 31: 937-942.

[133] Janoušek O, Ronzhina M, Hejč J, et al. The effect of voltage-sensitive dye di-4-ANEPPS on heart rate variability in Langendorff-perfused isolated rabbit heart. In Computing in Cardiology 2015: 1049-1052.

[134] Olejníčková V, Ronzhina M, Janoušek O, et al. Voltage sensitive dye di-4-ANNEPS prolongs impulse conduction through ventricles, but not through AV node in isolated rabbit heart. In Computing in Cardiology 2015: 1-4.

[135] Veselý P, Ronzhina M, Fialová , et al. The effect of voltage sensitive dye di-4-ANEPPS on the RT/ RR coupling in rabbit isolated heart. In Computing in Cardiology 2015: 1137-1140.

[136] Čmiel V, Odstrčilík J, Ronzhina M, et al. Real-time measurement of cardiomyocyte contraction and calcium transients using fast image processing algorithms. In IFMBE Proceedings 2015: 256-259.

[137] Janoušek O, Kolářová J, Ronzhina M, et al. Motion artefact in voltage-sensitive fluorescent dye emission during repeated ischemia of isolated heart. Physiol Res 2013; 62: 371-378.

[138] Richardson ES, Xiao Y. Electrophysiology of Single Cardiomyocytes: Patch Clamp and Other Recording Methods. In Cardiac Electrophysiology Methods and Models (1st edition). DC Sigg, PA Iaizzo, Y-F Xiao, B He (eds). New York: Springer, 2010, p. 329-348, ISBN 978-1-4419-6657-5.

[139] Salama G. Optical mapping: background and historical perspective. In Optical Mapping of Cardiac Excitation and Arrhythmias. D.S. Rosenbaum, J. Jalife (eds). New York: Futura Publishing Company. Futura Publishing Company, 2001, p. 9-33, ISBN 0-87993-481-6.

[140] Johnson PL, Smith W, Bayhnam TC, et al. Errors caused by combination of di-4-ANEPPS and fluo 3/4 for simultaneous measurements of transmembrane potentials and intracellular calcium. Annals of Biomedical Engineering 1999; 27: 563-571.

[141] Cheng Y, Van Wagoner DR, Mazgalev TN, et al. Voltage-sensitive dye RH421 increases contractility of cardiac muscle. Can J Physiol Pharmacol 1998; 76: 1146–1150.

[142] Hardy MEL, Lawrence CL, Standen NB, et al. Can optical recordings of membrane potential be used to screen for drug-induced action potential prolongation in single cardiac myocytes? J Pharmacol Toxicol Methods 2006; 54:173-82.

[143] Hardy MEL, Pollard CE, Small BG, et al. Validation of a voltage-sensitive dye (di-4-ANEPPS)-based method for assessing drug-induced delayed repolarisation in beagle dog left ventricular midmyocardial myocytes. J Pharmacol Toxicol Methods 2009; 60: 94–106.

[144] Larsen AP, Olesen SP, Grunnet M, et al. Pharmacological activation of IKr impairs conduction in guinea pig hearts. J Cardiovasc Electrophysiol 2010; 21: 923-929.

[145] Fialová K, Kolařová J, Provazník I, et al. Comparison of voltage-sensitive dye di-4-ANEPPS effects in isolated hearts of rat, guinea pig, and rabbit. In Computing in Cardiology 2010; 37: 565-568.

[146] Larsen PL, Sciuto KJ, Moreno AP, et al. The voltage-sensitive dye di-4-ANEPPS slows conduction velocity in isolated guinea pig hearts. Heart Rhythm. 2012; 9: 1493-1500.

[147] Nygren A, Kondo C, Clark RB, et al Voltage-sensitive dye mapping in Langendorff-perfused rat hearts. Am J Physiol Heart Circ. 2003; 284: H892-H902.

[148] Fialová K, Kolařová J, Janoušek O, et al. Effects of voltage-sensitive dye di-4-ANEPPS on isolated rat heart electrogram. In Computing in Cardiology 2011; 38: 721-724.

[149] Nygren A, Clark RB, Belke DD, et al. Voltage-sensitive dye mapping of activation and conduction in adult mouse hearts. Ann Biomed Eng 2000; 28: 958–967.

[150] Liang Q, Sohn K, Punske BB. Propagation and electrical impedance changes due to ischemia, hypoxia and reperfusion in mouse hearts. In Conf Proc IEEE Eng Med Biol Soc 2006; 1: 1560–1563.

[151] Nováková M, Nogová K, Bardoňová J, et al. Comparison of two procedures of loading with voltage-sensitive dye di-4-ANEPPS in rabbit isolated heart. In Computers in Cardiology 2008; 1081-1084.

[152] Shattock MJ, Rosen MR. The control of heart rate: the Physiology of the sinoatrial node and the role of the I_f current. Dialogues Cardiovasc Med. 2006; 11: 5-17.

[153] Ng FS, Shadi IT, Peters NS, et al. Selective heart rate reduction with ivabradine slows ischaemia-induced electrophysiological changes and reduces ischaemia-reperfusion-induced ventricular arrhythmias. J Mol Cell Cardiol 2013; 59: 67-75.

[154] Varró A, Lathrop DA, Hester SB, et al. Ionic currents and action potentials in rabbit, rat, and guinea pig ventricular myocytes. Basic Res Cardiol 1993; 88: 93-102.

[155] Baker LC, Wolk R, Choi BR, et al. Effects of mechanical uncouplers, 134iacetyl monoxime, and cytochalasin-D on the electrophysiology of perfused mouse hearts. Am J Physiol Heart Circ Physiol 2004; 287: H1771-H1779.

[156] Swift LM, Asfour H, Posnack NG, et al. Properties of blebbistatin for cardiac optical mapping and other imaging applications. Pflugers Arch 2012; 464: 503-512.

[157] Bernier M, Curtis MJ, Hearse DJ. Ischemia-induced and reperfusion-induced arrhythmias: importance of heart rate. Am J Physiol 1989; 256: H21–H31.

[158] Ceconi C, Cargnoni A, Francolini G, et al. Heart rate reduction with ivabradine improves energy metabolism and mechanical function of isolated ischaemic rabbit heart. Cardiovasc Res 2009; 84: 72–82.

[159] Ronzhina M, Potočňák T, Janoušek O, et al. Spectral and higher-order statistics analysis of ECG: application to study of ischemia in rabbit isolated hearts. In Computing in Cardiology 2012: 645-648.

[160] Ronzhina M, Maršánová L, Smíšek R, et al. Classification of ventricular premature and ischemic beats in animal electrograms. In Computing in Cardiology 2015: 1137-1140.

[161] Maršánová L, Ronzhina M, Vítek M. Automatická klasifikace EKG s použitím morfologických parametrů. Elektrorevue 2015; 17: 115-123.

[162] Maršánová L, Ronzhina M, Smíšek R, et al. Použití kumulantů vyšších řádů pro automatickou klasifikaci EKG. Elektrorevue 2016; 18: 103-111.

[163] Brailer DJ, Kroch E, Pauly MV. The impact of computer-assisted test interpretation on physician decision making: the case of electrocardiogram. Med Decis Making 1997; 17: 80-86.

[164] Salerno SM, Alguire PC, Waxman HS. Competency in interpretation of 12-lead electrocardiograms: a summary and appraisal of published evidence. Ann Intern med 2003; 138: 751-760.

[165] Taddei A, Distante G, Emdin M, et al. The Europen ST-T Database: standard for evaluating systems for the analysis of ST-T changes in ambulatory electrocardiography. European Heart Journal 1992; 13: 1164-1172.

[166] Holmvang L, Hasbak P, Clemmensen P, et al. Differences between local investigator and core laboratory interpretation of the admission electrocardiogram in patients with unstable angina pecroris or non-Q-wave myocardial infarction. Am J Cardiol 1998; 82: 54-60.

[167] Tsai TL, Fridsma DB, Gatti G. Computer decision support as a source of interpretation error: the case of electrocardiograms. J Am Med Inform Assoc 2003; 10: 478-483.

[168] May R, Dandy G, Maier H. Review of input variable selection methods for artificial neural networks. In Artificial neural networks – methodological advances and biomedical applications. K. Suzuki (eds.). InTech, 2011, p. 374, ISBN 978-953-307-243-2.

[169] Guyon I, Elisseeff A. An introduction to variable and feature selection. J Mach Learn Res 2003; 3: 1157-1182.

[170] Laguna P, Sörnmo L. The STAFF III ECG database and its significance for methodological development and evaluation. J Electrocardiol 2014; 47: 408-417.

[171] Murugan S. Rule based classification of ischemic ECG beats using ANT-Miner. IJEST 2010; 2: 3929-3935.

[172] Xu M, Wei S, Qin X, et al. Rule-based method for morphological classification of ST segment in ECG signals. J Med Biol 2015; 35: 816-823.

[173] Kumar A, Singh M. Ischemia detection using isoelectric energy function. Comput Biol Med 2016; 68: 76-83.

[174] Smrdel A, Jager F. Automatic classification of long-term ambulatory ECG records according to type of ischemic heart disease. Biomed Eng Online 2011; 10:1-13.

[175] Dranca L, Goni A, Illarramendi A. Tuning real-time detector of transient cardiac ischemic episodes on the Long-Term ST Database according to the annotation protocol B. In Computing in Cardiology 2013; 40: 583-586.

[176] Papaloukas C, Fotiadis DI, Likas A, et al. An ischemia detection method based on artificial neural networks. Artif Intell Med 2002; 24: 167-178.

[177] Murthy HSN, Meenakshi M. ANN, SVM and KNN classifiers for prognosis of cardic ischemia – a comparison. IJRCE 2015; 5: 7-11.

[178] Llamedo M, Martínez JP, Albertal M, et al. Morphologica features of the ECG for detection of stress-induced ischemia. In Computing in Cardiology 2013; 40: 591-594.

[179] Garciá J, Wagner G, Sörnmo L, et al. Identification of the occluded artery in patients with myocardial ischemia induced by prolonged percutaneous transluminal coronary angioplasty using traditional vs transformed ECG-based indexes. Comput Biomed Res 1999; 32: 470-482.

[180] Tseng Y-L, Lin K-S, Jaw F-S. Comparison of support-vector machine and sparse representation using a modified rule-based method for automated myocardial ischemia detection. Comput Math Methods Med 2016: 1-8.

[181] Meloun M, Militký J. Statistická analýza experimentálních dat. Academia, 2004, p. 953, ISBN 80-200-1254-0.

[182] Zou H, Hastie T, Tibshirani R. Sparse principal component analysis. J Comput Graph Statist 2006; 5: 265-286.

[183] Tibshirani R. Regression shrinkage and selection via the lasso. J Royal Statist Soc B 1996; 267-288.

[184] Lu Y, Cohen I, Zhou XS, et al. Feature selection using principal feature analysis. Proceedings of the 15th ACM international conference on Multimedia 2007: 301-304.

[185] Jolliffee IT. Principal component analysis (2nd edition). Springer, 2002, p. 487, ISBN 0-387-95442-2.

[186] Dougherty G. Pattern recognition and classification. An introduction. Springer, New York, 2013, p. 196, ISBN 978-1-4614-5322-2.

[187] Gastwirtth JL, Gel YR, Miao W. The impact of Levene's test of equality of variances on statistical theory and practice. Statistical Science 2009; 24: 343-360.

[188] Ghosh AK. On optimum choice of k in nearest neighbor classification. Comput Stat Data Anal 2006; 50: 3113-3123.

[189] Ronzhina M, Janoušek O, Kolářová J, et al. Sleep scoring using artificial neural networks. Sleep Med Rev 2012; 16: 251-263.

[190] Arlot S. A survey of cross-validation procedures for model selection. Statistics Suveys 2010; 4: 40-79.

[191] Tan PN, Steinbach M, Kumar V. Introduction to data mining. Pearson 2005, p. 769, ISBN-10 0321321367.

[192] Labatut V, Cherifi H. Accuracy measures for the comparison of classifiers. In Proceedings of The 5th International Conference on Information Technology 2011, 1-5.

[193] Hejč J, Ronzhina M, Janoušek O, et al. The effect of heart orientation on high frequency QRS components in multiple bandwidths. In Computing in Cardiology 2015: 1121-1124.

LIST OF ABBREVIATIONS

Acc	accuracy
ANN	artificial neural network
ANOVA	analysis of variance
AP	action potential
APD	action potential duration
AUC	area under curve
AUCROC	area under ROC curve
AV	atrioventricular
AVB	atrioventricular block
BUT	Brno University of Technology
BW	body weight
CV	cross-validation
DR	decision rule
DT	decision tree
ECG	electrocardiogram
EG	electrogram
FIR	finite impulse response
FN	false negative
FP	false positive
HF	high frequency
HW	heart weight
K-H	Krebs-Henseleit
KLT	Karhunen-Loève transform
k-NN	k-nearest neighbors
LAD	left anterior descending artery
LCX	left circumflex artery
LDF	linear discriminant function
LOO	leave-one-out
LV	left ventricle
LVT	left ventricular thickness
LVW	left ventricular weight
MAP	monophasic action potential
NOD	junctional rhythm
PC	principal component
PCA	principal component analysis
PTCA	percutaneous transluminal coronary angioplasty
QDF	quadratic discriminant function
RBF	radial basis function
RCA	right coronary artery
RMS	root mean square
ROC	receiver operating characteristic
SA	sinoatrial
SD	standard deviation
Se	sensitivity
Sp	specificity
SVES	supraventricular extrasystole
SVM	support vector machine
TC	computational time
TD	time moment of ischemia detection
TN	true negative
TP	true positive
UPGMA	unweighted pair group method with atithmetic mean
VCG	vectorcardiogram
VG	ventricular gradient
VPB	ventricular premature beat
VSD	voltage-sensitive dye

LIST OF FIGURES

Figure 1. Electrical activity of the heart. 10
Figure 2. Electrophysiological manifestations of myocardial schemia. 12
Figure 3. Experimental protocols. 20
Figure 4. Orthogonal system of electrodes. 21
Figure 5. Flowchart of electrogram processing and analysis (fixed orientation of the heart). 21
Figure 6. Baseline wander elimination in electrogram. 22
Figure 7. QRS complexes detection in electrograms from the first half of ischemic period. 23
Figure 8. Example of two-level clustering of electrograms from one experiment. 25
Figure 9. The main window of software for delineation and annotation of electrocardiographic data. 26
Figure 10. Example of QRS-T baseline correction. 26
Figure 11. Flowchart of electrogram processing in case of data from rotated heart. 26
Figure 12. Scheme of EG reconstruction. 28
Figure 13. Illustration of interval and voltage based parameters. 29
Figure 14. Illustration of VCG based parameters. 30
Figure 15. Coordinate systems used for VCG reconstruction. 30
Figure 16. Illustration of 2D QRS loop area calculation. 32
Figure 17. Illustration of QRS loops based parameters. 33
Figure 18. Main interval characteristics of electrograms. 34
Figure 19. Example of QRS-T segments recorded during stabilization period. 38
Figure 20. Correlation maps (Spearman's ρ) for data recorded in range from -90° to +90°. 38
Figure 21. Distribution of +/-AUC_{QRS} (a) and AUC_{JT} (b) in stabilization period. 39
Figure 22. QRS-T (from one experiment) in selected recording positions for different rotation sessions. 40
Figure 23. Correlation maps (Spearman's ρ) from data during various experimental periods. 41
Figure 24. Correlation maps (Spearman's ρ) between data from stabilization and other rotation sessions. 42
Figure 25. Boxplots of +AUC_{JT}R' and ST20 in different experimental periods and recording positions. 42
Figure 26. Values of T_A, ST20, -AUC_{QRS}R', and –AUC_{QRS}Rq' from one experiment. 44
Figure 27. Mean values of AUCROC of various electrogram parameters. 45
Figure 28. Mean values of AUCROC for EG parameters in different recording positions. 45
Figure 29. 2D EG loops and main VCG parameters during ischemia (standard VCG axes). 46
Figure 30. Mean values of AUCROC for VCG parameters in different recording positions. 46
Figure 31. Typical time-course of electrogram recorded from rabbit isolated heart. 48
Figure 32. Time-course of the main parameters of rabbit isolated heart electrogram. 49
Figure 33. Time progress of the main visual changes in electrograms and VCG of rabbit isolated heart induced by 10 minutes long global ischemia. 49
Figure 34. AUCROC of all lead I and lead II parameters and joint&VCG parameters during three ischemic (I) and reperfusion (R) periods. 51
Figure 35. Se and Sp for all parameters from lead I, lead II and joint&VCG during particular ischemic (I) periods. 52
Figure 36. Percent of parameters with AUCROC > 0.7, 0.8 and 0.9 during particular ischemic (I) periods. 53
Figure 37. AUCROC, Se and Sp for QRS and ST-T (JT) based parameters during the first ischemia. 53
Figure 38. Time course of AUCROC of common parameters calculated from lead I and lead II (a) and joint&VCG (b-c) during the first ischemia. 54
Figure 39. ΔAUC_{JT} from the end of ischemic (I, top) and reperfusion (R, bottom) periods and lines fitted through ΔAUC_{JT} from all experiments for slope calculation. 55
Figure 40. Results of histological analysis of myocardium tissue. 60
Figure 41. Averaged QRS complexes recorded in hearts with low (L) and high (H) LV mass fraction. 62
Figure 42. Median values of EG parameters recorded in hearts with low (L) and high (H) LV mass fraction. 62

Figure 43. Mean QRS loops at horizontal, frontal, and sagittal plane calculated for hearts with low (L) and high (H) LV mass fraction. 63
Figure 44. AUCROC for LV mass increase detection using parameters in the range from -90° to 90°. 63
Figure 45. ROC curves of EG parameters proposed for the detection of LV mass increase. 63
Figure 46. Distribution of QRS_D (a) and AUC_{QRS} (b) during experiments. 65
Figure 47. AUCROC of selected parameters from lead II EG. 67
Figure 48. Discrimination ability of selected EG parameters. 68
Figure 49. Duration of P wave, PQ interval and QRS complex in stained and non-stained hearts. 74
Figure 50. Duration of RR and QT interval and the ratio between them in stained and non-stained hearts. 75
Figure 51. Distribution of differences between adjacent minutes for RR and QT interval duration. 76
Figure 52. Distribution of most frequently observed types of cardiac rhythm in electrograms. 77
Figure 53. Results of patch clamp analysis of sodium channels in differentiated cells. 77
Figure 54. Main interval EG characteristics from stained (black) and non-stained (grey) hearts. 79
Figure 55. Distribution of different types of cardiac rhythm during ischemia and reperfusion. 80
Figure 56. Total number of ventricular premature beats (VPBs) in ischemia and reperfusion. 80
Figure 57. Course of AUCROC calculated for different groups of parameters during the first ischemia. 81
Figure 58. AUCROC, Se and Sp for main lead I & VCG (a) and lead II & joint & VCG (b) parameters calculated for stained and non-stained hearts. 82
Figure 59. Distribution of the parameters' Δ in stained (black) and non-stained (grey) hearts groups. 84
Figure 60. Distribution of AUC_{QRS} in different experimental groups. 85
Figure 61. Classification of experimental data. 93
Figure 62. Correlation based feature selection. 94
Figure 63. PCA-based ranking of the features. 95
Figure 64. Selection of optimal feature number using linear discriminant function. 101
Figure 65. Distribution of $AUC_{JTmax}R'$ values before and during ischemic period. 105
Figure 66. Selection of optimal 'k' parameter of k-NN classifier. 109
Figure 67. Confusion matrices for best single- and multi-feature binary ischemia detectors for control group data (LOO validation). 110
Figure 68. Selection of optimal decision tree for 4-class single-feature classification. 112
Figure 69. Cross-ischemia validation of decision tree 4-class classification using φ. 114
Figure 70. Outcomes of the best 4-class SVM based classifiers. 115
Figure 71. Cross-ischemia validation of 4-class LDF classification using F51 feature set. 116
Figure 72. Sensitivity and specificity distribution for the best 11-calss SVM classifier. 117

LIST OF TABLES

Table 1. Beginning of particular rotation sessions (i1-i5 and r1-r5) regarding the beginning of ischemic (I) and reperfusion (R) period..... 39
Table 2. Percent of parameters with averaged AUCROC (through all positions) higher than 0.7..... 45
Table 3. Number of recording positions with averaged overall AUCROC higher than 0.7..... 46
Table 4. Basic ECG parameters of White New Zealand rabbit..... 56
Table 5. Onset of significant ischemia-induced changes ($p < 0.05$) in EG and VCG parameters calculated for the hearts with low and high LV mass fraction..... 65
Table 6. Accuracy characteristics of myocardial ischemia detection..... 67
Table 7. Main interval characteristics in two experimental groups..... 76
Table 8. Onset of significant ischemia-induced changes ($p < 0.05$, Wilcoxon signed-rank test) in EG and VCG parameters from experiments with and without di-4-ANEPPS administration..... 78
Table 9. Onset of significant ischemia-induced changes ($p < 0.05$, Wilcoxon signed-rank test) in EG and VCG parameters from experiments with and without di-4-ANEPPS administration..... 81
Table 10. Discrimination ability indices of selected parameters in non-stained and stained hearts. 83
Table 11. Decision rule-based and tree classification approaches..... 91
Table 12. Supervised classification approaches (not based on decision rules)..... 92
Table 13. List of feature sets selected by proposed approaches. 96
Table 14. Average size of training and testing data sets in one cycle of LOO validation. 99
Table 15. Best results obtained by decision rule method in control group..... 103
Table 16. Best results obtained by decision rule method in H group. 103
Table 17. Best results obtained by decision rule method in stained hearts..... 104
Table 18. Results obtained by decision rule using features calculated without delineation outcomes. 105
Table 19. Performance of decision rule method for various definition of ischemic period beginning. 106
Table 20. Results of cross-group validation of single-feature decision rule method. 107
Table 21. Results of cross-ischemia validation of single-feature decision rule method. 108
Table 22. Overall performance indices of the best binary multi-feature classification approaches..... 110
Table 23. Dependence of performance of SVM trained on F7 (control group) on definition of ischemia beginning……111
Table 24. Best results of cross-group validation of binary multi-feature classifiers..... 111
Table 25. Results of cross-ischemia validation of the best binary multi-feature classifier in control group. 111
Table 26. Best results obtained by single-feature decision tree method. 113
Table 27. Results of cross-ischemia validation of single-feature decision tree method in control group..... 114
Table 28. Overall performance indices of the best 4-class multi-feature approaches. Shown as mean ± SD…..... 115
Table 29. Results of cross-ischemia validation of the best 4-class multi-feature classifier in control group…… 116

APPENDIX A – PARAMETERS CALCULATED FROM ELECTROGRAMS AND VECTORCARDIOGRAMS

Table A-1. Groups of electrogram based parameters.

Name	Description, unit
Interval parameters(joint for all leads):	
RR	RR interval duration, ms
QRS_D	QRS complex duration, ms
QT	QT interval duration, ms
JTmax	Time interval from J point to maximal deviation of ST-T, ms
PQ	PQ interval duration, ms
Voltage parameters:	
QRS_A	Maximal absolute deviation of QRS complex, mV
$+QRS_A$	Maximal positive deviation of QRS complex, mV
$-QRS_A$	Maximal negative deviation of QRS complex, mV
ST20	Deviation of ST-T at J+20 ms point, mV
T_A	Maximal deviation of ST-T, mV
AUC based parameters I:	
AUC_{QRST}	Area under QRS-T, mV·ms
AUC_{QRS}	Area under QRS complex, mV·ms
AUC_{JT}	Area under ST-T, mV·ms
$+AUC_{QRS}$	Area under positive part of QRS complex, mV·ms
$-AUC_{QRS}$	Area under negative part of QRS complex, mV·ms
+/- AUC_{QRS}	Ratio between areas under positive and negative parts of QRS complex: $+AUC_{QRS}$ / $-AUC_{QRS}$, -
AUC_{JTmax}	Area under curve from J point to maximal deviation of ST-T, mV·ms
$AUC_{TmaxTend}$	Area under curve from maximal deviation of ST-T to the end of T wave, mV·ms
$AUC_{JTmax/TmaxTend}$	Ratio between areas under ST-T curve before and after maximal deviation of ST-T: AUC_{JTmax} / $AUC_{TmaxTend}$, -
$+AUC_{JT}$	Area under positive part of ST-T, mV·ms
$-AUC_{JT}$	Area under negative part of ST-T, mV·ms
AUC based parameters II:	
AUC_{QRST}'	Area under |QRS-T|, where |.|- absolute value, mV·ms
AUC_{QRS}'	Area under |QRS|, mV·ms
AUC_{JT}'	Area under |ST-T|, mV·ms
AUC_{JTmax}'	Area under absolute values from J point to maximal deviation of ST-T, mV·ms
$AUC_{TmaxTend}'$	Area under absolute values from maximal deviation of ST-T and end of T wave, mV·ms
AUC based parameters III:	
$AUC_{QRS}R'$	Relative AUC_{QRS}': AUC_{QRS}' / AUC_{QRST}', -
$AUC_{JT}R'$	Relative AUC_{JT}': AUC_{JT}' / AUC_{QRST}', -
$+AUC_{QRS}R'$	Relative $+AUC_{QRS}$: $+AUC_{QRS}$ / AUC_{QRST}', -
$-AUC_{QRS}R'$	Relative $\|-AUC_{QRS}\|$: $\|-AUC_{QRS}\|$ / AUC_{QRST}', -
$+AUC_{QRS}Rq'$	Relative $+AUC_{QRS}$: $+AUC_{QRS}$ / AUC_{QRS}', -
$-AUC_{QRS}Rq'$	Relative absolute value of $-AUC_{QRS}$: $\|-AUC_{QRS}\|$ / AUC_{QRS}', -
$AUC_{JTmax}R'$	Relative AUC_{JTmax}': AUC_{JTmax}' / AUC_{QRST}', -
$AUC_{TmaxTend}R'$	Relative $AUC_{TmaxTend}'$: $AUC_{TmaxTend}'$ / AUC_{QRST}', -
$+AUC_{JT}R'$	Relative $+AUC_{JT}$: $+AUC_{JT}$ / AUC_{QRST}', -
$-AUC_{JT}R'$	Relative absolute value of $-AUC_{JT}$: $\|-AUC_{JT}\|$ / AUC_{QRST}', -

Table A-2. Groups of VCG based parameters.

Name	**Description, unit**
Common parameters:	
L_{qrs}	Maximal QRS spatial vector magnitude, mV
L_{jt}	Maximal ST-T spatial vector magnitude, mV
α_{qrs}	Angle of maximal QRS vector in frontal plane, °
β_{qrs}	Angle of maximal QRS vector in horizontal plane, °
γ_{qrs}	Angle of maximal QRS vector in sagittal plane, °
α_{jt}	Angle of maximal ST-T vector in frontal plane, °
β_{jt}	Angle of maximal ST-T vector in horizontal plane, °
γ_{jt}	Angle of maximal ST-T vector in sagittal plane, °
3D loop parameters:	
P_{qrs}	Perimeter of 3D QRS loop, mV
P_{jt}	Perimeter of 3D ST-T loop, mV
D	Distance between maximal QRS and ST-T vector, mV
φ	Angle between maximal QRS and ST-T spatial vector, °
2D loop area based parameters:	
$A_{qrs}xy$	Area of 2D QRS loop in frontal plane, mV^2
$A_{qrs}xz$	Area of 2D QRS loop in horizontal plane, mV^2
$A_{qrs}zy$	Area of 2D QRS loop in sagittal plane, mV^2
$A_{jt}xy$	Area of 2D ST-T loop in frontal plane, mV^2
$A_{jt}xz$	Area of 2D ST-T loop in horizontal plane, mV^2
$A_{jt}zy$	Area of 2D ST-T loop in sagittal plane, mV^2
2D loop centroid based parameters:	
$D^c_{qrs}xy$	Distance between main QRS and centroid vectors in frontal plane, mV
$D^c_{qrs}xz$	Distance between main QRS and centroid vectors in horizontal plane, mV
$D^c_{qrs}zy$	Distance between main QRS and centroid vectors in sagittal plane, mV
$D^c_{jt}xy$	Distance between main ST-T and centroid vectors in frontal plane, mV
$D^c_{jt}xz$	Distance between main ST-T and centroid vectors in horizontal plane, mV
$D^c_{jt}zy$	Distance between main ST-T and centroid vectors in sagittal plane, mV
$\varphi^c_{qrs}xy$	Angle between main QRS and centroid vectors in frontal plane, °
$\varphi^c_{qrs}xz$	Angle between main QRS and centroid vectors in horizontal plane, °
$\varphi^c_{qrs}zy$	Angle between main QRS and centroid vectors in sagittal plane, °
$\varphi^c_{jt}xy$	Angle between main ST-T and centroid vectors in frontal plane, °
$\varphi^c_{jt}xz$	Angle between main ST-T and centroid vectors in horizontal plane, °
$\varphi^c_{jt}zy$	Angle between main ST-T and centroid vectors in sagittal plane, °

APPENDIX B – ELECTROGRAM AND VCG DURING ISCHEMIA

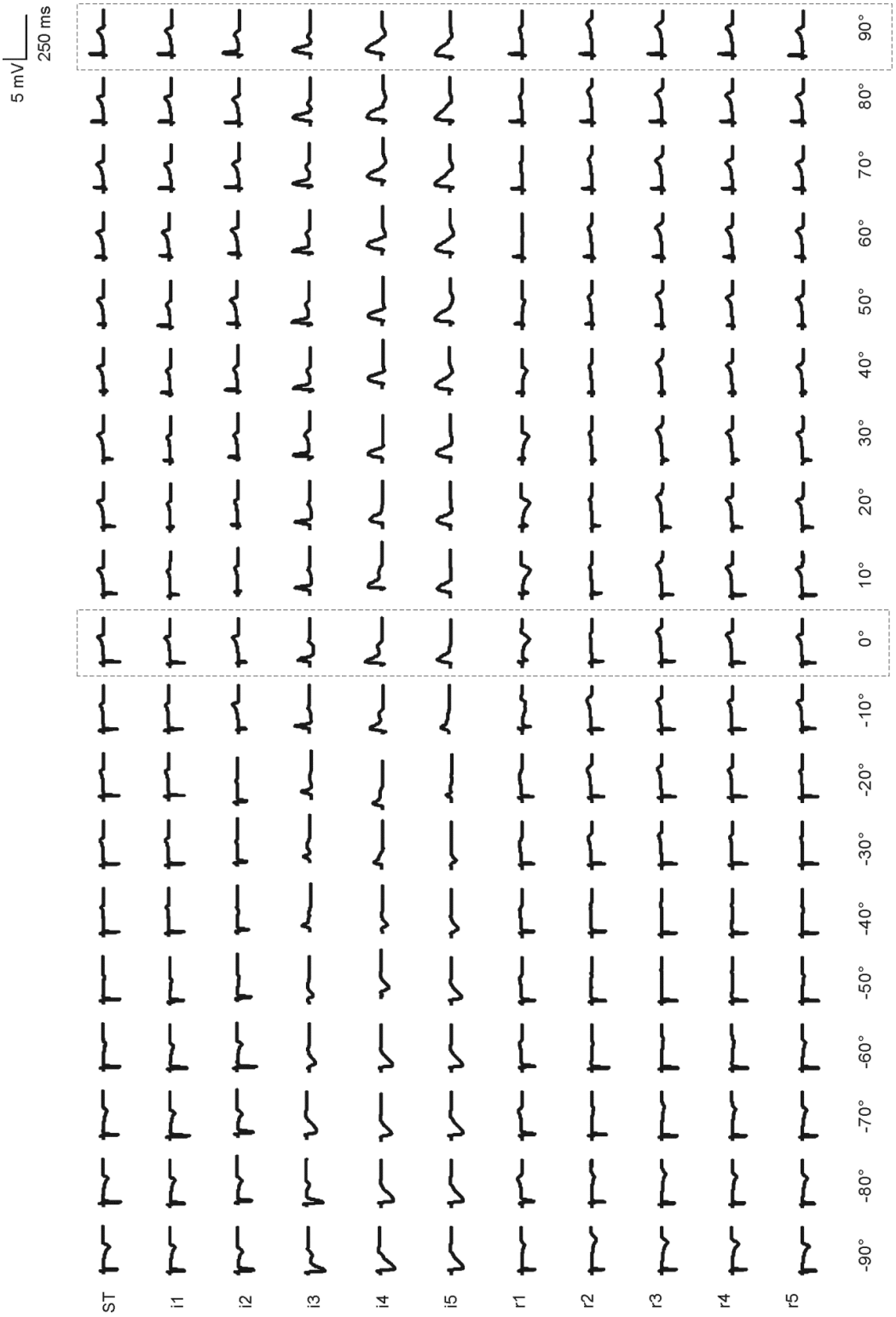

Figure B-1. QRS-T from electrogram recorded from different areas of LV at various time moments during ischemia (see text for more detail).

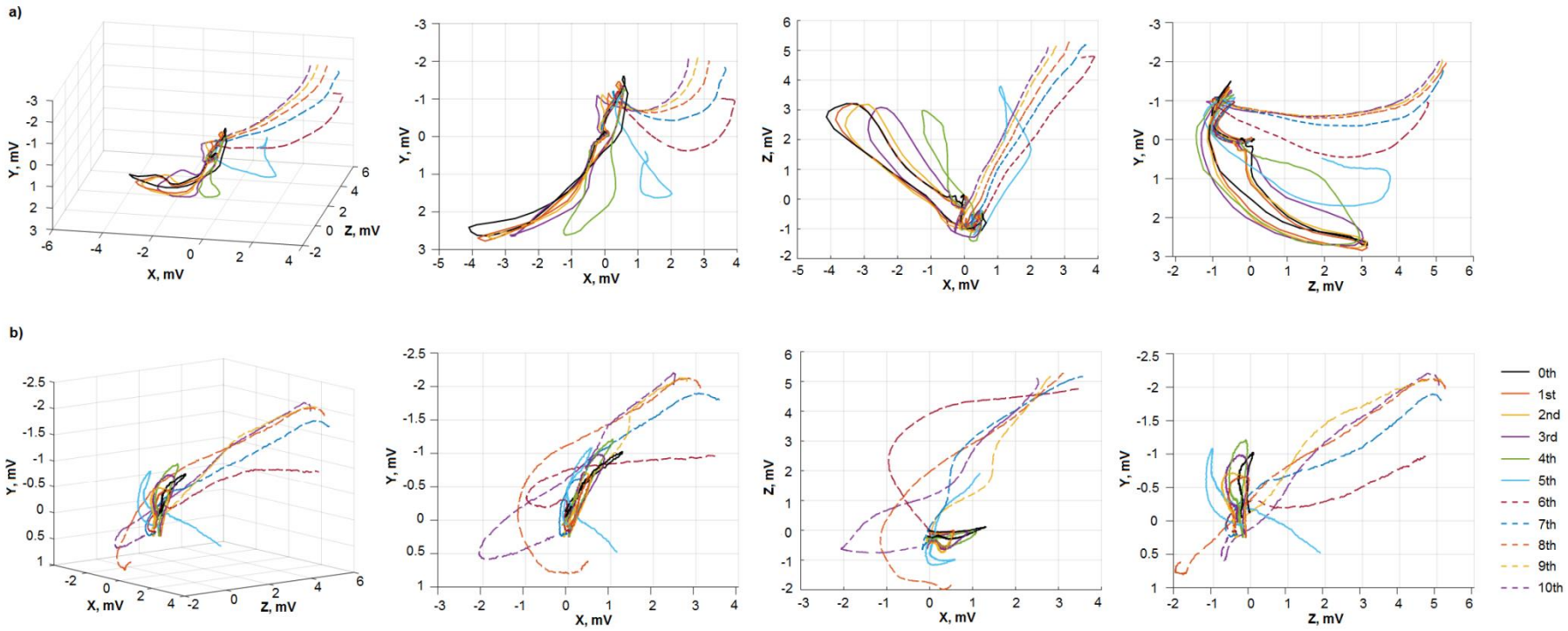

Figure B-2. 3D QRS and ST-T (a and b, left) and 2D QRS and ST-T loops in three planes (a and b, right) recorded in various time moments during ischemia.

APPENDIX C – VALUES OF PARAMETERS IN STABILIZATION AND ISCHEMIA

Table C-1. Values of lead I parameters at the beginning of ischemia (i.e. the end of stabilization) (0^{th} minute) and the end of the 2^{nd}, 5^{th}, 8^{th}, and 10^{th} minute of ischemia. Expressed as median and 25^{th} and 75^{th} percentiles.

Parameter	Time period during ischemia														
	0^{th} minute			2^{nd} minute			5^{th} minute			8^{th} minute			10^{th} minute		
	Mdn	**25^{th} perc**	**75^{th} perc**	**Mdn**	**25^{th} perc**	**75^{th} perc**	**Mdn**	**25^{th} perc**	**75^{th} perc**	**Mdn**	**25^{th} perc**	**75^{th} perc**	**Mdn**	**25^{th} perc**	**75^{th} perc**
$-AUC_{JT}R'$	**0.05**	0.04	0.55	**0.25**	0.02	0.42	**0.08**	0.05	0.26	**0.10**	0.03	0.16	**0.07**	0.02	0.08
$+AUC_{JT}R'$	**0.50**	0.01	0.76	**0.13**	0.01	0.77	**0.43**	0.23	0.60	**0.63**	0.51	0.67	**0.64**	0.42	0.71
$AUC_{TmaxTend}R'$	**0.17**	0.14	0.19	**0.17**	0.07	0.20	**0.64**	0.45	0.68	**0.66**	0.53	0.74	**0.67**	0.55	0.74
$AUC_{JTmax}R'$	**0.48**	0.45	0.56	**0.47**	0.30	0.59	**0.00**	0.00	0.03	**0.00**	0.00	0.08	**0.01**	0.00	0.06
$-AUC_{QRS}Rq'$	**0.29**	0.15	0.41	**0.30**	0.11	0.37	**0.09**	0.05	0.12	**0.09**	0.08	0.13	**0.10**	0.08	0.17
$+AUC_{QRS}Rq'$	**0.70**	0.59	0.85	**0.70**	0.63	0.89	**0.91**	0.87	0.95	**0.91**	0.87	0.92	**0.89**	0.83	0.92
$-AUC_{QRS}R'$	**0.08**	0.07	0.11	**0.06**	0.06	0.09	**0.03**	0.02	0.06	**0.02**	0.02	0.04	**0.03**	0.02	0.04
$+AUC_{QRS}R'$	**0.20**	0.15	0.35	**0.19**	0.13	0.56	**0.33**	0.24	0.50	**0.20**	0.18	0.34	**0.21**	0.20	0.32
$AUC_{JT}R'$	**0.66**	0.60	0.78	**0.78**	0.37	0.79	**0.64**	0.47	0.71	**0.77**	0.63	0.78	**0.76**	0.55	0.77
$AUC_{QRS}R'$	**0.34**	0.22	0.40	**0.22**	0.21	0.63	**0.36**	0.29	0.53	**0.23**	0.22	0.37	**0.24**	0.23	0.45
$AUC_{TmaxTend}'$	**24.0**	21.2	39.7	**39.1**	10.5	62.5	**253**	67.9	434.3	**388**	254	618	**354**	257	603
AUC_{JTmax}'	**74.8**	52.9	108.2	**99.7**	47.5	157.8	**0.0**	0.0	15.3	**1.6**	0.0	52.0	**2.2**	0.0	47.7
AUC_{JT}'	**101**	74.9	149.0	**180**	59.7	208.3	**256**	88.1	442	**393**	258	633	**358**	263	630
AUC_{QRS}'	**58.8**	39.5	79.1	**58.5**	42.9	84.3	**148**	136.1	203	**173**	118	254	**175**	113	236
AUC_{QRST}'	**159**	134	232	**208**	160	264	**397**	242.0	717	**610**	472	811	**620**	437	802
$-AUC_{JT}$	**-7.7**	-103	-4.1	**-25.8**	-95.1	-5.6	**-30.4**	-117	-15.4	**-49.6**	-110	-13.9	**-43.6**	-69.7	-8.3
$+AUC_{JT}$	**54.0**	0.7	102.0	**12.4**	1.2	179.2	**156**	67.7	324	**326**	217	599	**349**	216	591
$AUC_{JTmax/TmaxTend}$	**3.4**	3.0	4.0	**4.0**	2.8	4.6	**0.0**	0.0	0.4	**0.1**	0.0	0.2	**0.0**	0.0	0.1
$AUC_{TmaxTend}$	**14.2**	-23.7	23.2	**4.3**	-18.8	39.4	**50.9**	25.0	260	**315**	132	483	**337**	144	467
AUC_{JTmax}	**24.5**	-78.4	70.9	**-18.4**	-74.7	111	**0.0**	0.0	4.0	**1.6**	0.0	52.0	**2.2**	0.0	47.7
$+/-AUC_{QRS}$	**2.4**	1.5	6.0	**2.4**	1.7	8.2	**10.2**	7.5	18.8	**9.8**	6.8	12.4	**8.6**	4.9	12.1
$-AUC_{QRS}$	**-14.5**	-18.0	-9.8	**-13.7**	-18.8	-10.1	**-16.3**	-22.3	-9.5	**-16.6**	-20.4	-12.2	**-20.4**	-23.7	-13.0
$+AUC_{QRS}$	**49.6**	24.0	62.1	**48.8**	28.9	72.8	**134**	122	193	**159**	107.4	236	**143**	99.7	217
AUC_{JT}	**39.5**	-102	95.5	**-13.5**	-94.0	176	**62.0**	33.5	264	**319**	136.7	539	**341**	150	528
AUC_{QRS}	**29.3**	8.9	53.1	**28.2**	11.9	63.9	**126**	107	182	**143**	95.9	217	**110**	86.2	196
AUC_{QRST}	**66.2**	-54.9	133.2	**57.9**	-21.1	184	**213**	106	416	**510**	262	684	**578**	256	656
T_A	**0.76**	-0.51	1.28	**0.68**	-0.54	1.43	**3.15**	1.31	4.99	**4.31**	3.95	5.30	**4.10**	3.96	5.09
ST20	**-0.10**	-0.23	0.08	**-0.11**	-0.22	0.24	**1.10**	0.29	3.29	**2.86**	1.69	4.96	**3.04**	1.68	4.65
QRS_A	**3.91**	2.04	5.19	**3.19**	2.54	5.14	**4.57**	3.70	6.04	**4.66**	4.06	5.60	**4.84**	4.08	5.50
$-QRS_A$	**-1.20**	-1.46	-0.97	**-1.15**	-1.31	-0.84	**-1.01**	-1.18	-0.69	**-0.91**	-1.11	-0.75	**-1.02**	-1.18	-0.85
$+QRS_A$	**3.91**	2.04	5.19	**3.19**	2.54	5.14	**4.57**	3.70	6.04	**4.66**	4.06	5.60	**4.84**	4.08	5.50
JTmax	**118**	105.8	130.5	**129.8**	100.2	143.0	**1.00**	1.00	6.57	**1.09**	1.00	6.82	**1.18**	1.00	5.07

Unites of particular parameters can be found in Appendix A

Table C-2. Values of lead II parameters at the beginning of ischemia (i.e. the end of stabilization) (0^{th} minute) and the end of the 2^{nd}, 5^{th}, 8^{th}, and 10^{th} minute of ischemia. Expressed as median and 25^{th} and 75^{th} percentiles.

Parameter	Time period during ischemia														
	0^{th} minute			2^{nd} minute			5^{th} minute			8^{th} minute			10^{th} minute		
	Mdn	**25^{th} perc**	**75^{th} perc**	**Mdn**	**25^{th} perc**	**75^{th} perc**	**Mdn**	**25^{th} perc**	**75^{th} perc**	**Mdn**	**25^{th} perc**	**75^{th} perc**	**Mdn**	**25^{th} perc**	**75^{th} perc**
$-AUC_{JT}R'$	**0.00**	0.00	0.03	**0.00**	0.00	0.07	**0.03**	0.02	0.11	**0.05**	0.01	0.15	**0.10**	0.04	0.25
$+AUC_{JT}R'$	**0.82**	0.49	0.83	**0.62**	0.50	0.86	**0.54**	0.44	0.68	**0.62**	0.39	0.65	**0.46**	0.33	0.60
$AUC_{TmaxTend}R'$	**0.17**	0.12	0.18	**0.17**	0.13	0.30	**0.39**	0.24	0.49	**0.64**	0.34	0.67	**0.51**	0.30	0.62
$AUC_{JTmax}R'$	**0.59**	0.43	0.66	**0.45**	0.38	0.62	**0.29**	0.04	0.38	**0.01**	0.00	0.16	**0.04**	0.00	0.18
$-AUC_{QRS}Rq'$	**0.89**	0.78	0.94	**0.78**	0.55	0.93	**0.07**	0.02	0.15	**0.05**	0.02	0.15	**0.08**	0.05	0.25
$+AUC_{QRS}Rq'$	**0.11**	0.05	0.22	**0.22**	0.07	0.45	**0.93**	0.85	0.98	**0.95**	0.85	0.98	**0.92**	0.75	0.95
$-AUC_{QRS}R'$	**0.18**	0.14	0.35	**0.24**	0.08	0.38	**0.02**	0.01	0.03	**0.03**	0.00	0.04	**0.03**	0.02	0.06
$+AUC_{QRS}R'$	**0.03**	0.01	0.05	**0.06**	0.03	0.09	**0.42**	0.12	0.47	**0.32**	0.17	0.40	**0.39**	0.13	0.46
$AUC_{JT}R'$	**0.82**	0.58	0.83	**0.70**	0.55	0.87	**0.55**	0.51	0.75	**0.65**	0.59	0.78	**0.60**	0.50	0.73
$AUC_{QRS}R'$	**0.18**	0.17	0.42	**0.30**	0.13	0.45	**0.45**	0.25	0.49	**0.35**	0.22	0.41	**0.40**	0.27	0.50
$AUC_{TmaxTend}'$	**26.3**	19.8	55.0	**22.8**	7.9	49.1	**87.7**	60.5	134	**223**	51.2	354	**151**	41.6	254
AUC_{JTmax}'	**104**	54.7	194	**59.1**	39.1	151	**58.3**	5.6	105	**6.7**	0.0	31.5	**11.0**	0.0	49.3
AUC_{JT}'	**132**	75.5	243	**82.9**	52.6	209	**167**	133	201	**226**	110	364	**154**	121	265
AUC_{QRS}'	**48.3**	34.1	58.9	**30.2**	20.4	51.0	**104**	49.2	141	**118**	86.4	154	**118**	64.6	141
AUC_{QRST}'	**197**	130	285	**131**	73.8	241.4	**271**	188	359	**407**	220	525	**327**	191	445
$-AUC_{JT}$	**-0.8**	-5.2	-0.1	**-0.8**	-5.3	-0.1	**-7.2**	-46.6	-2.9	**-13.8**	-46.1	-4.6	**-20.9**	-71.3	-11.5
$+AUC_{JT}$	**126**	65.6	243	**81.1**	42.6	209	**144**	77.0	176	**135**	93.2	353	**102**	70.1	253
$AUC_{JTmax/TmaxTend}$	**3.5**	2.1	4.0	**1.9**	1.6	4.2	**0.5**	0.1	1.1	**0.0**	0.0	0.1	**0.1**	0.0	0.5
$AUC_{TmaxTend}$	**25.6**	19.1	53.8	**22.8**	7.9	49.0	**64.7**	38.1	93.3	**56.2**	47.5	307	**46.9**	30.6	133
AUC_{JTmax}	**93.7**	40.2	194	**55.5**	27.4	151.7	**50.9**	5.6	75.7	**0.0**	0.0	15.6	**0.0**	0.0	17.4
$+/-AUC_{QRS}$	**0.1**	0.1	0.3	**0.3**	0.1	0.9	**13.5**	6.2	45.7	**17.3**	6.7	60.0	**11.7**	6.2	20.2
$-AUC_{QRS}$	**-43.4**	-55.2	-24.9	**-20.0**	-38.7	-14.8	**-4.4**	-11.8	-2.5	**-6.6**	-14.7	-1.5	**-9.4**	-16.2	-5.1
$+AUC_{QRS}$	**6.3**	2.6	11.1	**6.1**	3.2	14.1	**58.9**	25.6	139	**105**	31.8	147	**107**	26.5	131
AUC_{JT}	**120**	58.2	242	**79.3**	33.8	208	**134**	63.4	172	**85.2**	56.4	316	**50.0**	34.4	142
AUC_{QRS}	**-37.9**	-50.7	-21.5	**-18.1**	-31.1	-4.6	**55.9**	21.3	138	**98.8**	30.0	142	**99.9**	20.3	121
AUC_{QRST}	**90.0**	20.7	209	**52.9**	10.1	197	**182**	115	248	**356**	90.5	425	**172**	54.6	338
T_A	**1.31**	0.93	2.05	**0.72**	0.44	1.70	**1.88**	1.45	2.35	**3.06**	1.27	3.62	**2.50**	1.09	3.16
ST20	**0.10**	0.00	0.32	**0.15**	0.00	0.31	**0.14**	-0.06	0.74	**0.98**	-0.30	1.93	**0.74**	-0.42	1.40
QRS_A	**-3.88**	-4.36	-2.51	**-2.07**	-3.10	-0.72	**2.35**	1.30	4.85	**3.74**	1.15	4.94	**3.40**	0.43	4.34
$-QRS_A$	**-3.88**	-4.36	-2.51	**-2.07**	-3.10	-0.97	**-0.52**	-0.81	-0.34	**-0.75**	-0.92	-0.19	**-0.74**	-1.01	-0.29
$+QRS_A$	**0.71**	0.51	1.03	**0.53**	0.38	1.38	**2.35**	1.36	4.85	**3.74**	1.17	4.94	**3.40**	1.00	4.34
JTmax	**129**	120	142	**138**	86.3	146	**60.7**	3.18	89.7	**1.82**	1.00	20.50	**2.64**	1.00	23.2

Unites of particular parameters can be found in Appendix A

Table C-3. Values of VCG parameters at the beginning of ischemia (i.e. the end of stabilization) (0^{th} minute) and the end of the 2^{nd}, 5^{th}, 8^{th}, and 10^{th} minute of ischemia. Expressed as median and 25^{th} and 75^{th} percentiles.

Parameter	Time period during ischemia														
	0^{th} minute			2^{nd} minute			5^{th} minute			8^{th} minute			10^{th} minute		
	Mdn	**25^{th} perc**	**75^{th} perc**	**Mdn**	**25^{th} perc**	**75^{th} perc**	**Mdn**	**25^{th} perc**	**75^{th} perc**	**Mdn**	**25^{th} perc**	**75^{th} perc**	**Mdn**	**25^{th} perc**	**75^{th} perc**
P_{jt}	**7.84**	6.08	9.20	**6.80**	6.42	9.02	**10.71**	8.89	13.11	**10.54**	9.43	11.17	**10.48**	9.77	10.94
P_{qrs}	**17.05**	15.02	22.03	**15.25**	13.57	17.38	**13.87**	10.82	17.26	**10.38**	9.32	14.08	**10.97**	9.00	13.41
$A_{jt}zy$	**0.17**	0.11	0.21	**0.32**	0.13	0.40	**1.15**	0.67	5.43	**1.96**	1.49	3.18	**1.69**	1.15	3.72
$A_{jt}xz$	**0.30**	0.18	0.37	**0.26**	0.20	0.55	**2.28**	1.01	5.00	**3.88**	3.34	6.19	**3.86**	3.01	8.31
$A_{jt}xy$	**0.19**	0.16	0.26	**0.22**	0.17	0.25	**0.63**	0.58	1.39	**0.82**	0.66	2.67	**0.99**	0.61	3.05
$A_{qrs}zy$	**3.31**	1.96	6.06	**3.22**	1.12	5.65	**5.13**	3.41	5.61	**3.79**	3.03	5.62	**4.73**	1.68	5.50
$A_{qrs}xz$	**4.44**	3.36	5.06	**4.08**	3.65	5.24	**6.26**	3.57	9.27	**4.50**	2.60	6.80	**4.74**	2.94	6.58
$A_{qrs}xy$	**3.72**	2.16	9.32	**1.79**	1.44	5.46	**2.39**	1.39	4.87	**2.21**	1.42	4.33	**2.25**	1.07	4.67
$\varphi^{c}_{jt}zy$	**75**	53	143	**98**	62	117	**32**	17	83	**16**	10	30	**16**	11	23
$\varphi^{c}_{jt}xz$	**9**	8	14	**8**	5	19	**22**	17	36	**15**	4	19	**14**	3	22
$\varphi^{c}_{jt}xy$	**4**	2	10	**6**	3	10	**26**	19	54	**28**	15	30	**28**	9	32
$\varphi^{c}_{qrs}zy$	**12**	7	28	**16**	1	25	**4**	3	13	**9**	3	22	**12**	4	21
$\varphi^{c}_{qrs}xz$	**11**	6	17	**16**	2	26	**12**	7	29	**7**	5	18	**8**	2	16
$\varphi^{c}_{qrs}xy$	**10**	5	41	**31**	13	44	**10**	4	19	**5**	2	11	**7**	5	12
$D^{c}_{jt}zy$	**0.63**	0.57	0.92	**0.66**	0.54	0.97	**2.46**	0.60	3.68	**2.74**	2.20	3.31	**2.73**	2.33	3.07
$D^{c}_{jt}xz$	**1.03**	0.75	1.32	**0.68**	0.42	1.14	**2.41**	1.40	4.66	**3.85**	2.39	4.19	**3.50**	2.52	3.98
$D^{c}_{jt}xy$	**0.93**	0.69	1.20	**0.66**	0.41	0.99	**1.19**	0.85	2.25	**2.09**	0.51	2.93	**1.98**	0.48	2.87
$D^{c}_{qrs}zy$	**3.06**	1.39	3.45	**2.75**	1.62	3.65	**2.78**	1.64	3.13	**3.05**	2.24	3.59	**3.05**	2.44	3.42
$D^{c}_{qrs}xz$	**3.40**	3.22	3.89	**2.85**	2.44	3.56	**3.11**	2.57	3.84	**3.81**	3.10	4.04	**3.66**	3.10	3.80
$D^{c}_{qrs}xy$	**3.23**	2.46	3.58	**2.26**	1.28	2.57	**1.39**	1.12	3.18	**2.17**	1.43	2.99	**1.89**	1.59	2.66
D	**6.33**	5.23	8.25	**5.31**	4.80	6.48	**2.73**	1.90	3.48	**0.22**	0.18	1.55	**0.30**	0.25	1.18
φ	**115**	92	131	**110**	96	132	**20**	12	46	**2**	1	15	**4**	2	7
L_{jt}	**2.1**	1.4	2.5	**1.6**	1.4	2.3	**3.3**	2.0	7.6	**6.3**	4.1	6.9	**5.6**	4.1	6.6
L_{qrs}	**5.5**	4.8	6.8	**5.0**	3.8	5.6	**5.6**	4.2	8.9	**6.8**	5.0	7.8	**6.5**	5.0	7.3
γ_{jt}	**-28.9**	-59.6	4.7	**-29.1**	-70.4	14.0	**-15.2**	-56.1	4.9	**-12.6**	-17.8	-1.7	**-11.5**	-23.8	-1.4
β_{jt}	**19**	-4	40	**24**	-72	46	**61**	26	85	**60**	51	81	**65**	53	85
α_{jt}	**-21**	-34	3	**-29**	-67	7	**-28**	-47	31	**-27**	-62	-2	**-40**	-70	-3
γ_{qrs}	**10**	-1	41	**21**	7	43	**17**	-1	20	**-7**	-15	13	**-8**	-21	2
β_{qrs}	**137**	119	150	**111**	87	141	**68**	35	72	**57**	42	72	**63**	48	75
α_{qrs}	**150**	71	162	**135**	10	150	**14**	-9	47	**-6**	-53	10	**-35**	-68	4
QT_D	**178**	169	190	**176**	170	201	**176**	159	187	**166**	151	186	**164**	142	184
QRS_D	**24.0**	22.7	26.8	**26.0**	21.5	31.0	**35.0**	33.4	39.5	**36.0**	32.0	41.3	**37.0**	32.8	41.3
RR	**344**	327	379	**373**	362	409	**505**	462	527	**561**	489	639	**581**	512	676

Unites of particular parameters can be found in Appendix A

APPPENDIX D – RESULTS OF PAIRED TEST FOR CONTROL GROUP PARAMETERS

lead I parameters:

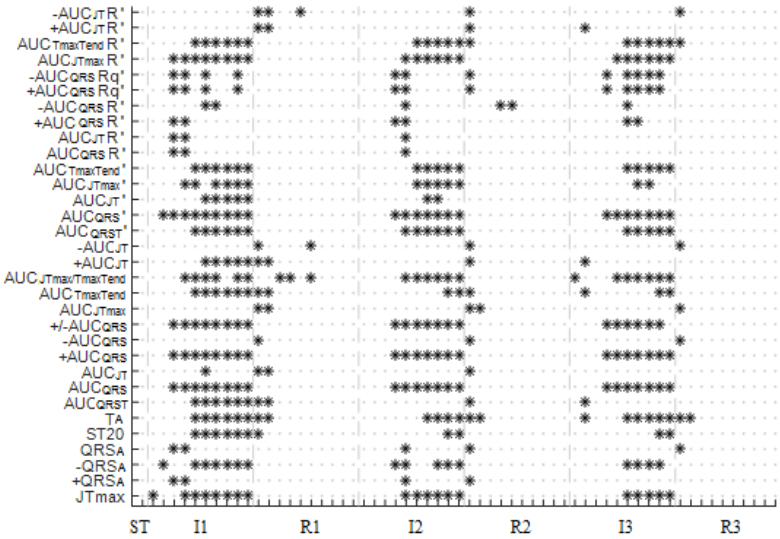

lead II parameters:

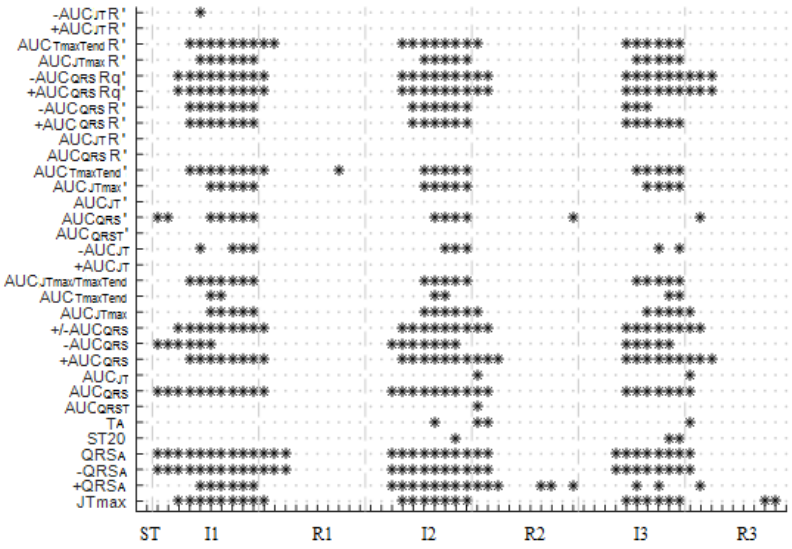

VCG and joint parameters:

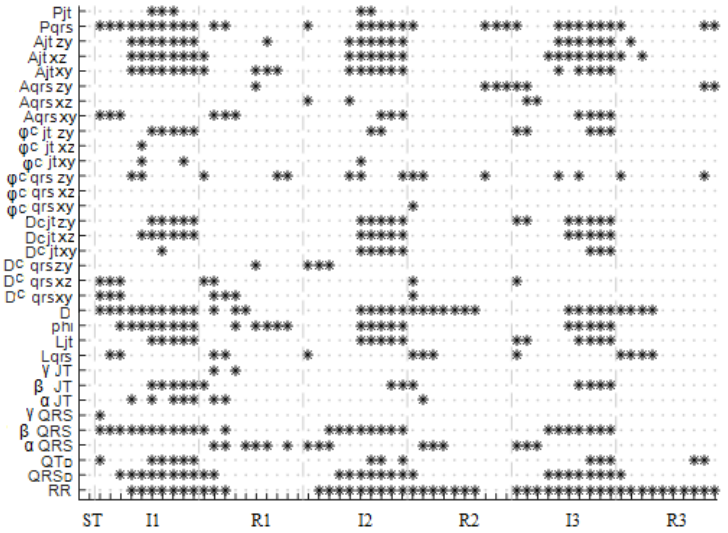

Figure D-1. Results of Wilcoxon signed-rank test for comparison of parameters from the end of stabilization and at each minute of three ischemia-reperfusion repetitions in control group (hearts with low LV mass fraction from experiments without voltage-sensitive dye application). * for $p < 0.05$.

APPENDIX E – DISCRIMINATING ABILITY INDEXES IN CONTROL GROUP DURING ISCHEMIA

Table E-1. Time instances, where AUCROC of lead I parameters from the control group reaches value higher than 0.7, 0.8 and 0.9 and corresponding Se, Sp and cut-off. Indexes with both Se and Sp in the range <0.7 - 0.8>, <0.8 - 0.9> or <0.9 - 1> (one of them may exceed the range) are highlighted by orange, green and blue, respectively.

Parameter	Time, min			Se, %			Sp, %			Cut-off*		
	> 0.7	> 0.8	> 0.9	> 0.7	> 0.8	> 0.9	> 0.7	> 0.8	> 0.9	> 0.7	> 0.8	> 0.9
-$AUC_{JT}R'$	-	-	-	-	-	-	-	-	-	-	-	-
+$AUC_{JT}R'$	-	-	-	-	-	-	-	-	-	-	-	-
$AUC_{TmaxTend}R'$	4	**5**	**6**	48.4	**86.1**	**100.0**	92.3	**92.3**	**99.6**	0.22	**0.22**	**0.37**
$AUC_{JTmax}R'$	3	4	**4**	76.1	89.8	**89.8**	61.0	80.1	**80.1**	0.46	0.39	**0.39**
-$AUC_{QRS}Rq'$	4	4	**8**	95.5	95.5	**84.2**	50.1	50.1	**82.4**	0.09	0.09	**0.12**
+$AUC_{QRS}Rq'$	4	4	**7**	64.2	64.2	**71.4**	85.0	85.0	**95.1**	0.88	0.88	**0.91**
-$AUC_{QRS}R'$	**5**	6	**6**	**78.1**	84.3	**84.3**	**70.3**	87.4	**87.4**	**0.04**	0.03	**0.03**
+$AUC_{QRS}R'$	4	4	-	91.4	91.4	-	65.9	65.9	-	0.23	0.23	-
$AUC_{JT}R'$	**4**	-	-	**74.5**	-	-	**71.2**	-	-	**0.60**	-	-
$AUC_{QRS}R'$	**4**	-	-	**71.2**	-	-	**74.5**	-	-	**0.40**	-	-
$AUC_{TmaxTend}'$	5	**5**	**6**	73.6	**73.6**	**100.0**	99.7	**99.7**	**99.1**	67.9	**67.9**	**57.9**
AUC_{JTmax}'	4	**4**	**5**	90.7	**90.7**	**92.2**	70.2	**70.2**	**94.3**	46.2	**46.2**	**44.8**
AUC_{JT}'	6	6	**6**	79.3	79.3	**79.3**	99.9	99.9	**99.9**	266. 6	266.6	**266.6**
AUC_{QRS}'	4	**4**	**5**	95.2	**95.2**	**85.0**	74.9	**74.9**	**98.4**	69.9	**69.9**	**116.4**
AUC_{QRST}'	5	5	**6**	58.6	58.6	**94.7**	99.7	99.7	**100.0**	327.8	327.8	**334.8**
-AUC_{JT}	-	-	-	-	-	-	-	-	-	-	-	-
+AUC_{JT}	5	6	6	28.3	64.3	64.3	99.7	99.3	99.3	260.8	256.2	256.2
$AUC_{JTmax/TmaxTend}$	3	**4**	**5**	82.6	**84.6**	**96.9**	63.6	**86.1**	**90.4**	2.80	**2.67**	**1.20**
$AUC_{TmaxTend}$	6	6	**6**	87.8	87.8	**87.8**	99.2	99.2	**99.2**	51.6	51.6	**51.6**
AUC_{JTmax}	-	-	-	-	-	-	-	-	-	-	-	-
+/-AUC_{QRS}	4	4	**8**	50.1	50.1	**82.4**	95.6	95.6	**84.2**	10.5	10.5	**7.5**
-AUC_{QRS}	-	-	-	-	-	-	-	-	-	-	-	-
+AUC_{QRS}	4	4	**5**	94.0	94.0	**83.8**	69.1	69.1	**95.8**	51.2	51.2	**94.6**
AUC_{JT}	6	6	-	51.5	51.5	-	99.5	99.5	-	254.9	254.9	-
AUC_{QRS}	4	4	**5**	64.8	64.8	**89.5**	90.7	90.7	**91.2**	72.2	72.2	**73.1**
AUC_{QRST}	5	6	**6**	36.1	76.5	**76.5**	99.7	99.9	**99.9**	308.8	311.7	**311.7**
T_A	5	5	**6**	68.6	68.6	**100.0**	100.0	100.0	**100.0**	2.1	2.1	**2.1**
ST20	5	5	**6**	58.8	58.8	**85.8**	99.9	99.9	**100.0**	0.68	0.68	**0.69**
QRS_A	7	-	-	95.8	-	-	59.9	-	-	3.98	-	-
-QRS_A	-	-	-	-	-	-		-	-	-	-	-
+QRS_A	8	-	-	98.5	-	-	59.0	-	-	3.95	-	-
JTmax	4	4	**5**	97.9	97.9	**95.9**	59.7	59.7	**92.2**	99	99	**102**

* Unites of particular parameters can be found in Appendix A

Table E-2. Time instances, where AUCROC of lead II parameters from the control group reaches value higher than 0.7, 0.8 and 0.9 and corresponding Se, Sp and cut-off. Indexes with both Se and Sp in the range <0.7 - 0.8>, <0.8 - 0.9> or <0.9 - 1> (one of them may exceed the range) are highlighted by orange, green and blue, respectively.

Parameter	Time, min			Se, %			Sp, %			Cut-off*		
	> 0.7	> 0.8	> 0.9	> 0.7	> 0.8	> 0.9	> 0.7	> 0.8	> 0.9	> 0.7	> 0.8	> 0.9
-$AUC_{JT}R'$	8	-	-	61.0	-	-	75.3	-	-	0.05	-	-
+$AUC_{JT}R'$	-	-	-	-	-	-	-	-	-	-	-	-
$AUC_{TmaxTend}R'$	3	4	**4**	55.3	72.6	**72.6**	97.2	93.5	**93.5**	0.21	0.20	**0.20**
$AUC_{JTmax}R'$	4	**5**	6	59.6	**80.3**	100.0	86.1	**73.8**	74.4	0.53	**0.41**	0.08
-$AUC_{QRS}Rq'$	3	3	**4**	93.9	93.9	**100.0**	58.6	58.6	**70.5**	0.65	0.65	**0.40**
+$AUC_{QRS}Rq'$	3	3	**4**	58.6	58.6	**70.3**	93.9	93.9	**100.0**	0.35	0.35	**0.59**
-$AUC_{QRS}R'$	3	**4**	**5**	77.6	**87.5**	**87.8**	55.1	**76.5**	**87.1**	0.16	**0.09**	**0.09**
+$AUC_{QRS}R'$	3	**4**	5	71.2	**84.6**	71.1	78.2	**79.7**	100.0	0.05	**0.05**	0.20
$AUC_{JT}R'$	-	-	-	-	-	-	-	-	-	-	-	-
$AUC_{QRS}R'$	-	-	-	-	-	-	-	-	-	-	-	-
$AUC_{TmaxTend}'$	4	5	**6**	67.6	69.5	**73.6**	82.7	88.3	**99.9**	47.61	64.50	**103.56**
AUC_{JTmax}'	6	6	**6**	100.0	100.0	**100.0**	71.8	71.8	**71.8**	7.72	7.72	**7.72**
AUC_{JT}'	7	-	-	57.4	-	-	85.8	-	-	243.36	-	-
AUC_{QRS}'	5	6	**6**	59.6	83.8	**83.8**	100.0	100.0	**100.0**	88.26	88.34	**88.34**
AUC_{QRST}'	5	**6**	-	59.2	**70.2**	-	78.5	**87.0**	-	267.03	**310.46**	-
-AUC_{JT}	5	**7**	-	73.0	**80.5**	-	61.7	**71.2**	-	-4.13	**-6.59**	-
+AUC_{JT}	-	-	-	-	-	-	-	-	-	-	-	-
$AUC_{JTmax/TmaxTend}$	4	**5**	**6**	62.8	**76.0**	**83.3**	97.1	**86.1**	**97.8**	3.17	**1.45**	**0.92**
$AUC_{TmaxTend}$	5	6	**6**	61.7	84.6	**84.6**	81.7	87.1	**87.1**	45.41	58.29	**58.29**
AUC_{JTmax}	6	**6**	-	94.0	**94.0**	-	70.0	**70.0**	-	0.10	**0.10**	-
+/-AUC_{QRS}	3	3	**4**	58.6	58.6	**70.3**	93.9	93.9	**100.0**	0.54	0.54	**1.50**
-AUC_{QRS}	3	**4**	-	68.2	**77.7**	-	87.6	**87.8**	-	-22.66	**-21.71**	-
+AUC_{QRS}	3	4	**5**	69.1	61.1	**84.4**	86.1	100.0	**99.9**	14.28	27.94	**19.36**
AUC_{JT}	-	-	-	-	-	-	-	-	-	-	-	-
AUC_{QRS}	**3**	4	-	**79.6**	77.7	-	**77.2**	94.0	-	**-20.04**	-5.81	-
AUC_{QRST}	5	7	-	44.7	56.5	-	87.4	93.6	-	226.9	341.4	-
T_A	**5**	-	-	**73.8**	-	-	**70.4**	-	-	**1.52**	-	-
ST20	-	-	-	-	-	-	-	-	-	-	-	-
QRS_A	2	**3**	4	86.0	**75.3**	77.7	56.7	**86.7**	98.8	-3.73	**-2.15**	-0.91
-QRS_A	2	**3**	4	86.0	**75.3**	77.4	56.7	**86.7**	95.4	-3.73	**-2.15**	-1.16
+QRS_A	**4**	4	5	**72.2**	72.2	94.7	**83.8**	83.8	82.2	**1.35**	1.35	1.07
JTmax	3	4	**5**	82.9	99.1	**100.0**	54.8	60.0	**81.3**	114	104	**103**

* Unites of particular parameters can be found in Appendix A

Table E-3. Time instances, where AUCROC of joint & VCG parameters from the control group reaches value higher than 0.7, 0.8 and 0.9 and corresponding Se, Sp and cut-off. Indexes with both Se and Sp in the range <0.7 - 0.8>, <0.8 - 0.9> or <0.9 - 1> (one of them may exceed the range) are highlighted by orange, green and blue, respectively.

Parameter	Time, min			Se, %			Sp, %			Cut-off*		
	> 0.7	> 0.8	> 0.9	> 0.7	> 0.8	> 0.9	> 0.7	> 0.8	> 0.9	> 0.7	> 0.8	> 0.9
P_{jt}	5	5	**7**	48.8	48.8	**88.9**	100.0	100.0	**82.7**	10.5	10.5	**9.5**
P_{qrs}	6	6	-	100.0	100.0	-	53.5	53.5	-	12.8	12.8	-
$A_{jt}zy$	3	**4**	5	60.4	**82.3**	90.2	85.8	**85.8**	83.9	0.34	**0.34**	0.31
$A_{jt}xz$	4	**5**	**6**	50.3	**72.5**	**99.8**	90.7	**93.1**	**100.0**	0.64	**0.76**	**1.34**
$A_{jt}xy$	3	**3**	**4**	77.5	**77.5**	**88.0**	88.4	**88.4**	**88.6**	0.31	**0.31**	**0.31**
$A_{qrs}zy$	-	-	-	-	-	-	-	-	-	-	-	-
$A_{qrs}xz$	-	-	-	-	-	-	-	-	-	-	-	-
$A_{qrs}xy$	-	-	-	-	-	-	-	-	-	-	-	-
$\varphi^c_{jt}zy$	5	6	**6**	88.3	89.6	**89.6**	55.3	87.2	**87.2**	38	34	**34**
$\varphi^c_{jt}xz$	-	-	-	-	-	-	-	-	-	-	-	-
$\varphi^c_{jt}xy$	5	5	-	60.7	60.7	-	88.7	88.7	-	20	20	-
$\varphi^c_{qrs}zy$	5	-	-	90.8	-	-	35.0	-	-	3	-	-
$\varphi^c_{qrs}xz$	-	-	-	-	-	-	-	-	-	-	-	-
$\varphi^c_{qrs}xy$	7	-	-	90.3	-	-	41.4	-	-	4	-	-
$D^c_{jt}zy$	5	6	**6**	68.6	93.5	**93.5**	100.0	100.0	**100.0**	1.6	1.4	**1.4**
$D^c_{jt}xz$	4	5	**6**	69.6	68.4	**90.9**	76.4	100.0	**100.0**	1.2	1.7	**1.7**
$D^c_{jt}xy$	4	**7**	-	65.2	**75.6**	-	73.0	**100.0**	-	1.0	**1.9**	-
$D^c_{qrs}zy$	-	-	-	-	-	-	-	-	-	-	-	-
$D^c_{qrs}xz$	-	-	-	-	-	-	-	-	-	-	-	-
$D^c_{qrs}xy$	2	-	-	68.8	-	-	84.1	-	-	2.8	-	-
D	4	5	**5**	100.0	93.9	**93.9**	37.2	80.9	**80.9**	3.8	4.5	**4.5**
φ	4	4	**5**	97.9	97.9	**99.9**	52.8	52.8	**84.6**	54	54	**53**
L_{jt}	4	5	**6**	44.8	55.3	**81.9**	85.5	100.0	**99.7**	2.4	3.4	**3.3**
L_{qrs}	7	-	-	46.2	-	-	89.9	-	-	7.6	-	-
γ_{jt}	**6**	-	-	**81.9**	-	-	**77.7**	-	-	**-20**	-	-
β_{jt}	5	6	-	42.0	100.0	-	88.3	68.4	-	72	40	-
α_{jt}	-	-	-	-	-	-	-	-	-	-	-	-
γ_{qrs}	**6**	-	-	**76.0**	-	-	**87.6**	-	-	7	-	-
β_{qrs}	3	4	**4**	84.1	97.9	**97.9**	62.9	72.6	**72.6**	112	98	**98**
α_{qrs}	**4**	10		**75.8**	76.9		**87.0**	100.0		**132**	102	
QT_D	-	-	-	-	-	-	-	-	-	-	-	-
QRS_D	3	4	**5**	37.7	60.9	**87.1**	98.1	98.1	**98.1**	31	31	**31**
RR	**3**	**4**	7	**88.9**	**88.9**	88.9	**77.8**	**88.9**	100.0	**377.5**	**425.0**	469.5

* Unites of particular parameters can be found in Appendix A

APPENDIX F – DISCRIMINATING ABILITY INDEXES IN DIFFERENT GROUPS OF PARAMETERS IN CONTROL HEART GROUP

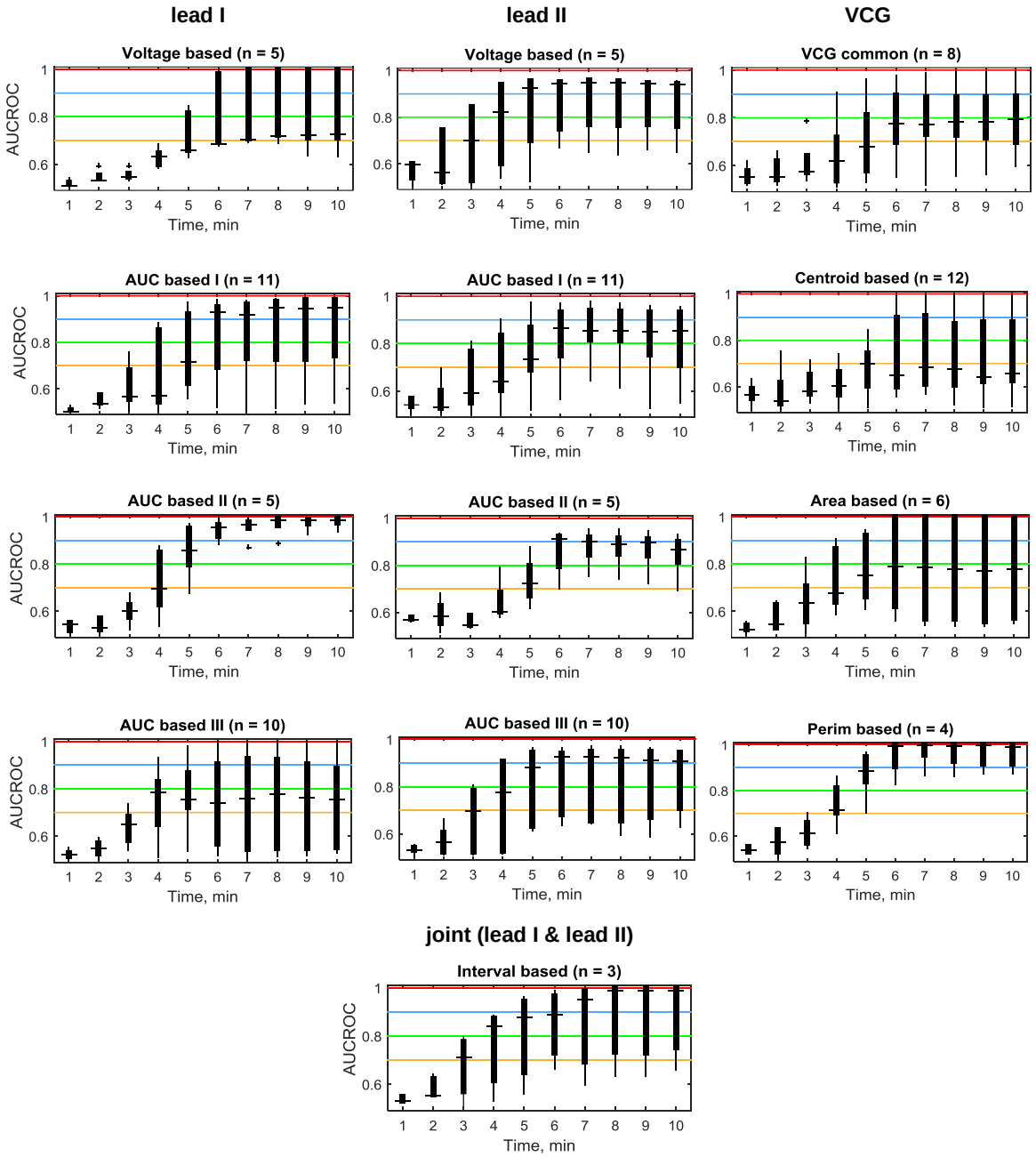

Figure F-1. Distribution of AUCROC of different parameters groups during ischemia.

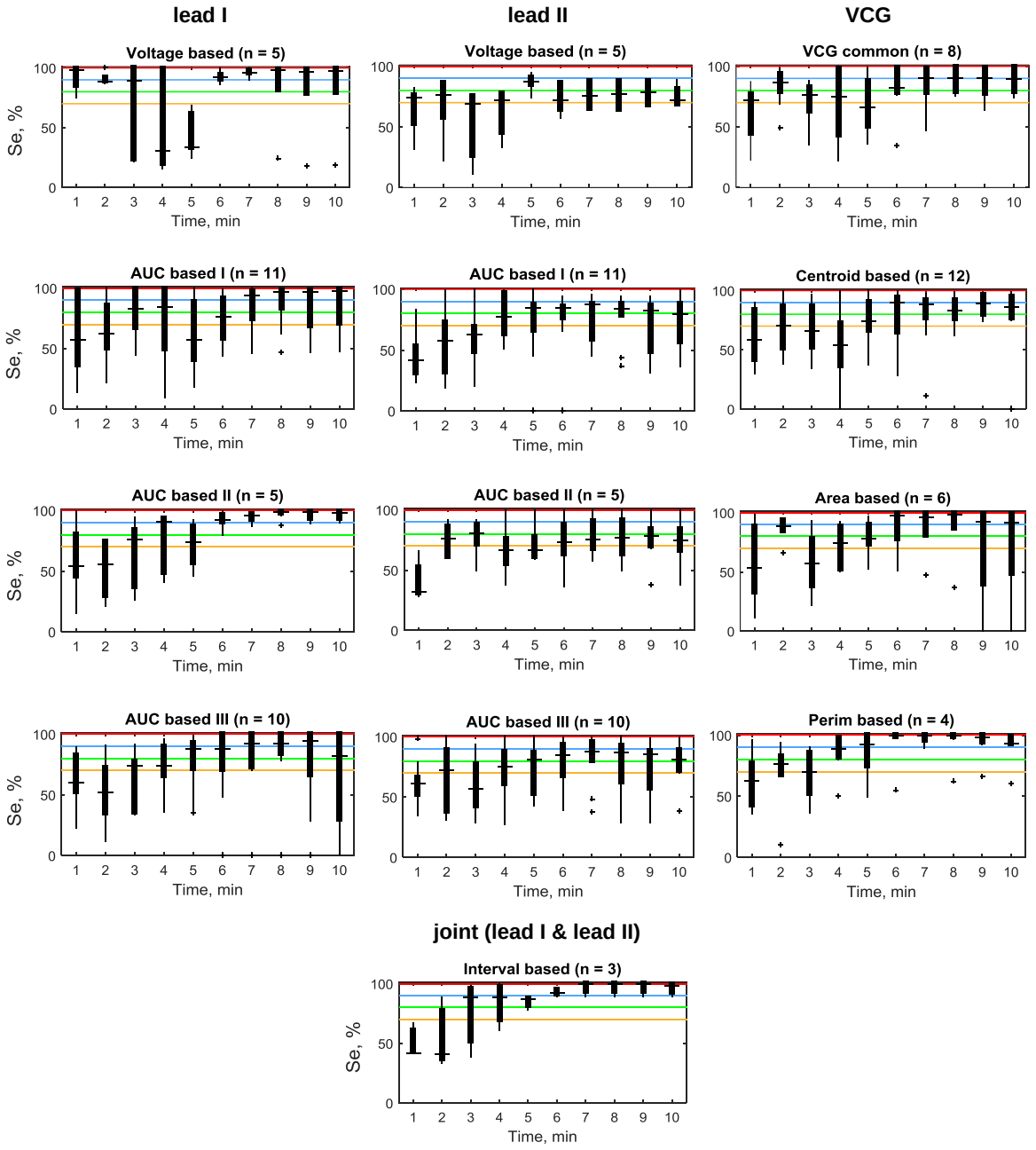

Figure F-2. Distribution of Se of different parameters groups during ischemia.

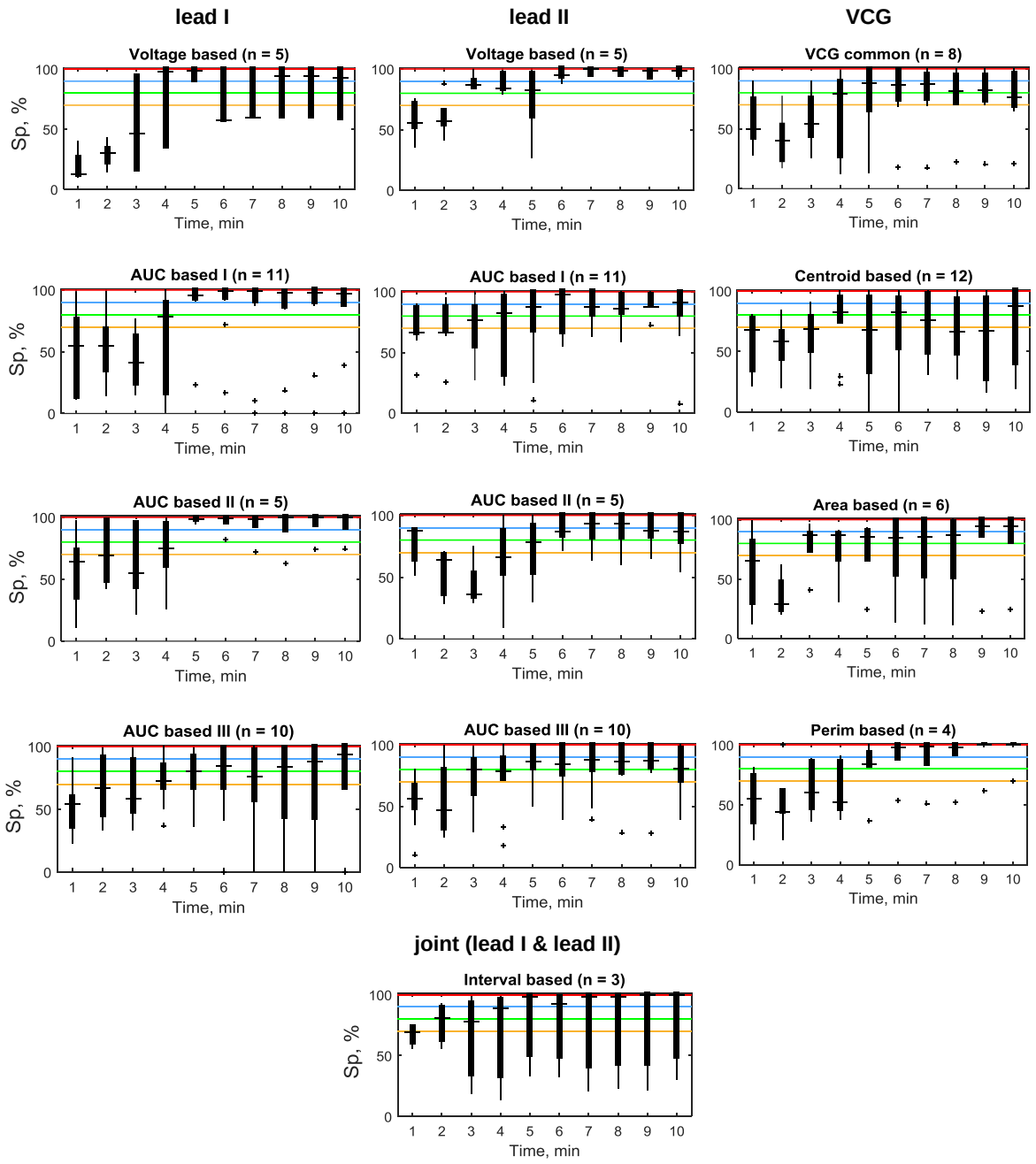

Figure F-3. Distribution of Sp of different parameters groups during ischemia.

APPENDIX G - DISCRIMINATING ABILITY OF LEAD III PARAMETERS

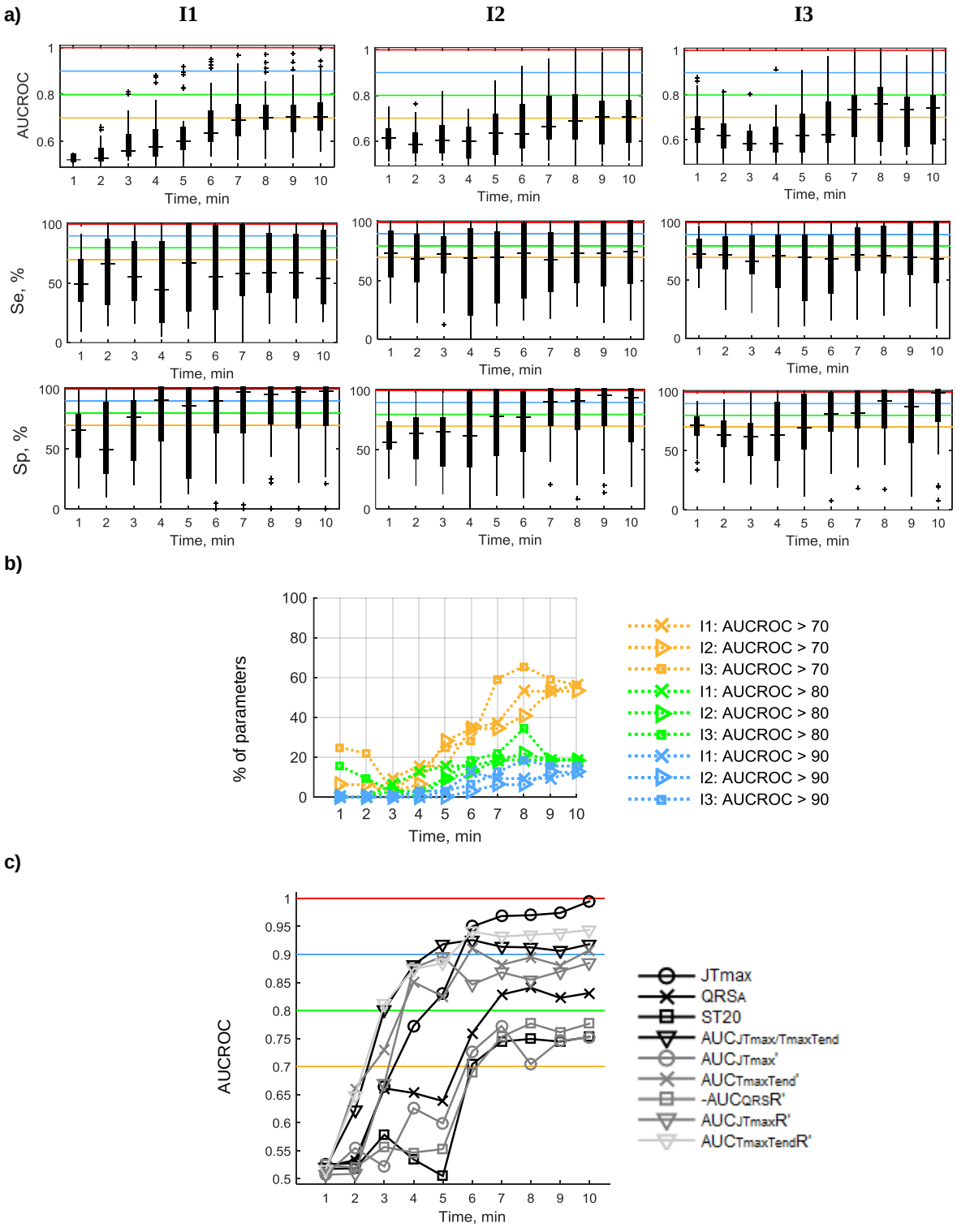

Figure G-6. Indexes of discriminating ability of morphological parameters calculated from lead III: AUCROC, Se and Sp distribution during three ischemic periods (a), percent of parameters with AUCROC reached high level during ischemic periods (b), time course of AUCROC of parameters with the best discriminating ability (c).

APPENDIX H – RESULTS OF PAIRED TEST FOR THE HEARTS WITH HIGH LV MASS FRACTION

Lead I data:

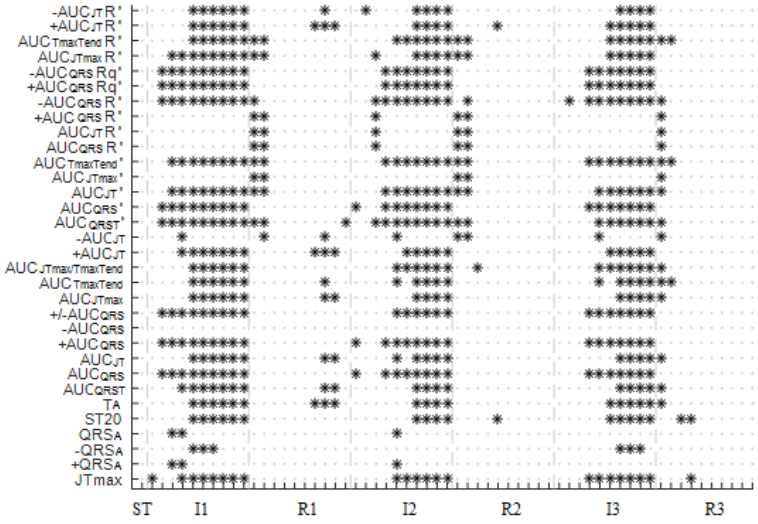

Lead II data:

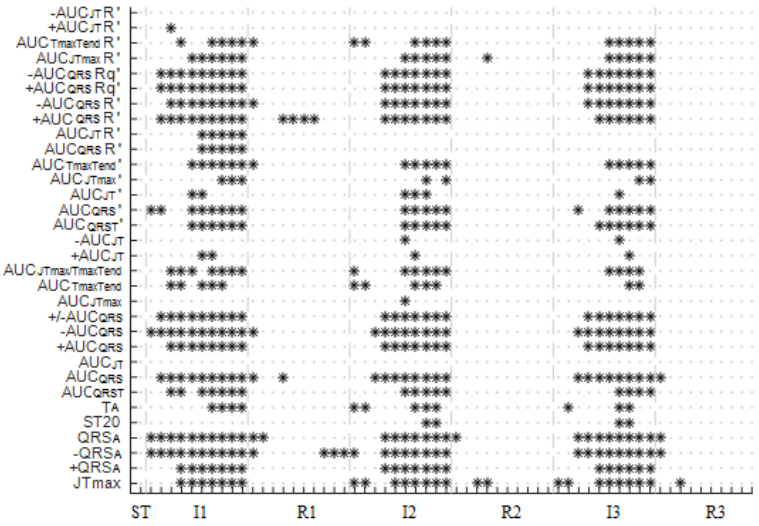

VCG and joint data:

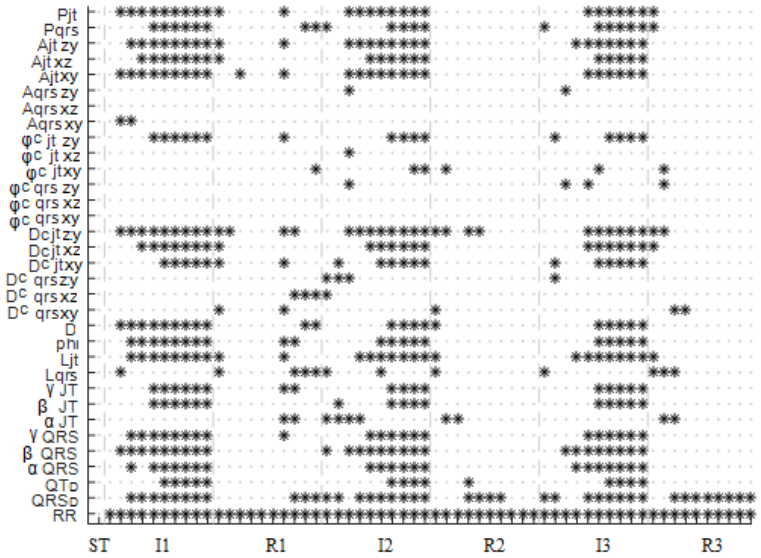

Figure H-1. Results of Wilcoxon signed-rank test for comparison of parameters from the end of stabilization and at each minute of three ischemia-reperfusion repetitions in the hearts with high LV mass fraction (experiments without voltage-sensitive dye application). * for $p < 0.05$.

APPENDIX I – DISCRIMINATING ABILITY INDEXES IN HEARTS WITH HIGH LV MASS FRACTION DURING ISCHEMIA

Table I-1. Time instances, where AUCROC of lead I parameters from the hearts with high LV mass fraction reaches value higher than 0.7, 0.8 and 0.9 and corresponding Se, Sp and cut-off. Indexes with both Se and Sp in the range <0.7 - 0.8>, <0.8 - 0.9> or <0.9 - 1> (one of them may exceed the range) are highlighted by orange, green and blue, respectively.

Parameter	Time, min			Se, %			Sp, %			Cut-off*		
	> 0.7	> 0.8	> 0.9	> 0.7	> 0.8	> 0.9	> 0.7	> 0.8	> 0.9	> 0.7	> 0.8	> 0.9
$-AUC_{JT}R'$	5	5	**6**	65.5	65.5	**97.3**	93.4	93.4	**72.0**	0.193	0.193	**0.101**
$+AUC_{JT}R'$	5	5	**5**	99.8	99.8	**99.8**	71.4	71.4	**71.4**	0.049	0.049	**0.049**
$AUC_{TmaxTend}R'$	3	**4**	**5**	59.8	**78.6**	**100.0**	82.2	**88.8**	**99.5**	0.097	**0.104**	**0.196**
$AUC_{JTmax}R'$	4	5	**5**	81.2	99.7	**99.7**	68.5	97.9	**97.9**	0.189	0.122	**0.122**
$-AUC_{QRS}Rq'$	3	**4**	**5**	81.6	**100.0**	**100.0**	66.6	**71.7**	**86.3**	0.125	**0.106**	**0.106**
$+AUC_{QRS}Rq'$	3	**4**	**5**	66.2	**71.7**	**86.3**	82.1	**100.0**	**100.0**	0.873	**0.900**	**0.912**
$-AUC_{QRS}R'$	4	5	**5**	98.8	86.1	**86.1**	42.7	96.1	**96.1**	0.042	0.059	**0.059**
$+AUC_{QRS}R'$	-	-	-	-	-	-	-	-	-	-	-	-
$AUC_{JT}R'$	6	-	-	45.4	-	-	91.1	-	-	0.694	-	-
$AUC_{QRS}R'$	6	-	-	91.1	-	-	45.4	-	-	0.306	-	-
$AUC_{TmaxTend}'$	3	**3**	4	80.6	**80.6**	77.8	72.2	**72.2**	91.8	15.9	**15.9**	29.5
AUC_{JTmax}'	5	5	**5**	100.0	100.0	**100.0**	80.9	80.9	**80.9**	12.0	12.0	**12.0**
AUC_{JT}'	3	5	**6**	85.6	62.7	**79.8**	57.3	98.3	**99.8**	58.6	300.8	**334.7**
AUC_{QRS}'	3	4	4	93.4	65.9	65.9	58.3	100.0	100.0	84.7	165.7	165.7
AUC_{QRST}'	**3**	**4**	5	**87.1**	**86.6**	100.0	**76.4**	**86.4**	86.4	**199.8**	**266.8**	237.7
$-AUC_{JT}$	-	-	-	-	-	-	-	-	-	-	-	-
$+AUC_{JT}$	4	5	**5**	66.7	85.3	**85.3**	85.8	100.0	**100.0**	16.5	38.6	**38.6**
$AUC_{JTmax/TmaxTend}$	4	4	**5**	66.0	66.0	**98.5**	85.8	85.8	**100.0**	3.2	3.2	**0.2**
$AUC_{TmaxTend}$	5	6	**6**	67.0	100.0	**100.0**	99.7	100.0	**100.0**	3.4	37.3	**37.3**
AUC_{JTmax}	5	5	**5**	100.0	100.0	**100.0**	87.8	87.8	**87.8**	0	0	**0**
$+/-AUC_{QRS}$	3	**4**	**5**	66.6	**71.7**	**86.3**	81.6	**100.0**	**100.0**	6.9	**9.1**	**10.6**
$-AUC_{QRS}$	-	-	-	-	-	-	-	-	-	-	-	-
$+AUC_{QRS}$	3	4	4	98.5	68.1	68.1	58.1	100.0	100.0	66.5	146.6	146.6
AUC_{JT}	5	5	**6**	63.1	63.1	**100.0**	100.0	100.0	**100.0**	24.6	24.6	**40.4**
AUC_{QRS}	3	**4**	**5**	84.3	**70.7**	**86.3**	58.0	**100.0**	**100.0**	50.7	**126.0**	**160.5**
AUC_{QRST}	5	5	**5**	99.4	99.4	**99.4**	100.0	100.0	**100.0**	121.4	121.4	**121.4**
T_A	5	5	**5**	95.6	95.6	**95.6**	100.0	100.0	**100.0**	0.59	0.59	**0.59**
ST20	5	**5**	**6**	71.4	**71.4**	**100.0**	100.0	**100.0**	**100.0**	-0.02	**-0.02**	**0.28**
QRS_A	-	-	-	-	-	-	-	-	-	-	-	-
$-QRS_A$	5	-	-	56.8	-	-	83.2	-	-	-1.51	-	-
$+QRS_A$	-	-	-	-	-	-	-	-	-	-	-	-
JTmax	3	4	**4**	63.5	95.0	**95.0**	81.2	87.0	**87.0**	132	114	**114**

*Unites of particular parameters can be found in Appendix A

Table I-2. Time instances, where AUCROC of lead II parameters from the hearts with high LV mass fraction reaches value higher than 0.7, 0.8 and 0.9 and corresponding Se, Sp and cut-off. Indexes with both Se and Sp in the range <0.7 - 0.8>, <0.8 - 0.9> or <0.9 - 1> (one of them may exceed the range) are highlighted by orange, green and blue, respectively.

Parameter	Time, min			Se, %			Sp, %			Cut-off*		
	> 0.7	> 0.8	> 0.9	> 0.7	> 0.8	> 0.9	> 0.7	> 0.8	> 0.9	> 0.7	> 0.8	> 0.9
-AUC_{JT}R'	-	-	-	-	-	-	-	-	-	-	-	-
+AUC_{JT}R'	3	-	-	61.3	-	-	78.4	-	-	0.546	-	-
$AUC_{TmaxTend}$R'	3	**3**	**7**	95.8	**95.8**	**99.8**	77.4	**77.4**	**81.6**	0.125	**0.125**	**0.154**
AUC_{JTmax}R'	5	6	**6**	52.1	71.7	**71.7**	92.1	95.5	**95.5**	0.413	0.328	**0.328**
-AUC_{QRS}Rq'	3	4	**4**	84.3	100.0	**100.0**	60.9	81.8	**81.8**	0.783	0.458	**0.458**
+AUC_{QRS}Rq'	3	4	**4**	60.9	81.8	**81.8**	84.3	100.0	**100.0**	0.216	0.568	**0.568**
-AUC_{QRS}R'	3	3	**4**	64.2	64.2	**78.2**	92.2	92.2	**100.0**	0.426	0.426	**0.261**
+AUC_{QRS}R'	3	4	**4**	50.5	82.4	**82.4**	100.0	100.0	**100.0**	0.108	0.108	**0.108**
AUC_{JT}R'	3	-	-	81.6	-	-	58.5	-	-	0.546	-	-
AUC_{QRS}R'	3	-	-	42.7	-	-	99.4	-	-	0.500	-	-
$AUC_{TmaxTend}$'	3	**4**	6	67.9	**79.6**	77.9	74.2	**76.5**	96.1	21.6	**23.1**	56.3
AUC_{JTmax}'	7	**8**	-	100.0	**100.0**	-	59.5	**70.5**	-	18.2	**18.2**	-
AUC_{JT}'	5	6	-	98.5	62.0	-	50.1	91.8	-	75.8	133.3	-
AUC_{QRS}'	5	5	**5**	88.2	88.2	**88.2**	82.6	82.6	**82.6**	86.8	86.8	**86.8**
AUC_{QRST}'	5	**5**	**6**	72.8	**72.8**	**81.7**	88.1	**88.1**	**99.3**	199.9	**199.9**	**284.6**
-AUC_{JT}	9	-	-	83.8	-	-	67.7	-	-	-23.3	-	-
+AUC_{JT}	4	7	-	54.3	69.7	-	81.9	88.8	-	100.7	110.3	-
$AUC_{JTmax/TmaxTend}$	4	**5**	**7**	47.9	**76.0**	**81.6**	99.0	**77.2**	**98.1**	2.5	**1.4**	**1.2**
$AUC_{TmaxTend}$	3	3	**4**	67.0	67.0	**82.8**	91.1	91.1	**90.8**	20.4	20.4	**20.0**
AUC_{JTmax}	**10**	-	-	**81.9**	-	-	**72.2**	-	-	**0.02**	-	-
+/-AUC_{QRS}	3	4	**4**	60.5	81.8	**81.8**	84.6	100.0	**100.0**	0.287	1.32	**1.32**
-AUC_{QRS}	3	4	**4**	100.0	99.6	**99.6**	59.3	85.1	**85.1**	-65.6	-37.9	**-37.9**
+AUC_{QRS}	3	4	**4**	49.1	79.8	**79.8**	100.0	99.7	**99.7**	17.3	16.8	**16.8**
AUC_{JT}	4	7	-	54.3	57.4	-	83.2	90.8	-	100.4	118.9	-
AUC_{QRS}	3	3	**4**	100.0	100.0	**99.6**	58.0	58.0	**85.4**	-59.9	-59.9	**-30.5**
AUC_{QRST}	3	**3**	**4**	90.7	**90.7**	**99.8**	72.7	**72.7**	**91.0**	12.3	**12.3**	**65.7**
T_A	5	7	**8**	50.8	67.6	**80.1**	98.3	100.0	**97.8**	1.42	1.48	**1.42**
ST20	7	-	-	60.4	-	-	100.0	-	-	0.32	-	-
QRS_A	3	**3**	**4**	91.3	**91.3**	**100.0**	74.7	**74.7**	**83.2**	-3.87	**-3.87**	**-2.79**
-QRS_A	3	**3**	**4**	91.3	**91.3**	**100.0**	74.7	**74.7**	**83.2**	-3.87	**-3.87**	**-2.79**
+QRS_A	4	4	**4**	76.4	76.4	**76.4**	99.5	99.5	**99.5**	1.73	1.73	**1.73**
JTmax	4	4	**5**	62.1	62.1	**85.4**	99.8	99.8	**100.0**	131	131	**109**

*Unites of particular parameters can be found in Appendix A

Table I-3. Time instances, where AUCROC of joint & VCG parameters from the hearts with high LV mass fraction reaches value higher than 0.7, 0.8 and 0.9 and corresponding Se, Sp and cut-off. Indexes with both Se and Sp in the range <0.7 - 0.8>, <0.8 - 0.9> or <0.9 - 1> (one of them may exceed the range) are highlighted by orange, green and blue, respectively.

Parameter	Time. min			Se. %			Sp. %			Cut-off*		
	> 0.7	> 0.8	> 0.9	> 0.7	> 0.8	> 0.9	> 0.7	> 0.8	> 0.9	> 0.7	> 0.8	> 0.9
P_{jt}	**3**	4	**5**	**71.7**	93.0	**81.1**	**80.6**	78.7	**96.0**	**6.7**	6.6	**7.9**
P_{qrs}	5	**6**	**7**	43.2	**73.4**	**87.1**	97.7	**96.7**	**98.8**	21.9	**18.6**	**16.5**
$A_{jt}zy$	2	3	**4**	86.8	91.8	**88.2**	64.5	67.3	**86.4**	0.225	0.236	**0.389**
$A_{jt}xz$	3	**4**	**5**	86.7	**71.3**	**87.6**	60.3	**82.4**	**96.8**	0.273	**0.407**	**0.721**
$A_{jt}xy$	2	2	**5**	79.7	79.7	**95.6**	69.5	69.5	**99.7**	0.293	0.293	**0.431**
$A_{qrs}zy$	**5**	-	-	**73.2**	-	-	**78.2**	-	-	**6.033**	-	-
$A_{qrs}xz$	-	-	-	-	-	-	-	-	-	-	-	-
$A_{qrs}xy$	-	-	-	-	-	-	-	-	-	-	-	-
$\varphi^{c}_{jt}zy$	5	5	**5**	91.3	91.3	**91.3**	84.2	84.2	**84.2**	60	60	**60**
$\varphi^{c}_{jt}xz$	-	-	-	-	-	-	-	-	-	-	-	-
$\varphi^{c}_{jt}xy$	3	-	-	88.1	-	-	57.3	-	-	10	-	-
$\varphi^{c}_{qrs}zy$	-	-	-	-	-	-	-	-	-	-	-	-
$\varphi^{c}_{qrs}xz$	4	-	-	38.7	-	-	95.5	-	-	24	-	-
$\varphi^{c}_{qrs}xy$	**4**	-	-	**92.4**	-	-	**72.0**	-	-	**9**	-	-
$D^{c}_{jt}zy$	3	**3**	4	88.8	**88.8**	97.6	81.7	**81.7**	87.3	0.54	**0.54**	0.60
$D^{c}_{jt}xz$	**3**	4	**5**	**70.0**	66.9	**82.2**	**72.0**	92.1	**100.0**	**0.76**	0.89	**1.79**
$D^{c}_{jt}xy$	3	**4**	-	67.9	**72.1**	-	88.9	**89.3**	-	0.88	**0.89**	-
$D^{c}_{qrs}zy$	-	-	-	-	-	-	-	-	-	-	-	-
$D^{c}_{qrs}xz$	-	-	-	-	-	-	-	-	-	-	-	-
$D^{c}_{qrs}xy$	3	-	-	82.9	-	-	57.7	-	-	2.60	-	-
D	4	5	**5**	85.4	99.5	**99.5**	55.3	88.0	**88.0**	6.6	5.9	**5.9**
φ	3	4	**4**	46.6	71.4	**71.4**	91.7	100.0	**100.0**	148	128	**128**
L_{jt}	3	3	**4**	98.5	98.5	**96.8**	66.5	66.5	**88.6**	1.4	1.4	**1.8**
L_{qrs}	-	-	-	-	-	-	-	-	-	-	-	-
γ_{jt}	5	5	**5**	82.2	82.2	**82.2**	99.3	99.3	**99.3**	-27	-27	**-27**
β_{jt}	5	**5**	-	82.2	**82.2**	-	89.1	**89.1**	-	58	**58**	-
α_{jt}	**5**	-	-	**76.5**	-	-	**73.9**	-	-	**-58**	-	-
γ_{qrs}	3	4	**4**	57.3	93.8	**93.8**	100.0	77.4	**77.4**	34	8	**8**
β_{qrs}	**3**	4	4	**71.9**	73.2	73.2	**77.2**	99.8	99.8	**127**	121	121
α_{qrs}	3	5	**5**	84.6	99.2	**99.2**	67.2	100.0	**100.0**	135	31	**31**
QT_D	5	**7**	8	76.4	**82.9**	87.4	63.3	**90.0**	93.7	180	**179**	174
QRS_D	3	**3**	**4**	88.4	**88.4**	**85.6**	72.5	**72.5**	**100.0**	30	**30**	**33**
RR	2	**3**	**4**	57.1	**71.4**	**100.0**	85.7	**85.7**	**85.7**	378	**384**	**375**

*Unites of particular parameters can be found in Appendix A

APPENDIX J – RESULTS OF PAIRED TEST FOR PARAMETERS FROM THE HEARTS STAINED WITH VSD DI-4-ANEPPS

Lead I data:

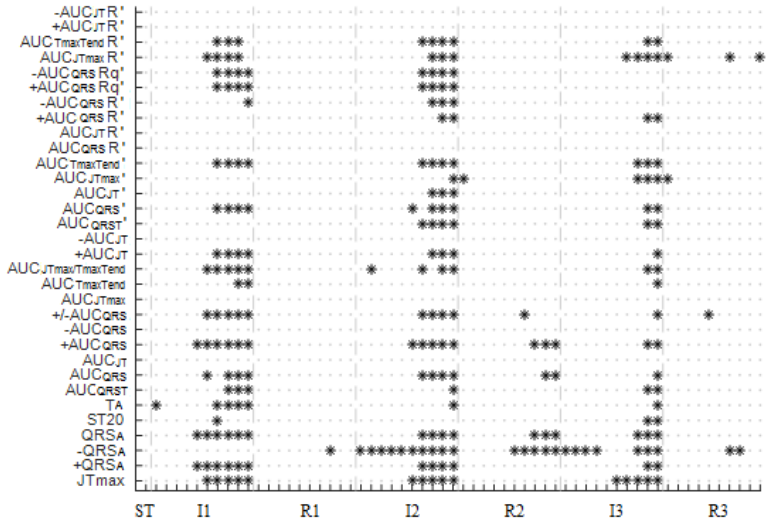

Lead II data:

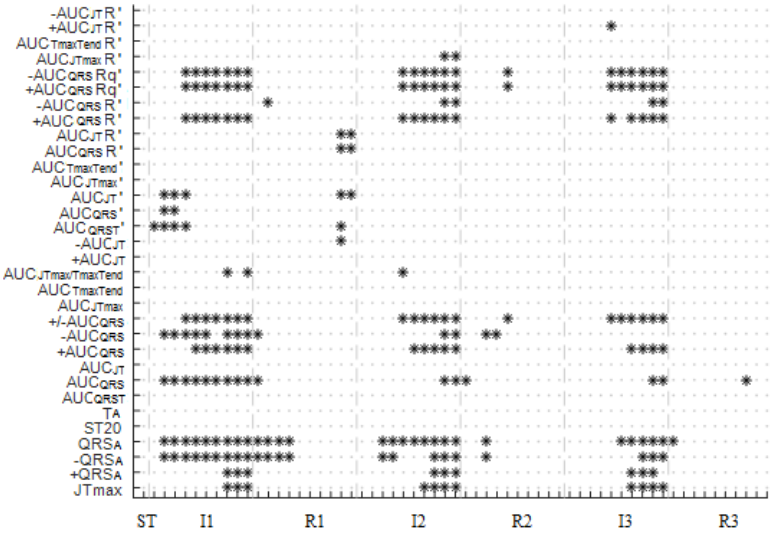

VCG and joint data:

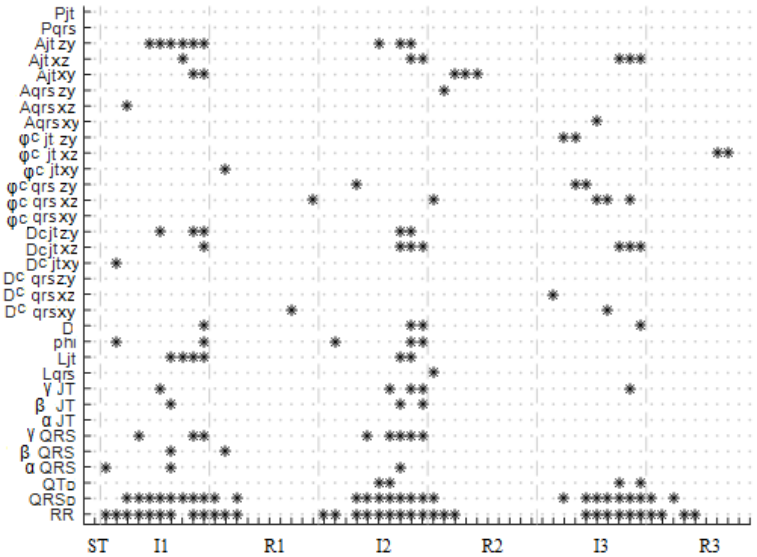

Figure J-1. Results of Wilcoxon signed-rank test for comparison of parameters from the end of stabilization and at each minute of three ischemia-reperfusion repetitions in the hearts stained with voltage-sensitive dye di-4-ANEPPS. * for $p < 0.05$.

APPENDIX K – DISCRIMINATING ABILITY INDEXES IN HEARTS STAINED WITH VSD DI-4-ANEPPS

Table K-1. Time instances, where AUCROC of lead I parameters from the hearts stained with voltage-sensitive dye di-4-ANEPPS reaches value higher than 0.7, 0.8 and 0.9 and corresponding Se, Sp and cut-off. Indexes with both Se and Sp in the range <0.7 - 0.8>, <0.8 - 0.9> or <0.9 - 1> (one of them may exceed the range) are highlighted by orange, green and blue, respectively.

Parameter	Time, min			Se, %			Sp, %			Cut-off*		
	> 0.7	> 0.8	> 0.9	> 0.7	> 0.8	> 0.9	> 0.7	> 0.8	> 0.9	> 0.7	> 0.8	> 0.9
-$AUC_{JT}R'$	10	-	-	57.5	-	-	100.0	-	-	0.367	-	-
+$AUC_{JT}R'$	9	-	-	89.2	-	-	58.5	-	-	0.206	-	-
$AUC_{TmaxTend}R'$	**7**	-	-	**76.0**	-	-	**75.8**	-	-	**0.269**	-	-
$AUC_{JTmax}R'$	6	**7**	-	56.7	**83.3**	-	96.2	**74.1**	-	0.526	**0.278**	-
-$AUC_{QRS}Rq'$	8	**10**	-	100.0	**72.9**	-	36.3	**89.9**	-	0.049	**0.338**	-
+$AUC_{QRS}Rq'$	8	**10**	-	36.3	**89.3**	-	100.0	**73.3**	-	0.952	**0.677**	-
-$AUC_{QRS}R'$	9	-	-	100.0	-	-	52.6	-	-	0.023	-	-
+$AUC_{QRS}R'$	**6**	-	-	**73.1**	-	-	**85.6**	-	-	**0.196**	-	-
$AUC_{JT}R'$	5	6	-	63.8	63.5	-	84.3	91.8	-	0.769	0.770	-
$AUC_{QRS}R'$	5	6	-	84.3	91.8	-	63.8	63.5	-	0.231	0.230	-
$AUC_{TmaxTend}'$	7	10	-	44.3	55.9	-	98.5	100.0	-	210.2	245.5	-
AUC_{JTmax}'	7	7	-	98.5	98.5	-	53.5	53.5	-	2.39	2.39	-
AUC_{JT}'	9	-	-	47.7	-	-	94.4	-	-	488.2	-	-
AUC_{QRS}'	6	7	**10**	48.9	48.7	**98.8**	99.4	100.0	**79.2**	175.9	179.2	**91.9**
AUC_{QRST}'	8	10	-	35.8	66.0	-	100.0	93.8	-	1264.9	552.8	-
-AUC_{JT}	-	-	-	-	-	-	-	-	-	-	-	-
+AUC_{JT}	**7**	8	-	**74.1**	66.3	-	**74.8**	88.8	-	**136.7**	261.1	-
$AUC_{JTmax/TmaxTend}$	7	7	-	98.5	98.5	-	53.5	53.5	-	0.049	0.049	-
$AUC_{TmaxTend}$	8	9	-	45.7	58.8	-	100.0	100.0	-	114.2	104.9	-
AUC_{JTmax}	-	-	-	-	-	-	-	-	-	-	-	-
+/-AUC_{QRS}	8	**10**	-	36.3	**89.3**	-	100.0	**73.3**	-	20.0	**2.1**	-
-AUC_{QRS}	-	-	-	-	-	-	-	-	-	-	-	-
+AUC_{QRS}	6	**9**	-	39.8	**84.4**	-	100.0	**74.4**	-	162.5	**48.4**	-
AUC_{JT}	9	9	-	53.9	53.9	-	97.1	97.1	-	382.0	382.0	-
AUC_{QRS}	7	**9**	-	43.5	**89.2**	-	100.0	**73.8**	-	79.0	**19.3**	-
AUC_{QRST}	8	9	-	46.0	66.6	-	88.3	88.5	-	232.2	240.4	-
T_A	7	7	-	88.6	88.6	-	66.7	66.7	-	1.57	1.57	-
ST20	6	7	-	38.5	59.3	-	89.8	91.5	-	0.12	0.15	-
QRS_A	7	-	-	38.7	-	-	100.0	-	-	7.71	-	-
-QRS_A	-	-	-	-	-	-	-	-	-	-	-	-
+QRS_A	7	-	-	38.7	-	-	100.0	-	-	7.71	-	-
JTmax	**6**	7	7	**74.2**	76.0	76.0	**78.3**	100.0	100.0	**131**	127	127

*Unites of particular parameters can be found in Appendix A

Table K-2. Time instances, where AUCROC of lead II parameters from the hearts stained with voltage-sensitive dye di-4-ANEPPS reaches value higher than 0.7, 0.8 and 0.9 and corresponding Se, Sp and cut-off. Indexes with both Se and Sp in the range <0.7 - 0.8>, <0.8 - 0.9> or <0.9 - 1> (one of them may exceed the range) are highlighted by orange, green and blue, respectively.

Parameter	Time, min			Se, %			Sp, %			Cut-off*		
	> 0.7	> 0.8	> 0.9	> 0.7	> 0.8	> 0.9	> 0.7	> 0.8	> 0.9	> 0.7	> 0.8	> 0.9
$-AUC_{JT}R'$	-	-	-	-	-	-	-	-	-	-	-	-
$+AUC_{JT}R'$	-	-	-	-	-	-	-	-	-	-	-	-
$AUC_{TmaxTend}R'$	9	-	-	70.6	-	-	69.4	-	-	0.284	-	-
$AUC_{JTmax}R'$	-	-	-	-	-	-	-	-	-	-	-	-
$-AUC_{QRS}Rq'$	6	8	9	100.0	96.3	68.1	42.9	55.4	98.1	0.439	0.499	0.828
$+AUC_{QRS}Rq'$	6	8	9	42.9	55.1	98.1	100.0	96.5	68.3	0.837	0.507	0.173
$-AUC_{QRS}R'$	6	**9**	-	97.1	**70.6**	-	41.8	**90.6**	-	0.055	**0.182**	-
$+AUC_{QRS}R'$	6	8	**9**	53.0	61.6	**91.6**	100.0	98.1	**75.8**	0.133	0.118	**0.054**
$AUC_{JT}R'$	-	-	-	-	-	-	-	-	-	-	-	-
$AUC_{QRS}R'$	-	-	-	-	-	-	-	-	-	-	-	-
$AUC_{TmaxTend}'$	8	-	-	97.9	-	-	45.6	-	-	39.8	-	-
AUC_{JTmax}'	-	-	-	-	-	-	-	-	-	-	-	-
AUC_{JT}'	-	-	-	-	-	-	-	-	-	-	-	-
AUC_{QRS}'	-	-	-	-	-	-	-	-	-	-	-	-
AUC_{QRST}'	-	-	-	-	-	-	-	-	-	-	-	-
$-AUC_{JT}$	-	-	-	-	-	-	-	-	-	-	-	-
$+AUC_{JT}$	-	-	-	-	-	-	-	-	-	-	-	-
$AUC_{JTmax/TmaxTend}$	**8**	-	-	**76.5**	-	-	**71.3**	-	-	**1.01**	-	-
$AUC_{TmaxTend}$	**10**	-	-	**78.4**	-	-	**72.3**	-	-	**44.4**	-	-
AUC_{JTmax}	-	-	-	-	-	-	-	-	-	-	-	-
$+/-AUC_{QRS}$	6	8	9	42.9	55.1	98.1	100.0	96.5	68.3	5.15	1.03	0.21
$-AUC_{QRS}$	6	10	-	45.9	63.4	-	99.8	100.0	-	-15.7	-11.6	-
$+AUC_{QRS}$	6	8	**10**	53.0	58.5	**89.9**	100.0	99.0	**90.4**	42.3	39.7	**21.2**
AUC_{JT}	-	-	-	-	-	-	-	-	-	-	-	-
AUC_{QRS}	6	**9**	-	42.9	**90.0**	-	100.0	**76.5**	-	35.2	**-26.4**	-
AUC_{QRST}	-	-	-	-	-	-	-	-	-	-	-	-
T_A	-	-	-	-	-	-	-	-	-	-	-	-
ST20	-	-	-	-	-	-	-	-	-	-	-	-
QRS_A	5	8	-	50.8	60.6	-	99.4	98.3	-	-0.86	-1.27	-
$-QRS_A$	5	8	-	50.8	59.3	-	100.0	100.0	-	-1.17	-0.84	-
$+QRS_A$	7	9	-	68.0	67.4	-	90.4	90.4	-	1.45	1.31	-
JTmax	8	-	-	64.6	-	-	89.6	-	-	122	-	-

*Unites of particular parameters can be found in Appendix A

Table K-3. Time instances, where AUCROC of joint&VCG parameters from the hearts stained with voltage-sensitive dye di-4-ANEPPS reaches value higher than 0.7, 0.8 and 0.9 and corresponding Se, Sp and cut-off. Indexes with both Se and Sp in the range <0.7 - 0.8>, <0.8 - 0.9> or <0.9 - 1> (one of them may exceed the range) are highlighted by orange, green and blue, respectively.

Parameter	Time. min			Se. %			Sp. %			Cut-off*		
	> 0.7	> 0.8	> 0.9	> 0.7	> 0.8	> 0.9	> 0.7	> 0.8	> 0.9	> 0.7	> 0.8	> 0.9
P_{jt}	-	-	-	-	-	-	-	-	-	-	-	-
P_{qrs}	-	-	-	-	-	-	-	-	-	-	-	-
$A_{jt}zy$	**7**	-	-	**76.9**	-	-	**75.6**	-	-	**4.19**	-	-
$A_{jt}xz$	6	7	-	57.4	52.1	-	80.8	94.4	-	1.28	3.05	-
$A_{jt}xy$	-	-	-	-	-	-	-	-	-	-	-	-
$A_{qrs}zy$	-	-	-	-	-	-	-	-	-	-	-	-
$A_{qrs}xz$	-	-	-	-	-	-	-	-	-	-	-	-
$A_{qrs}xy$	-	-	-	-	-	-	-	-	-	-	-	-
$\varphi^{c}_{jt}zy$	-	-	-	-	-	-	-	-	-	-	-	-
$\varphi^{c}_{jt}xz$	-	-	-	-	-	-	-	-	-	-	-	-
$\varphi^{c}_{jt}xy$	-	-	-	-	-	-	-	-	-	-	-	-
$\varphi^{c}_{qrs}zy$	-	-	-	-	-	-	-	-	-	-	-	-
$\varphi^{c}_{qrs}xz$	-	-	-	-	-	-	-	-	-	-	-	-
$\varphi^{c}_{qrs}xy$	-	-	-	-	-	-	-	-	-	-	-	-
$D^{c}_{jt}zy$	8	-	-	89.3	-	-	65.2	-	-	2.07	-	-
$D^{c}_{jt}xz$	7	-	-	38.7	-	-	100.0	-	-	4.84	-	-
$D^{c}_{jt}xy$	**9**	-	-	**79.0**	-	-	**70.0**	-	-	**1.71**	-	-
$D^{c}_{qrs}zy$	-	-	-	-	-	-	-	-	-	-	-	-
$D^{c}_{qrs}xz$	-	-	-	-	-	-	-	-	-	-	-	-
$D^{c}_{qrs}xy$	-	-	-	-	-	-	-	-	-	-	-	-
D	-	-	-	-	-	-	-	-	-	-	-	-
φ	10	-	-	57.5	-	-	81.0	-	-	108	-	-
L_{jt}	8	-	-	89.0	-	-	57.3	-	-	3.97	-	-
L_{qrs}	-	-	-	-	-	-	-	-	-	-	-	-
γ_{jt}	-	-	-	-	-	-	-	-	-	-	-	-
β_{jt}	7	**8**	-	54.3	**73.4**	-	94.8	**79.0**	-	78	**58**	-
α_{jt}	-	-	-	-	-	-	-	-	-	-	-	-
γ_{qrs}	10	-	-	87.7	-	-	53.0	-	-	24	-	-
β_{qrs}	-	-	-	-	-	-	-	-	-	-	-	-
α_{qrs}	7	-	-	79.4	-	-	66.3	-	-	91	-	-
QT_D	-	-	-	-	-	-	-	-	-	-	-	-
QRS_D	4	6	**6**	83.8	86.0	**86.0**	60.6	87.7	**87.7**	29	34	**34**
RR	2	7	-	100.0	88.9	-	55.6	66.7	-	535	564	

*Unites of particular parameters can be found in Appendix A

APPENDIX L – SELECTED CLASSIFICATION FEATURES

Table L-1. Feature sets selected by different feature selection methods from control group data.

	Feature selection method	
	Ranked Spearman's ρ	**Ranked weighted principal component loadings**
BINARY:		
F2	**F21**	**F22**
	+/-AUC_{QRS} (II), +/-AUC_{QRS} (I), $AUC_{JTmax/TmaxTend}$ (I), $AUC_{JTmax/TmaxTend}$ (II), -QRS_A (I) , $A_{qrs}xy$ **(6 / 69)**	QRS_A (I), +QRS_A (I), $D^c_{qrs}xz$, -AUC_{QRS} (II), L_{qrs}, AUC_{JTmax}' (II), AUC_{JTmax} (II), -$AUC_{QRS}R'$ (II), +$AUC_{QRS}R'$ (I), $AUC_{QRS}R'$ (I), $AUC_{JT}R'$ (I) **(11 / 69)**
F3	**F31**	**F32**
	$AUC_{JTmax/TmaxTend}$ (I), +/-AUC_{QRS} (I), -QRS_A (I) **(3 / 26)**	$AUC_{QRS}R'$ (I), $AUC_{JT}R'$ (I), +$AUC_{QRS}R'$ (I), AUC_{JT}' (I), QRS_A (I), +QRS_A (I), +AUC_{JT} (I), +$AUC_{QRS}Rq'$ (I), -$AUC_{QRS}Rq'$ (I) **(9 / 26)**
F4	**F41**	**F42**
	+/-AUC_{QRS} (II), $AUC_{JTmax/TmaxTend}$ (II), -AUC_{JT} (II), AUC_{JTmax} (II), AUC_{JTmax}' (II), $AUC_{TmaxTend}$ (II), -AUC_{QRS} (II) **(7 / 21)**	$AUC_{JTmax}R'$ (II), QRS_A (II), JTmax (II), +$AUC_{QRS}Rq'$ (II), -$AUC_{QRS}Rq'$ (II) **(5 / 21)**
F5	**F51**	**F52**
	$\varphi^c_{qrs}zy$, QT_D, $A_{qrs}xy$, α_{jt}, $D^c_{qrs}xz$, $D^c_{qrs}xy$, β_{qrs} **(7 / 22)**	QT_D, $A_{qrs}xy$, α_{jt}, L_{qrs}, $D^c_{qrs}xy$, $\varphi^c_{qrs}zy$, β_{jt}, P_{qrs}, φ **(9 / 22)**
F6	QRS_D, QRS_A (I), ST20 (I), T_A (I), QRS_A (II), ST20 (II), T_A (II) **(7 / 69)**	
F7	+$AUC_{QRS}Rq'$ (I), QRS_A (II), $AUC_{JTmax/TmaxTend}$ (II), D, $A_{jt}xy$ **(5 / 69)**	
4-CLASS:		
F2	**F21**	**F22**
	+/-AUC_{QRS} (II), +/-AUC_{QRS} (I), $AUC_{JTmax/TmaxTend}$ (I), $AUC_{JTmax/TmaxTend}$ (II), -QRS_A (I) , $A_{qrs}xy$, QT_D, α_{jt}, $D^c_{qrs}xy$, $\varphi^c_{qrs}zy$, $D^c_{qrs}xz$, +$AUC_{QRS}R'$ (I), -AUC_{JT} (II), $AUC_{QRS}R'$ (I), $AUC_{JT}R'$ (I), AUC_{JTmax} (II), AUC_{JTmax}' (I), AUC_{JTmax}' (II), β_{jt}, -AUC_{QRS} (II), RR, P_{qrs} **(n = 22)**	QRS_A (I), +QRS_A (I), $D^c_{qrs}xz$, -AUC_{QRS} (II), L_{qrs}, AUC_{JTmax}' (II), AUC_{JTmax} (II), -$AUC_{QRS}R'$ (II), +$AUC_{QRS}R'$ (I), $AUC_{QRS}R'$ (I), $AUC_{JT}R'$ (I), AUC_{JTmax}' (I), AUC_{QRS}' (II), $AUC_{JTmax}R'$ (I), +$AUC_{QRS}R'$ (II), P_{qrs}, β_{jt}, -QRS_A (II), $D^c_{qrs}xy$, +AUC_{QRS} (II), -$AUC_{QRS}Rq'$ (I), +$AUC_{QRS}Rq'$ (I), QRS_D **(n = 23)**
F3	**F31**	**F32**
	$AUC_{JTmax/TmaxTend}$ (I), +/-AUC_{QRS} (I), -QRS_A (I), AUC_{JTmax}' (I), +$AUC_{QRS}R'$ (I), $AUC_{QRS}R'$ (I), $AUC_{JT}R'$ (I), QRS_A (I), +QRS_A (I), -$AUC_{QRS}Rq'$ (I), -$AUC_{QRS}R'$ (I), +$AUC_{QRS}Rq'$ (I), $AUC_{JTmax}R'$ (I) **(n = 13)**	$AUC_{QRS}R'$ (I), $AUC_{JT}R'$ (I), +$AUC_{QRS}R'$ (I), AUC_{JT}' (I), QRS_A (I), +QRS_A (I), +AUC_{JT} (I), +$AUC_{QRS}Rq'$ (I), -$AUC_{QRS}Rq'$ (I), AUC_{QRS} (I) **(n = 10)**
F4	**F41**	**F42**
	+/-AUC_{QRS} (II), $AUC_{JTmax/TmaxTend}$ (II), -AUC_{JT} (II), AUC_{JTmax} (II), AUC_{JTmax}' (II), $AUC_{TmaxTend}$ (II), -AUC_{QRS} (II), $AUC_{TmaxTend}R'$ (II), $AUC_{TmaxTend}$' (II), -$AUC_{QRS}R'$ (II), AUC_{QRS}' (II), -QRS_A (II), $AUC_{JTmax}R'$ (II) **(n = 13)**	$AUC_{TmaxTend}R'$ (II), $AUC_{TmaxTend}$' (II), -AUC_{QRS} (II), $AUC_{JTmax}R'$ (II), AUC_{JTmax} (II), -$AUC_{QRS}R'$ (II), $AUC_{TmaxTend}$ (II), +$AUC_{QRS}R'$ (II), JTmax (II), AUC_{JTmax}' (II), AUC_{QRS}' (II), -QRS_A (II) **(n = 12)**
F5	**F51**	**F52**
	$\varphi^c_{qrs}zy$, QT_D, $A_{qrs}xy$, α_{jt}, $D^c_{qrs}xz$, $D^c_{qrs}xy$, β_{qrs}, RR, QRS_D, β_{jt}, $A_{jt}xy$, P_{qrs} **(n = 12)**	QT_D, $A_{qrs}xy$, α_{jt}, L_{qrs}, $D^c_{qrs}xy$, $\varphi^c_{qrs}zy$, β_{jt}, P_{qrs}, φ, QRS_D, $\varphi^c_{jt}zy$ **(n = 11)**
F6	QRS_D, QRS_A (I), ST20 (I), T_A (I), QRS_A (II), ST20 (II), T_A (II) **(n = 7)**	
F7	QRS_A (II), φ, -QRS_A (II), -AUC_{QRS} (II), $AUC_{TmaxTend}R'$ (II) **(n = 5)**	

Table L-2. Feature sets selected by different feature selection methods from H group data.

	Feature selection method	
	Ranked Spearman's ρ	**Ranked weighted principal component loadings**
BINARY:		
F2	**F21**	**F22**
	$AUC_{JTmax/TmaxTend}$ (I), $AUC_{JTmax/TmaxTend}$ (II), +/-AUC_{QRS} (I), $A_{qrs}xy$, QRS_A (I), +QRS_A (I), +/-AUC_{QRS} (II), -QRS_A (I), $AUC_{JT}R'$ (II), $AUC_{QRS}R'$ (I), AUC_{JTmax}' (II), +AUC_{JT} (II), AUC_{JTmax} (I) **(n = 13)**	+AUC_{JT} (II), +QRS_A (I), QRS_A (I), AUC_{JT}' (II), T_A (II), $AUC_{TmaxTend}$ (II), $D^c_{jt}xy$, -$AUC_{QRS}Rq'$ (I), +$AUC_{QRS}Rq'$ (I), -QRS_A (I) **(n = 10)**
F3	**F31**	**F32**
	$AUC_{JTmax/TmaxTend}$ (I), +/-AUC_{QRS} (I), -QRS_A (I), QRS_A (I), +QRS_A (I), AUC_{JTmax} (I), -$AUC_{QRS}Rq'$ (I), +$AUC_{QRS}Rq'$ (I), -$AUC_{QRS}R'$ **(n = 9)**	-$AUC_{QRS}Rq'$ (I), +$AUC_{QRS}Rq'$ (I), QRS_A (I) **(n = 3)**
F4	**F41**	**F42**
	$AUC_{JTmax/TmaxTend}$ (II), +/-AUC_{QRS} (II), $AUC_{JT}R'$ (II), $AUC_{QRS}R'$ (II), AUC_{JTmax}' (II), +AUC_{JT} (II), T_A (II) **(n = 7)**	AUC_{JT}' (II), $AUC_{QRS}R'$ (II), $AUC_{JT}R'$ (II), +AUC_{JT} (II), AUC_{JTmax}' (II), $AUC_{JTmax}R'$ (II) **(n = 6)**
F5	**F51**	**F52**
	$A_{qrs}xy$, QT_D, RR **(n = 3)**	P_{qrs}, $D^c_{jt}xy$, α_{qrs}, $\varphi^c_{jt}zy$ **(n = 4)**
F6	QRS_D, QRS_A (I), ST20 (I), T_A (I), QRS_A (II), ST20 (II), T_A (II) **(n = 7)**	
F7	AUC_{QRST}' (I), -QRS_A (II), +AUC_{QRS} (II), β_{qrs}, $D^c_{jt}zy$ **(n = 5)**	
4-CLASS:		
F2	**F21**	**F22**
	$AUC_{JTmax/TmaxTend}$ (I), $AUC_{JTmax/TmaxTend}$ (II), +/-AUC_{QRS} (I), $A_{qrs}xy$, QRS_A (I), +QRS_A (I), +/-AUC_{QRS} (II), -QRS_A (I), $AUC_{JT}R'$ (II), $AUC_{QRS}R'$ (I), AUC_{JTmax}' (II), +AUC_{JT} (II), AUC_{JTmax} (I), AUC_{JT}' (II), QT_D, -$AUC_{QRS}Rq'$ (I), +$AUC_{QRS}Rq'$ (I), T_A (II), $AUC_{TmaxTend}$ (II), RR, P_{qrs}, $D^c_{jt}xy$ **(n = 22)**	+AUC_{JT} (II), +QRS_A (I), QRS_A (I), AUC_{JT}' (II), T_A (II), $AUC_{TmaxTend}$ (II), $D^c_{jt}xy$, -$AUC_{QRS}Rq'$ (I), +$AUC_{QRS}Rq'$ (I), -QRS_A (I), $AUC_{TmaxTend}'$ (II), P_{qrs}, $A_{jt}xz$, AUC_{QRST} (II), $AUC_{QRS}R'$ (II), $AUC_{JT}R'$ (II), QRS_D, AUC_{JTmax}' (II), P_{jt}, AUC_{QRST}' (II), AUC_{JT} (I), AUC_{QRS} (I), +AUC_{JT} (I), ST20 (I), +AUC_{QRS} (I), AUC_{JT}' (I), AUC_{QRS}' (II), $AUC_{TmaxTend}$ (I), γ_{qrs}, AUC_{QRS}' (I), $AUC_{TmaxTend}'$ (I), $AUC_{JTmax}R'$ (II), AUC_{JTmax} (I), AUC_{QRST}' (I), QT_D **(n = 35)**
F3	**F31**	**F32**
	$AUC_{JTmax/TmaxTend}$ (I), +/-AUC_{QRS} (I), -QRS_A (I), QRS_A (I), +QRS_A (I), AUC_{JTmax} (I), -$AUC_{QRS}Rq'$ (I), +$AUC_{QRS}Rq'$ (I), -$AUC_{QRS}R'$ **(n = 9)**	-$AUC_{QRS}Rq'$ (I), +$AUC_{QRS}Rq'$ (I), QRS_A (I), +QRS_A (I), AUC_{JT} (I), AUC_{QRS} (I), +AUC_{QRS} (I), AUC_{QRS}' (I), ST20 (I), -$AUC_{QRS}R'$ (I), AUC_{JTmax} (I) **(n = 11)**
F4	**F41**	**F42**
	$AUC_{JTmax/TmaxTend}$ (II), +/-AUC_{QRS} (II), $AUC_{JT}R'$ (II), $AUC_{QRS}R'$ (II), AUC_{JTmax}' (II), +AUC_{JT} (II), T_A (II), AUC_{JT}' (II), $AUC_{TmaxTend}$ (II), -QRS_A (II), $AUC_{TmaxTend}R'$ (II), $AUC_{JTmax}R'$ (II), -$AUC_{QRS}R'$ (II), -AUC_{QRS} (II), AUC_{QRST}' (II), AUC_{QRS}' (II) **(n = 16)**	AUC_{JT}' (II), $AUC_{QRS}R'$ (II), $AUC_{JT}R'$ (II), +AUC_{JT} (II), AUC_{JTmax}' (II), $AUC_{JTmax}R'$ (II), +$AUC_{QRS}R'$ (II), $AUC_{TmaxTend}$ (II), AUC_{QRST}' (II), AUC_{QRST} (II), $AUC_{TmaxTend}'$ (II), -$AUC_{QRS}R'$ (II), +AUC_{QRS} (II), AUC_{QRS}' (II), AUC_{QRS} (II), JTmax (II), $AUC_{TmaxTend}R'$ (II), +QRS_A (II), +$AUC_{QRS}Rq'$ (II), -$AUC_{QRS}Rq'$ (II), QRS_A (II), -AUC_{QRS} (II) **(n = 22)**
F5	**F51**	**F52**
	$A_{qrs}xy$, QT_D, RR, P_{qrs}, $D^c_{jt}xy$, β_{jt}, QRS_D, α_{qrs} **(n = 8)**	P_{qrs}, $D^c_{jt}xy$, α_{qrs}, $\varphi^c_{jt}zy$, $A_{qrs}xy$, $A_{jt}xz$, $A_{jt}xy$, P_{jt}, β_{qrs}, $D^c_{jt}zy$, D, QT_D **(n = 12)**
F6	QRS_D, QRS_A (I), ST20 (I), T_A (I), QRS_A (II), ST20 (II), T_A (II) **(n = 7)**	
F7	AUC_{QRST} (I), $D^c_{jt}zy$, AUC_{QRST}' (I), +/-AUC_{QRS} (II), -QRS_A (II) **(n = 5)**	

Table L-3. Feature sets selected by different feature selection methods from data recorded in experiments with di-4-ANEPPS administration.

	Feature selection method	
	Ranked Spearman's ρ	**Ranked weighted principal component loadings**
BINARY:		
F2	**F21**	**F22**
	$AUC_{JTmax/TmaxTend}$ (I), +/-AUC_{QRS} (I), RR, $A_{jt}zy$, $A_{jt}xy$, L_{jt}, γ_{qrs}, -QRS_A (I), JTmax (II), $AUC_{TmaxTend}$ (I), -$AUC_{QRS}Rq'$ (I) **(n = 11)**	L_{jt}, +$AUC_{QRS}Rq'$ (I), -$AUC_{QRS}Rq'$ (I), -QRS_A (II), -$AUC_{QRS}Rq'$ (II) **(n = 5)**
F3	**F31**	**F32**
	$AUC_{JTmax/TmaxTend}$ (I), +/-AUC_{QRS} (I), -QRS_A (I), $AUC_{JTmax}R'$ (I), $AUC_{TmaxTend}$ (I), -$AUC_{QRS}Rq'$ (I), +$AUC_{QRS}Rq'$ (I) **(n = 7)**	QRS_A (I), $AUC_{TmaxTend}'$ (I), +$AUC_{QRS}Rq'$ (I), $AUC_{QRS}Rq'$ (I) **(n = 4)**
F4	**F41**	**F42**
	JTmax (II), -QRS_A (II) **(n = 2)**	AUC_{QRS}' (II), -AUC_{QRS} (II), -QRS_A (II) **(n = 3)**
F5	**F51**	**F52**
	RR, QRS_D, γ_{qrs}, $A_{jt}xz$, $A_{jt}zy$, L_{jt} **(n = 6)**	RR, γ_{qrs}, $A_{jt}xz$, $A_{jt}zy$ **(n = 3)**
F6	QRS_D, QRS_A (I), ST20 (I), T_A (I), QRS_A (II), ST20 (II), T_A (II) **(n = 7)**	
F7	JTmax (I), $AUC_{JTmax}R'$ (I), AUC_{QRS} (II), RR, QRS_D **(n = 5)**	
4-CLASS:		
F2	**F21**	**F22**
	$AUC_{JTmax/TmaxTend}$ (I), +/-AUC_{QRS} (I), RR, $A_{jt}zy$, $A_{jt}xy$, L_{jt}, γ_{qrs}, -QRS_A (I), JTmax (II), $AUC_{TmaxTend}$ (I), -$AUC_{QRS}Rq'$ (I), -QRS_A(II), +$AUC_{QRS}Rq'$ (I), -AUC_{QRS} (II), AUC_{QRS}' (II), $AUC_{JTmax}R'$ (I), QRS_A (I), QRS_D **(n = 18)**	-AUC_{QRS} (II), -QRS_A (II), AUC_{QRS}' (II), L_{jt}, $A_{jt}xy$, AUC_{QRST}' (II), -$AUC_{QRS}R'$ (II), JTmax (II), QRS_A (II), QRS_A (I) **(n = 10)**
F3	**F31**	**F32**
	$AUC_{JTmax/TmaxTend}$ (I), +/-AUC_{QRS} (I), -QRS_A (I), $AUC_{JTmax}R'$ (I), $AUC_{TmaxTend}$ (I), -$AUC_{QRS}Rq'$ (I), +$AUC_{QRS}Rq'$ (I), $AUC_{TmaxTend}R'$ (I), JTmax (I), AUC_{JT}' (I), QRS_A (I), AUC_{QRS}' (I) **(n = 12)**	QRS_A (I), $AUC_{TmaxTend}'$ (I), +$AUC_{QRS}Rq'$ (I), $AUC_{QRS}Rq'$ (I), +AUC_{JT} (I), +QRS_A (I), AUC_{QRS} (I) **(n = 7)**
F4	**F41**	**F42**
	JTmax (II), -QRS_A (II), -AUC_{QRS} (II), AUC_{QRS}' (II), AUC_{JT}' (II), AUC_{QRST}' (II), -$AUC_{QRS}R'$ (II), +QRS_A (II) **(n = 8)**	QRS_A (I), +QRS_A (II), +AUC_{QRS} (II), -$AUC_{QRS}R'$ (II), AUC_{QRST}' (II) **(n = 5)**
F5	**F51**	**F52**
	RR, QRS_D, γ_{qrs}, $A_{jt}xz$, $A_{jt}zy$ **(n = 5)**	RR, γ_{qrs}, $A_{jt}xz$, $A_{jt}zy$, QRS_D **(n = 5)**
F6	QRS_D, QRS_A (I), ST20 (I), T_A (I), QRS_A (II), ST20 (II), T_A (II) **(n = 7)**	
F7	JTmax (I), JTmax (II), $A_{jt}xy$, -QRS_A (II), $AUC_{TmaxTend}'$ (I) **(n = 5)**	